Role of brain-enriched microRNAs during neural development

Dissertation

zur Erlangung des akademischen Grades des

Doktors der Naturwissenschaften (Dr. rer. nat.)

eingereicht im Fachbereich Biologie, Chemie, Pharmazie

der Freien Universität Berlin

vorgelegt von

Heiko Fuchs

Berlin, Deutschland

Berlin 2010

1. Gutachter: Prof. Dr. Fritz Rathjen

2. Gutachter: Prof. Dr. Robert Nitsch

Disputation am: 12.07.2011

List

Abbreviations

3'UTR 3' untranslated region

αMEM α modified form of Eagle's minimal essential medium

µg Microgram

µM Micromolar

Ago1/2 Argonaute proteins 1 or 2

APS Ammonium phosphate sulfate

Bp Base pairs

BSA Bovine serum albumin

cm Centimeter

CMV Cytomegalovirus

CNS Central nervous system

CTP Cytosin-5'-triphosphat

DMEM Dulbecco's modified Eagle's medium

DMSO Dimethyl sulfoxide

dNTP Deoxynucleotidetriphosphat

dsRBD Double-stranded RNA binding domain

DTT 1,4-dithiothreitol

DRG Dorsal root ganglion

EDTA Ethylenediamine-tetraaceticacid

EC cells Embryonal carcinoma cells

eIF4E Eukaryotic translation initiation factor 4E

EMSA Electrophoretic mobility shift assay

ES cells Embryonic stem cells

et al. Et alter

FACS Fluorescence-Activated Cell Sorter

FBS Fetal bovine serum

FMRP Fragile X mental retardation protein

GAPDH Glyceraldehyde-3-phosphate degydrogenase

GFAP Glial fibrillary acidic protein

GFP Green fluorescent protein

h Hours

HEK293 Human embryonic kidney cell line 293

HRP Horseradish Peroxidase

ISH In situ hybridization

IHC Immunohistochemistry

L Liter

mAb Monoclonal antibody

min Minutes

miRNA microRNA

ml Milliliter

mM Millimolar

mm Millimeter

ng Nanogramm

nt Nucleotide

ORF Open reading frame

P19GM P19 growth medium

PACT PKR activating protein

PBS Phosphate buffered saline

PCR Polymerase chain reaction

PFA Paraformaldehyde

Pol II/ pol III Polymerase II or III

RIIID RNAse III domain

RA Retinoic acid

RISC RNA induced silencing complex

RT Room temperature

RT-PCR Reverse transcription polymerase chain reaction

SAP Shrimp Alkaline Phosphatase

SDS Sodium dodecyl sulfate

s Seconds

snRNA Small nuclear RNA

SSC Solution of sodium chloride and sodium citrate

TBE Buffer Tris-borate-EDTA buffer

TCA Trichloroacetic acid

TEMED N,N,N',N'-Tetramethylethylenediamine

RNP Ribonucleoprotein

TRBP transactivating response RNA binding protein

Tris Tris(hydroxymethyl)aminomethane

Tween20 Polyoxyethylensorbitanmonolaurat

U Units

UTP Uracil-5'-triphosphate

V Volt

Summary

The discovery of microRNAs has revealed an unexpected and spectacular additional level of fine tuning of the genome. MicroRNAs (miRNAs) are a class of 22 nucleotide, non-coding, regulatory RNAs that inhibit the translation of mRNAs by binding to cognate sites of imperfect complementarity found in 3' untranslated regions in their target genes. To date, thousand of miRNA genes have been identified and each miRNA may potentially target many different (ten to hundreds) mRNAs. miRNAs are particularly highly expressed in the brain and they are involved in brain development and function by controlling the temporal and spatial expression of target genes. Several intriguing studies have linked miRNAs as major regulators of the neuronal phenotype, and have implicated specific miRNAs in the regulation of synapse formation and plasticity. Dysfunction of miRNA pathway is also a potential important contributor to the pathogenesis of major neurodegenerative disorders such as Alzheimer's or Parkinson's diseases. Unfortunately, to date relatively little is known about the role of individual miRNAs in neural development and nervous system function. Therefore, the main aim of this work was to elucidate potential functions of brain enriched miRNAs (let-7, miR-125, miR-124 and miR-128) during neural development.

Functional assays were developed and used to compare the activities of four selected miRNAs: let-7, miR-125, miR-124 and miR-128 in embryomic stem (ES) cells, primary cortical neurons at stage E15 and E18 and in a neural stem cell line generated in the course of this thesis. Activity of let-7 and miR-125 was shown to start early in progenitor cell differentiation, suggesting a potential role of both miRNAs as inhibitors of ES cell self-renewal. miR-124 activity was observed in primary neurons at E15, consistent with a role in neuronal lineage determination. miR-128 was active after E15, suggesting a potential role during neuronal maturation.

As a starting point for the functional investigation of miR-124 and miR-128, gain of function experiments were performed *in vitro* and *in vivo*. miR-124 overexpression in NS cells undergoing astrocytic differentiation failed to adopt astrocytic morphology and showed certain characteristics of developing neurons. Ectopic overexpression of miR-124 was also performed in E12 cortical progenitors *in utero.* In this experiment, miR-124 expressing cells formed large aggregates and failed to distribute into the overlying cortical layers. Premature miR-128 expression in the E15 cortex resulted in aberrant migration, preventing migration into upper cortical layers in late embryonic development.

Summary

In order to identify functionally relevant genes as miRNA targets, an *in vitro* assay was established in Hek293 cells. GFP constructs bearing the 3'UTR of putative target genes were generated and co-transfected with appropriate miRNA mimics. With this assay, several predicted miRNA target genes could be confirmed. Moreover, two novel pluripotency genes, Lin-41 and Lin-28, were identified as let-7 and miR-125 targets.

Experiments with Lin-41 and Lin-28 revealed that both proteins act together in embryonic stem cells and inhibit the maturation and activity of let-7. In addition, let-7 and miR-125 competitive inhibition experiments were performed in neural stem cells. For this purpose miRNA sponge constructs, bearing up to 64 semi-complementary binding sites for a given miRNA were generated. Introduction of miR-125 or let-7 sponges in Lin-41⁻, Lin-28⁻ neural stem cells led to a de-repression of Lin-28 and Lin-41, resulting in posttranscriptional inhibition of let-7 and therefore a partial restoration of the pluripotent state. Taken together, these experiments defined previously unrecognized autoregulatory interactions among let-7, miR-125, Lin-28 and Lin-41 acting during stem cell commitment.

Zusammenfassung

MicroRNAs, eine Klasse nicht kodierender RNAs mit einer Länge von ca. 22 Nukleotiden, inhibieren die Translation von messenger-RNAs durch imperfekte Bindung an bestimmte Sequenzen in der 3'UTR ihrer Zielgene. Bis heute konnten tausende dieser regulatorischen miRNAs identifiziert werden. Jede dieser miRNAs besitzt potentiell die Möglichkeit, viele unterschiedliche (zehn bis hunderte) messenger-RNAs zu regulieren. Der Großteil aller miRNAs wird im zentralen Nervensystem (ZNS) exprimiert. miRNAs regulieren die Funktion und Entwicklung des ZNS durch räumliche und zeitliche Regulation ihrer Zielgene. Einige Studien haben miRNAs als Hauptregulatoren des neuronalen Phänotyps identifiziert, welche unter anderem die synaptische- und kortikale Plastizität regulieren. Die Pathogenese viele neuronaler Störungen, wie z.B. Alzheimer und Parkinson konnten mit funktionellen Störungen der miRNA-Biogenese in Verbindung gebracht werden.

Leider ist bis heute wenig über einzelne miRNAs und deren Einfluß auf die Neuralentwicklung und Funktion im ZNS bekannt. Deshalb war es ein Hauptziel dieser Arbeit, Funktionen der besonders stark im Gehirn angereicherter miRNAs (let-7, miR-125, miR-124 und miR-128) und deren Einfluß auf die Neuralentwicklung eingehender zu untersuchen. Hierzu wurde ein funktioneller Ansatz etabliert um die miRNA Aktivität von let-7, miR-125, miR-124 und miR-128 in embryonalen Stammzellen, in primären kortikalen Neuronenkulturen zweier Embryonalstadien E15 und E18 und in neuronalen Stammzellen zu bestimmen.

Die Aktivität von let-7 und mir-125 konnte bereits in neuronalen Vorläuferzellen nachgewiesen werden, was darauf hinweist, daß diese miRNAs die Selbsterneuerung embryonaler Stammzellen inhibiert. Die Aktivität von miR-124 konnte bereits in frühen kortikalen Neuronen im Entwicklungsstadium E15 nachgewiesen werden. miR-128 war dagegen erst in späten kortikalen Neuronen im Entwicklungsstadium E18 aktiv und könnte somit an der Hirnreifung beteiligt sein.

Für funktionelle Studien wurden gain-of-function Experimente von miR-124 und miR-128 sowohl *in vitro* als auch *in vivo* durchgeführt. Neuronale Vorläuferzellen, welche miR-124 ektopisch überexpremierten, waren nicht in der Lage in Astrocytendifferenzierungsmedium zu Astrozyten differenzierten und wiesen einen neuronalen Phänotyp auf. Überexpression von miR-124 wurde auch in kortikalen Vorläuferzellen von E12 Mausembryonen *in utero* überexprimiert. In diesem Experiment bildeten miR-124 überexprimierende Zellen große Zellanhäufungen welche nicht mehr in der Lage waren in den darüber liegenden Kortex zu immigrieren. Eine zu frühe Expression von miR-128 in E15 kortikalen Vorläuferzellen führte

dagegen zu einer anormalen Migration transfizierter Zellen innerhalb des Kortex, durch Verhinderung der Migration in darüber liegende kortikalen Schichten.

Um funktionell relevante Kandidaten-Gene als miRNA Zielgene zu identifizieren, wurde ein *in vitro* System in HEK293 Zellen etabliert. Hierzu wurden GFP Konstrukte, welche den 3'UTR möglicher miRNA Zielgene beinhalteten, generiert und mit entsprechenden miRNAs co-transfiziert. Mit Hilfe dieses Ansatzes konnten einige vorhergesagte Zielgene bestätigt werden. Zudem konnten zwei pluripotente Gene, Lin-41 und Lin-28 als let-7- und miR-125 Zielgene identifiziert werden. Weitergehende Untersuchungen von Lin-41 und Lin-28 konnten zeigen, daß beide Proteine zusammen die Reifung und Aktivität von let-7 in embryonalen Stammzellen verhindern und somit Rückkopplungskreis bilden.

Um miRNAs zu inhibieren, wurden miRNA "Schwamm"-Konstrukte, welche bis zu 64 halb-komplementäre Bindestellen für bestimmte miRNAs besitzen, generiert. Die Transfektion von Lin-28$^-$/Lin-41$^-$ neuronalen Stammzellen mit miR-125 oder let-7 Schwamm-Konstrukten führte zu einer de-Repression von Lin-28 und Lin-41 und somit zu einer post-transkriptionalen Inhibierung von let-7 und dadurch zu einer partiellen Restauration des pluripotenten Stadiums.

Zusammengefaßt zeigen diese Experimente eine zuvor nicht bekannte autoregulatorische Interaktion zwischen let-7, miR-125, Lin-28 und Lin-41, welche während des Stammzellstadiums aktiv ist.

1. Introduction

1.1 The discovery of miRNAs

The miRNA era began in 1980, when Horvitz and Sulston showed that the lin-4 (e912)- *C. elegans* mutant fails to stop molting at the normal time point and consequently undergoes additional larval stages (Horvitz and Sulston, 1980). In November 1993, the lab of Victor Ambros first published that lin-4 is a non-coding gene, which is upregulated during the late larval stage L1 and negatively regulates the protein coding gene lin-14 (Lee et al., 1993). Lin-4 encodes two small transcripts of 61 nt (lin-4L) and 21 nt (lin-4S) from which lin-4S shows high complementarity to different loci of the lin-14 3'UTR. One month later, Gary Ruvkun and co-workers showed the reciprocal, temporal expression of lin-14 and lin-5 from larval stage L1 to L4. They identified seven conserved elements in the 3'UTR of lin-14 which were complementary to lin-4 (Wightman et al., 1993). Seven years later, let-7, another miRNA, was found to regulate L4-adult transition in *C. elegans* by regulating multiple heterochronic genes such as lin-14, lin-28 and lin-41 (Reinhart et al., 2000). Let-7 has been found in ascidia, molluscs, annelida, arthrophodae, hemichordata and vertebrates (Pasquinelli et al., 2000). To date, thousands of miRNAs have been found and characterized in a wide range of animal species.

1.2 miRNA production and trafficking in vertebrates

miRNA processing begins in the nucleus, where the Microprocessor complex including the core-enzymes Drosha and DGRCR8, cleaves the primary miRNA transcripts at the base of the stem loop, releasing the 60-70 nt long precursor-miRNA (pre-miRNA). Precursor-miRNA is then actively exported to the cytoplasm via the Ran-GTP-dependent double-stranded RNA binding protein Exportin-5 (Bohnsack et al., 2004). In the cytoplasm, another RNase III endonuclease, Dicer, cleaves the double stranded pre-miRNA approximately 21-22 nt from the 3'-end, releasing an miRNA duplex of about 22 nt . One strand of the miRNA duplex is incorporated into the multi-protein **R**NA-**i**nduced **s**ilencing **c**omplex (RISC). RISC consists of a number of proteins, including the Argonaute protein family, which facilitates the association of the miRNA with its target gene. The following chapters elucidate the specific processing steps in detail.
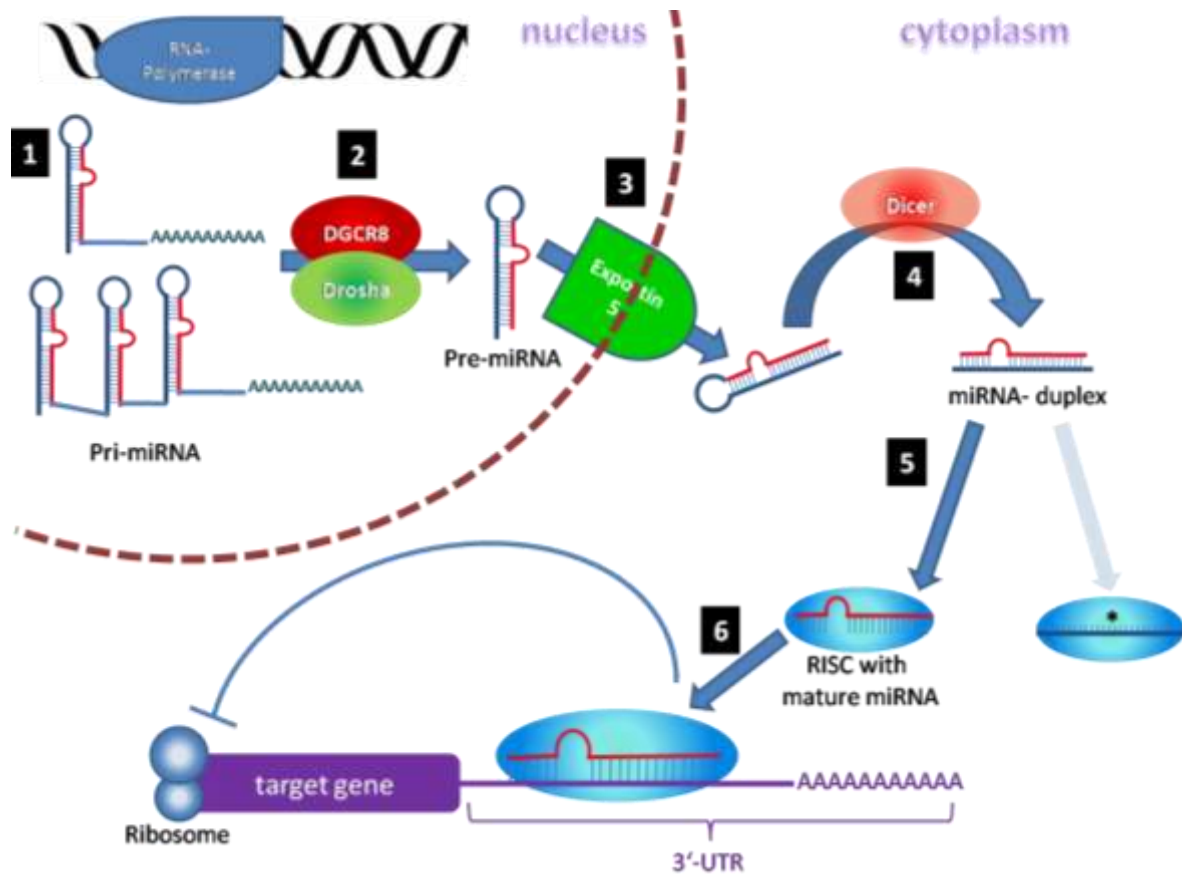
Figure 1.2: The miRNA pathway: an overview

1.2.1 miRNA transcription

The majority of miRNAs are located in intergenic regions and are transcribed by RNA-polymerase by their own promoters, while a subset of miRNAs is located within introns of protein coding genes. Most are found in sense orientation, suggesting that they are processed from the pre-mRNA transcripts. In *Drosophila melanogaster*, many miRNAs are located in polycistronic clusters, while in vertebrates the majority of miRNAs are monocistronic. miRNA processing occurs in two stages. First, the miRNA is transcribed by RNA-Polymerase II into an initial transcript which forms a large hairpin structure, termed primary miRNA (pri-miRNA) (Lee et al., 2002). The hairpin structure of the primary transcript can be subdivided into several specifiable sections: the single stranded basal segments, a ~11 nt long double stranded lower stem and a 22 nt upper stem, which contains the mature miRNA and a terminal loop (Figure 1.2.1).
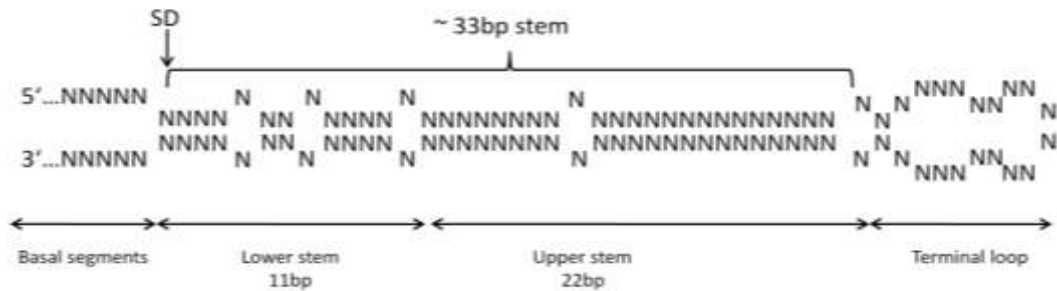
Figure 1.2.1: The average face of a pri-miRNA inferred from thermodynamic profiling.
A pri-miRNA can be divided into four parts: the basal segments, the lower stem, the upper stem and a terminal loop. The lower and upper stems together represent the 33bp long stem. The junction between the single stranded basal segment and the double stranded stem is referred to as the ssRNA-dsRNA junction (SD).

1.2.2 The Microprocessor complex

The pri-miRNA is processed by RNaseIII endonuclease Drosha (Lee et al., 2003) and the double-stranded-RNA-binding protein DGCR8, also known as Di George Syndrome Critical Region protein 8 (Denli et al., 2004). It has been shown that neither recombinant Drosha nor DGRC8 alone is able to crop the pri-miRNA but that a combination of both proteins restores this activity, indicating that both molecules are important in pri-miRNA processing (Gregory et al., 2004). Both proteins form a complex called the "Microprocessor", which crops the pri-miRNA and releases ~65 nt hairpin-shaped precursor miRNA (pre-mRNA).
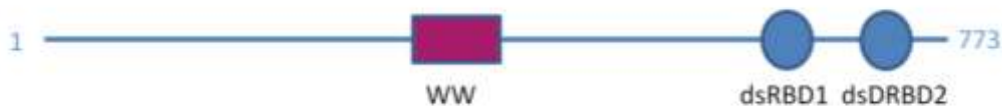
Figure 1.2.2a: Conserved protein domains of the double stranded RNA binding protein DGCR8:
WW-domain (two conserved tryptophan domains), dsRBD1+2 domain (double stranded RNA binding domains)

The mouse DGCR8 (Figure 1.2.2a) codes a protein of 773 aa that contains three highly conserved domains: WW, and two DRBD motifs. The WW domain, also called "two conserved tryptophan domain" consists of about 40 aa and functions as an interaction module in a diverse set of signalling proteins by binding proline-rich sequences. The double stranded RNA binding domains (DSRBD) bind double stranded RNA. However, the binding is not sequence-specific.

Figure 1.2.2b: Conserved protein domains of the ribonuclease III type Drosha: Proline- and serine-arginine-rich region, the RNAse III domains (RIIIDa and RIIIDb), and the double strand RNA binding domain (dsRBD).

Mouse Drosha (Figure 1.2.2b) is a 1303aa long protein with tandem RNase III domains (RIIIDs) and a double stranded RNA binding domain in the C-terminus. The N-terminus possesses a proline- and arginine-serine-rich region of unknown function. The two RIIIDs interact with each other to a constitute a processing center, at which two catalytic sites are placed 2nt away from where each RIIID cleaves one strand of the RNA duplex. The C-terminal RIIID (RIIIDb) cleaves the 5'-strand of the hairpin, while the N-terminal RIIID (RIIIDa) cleaves the 3'-strand, which creates a 2 nt overhang at the 3'end of its product.
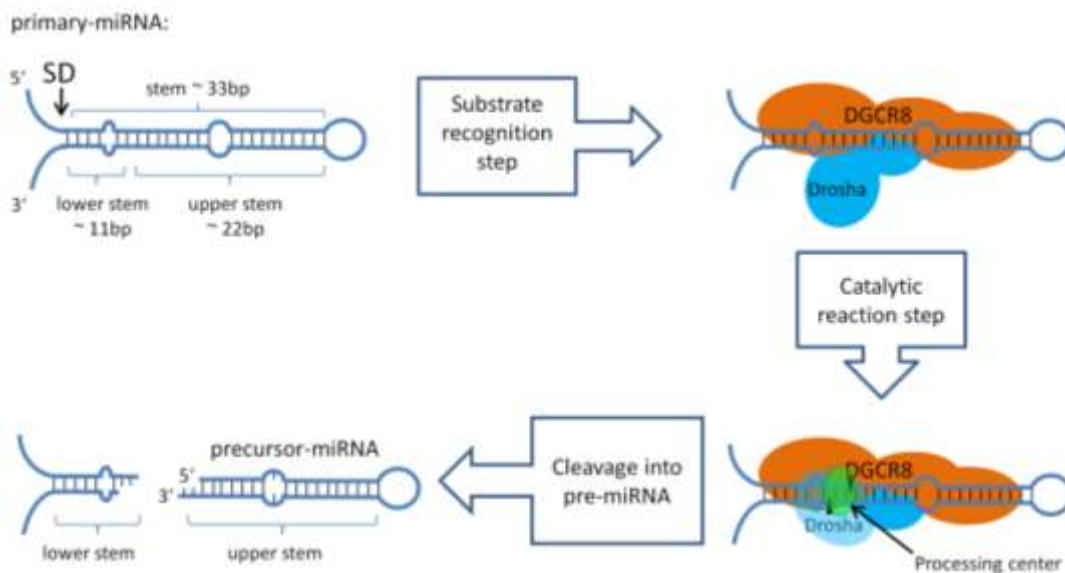
Figure 1.2.2c: A "ssRNA-dsRNA junction anchoring" model of the processing of pri-miRNA

The question arises how the Drosha-DGRC8-complex is able to cleave the many different kinds of pri-miRNAs into the correct precursor-miRNAs. Narry Kim and co-workers have shown that DRGC8 interacts preferentially and directly with pri-miRNAs by anchoring itself at the single-stranded-double-stranded junction (Figure 1.2.2c) Han et al., 2006). After this substrate recognition step, Drosha is recruited via WW-proline-rich mediated interaction and builds its processing center 11 bp upstream from the SD junction (Han et al., 2006) . After cleavage, the precursor-miRNA consisting of the 2 nt overhang at the 3'end, the ~22 bp upper stem and the terminal loop are released.

1.2.3 Nuclear export of precursor miRNA to the cytoplasm

After the Microprocessor complex has cropped the pre-miRNA into its precursor form, it is exported from the nucleus to the cytoplasm. Previous data has shown that exportin-5 (Exp-5) is involved in exporting tRNAs and VA1, a 160 nt non-coding RNA from adenovirus out of the nucleus. In the case of VA1, Exp-5 binding requires a terminal dsRNA of 14 bp and a 3' extension of 3 nt. As these structural determinants bear a striking similarity to pre-miRNAs, Rui Yi et al. investigated whether Exp-5 also mediates pre-miRNA export. Their results showed that Exp-5 is indeed the right pre-miRNA binding partner:

- siRNA targeting Exp-5 in T293 cells results in a decrease of exogenous miR-21 activity, a miRNA that is normally active in these cells.

- Overexpression of endogenous miR-30 in siExp-5 transfected T293 cells results in an increase of pre-miR-30 in the nucleus but less miR-30 in the cytoplasm.

Furthermore, Yan Zeng et al. determined the double stranded RNA motif that is necessary for pre-miRNAs to be bound by Exportin-5. They have shown that Exportin-5 binds preferably on double stranded RNA with a stem of 18-21 bp with a 3' overhang or blunt end at the stem. Exp-5 binding was significantly reduced using a modified pre-miR-30 containing either a truncated stem of 12 to 15 bp or a 5' overhang at the stem.

In vitro analysis showed that Exp-5 binds pre-miRNA in the presence of Ran-GTP while hydrolysis of Ran-GTP to Ran-GDP abolishes the binding of Exp-5. Ran-GTP is not distributed ubiquitously in the cell: transition of Ran-GTP to Ran-GDP and vice versa is regulated in the nucleus by **g**uanine nucleotide **e**xchange **f**actor (GEF), termed RCC1 (regulator of chromosome condensation 1) and in the cytoplasm, by the GTPase- activating protein RanGAP1 (Figure 1.2.3). Hydrolysis by RanGAP1 requires an additional factor, RanBP1, which possesses a RanGTP-binding domain (Richards et al., 1995). The asymmetric localization of these regulators creates a Ran-GTP gradient across the cell: the Ran-GTP level is higher in the nucleus because RCC1 is predominantly chromatin-bound while Ran-GAP and RanBP1 are distributed perinuclearly. In the nucleus, the chromatin-bound guanine nucleotide exchange factor RCC1 transforms Ran-GDP to its active form Ran-GTP. Ran-GTP activates Exportin-5 to bind double stranded precursor miRNA (Part 1 of Figure 1.2.3). In the cytoplasm, Ran-GTP is hydrolised by Ran-GAP/Ran-BP1 complex which induces the release of precursor miRNA by Exportin-5 (Part 2 of Figure 1.2.3).
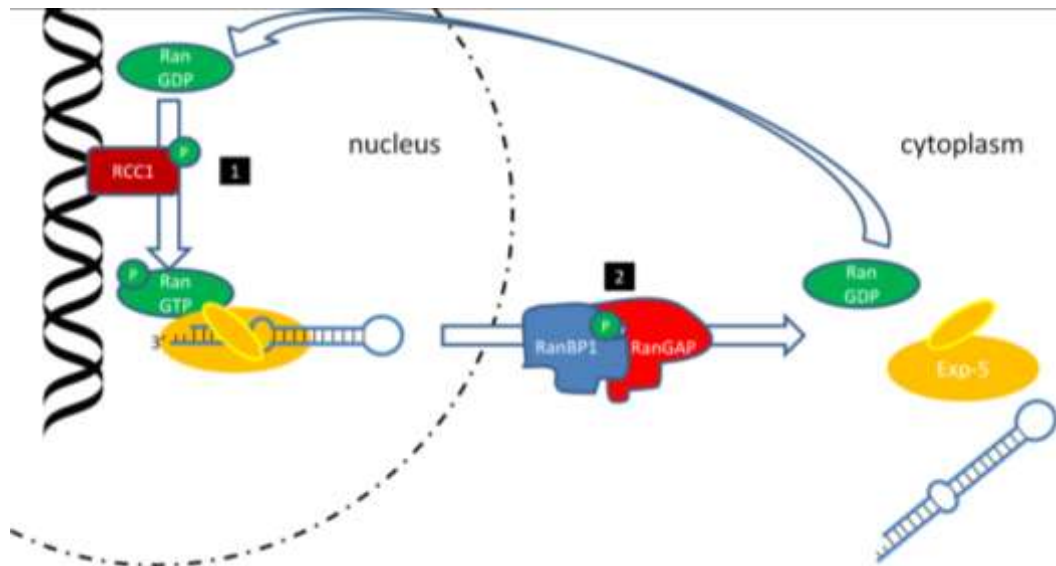
Figure 1.2.3: Precursor miRNAs are transported from the nucleus to the cytoplasm by the Ran-GTP-dependent ds RNA binding protein Exportin-5

1.2.4 Precursor miRNA processing

In the cytoplasm, the pre-miRNA processing complex cleaves the 70 bp pre-miRNA product generated by the Microprocessor complex into a miRNA duplex of ~ 21-23 bp. The Core-enzymes of pre-miRNA processing complex are the ribonuclease Dicer and the TAR RNA binding protein (TRBP).

Dicer is responsible for the generation of miRNA duplexes with a 5' phosphate, a 3' hydroxylated end and a 2-nt overhang. In mammals the presence of Dicer is essential, as Dicer-deficient mice die early at the embryonic stage. The mouse homolog of Dicer consists of several conserved domains: two RNaseIII domains at the C-term followed by a double stranded RNA binding domain, the N term includes a DEX/ATPase, RNA Helicase, the DUF283 domain and a PAZ domain (Figure 1.2.4a).
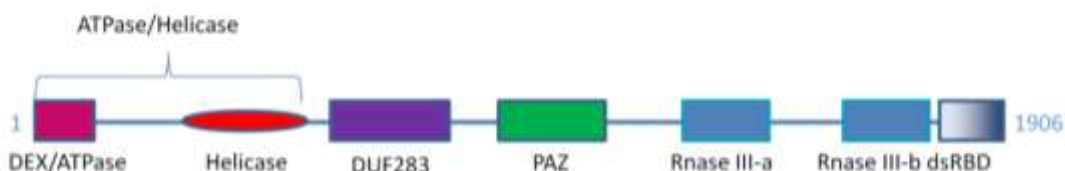
Figure 1.2.4a: Conserved protein domains of the ribonuclease III type Dicer: DEX/ATPase, RNA-helicase, the DUF283 domain, the PAZ domain, the RIIID a and b domains, the dsRBD (double stranded RNA binding domain)

As previously described above in the Drosha model, Dicer function is likely characterized by the intramolecular dimerization of its two RNAse II domains, assisted by the PAZ and dsRBD domains. The central PAZ domain specifically recognizes the 2-nt 3' overhang present in the pre-miRNA. The PAZ and the two RNAse III domains may act as a spacer in generating similarly sized double stranded miRNA.

In vitro studies have shown that while recombinant Dicer alone is able to cut the precursor miRNA into an 21-23 nt RNA duplex, it merges with TRBP during the miRNA precursor cleavage step. TRBP has been identified as a cellular factor acting in synergy with the viral TAT protein in the transactivation of the long terminal repeats (LTR) of HIV-1. It possesses two dsRBDs and is present in two isoforms (TRBP1 and TRBP2) (Figure 1.2.4b).
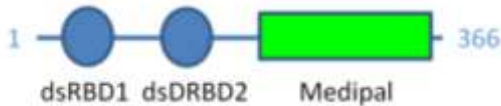
Figure 1.2.4b: Conserved protein domains of the TAR RNA binding protein (TRBP2): Double stranded RNA binding domains (dsRBD1+2) and the Medipal domain

TRBP knockout studies demonstrated that TRBP seems to facilitate, together with Dicer, RNA interference by shRNA and miRNA. TRBP was found to interact directly with Dicer by yeast two hybrid screens. The C-terminal part (aa 298-366) of the Medipal domain of TRBP (Figure 1.2.4b) interacts with a unique domain (aa 267-431) located between the ATPase and the Helicase motif of Dicer (Daniels et al., 2009).

1.2.5 The miRNA- containing ribonucleoprotein (miRNP) complex

Mature miRNAs are incorporated into the effector complex, which is known as the miRNP or miRISC (**mi**RNA-containing **R**NA-**i**nduced **s**ilencing **c**omplex). This mechanism uses small double stranded RNA, named small interfering RNA (siRNA) and miRNA schematically displayed in figure 1.2.5.
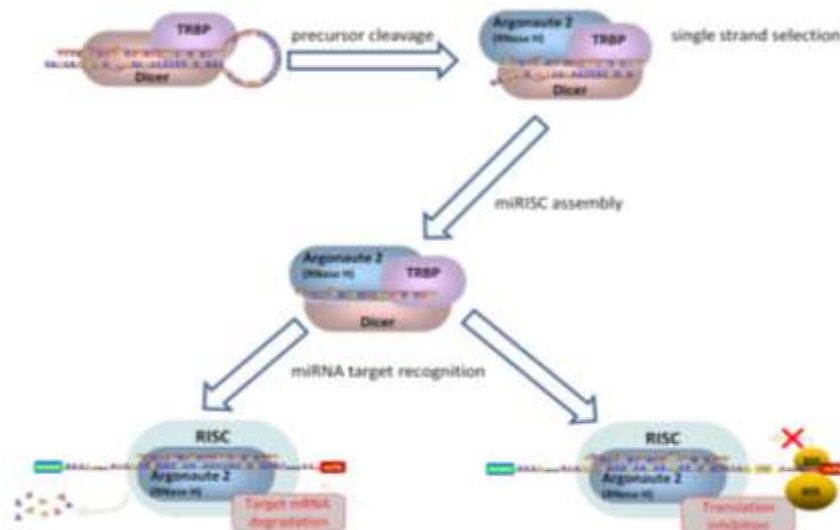
Figure 1.2.5: Formation of the miRNA-containing RNA-induced silencing complex (adapted from scienceslices)

The human RNA induced silencing complex is composed of at least three different core proteins: Dicer, TRBP and Argonaute2 (Ago2). Within the RNA induced silencing complex, TRBP loads the dsRNA and recruits Dicer to Ago2 (Chendrimada et al., 2005). After the dsRNA is asymmetrically unwound one of both strands retained for binding to partially

complementary sequences within the 3'UTR of the target mRNA (Diederichs and Haber, 2007; Gregory et al., 2005; Maniataki and Mourelatos, 2005). miRISC-bound mRNA transcripts are subject to several alternative fates, including translational suppression, destabilization by deadenylation or degradation by Ago2 RNase activity (Doench et al., 2003) (Chendrimada et al., 2005). The core components of the miRISC are Argonaute (Ago) family proteins. In addition, a number of Ago-associated proteins have been identified, including RNA-binding proteins and ribonucleases (Omarov et al., 2007; Pham et al., 2004).

Figure 1.2.5: Conserved protein domains of the mouse Argonaute2 protein (Ago2): the PAZ, the MC and the PIWI domain.

Ago2, the so-called Slicer RNAse in the RNAi pathway, has cleavage activity and degrades target mRNAs that are complementary to the guiding siRNAs. If the miRISC/mRNA complex is partial complementary, Ago2 fails to cleave, but inhibits translation of the target mRNA (Chendrimada et al., 2005; Kiriakidou et al., 2007; Li et al., 2008). The PAZ domain interferes with the 3' overhangs of dsRNAs (Song et al., 2003). The PIWI domain of Ago2 shows similarity to the RNase H domain and facilitates interaction with TRBP2 and Dicer during RISC assembly (Choudhary et al., 2007; Liu et al., 2004; Ma et al., 2005).

Other mammalian Ago proteins are also part of miRNA effector complexes that mediate translational inhibition of target mRNAs (Diederichs and Haber, 2007; Iwasaki et al., 2009; Miyoshi et al., 2005).

Another member of the complex is fragile X mental retardation protein (FMRP). FMRP is an RNA-binding protein with an RGG box that binds to G-quartet stem loops of mRNAs that are known to be involved in the regulation of mRNA translation (Darnell et al., 2001; Darnell et al., 2004). Studies from Provost and co-workers demonstrated that FMRP can act as a miRNA acceptor protein for the ribonuclease Dicer and facilitate the assembly of miRNAs on specific target RNA sequences (Plante et al., 2006). Phosphorylation of FMRP disrupts this assembly, leading to an increase of pre-miRNA *in vivo* (Cheever and Ceman, 2009). Recently, it was demonstrated that human FMRP can act as a miRNA acceptor protein for Dicer and facilitates assembly of miRNAs on specific target RNA sequences (Plante et al., 2006). Recently, a link between miRNA-RNP and P-bodies has been described (Jabri, 2005; Liu et al., 2005b).

1.2.6 P-bodies

P-bodies are large cytoplasmatic foci that are involved in the post-transcriptional regulation of gene expression (Sheth and Parker, 2003). Recent studies have revealed that P-bodies containing untranslated mRNAs and serve as foci of mRNA degradation. P-bodies consist of a large number of proteins that are involved in mRNA silencing, including the Ago protein family (Liu et al., 2005b; Zhou et al., 2009), mRNA decapping enzymes and their activators as well as enzymes required for deadenylation. The P-body protein GW182 is one of the core mediators for miRNA-mediated gene silencing and direct interacts with Ago2 (Lian et al., 2009; Liu et al., 2005a). GW182 is involved in both, decapping and deadenylation of mRNAs (Behm-Ansmant et al., 2006a; Rehwinkel et al., 2005). The P-body mRNA decapping machinery includes the decapping enzymes Dcp1p/ Dcp2p and decapping activators like Dhh1p, Rbp1p and RAP55/Scd6p (Brengues and Parker, 2007; Ingelfinger et al., 2002; Jang et al., 2006). Proteins that are involved in deadenylation like poly(A) binding protein 1 (Pab1p), CAF1 and CCR4 are enriched in P-bodies (Brengues and Parker, 2007; Tucker et al., 2001). The mechanisms by which miRNA regulate their target gene expression are elucidated in the following paragraph.

1.3 Regulation of gene expression by miRNAs

The effects of miRNAs on target genes have been contradictory. Several studies report mRNA degradation as an important aspect of miRNA–mediated repression of gene expression either by decapping or deadenylation (Hausser et al., 2009; Rehwinkel et al., 2005; Yu et al., 2005). In contrast to these studies several publications have shown that in many cases miRNAs do not promote degradation of their targets but inhibit the translation step by preventing the initation or elongation step of translation (Mathonnet et al., 2007; Pillai et al., 2004). Other studies report that miRNAs inhibit their target gene expression on both levels.
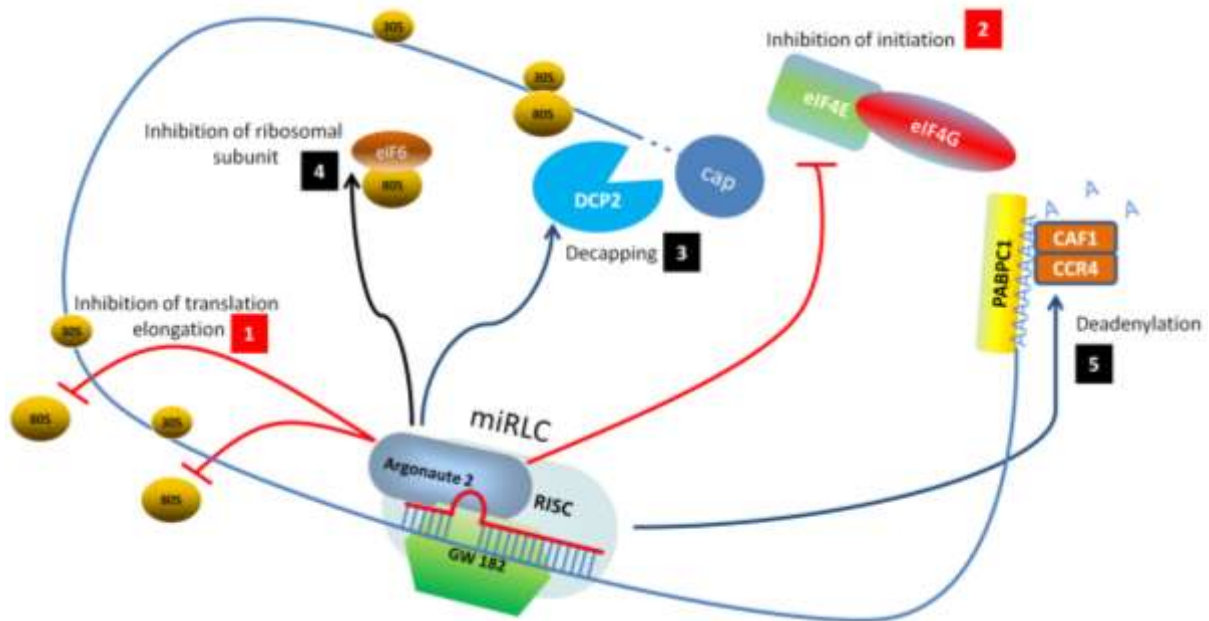
Figure 1.3: Several options for an miRNA to regulate the translation of its target genes. For a more detailed explanation please refer the part 1.3.1 to 1.3.3.

1.3.1 miRNAs may interfere with the initiation step of translation

The observation that the presence of miRNAs shifts the target mRNAs from active polysomes to lighter sucrose gradient fractions containing translationally inactive mRNA ribonucleoprotein particles (No.1 of Figure 1.3) suggests they are involved in the initiation step of translation (Pillai et al., 2004). Recent publications (Kiriakidou et al., 2007; Mathonnet et al., 2007) have emphasized that Ago proteins may compete with eIF4E in binding to the mRNAs 5' cap structure or that Ago proteins may directly recruit the translational repressor eIF6 on target mRNAs (No.2 of Figure 1.3) (Chendrimada et al., 2007; Wang et al., 2009).

1.3.2 miRNAs may inhibit post-initiation steps of translation

The first evidence for miRNA mediated repression at the post-initiation step of translation was based on studies of the lin-4 mediated repression of *lin-14* in *C. Elegans*. A significant percentage of *lin-14* mRNA was found to be associated with polyribosomes (Olsen and Ambros, 1999). A similar result was reached in the analysis of the lin-4 target gene *lin-28* (Seggerson et al., 2002), proposing translational arrest of elongation (No.4 of Figure 1.3). miRNAs and miRNPs were shown to be associated with polyribosomes in vertebrates (Krichevsky et al., 2003). Another study examined gene regulation by the 3′ UTR of the *C. Elegans* gene *lin-41* in Hela cells. In this study let-7 and its target mRNAs were associated with actively translating polysomes as determined by sucrose sedimentation profiles, suggesting that that let-7 miRNP complex interferes with the accumulation of growing polypeptides (Nottrott et al., 2006). Further evidence supporting translational inhibition after initiation was the fact that miRNA-mediated silencing occurs in the presence of an internal

ribosome-binding site (IRES), thus bypassing the requirement for the cap (Petersen et al., 2006).

1.3.3 miRNAs can promote target mRNA degradation

Microarray profiling of mRNAs showed that ectopic overexpression of lineage specific miRNA decreases the abundance of specific subsets of mRNAs (Liu et al., 2007; Yan et al., 2007). The hypothesis that miRNAs could regulate target mRNAs expression by affecting their stability, mRNA either by decapping or deadenylation (No.3 and 5 of Figure 1.3) has been reported by several groups (Fabian et al., 2009; Ronemus et al., 2006; Wu et al., 2006; Zekri et al., 2009). miRNA-mediated acceleration of target mRNA degradation through the normal pathway of deadenylation has been recently reported (Eulalio et al., 2009; Fabian et al., 2009). miRNPs recruit PABP, NOT1 and CAF1 leading to deadenylation, followed by decapping and subsequent degradation of the mRNA by 5'→ 3' exonuclease activity (No.5 of Figure 1.3) (Eulalio et al., 2009) (Fabian et al., 2009). Several protein complexes were identified for miRNA induced decapping such as the DCP1/DCP2 decapping complex and their activator HPat (No.3 of Figure 1.3) (Behm-Ansmant et al., 2006a; Jager and Dorner, 2010; Rehwinkel et al., 2005). Other studies demonstrated that the miRNA-mediated silencing of mRNA targets may occur by inducing their relocation to P-bodies (Behm-Ansmant et al., 2006b; Bhattacharyya et al., 2006; Hillebrand et al., 2007).

1.4 Prediction of miRNA targets

To determinate if given gene is a target of miRNAs, individual gene sequences (i.e. 3′-UTR mRNA sequences) have to be analyzed by various computational algorithms that utilize distinct parameters to predict the probability of a functional miRNA binding site within a given mRNA target. The first miRNA target predictions were based on a very limited set of experimentally identified possible target sites for a few miRNAs in *Drosophila* and *C. elegans*. To date, several computational methods have been employed in the prediction of target genes for invertebrate and vertebrate miRNA. Figure 1.4 shows two different classes of miRNA target sequences and exemplifies the current major problem of accurate target gene predictions.
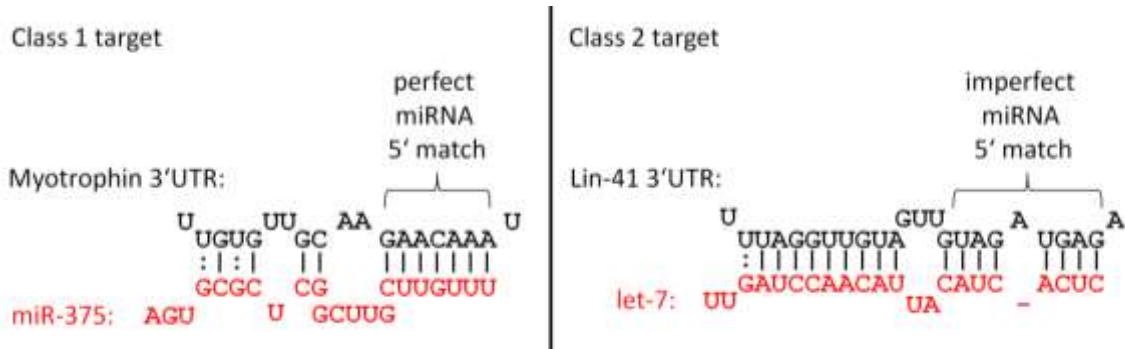
Figure 1.4: Two classes of validated miRNA target sequences in C. elegans. (Adopted from Rajewsky, 2006) Standard base pairing is indicated with (|), G:U pairs with (:).

Class 1 targets have perfect complementary base pairings between the 5'-end (6-8 bp) of the miRNA and the 3'UTR of the target sites (seed), but insignificant complementarity to the rest of the miRNA, whereas Class 2 targets have significant complementarity between the miRNA and the targets, but show an imperfect complementarity in the seed region. The multitude of possible conformations of miRNA-mRNA duplexes makes it difficult to trace miRNA binding sites within 3'UTRs of target genes. Therefore computational methods for identifying common targets use additional criteria such as the thermal stability of the miRNA-mRNA duplexes, presence of multiple target sites in the same gene, and their target site conservation across species. The miRNA target prediction programs that were used are described in Table 1.4.

Table 1.4: miRNA- target gene prediction algorithms that have been used to validate miRNA regulated target genes

prediction algorithm	Main-parameters of miRNA target site recognition	Reference
PicTar	- Perfect matches between the mRNA and the 5' seed region of the miRNA - Required target conservation across several species - Biased toward perfect seed region complementarity	(Krek et al., 2005)
TargetScan	- Perfect matches between the mRNA and the 5' seed region of the miRNA with extension of matches as far as possible, allowing G:U wobble pairing - Optimize base pairing of the remaining sequence using RNAfold to calculate the thermodynamic free energy of bindings	(Lewis et al., 2005) (Grimson et al., 2007)
MicroInspector	- Scans any given RNA sequence for at least 4 to 6 Watson-Crick base pairs and 2 to 0 G:U base pairs between the mRNA and the 5' seed region of the miRNA (nt 1-6 or nt 2-7)	(Rusinov et al., 2005)

	- The sequence upstream to the seed region is subjected to a pair-wise hybridization folding algorithm - Calculates free energy of miRNA-RNA duplexes	

The table shows that these miRNA prediction algorithms are potentially able to detect Class 1 target genes, but not Class 2 target genes. This is because they all scan for miRNA seed regions. While PicTar and TargetScan are online databases that provide details of 3' UTR alignments with predicted sites, MicroInspector analyses whether, in a given mRNA sequence a binding site can be found for any miRNA that is available in the database. Even though the main parameters chosen to detect miRNA binding sites, are quite similar for each algorithm, they differ considerable in their miRNA target gene predictions. These differences are caused by different shifts of these parameters the single algorithms they are assigned too. It is important to reiterate that multiple algorithms are utilized since these programs will often predict distinct miRNA binding sites. For example, when the mouse Lin-28 homolog was analyzed for putative miRNA binding sites, PicTar predicted 18 miRNA binding sites within the Lin-28 3′-UTR. TargetScan predicted that over 41 miRNA binding sites were harboured within the 3'UTR. In this case, 16 of the predicted miRNA binding sites overlap in these two bioinformatic algorithms. However, PicTar predicted two and TargetScan 25 additional miRNA binding sites. Therefore, it is very important to validate miRNA target genes.

The magnitude of miRNA-mediated target gene repression depends on several factors. Beside the expression level of miRNAs, several studies showed that the length of the targeted 3'UTR, number of binding sites and the distance between them influence the repression of the target gene.

A study from Hon and Zang reveals following correlations:
- shorter 3' UTRs of target genes are more strongly repressed by their predicted cognate miRNAs
- target genes with more binding sites are more strongly repressed
- pairs of binding sites targeted by the same miRNA that are between 16 and 30 bp apart have   significantly increased repression
- 3'UTRs with multiple pairs of extensively overlapping sites, whose start positions are within 10 bp of each other, have increased repression

These correlations seem to be of biological importance for fine-tuning repression of target genes, since a lot of binding sites, their number and arrangement within the 3'UTR are conserved among species.

1.5 miRNA target validation

Validation of miRNA targets is one of the major goals in miRNA research. Therefore several strategies have been established such as GFP or Luciferase based reporter gene constructs (Krek et al., 2005; Lewis et al., 2003) and mutation studies (Brennecke et al., 2005). Luciferase or GFP reporter gene constructs are usually generated by insertion of the whole or partial 3'UTR sequence of a predicted miRNA regulated target gene into the 3'UTR of the Luciferase or GFP gene (Lin et al., 2003). Next, the reporter gene construct can be co-transfected with miRNA-mimics to check if the reporter is repressed in the presence of the predicted miRNA. However repression of the reporter gene by a predicted miRNA does not answer the question how many binding sites are present in 3'UTR of target gene. In order to identify single binding sites, the seed regions of the predicted binding sites have to be mutagenized. A de-repression of the mutagenized reporter gene due to co-transfection with predicted miRNA-mimics reveals the biological relevance of the predicted miRNA binding sites. The procedure to identify single miRNA binding sites using GFP-reporter constructs is schematically shown in Figure 1.5.

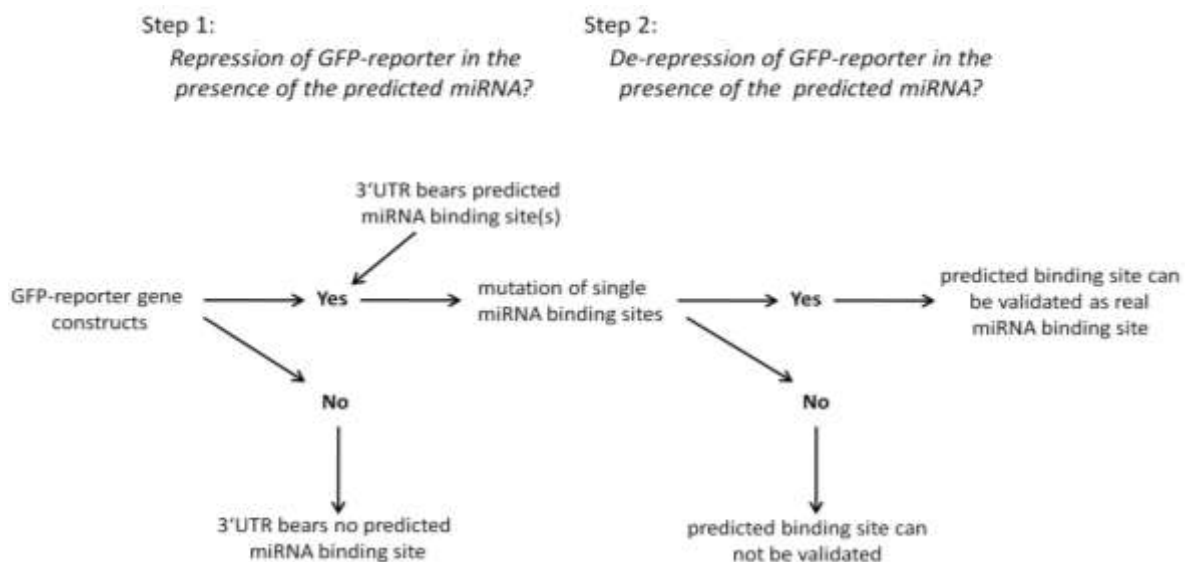**Figure 1.5: Procedure to detect miRNA binding sites in 3'UTRs of target genes using a GFP based reporter gene construct**

1.6 miRNA function

The discovery of large numbers of miRNAs following progress in experimental approaches reveals that miRNAs are involved in a multitude of cellular processes. The first miRNAs described, lin-4 (homolog of vertebrate miR-125) and let-7 are important temporal regulators

at the larval to adult transition in *C. Elegans* which indicated a role for miRNAs in animal development. Northern blot and *in situ* hybridization analyses show that miRNAs are very often temporal and tissue specific expressed. Other studies have pointed out the role of miRNAs during cell differentiation and specification by the suppression of alternative lineages. miRNA expression is highly enriched in CNS and distinct expression profiles are seen in germ cells, embryonic stem cells and in the developing brain. Since this thesis is concerned with miRNA function during stem cell commitment and neural development, these points are further characterized in the following sections.

1.6.1 miRNAs and stem cell function

Stem cells are characterized by self-renewal and pluripotency. The mechanisms by which stem cells maintain these remarkable dual properties are still unclear. Recent studies indicate that the expression profile of miRNAs in stem cells is different from other tissues and suggest that miRNAs may play an essential role in stem cell self-renewal and differentiation. Several stem cell specific miRNAs have been identified in vertebrates. In the mouse, six stem cell-specific miRNAs (miR-290-295) are arranged in a polycistronic cluster. In human stem cells, similar miRNAs clusters could be identified. One cluster contains eight miRNA genes (miR-302b*, miR-302b, miR-302c, miR-302c*, miR-302a, miR-302a*, miR-302d, miR-367), while the other cluster contains four different miRNAs (miR-371, miR-372, miR-373, miR-373*).

Since Dicer is essential for the biogenesis of miRNAs, Dicer knockout studies gave new insights into miRNA function. Loss of Dicer activity in embryonic stem cells causes proliferation defects, indicating that miRNAs regulate stem cell division. In addition, disruption of the miRNA pathway by the removal of Dicer from mouse ES cells results in a failure to differentiate, even though ES cell markers continue to be expressed (Kanellopoulou et al., 2005). Dicer knock-out in mouse is lethal at early E7.5 stage, with complete loss of pluripotent cells. Lack of *Dicer-1* in ovarian germline stem cells (GMCs) of *Drosophila* leads to a delayed transition from G1 to S phase during cell cycle, and therefore to a reduction of cell division. In adults, ovarian GMCs deficient in Dicer-1 fail to be maintained in the GSC niche, revealing a role of embryonic stem cell-specific miRNAs in stem cell commitment. miRNAs are also involved in regulating stem cells differentiation, cell lineage differentiation and development (Giraldez et al., 2005; Kanellopoulou et al., 2005; Smirnova et al., 2005).

1.6.2 miRNAs in the nervous system

miRNA expression is highly enriched in the nervous system. Approximately 70% of experimentally detectable miRNAs are expressed in the brain. Its development and function

requires precise temporal and spatial control of gene expression at transcriptional and translational level. Not surprisingly, the miRNA expression levels change dramatically upon neural differentiation (Gangaraju and Lin, 2009; Miska et al., 2004; Smirnova et al., 2005). It has been show by *in vitro* experiments that in retinoic acid (RA) treated EC (embryonic carcinoma) cells numerous brain-specific, brain enriched and few non-brain specific miRNAs are induced (Sempere et al., 2004), while for example miR-17, which blocks neural differentiation is repressed by RA (Beveridge et al., 2009).

Different Cre-loxP-Dicer mutants have been generated in mice. Some of these generated conditional knock-out mice lack Dicer expression at different stages in distinct areas of the developing brain. Table 1.6.2 presents two strains which lack Dicer expression and therefore show reduced miRNA expression at different time points and brain areas.

Table 1.6.2a: Depletion of miRNA expression in the mouse brain due to study of conditional Dicer knock-out in the developing mouse brain

	Foxg1-Cre;DicerloxP/loxP	Rag1AG-Cre (a-CamKII Promoter); DicerloxP/loxP
Time/location of Dicer loss	From E9.5 in the dorsal telencephalon	From E15.5 in cortex and hippocampus
Time of miRNA reduction	E10.5	n.a. but for miR132 14%–20% reduction at P15
Lethal at stage	Death by P1	homozygotes die postnaly (40% at P2, 100% at P20)
Abnormalities	small forebrain; widespread apoptosis by E14,5; decreased proliferation in the ventricular zone leads to reduced cortical thickness -> distinct cortical layers fail to form	small forebrain; enlarged lateral ventricles and smaller cortex; apoptotic cells near the VZ at P0, decreased dendritic branching
Reference	De Pietri Tonelli 2008	Davis 2008

Table 1.6.2a emphasize the importance of miRNA function in the developing brain. Not surprisingly, the loss of Dicer at E10.5 has a more dramatic phenotype compared to mice lacking Dicer at E15.5. A lot of effort was made to identify miRNAs that play a decisive role in the development of the nervous system. It has been found that loss of the let-7 target gene, mouse Lin-41, causes neural tube defects, indicating a role for let-7 in neural tube closure in mouse (Maller Schulman et al., 2008). Additional examples are listed in Table 1.6.2b.

Table 1.6.2b: miRNAs in brain development

miRNA	Function	Specifity	Reference
miR-9	promotes NPC differentiation in mouse cortex	brain specific and neural related	Conaco 2006, Miska 2004, Zhao 2009
miR-124	promotes neuronal transcriptome/ neurogenesis	brain specific and neural related	Conaco 2006
miR-125	NMDA receptor subunit NR2A which is essential for synaptic plasticity	brain enriched	Edbauer 2010
miR-128	synaptogenesis	brain enriched, lineage specific to neurons	Smirnova 2005
miR-23	regulates oligodendrocyte development and myelination	brain enriched, lineage specific to astrocytes	Lagos-Qintana 2002 Smirnova 2005 Lin 2009
miR-134	controls dendritic spine development which is essential for synaptic plasticity	brain specific	Schratt 2006, Rowan 2006

The table shows miRNAs that are enriched or specifically expressed in the brain. For example, miR-9 promotes differentiation of neural progenitor cells, which leads to the conclusion that this miRNA inhibits the translation of neural stem cell specific genes. Indeed miR-9 suppresses TLX expression in neural stem cells, an essential regulator of neural stem cell self-renewal (Zhao et al., 2009). Other miRNAs, like miR-124 and miR-128, are restricted to neurons, while miR-23 is related to astrocytes (Conaco et al., 2006; Maiorano and Mallamaci, 2009; Makeyev et al., 2007; Smirnova et al., 2005). miR-125 and miR-134 are important regulators for synaptic plasticity. In hippocampal neurons, the NMDA receptor (NMDAR) subunit NR2A expression is negatively regulated by miR-125 (Edbauer et al., 2010). NMDAR, a glutamate receptor, is the predominant molecular device for controlling synaptic plasticity and memory function. miR-134 negatively regulates Limk1, a protein kinase, that controls spine development in rat hippocampal neurons.

Several *in vivo* experiments were performed for this thesis in order to elucidate miRNA functions during neurogenesis. Therefore miRNAs or their target genes were over expressed in the neural tube *in ovo* and in the brain *in utero*. The last two Chapters concern with the development of the neural tube and the development of the brain.

1.7 Development of the neural tube

The differentiated cell types that comprise the vertebrate CNS are generated during embryonic development. In a first step, primary neurulation occurs in response to soluble growth factors secreted by the notochord. Ectodermal cells are induced to form the neuroectoderm (also called the neural plate) (Figure 1.7a).
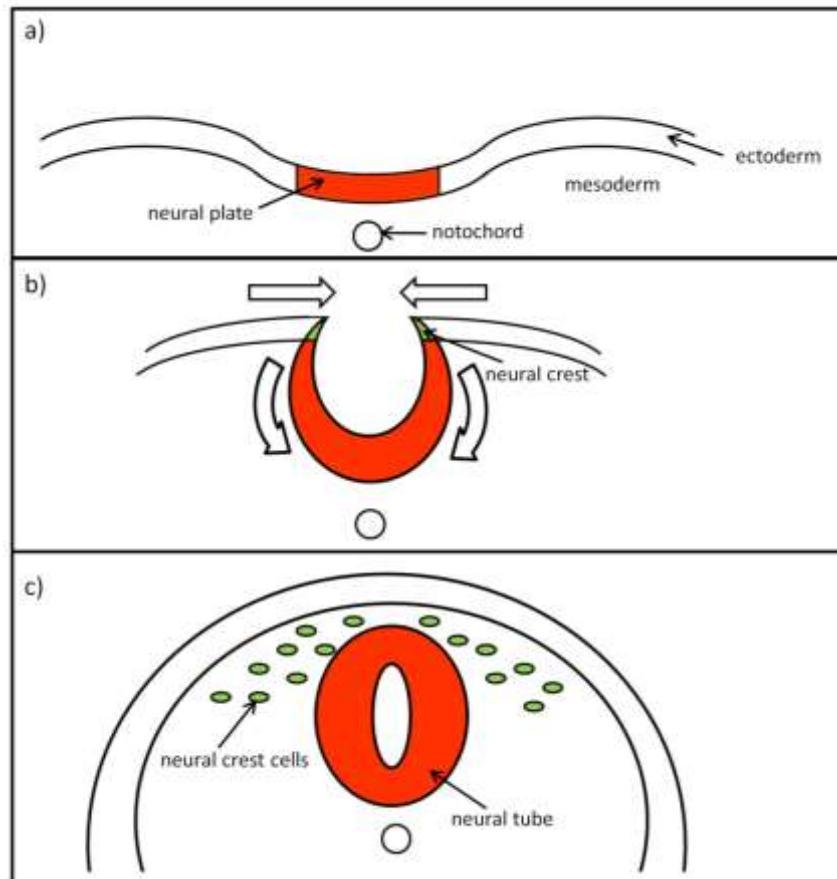
Figure 1.7a: Schematic transverse sections that show the progression of the neural plate to the neural tube from top to bottom For a detailed explanation please refer to text.

The rapid growth of these cells leads to an invagination of the neural plate resulting in the neural fold. Neural crest cells, shown in green, differentiate from the neural fold at both ends. Variable allocations of a number of cell adhesion molecules between the neural crest and the neural fold result in a fusion at the midline, detachment from the epidermis and release of the neural crest cells (Figure 1.7a).
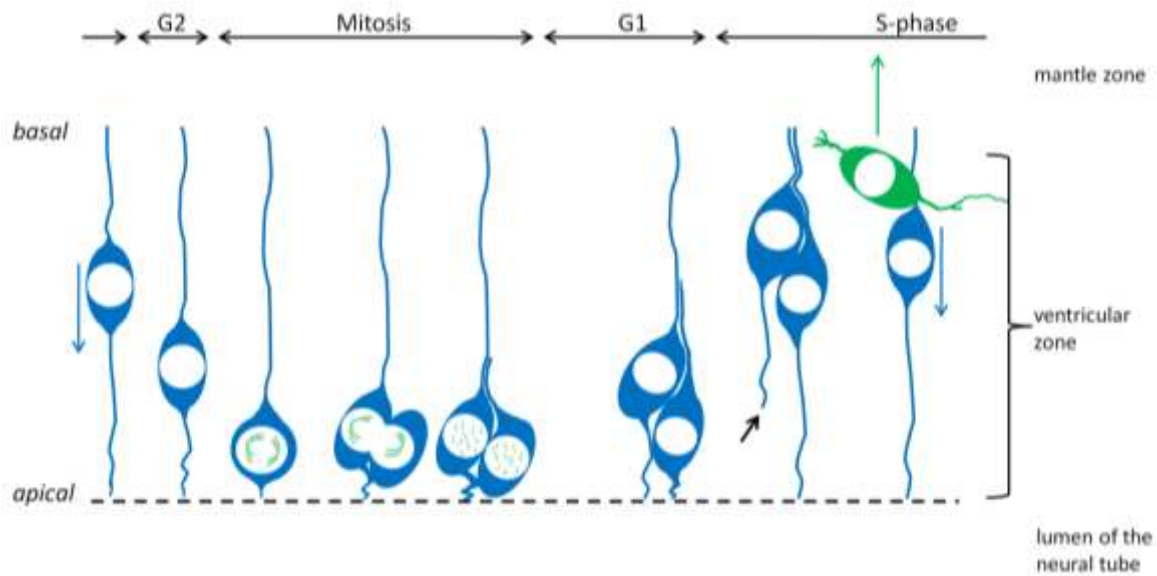
Figure 1.7 b: Illustration of an asymmetrically dividing multipotent neural stem cell in the ventricular zone of the neural tube For a detailed explanation please refer to text.

Within the neural tube, the processes of a neural stem cell (NSC) span the ventricular zone from the apical lumen to the basal marginal zone. During the late S-phase and G2-phase the soma of the neural stem cell moves apical towards the lumen of the neural tube. After mitosis and cell division in the apical layer of the ventricular zone, one daughter cell maintains the radial processes of the mother cell whereas the other daughter cell generates new outgrowths. Asymmetry of neuroepithelial cells is attributed to asymmetric inheritance of apical determinants (black arrow) (Nagele et al., 1987). The daughter cell destined to become a neuroblast migrates into the marginal layer of the neural tube (green cell), while the other remains a dividing neural stem cell.

In addition to this classical view of cell fate decisions in the neural tube, fate mapping using live imaging has revealed alternate pathways. A schematic view of the results reported by Wilcox is presented in Figure 1.7c.
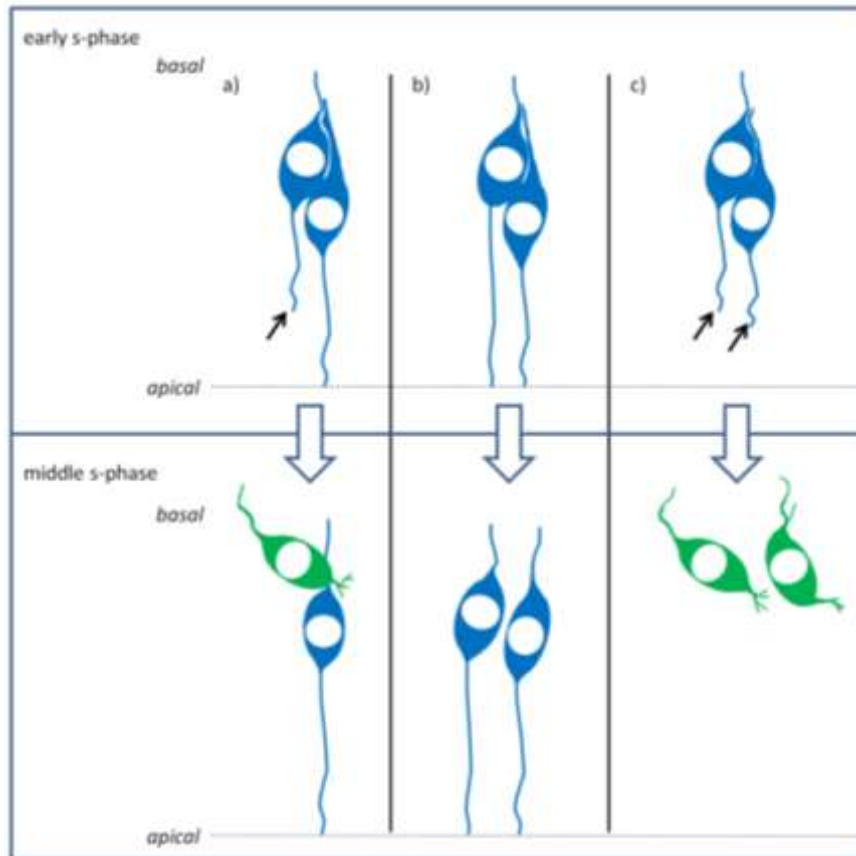
Figure 1.7c: Cell fate of neural stem daughter cells after cell division in the early s-phase (upper row) and middle s-phase (lower row) of the neural tube a) asymmetric neuroblast production b) symmetric neural stem cell renewal c) symmetric neuroblast production. Multipotent neural stem cells are shown in blue, neuroblasts highlighted in green. For a detailed explanation please refer to text below.

In addition to symmetrical proliferative divisions generating two progenitor cells, in some cases symmetric division results in generation of two neuroblasts.

In addition to these different cell fates of dividing neural stem cells within the ventricular zone, the patterning of the developing spinal cord is characterized by variable signals. These signals include homeodomain transcription factors that are variably secreted from dorsal lying cells of the roof plate and ventral lying cells of the floor plate (Figure 1.7d). Depending on their spatial concentration, these transcription factors divide the neural tube into different regions along the dorso-ventral axis and thereby specify neural subtype identity for distinct zones. The main subtypes that arise during development of the neural tube are shown in the following Figure 1.7c.
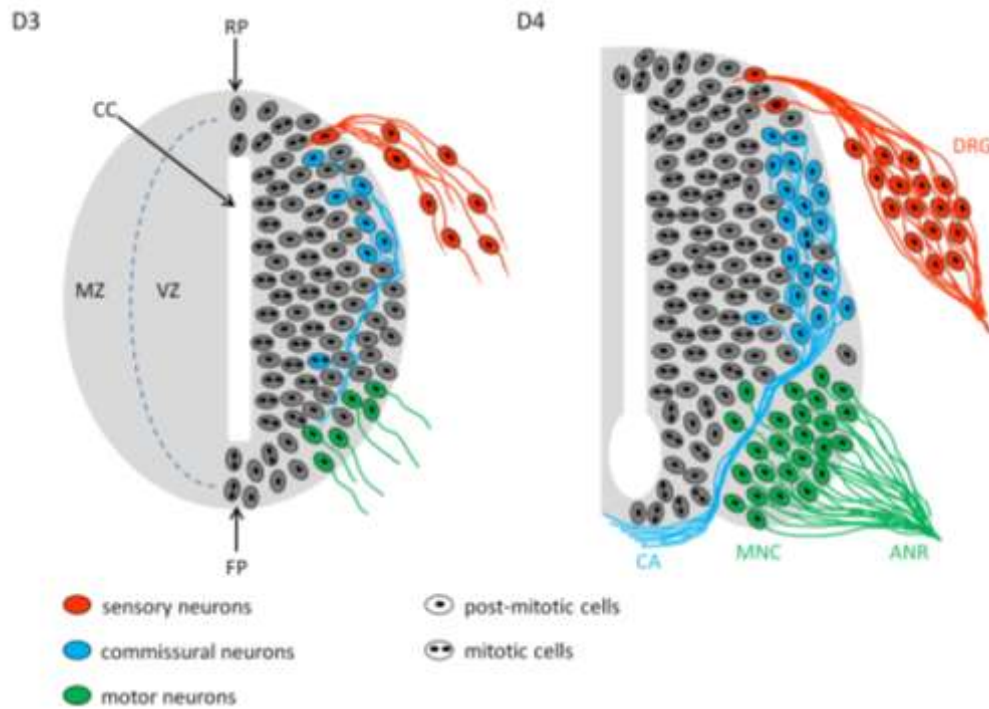
Figure 1.7d: Schematic horizontal sections of the neural tube of a day 3 and 4 chick embryo VZ: ventricular zone, MZ: mantle zone, CC: central canal, RP: roof plate, FP: floor plate, DRG: dorsal root ganglion, MNC: motor neural column, ANR: anterior neural root, CA: commissural axons. For a detailed explanation please refer to text.

In the embryonic chicken at day 3, the first post-mitotic neuroblasts migrate from the ventricular zone into the mantle layer of the growing neural tube. At this time point the first motor neurons (green cells), neurons that form commissural axons (blue cells), and the first sensory neurons (red cells) appear. 24 hours later, the nuclei of the sensory neurons are arranged in a complex called the dorsal root ganglion (DRG). The cell bodies of the motor neurons (green cells) migrate to the ventral outer area of the neural tube. Their axons bundle together into the anterior neural root (ANR) and grow out to innervate the developing muscle cells.

1.8 Development of the mouse brain: a short introduction

The development of the neural tube before encephalization is previously described in Chapter 1.7. At the posterior part of the neural tube the cranial canal swells to form three bulges that are the precursor structures of the forebrain, midbrain and hindbrain. In the next step the forebrain divides into two vesicles: the telencephalon which will form the neocortex and basal ganglia and the diencephalon which will form the thalamus and hypothalamus. The hindbrain splits into the metencephalon and the myelencephalon. Each of these vesicles contain proliferative zones. Around E12 the two lateral ventricles (Lv 1 an Lv 2), the third and the fourth ventricles are formed. Each lateral ventricle is connected to the third ventricle,

which in turn passes into the fourth ventricle. The narrow layer surrounding these ventricles is termed the ventricular zone where neuroblasts and glia cells are generated.

Early in development, neuroepithelial stem cells reside in the luminar layer close to the ventricle, where they divide rapidly. Initially these cells generate radial glia cells and some neuroblasts as well. One process of the radial glia cells extends towards the pial surface of the cortex while the other retains contact to the luminar layer of the neuroepithelium. The radial glia cells thus form a radial scaffold that reaches from the inner ventricular layer to the outer pial layer (shown in the first picture of Figure 3.3.3.1a).
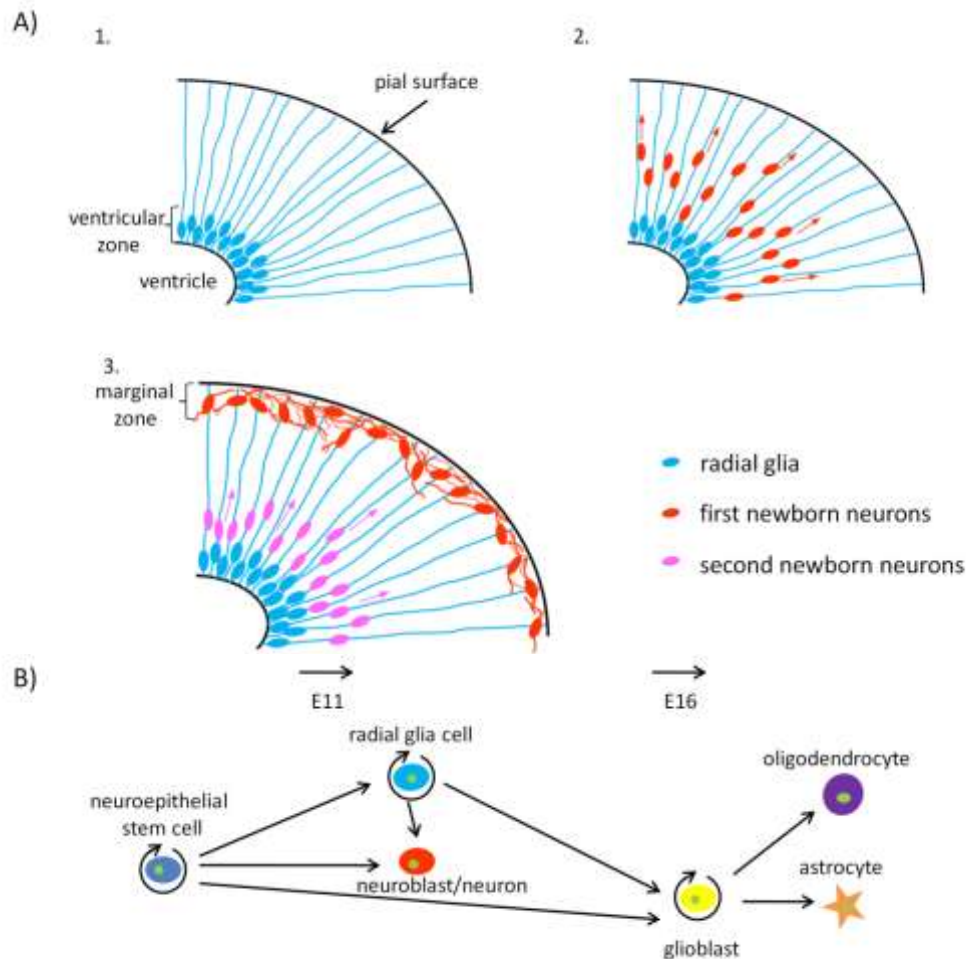
Figure 1.8: Schematic illustration of the neocortex development A) temporal illustration of the development of the neocortex .**B)** Cell-fate map of an neuroepithelial stem cell. For a detailed explanation please refer to text.

At E13.5, the earliest derived neurons use these radial glia cells as tracks to migrate towards the pial surface where they differentiate and form the first cortical layer in the marginal zone (second and third picture of Figure 1.8). In the next step a new wave of neurons migrates out of the ventricular zone and takes a position below the marginal layer. Successive waves of neurons then migrate in an inside-out pattern in which the earliest born neurons are found in the deepest cortical layers while the later born neurons move to the more superficial layers. After the neurons have taken their proper laminar positions, they develop characteristic

synaptic connections with nearby neurons as well as more distant neurons in associated regions of the cortex. Later in neocortex development oligodendrocytes and astrocytes are generated that migrate to the cortical layers as well. At E16 when neuron formation subsides, radial glia cells in the VZ begin to generate glioblasts (Panel B of Figure 1.8). These glioblasts migrate out into the adjacent subventricular zone (SVZ) where they proliferate and differentiate into astrocytes and oligodendrocytes.

1.9 Aim of this thesis

The major aim of this thesis was to investigate the expression and developmental function of brain enriched miRNAs: let-7, miR-125, miR-124 and miR-128. In pursuit of this goal the following question were addressed and experimental approaches adopted:

What is the temporal and cell specific expression of these miRNAs during neuronal development?

- Generation of E12 mouse neural stem cells (NSC's) along the neural lineage
- FACS analysis of miRNAs activity in embryonic carcinoma, E12 neural stem cells, primary cortical neurons at stage E15 and E18 using GFP based constructs, containing specific binding sites miRNAs

What are potential roles of the neuronal lineage specific miRNAs, miR-124 and miR-128, during neural development?

- *in vitro*: ectopic overexpression of miR-124 in NSC's undergoing astrocytic
      lineage differentiation
- *in vivo*:
        - miRNA overexpression in the developing mouse brain *in utero*
        - misexpression of miR-124 in the neural tube of the chicken *in ovo*

Which genes are regulated by let-7, miR-125 and miR-128?

- Establishment of assay conditions in Hek293 cells to validate putative miRNA target genes using synthetic miRNA mimics
- Generation of GFP-miRNA target gene constructs, bearing 3'UTRs of certain predicted miRNA target genes
- FACS analysis of Hek293 that have been co-transfected with GFP-miRNA target gene constructs and appropriate miRNA mimics

What is the function of the let-7/miR-125 target genes Lin-28 and Lin-41?

- overexpression of Lin-41 in the neural tube of the chicken *in ovo*
- co-expression of Lin-41 and Myosin IV in the neural tube of the chicken *in ovo*
- overexpression of Lin-41 and Lin-28 in a miRNA-activity assay in Hek293 cells
- de-repression of Lin-28 and Lin-41 by competitive inhibition of miR-125/let-7 in neural stem cells using GFP-sponge constructs

2. Material and Methods

2.1 Materials

2.1.1 Chemicals

Chemicals for experiments were purchased from the following companies, unless indicated otherwise: Ambion, BD Clontech, Gibco, Sigma, Invitek, Invitrogen, Fermentas, Stratagene, Chemicon, BioLabs, Biochrom, Roth, Roche, Merck, Pierce, BioRad, Fluka, Serva, Promega. Anti-mLin-41 sera were generated by Pineda-Antikörper-Service.

2.1.1.1 Enzymes, Kits and Transfection Reagents:

- Advantage RT-for-PCR Kit (Clontech)
- CombiZyme DNA polymerase Mix (Invitek)
- GoTaq Master Mixes (Promega)
- Lipofectamine 2000 transfection reagent (Invitrogen)
- Lipofectamine LTX reagent (Invitrogen)
- Lipofectamine RNAiMAX reagent (Invitrogen)
- Mouse NSC (Neural Stem Cell) Nucleofector$^®$ Kit (Amaxa)
- Mouse NSC (Neural Stem Cell) Nucleofecto
- NucleoBond PC 100/PC 500 (Macherey-Nagel)
- NucleoBond Extra Midi EF (Macherey-Nagel)
- Phusion High-Fidelity DNA polymerase (Finnzymes)
- QIAquick Gel Extraction Kit (Qiagen)
- QIAquick Nucleotide removal Kit (Qiagen)
- Restriction endonucleases (BioLabs)
- Shrimp Alkaline Phosphatase (SAP) (Promega)
- T4 DNA Ligase (BioLabs)
- T4 Polynucleotide Kinase (Fermentas)
- T7 Transcription Kit (Fermentas)
- T7 TNT in vitro translation assay (Promega)
- Topo TA cloning Kit (Invitrogen)
- Trizol reagent (Invitrogen)

2.1.2 Equipment

- Amaxa Nucleofactor device

- Cell incubator (Hereaus Instruments)
- Centrifuges: Rotina 35 R (Hetich); 5417R, 5804R (Eppendorf); Biofuge pico (Heraeus)
- Confocal equipment TCS SL (Leica Microsystems)
- CUY21EDIT Square Wave electroporator
- DNA electrophoresis chamber (BioRad)
- ECM 830 electroporator (BTX)
- Egg breeding chamber BSS160-8103 (Grumbach)
- FACS CantoII(BD)
- Fluorescent microscope BX 51 (Olympus)
- Gel electrophoreses and blotting equipment (BioRad)
- Needle 45 Degree-Shape Exposed Platinum electrodes,1-3mm (CUY)
- PCR Block (MJ Research)
- pH Meter 537 (WTW)
- Photometer Ultrospec 2000 (Pharmacia Biotech)
- Power pac 200/300 (BioRad)
- Vibratome Serie 1000 (Pelco, Redding, USA)

2.1.3 Software

- Adobe Acrobat Reader 5.0
- Adobe Photoshop CS3/4
- BLAST (http://www.ncbi.nlm.nih.gov/BLAST/)
- CLUSTALW (http://align.genome.jp/)
- Ensembl genome browser (http://www.ensembl.org/index.html)
- WCIF-ImageJ (http://www.uhnresearch.ca/facilities/wcif/imagej)
- JaMBW (http://hometown.aol.com/lucatoldo/myhomepage/JaMBW/index.html?f=fs)
- Leica Confocal Software v. 2.61 Build 1537
- Magnafire
- MFOLD program (http://www.bioinfo.rpi.edu/applications/mfold/rna/form1.cgi)
- MicroInspector (http://bioinfo.uni-plovdiv.bg/microinspector/)
- Microsoft Office 2007
- Microsoft Windows Vista / Windows 7 64-bit
- miRanda software (http://www.miRNA.org/)
- miRNA database (http://www.sanger.ac.uk/Software/Rfam/mirna/)
- NCBI database (http://www.ncbi.nlm.nih.gov/)
- Primer3 program (http://frodo.wi.mit.edu/)
- PicTar (http://pictar.bio.nyu.edu/cgi-bin/new_PicTar_mouse.cgi)

- RNA22 (http://cbcsrv.watson.ibm.com/rna22.html)

- TargetScan software (http://genes.mit.edu/targetscan)

2.1.4 DNA and RNA Oligonucleotides

Table 2.1.4a: DNA- Oligonucleotides used to modify the pEGFP-C1 vector

Primer	Sequence	Usage
BglII- Stop-NotI-Hindfwd	gATCT**TAA**TAggCggCCgCCgAgCTCA	Insertion of a **stop** codon and NotI –SacII restriction site into BglII-HindIII digested pEGFP-C1 Vector → pWu
BglII- Stop-NotI-Hindrev	AgCTTgAgCTCggCggCCgCCTATTAA	
XhoIfwd	ggCCgCATCTCgAgA	Insertion of a XhoI restriction site into NotI-HindIII digested pWu → pXho
XhoIrev	AgCTTCTCgAgATgC	

Table 2.1.4b: DNA- Oligonucleotides to insert miRNA binding sites into modified pEGFP-C1 vector.

Primer	Sequence	Usage
let-7a-BSfwd	AATTCAACTATACAACCTACTACCTCAG	Insertion of a let-7a binding site into EcoRI/SalI digested pXho.
let-7a-BSrev	TCGACTGAGGTAGTAGGTTGTATAGTTG	
mir124-BSfwd	AATTCTCTTGGCATTCACCGCGTGCCTTAATTGG	Insertion of a miR-124 binding site into EcoRI/SalI digested pXho.
mir124-BSrev	TCGACCAATTAAGGCACGCGGTGAATGCCAAGAG	
mir-125-BSfwd	AATTCTCACAAGTTAGGGTCTCAGGGAG	Insertion of a miR-125 binding site into EcoRI/SalI digested pXho.
mir-125-BSrev	TCGACTCCCTGAGACCCTAACTTGTGAG	
mir-128-BSfwd	AATTCAAAAGAGACCGGTTCACTGTGAG	Insertion of a miR-128 binding site into EcoRI/SalI digested pXho.
mir-128-BSrev	TCGACTCACAGTGAACCGGTCTCTTTTG	

Table 2.1.4c: DNA- Oligonucleotides to insert miRNA sponge binding sites into modified pEGFP-C1 vector.

Oligonucleotide	Sequence
2xlet-7sp-fwd	AGCTTAACCCCCCAACCTACTACCTCAATATAACTATATTTTCTACTACCTCAG
2x let-7sp-rev	TCGACTGAGGTAGTAGAAAATATAGTTATATTGAGGTAGTAGGTTGGGGGGTTA
2x miR-128sp-fwd	AGCTTAAAGAGACAAAATCACTGTGAAAAAGAAGAGACAAAATCACTGTGAG
2x miR-128SP-rev	TCGACTCACAGTGATTTTGTCTCTTCTTTTTCACAGTGATTTTGTCTCTTTA
2x miR-125SP-fwd	AGCTTTCACAGGTTAAAAAATCTCAGGGAAAAATCACAAGTTAAAAAATCTCAGGGAG
2x miR-125SP-rev	TCGACTCCCTGAGATTTTTTAACTTGTGATTTTTTCCCTGAGATTTTTTAACCTGTGAA

2x miR-29SP-fwd	AGCTTTAACCGATTTACACTGGTGCTATTTTTAACCGATTTACACTGGTGCTAG
2x miR-29SP-rev	TCGACTAGCACCAGTGTAAATCGGTTAAAAATAGCACCAGTGTAAATCGGTTAA

PCR-Primers were designed using Primer3 program, and analyzed in BLAST for specificity.

Table 2.1.4d: Primers to generate GFP- miRNA target gene constructs

Primer	Sequence	T_M in °C	Amplified 3'UTR
D4Ertd22efwd	ACGGCTGGACTTGAGCAG	58	nt 591-917 of NM_001025608
D4Ertd22erev	AAATGAGAACTTCCCCACCC	58	
Mll1fwd	GGTAGCGTAGTCCGAGTGGA	56	nt 13890-14362 of NM_001081049
Mll1rev	CATGACCCATCAGTGCATTT	56	
RPS6ka5fwd	TCTTGGTTTTATGTAATATGGCACTT	60	nt 3425-3722 of NM_153587.2
RPS6ka5rev	TCTGCCTACAGGAGGAGCTG	56	
FoxP2fwd	TTTT***CTCGAG***GCTCACCTCAGCCACACATA	60	nt 2641-6124 of NM_053242
FoxP2rev	TTTT***GGTACC***ACAATACAACGGTGCCATGA	56	
ZBTB7afwd	TCTTGGTTTTATGTAATATGGCACTT	60	nt 2458-2774 of NM_010731
ZBTB7arev	AAGCAGAGATGGGAAGGTTG	58	
Arid3afwd	TAAAAATCAGGGCAAAGCAAAGA	56	nt 2492-4653 of NM_007880.3
Arid3arev	TGAAGGGTGACCAGGAAGGTTCT	57	
Arid3bfwd	TAACAGCAGCTCTCACTGCTCAC	57	nt 1706-3087 of NM_019689
Arid3brev	TAAGCATGCCAACAGAAGACAGA	61	
NR6a1fwd	TAACTGCACTCCTGCAAGACAAG	63	nt 1842-3781 of NM_010264.3
NR6a1rev	TAATGCACAGAGGTGCTGTCTCT	63	
Lin-41fwd	GGACTTTGGCAACAATCGAATCCTC	56	nt 3792-4338 of NM_001042503.1
Lin-41rev	CACAGTATTCTCAAGAACACAAATAC	62	
Lin-28fwd	AT***GAATTC***GGTTGTGATGACAGGCAAAG	58	nt 1187-2832 of NM_145833.1
Lin-28rev	TA***GGATCC***TCTCAAAACCACCAACCAAA	57	

Table 2.1.4e: Primers for vector based miRNA overexpression.

Primer	Sequence	RS	T_M in °C
preLet7afwdsac2	ATGATG***CCGCGG***TCATTACACAGGAAACCGGAAT	SacII	58
preLet7afwdpme1	ATGATG***GTTTAAAC***TCATTACACAGGAAACCGGAAT	PmeI	58
preLet7arevNot1	TCAT***GCGGCCGC***AAGCATGCATAGCATAAGCAAA	NotI	56
premir-128fwd	ATGATG***CCGCGG***CGTAGCTGCTTTCATTCTTGG	SacII	60
premir-128afwdpme1	ATGATG***GTTTAAAC***CGTAGCTGCTTTCATTCTTGG	PmeI	60
premir-128revNot1	TCAT***GCGGCCGC***AGGCAATGGAAAATATAAACAAAT	NotI	58
premir-29afwdpme1	ATGATG***GTTTAAAC***AAGCCTTCTCTGGAAGTGGA	PmeI	58
premir29revNot1	TCAT***GCGGCCGC***CCTTAGCATGTTTTGGTATTTGTTT	NotI	59

Table 2.1.4f: Primers used to generate and sequence 3xFLAG-tagged fusion proteins.

Primer	Sequence	T_M in °C	Usage:
predLin-41for#1	ATCCTCCGCCTTCCTGCTCA	63	These Primers have been used for cloning and sequencing of
predLin-41for#4	TCTTCACGTCTTGCCCTGCCT	63	
Xm_356199.3#6for	CGCCTCACCAAGGACCATTAC	63	
lin41 rev	ATCAAGCGTGCCCTTCAGGGGAAG	69	
predLin-41rev#1	GACTGCCAGGAACACCTGTGC	65	

predLin-41rev#2:	TACCTCCAGGATGCCCT	55	the 3xFLAG-
predLin-41rev#3:	ATCGAGCAGGCCCAGACTGT	63	Lin-41 vector.
predLin-41rev#4:	AGCTGCTGGCTGATGCCCAGC	67	
muLin41 3\'#5:	CACTGTCATGGGCTACGACCAC	66	
Lin28fwdPrimer	***GCGGCCGC***TATGGGCTCGGTGTCCAAC	60	These Primers
Lin-28ORF rev	***GAATTC***AACTCCCCATTAGCCAAAGAAT	66	have been
Lin28revBamHI	***GGATCC***TCAATTCTGGGCTTCTGG	56	used for
Lin28RTPrimer	GGGTTCTAGGGTGGTTCCTC	63	cloning and
Lin-28ORF fwd	***GAATTC***ACGGGCTCAGCAGACGACC	64	sequencing of the 3xFLAG-Lin-28 vector.

Table 2.1.4g: Primers used for site directed mutagenesis of pC3xFLAG-Lin-41

Primer	Sequence	Description
Linmutfwd	GACCGACTTCC<u>AGATCT</u>***TA***CTGCTG***GCC***AAGG AGATGTGCGGCT	- *Bgl*II site is underlined - exchanged nucleotides are in italics
Linmutrev	GCCCGTTCTTGGTGCCTTTCTCACCA	-
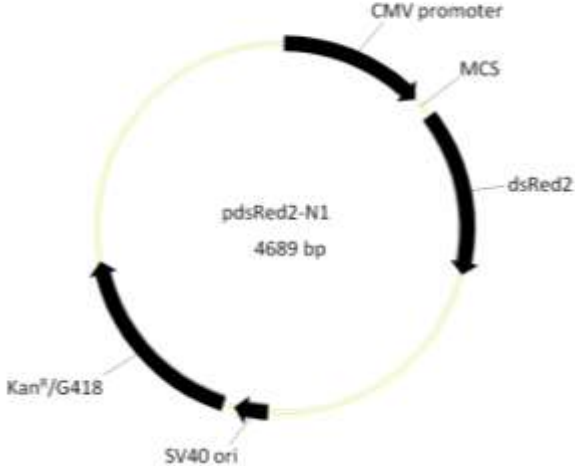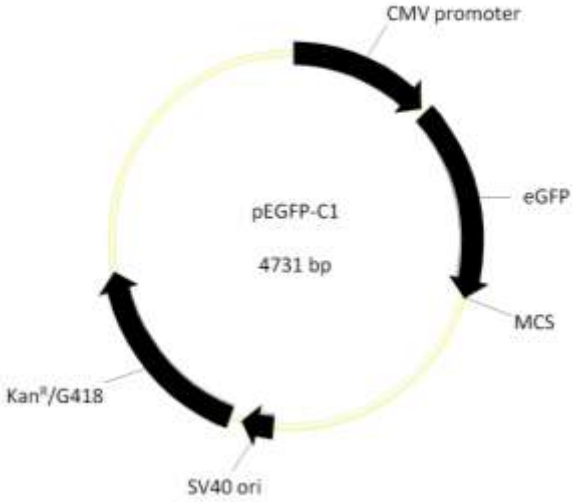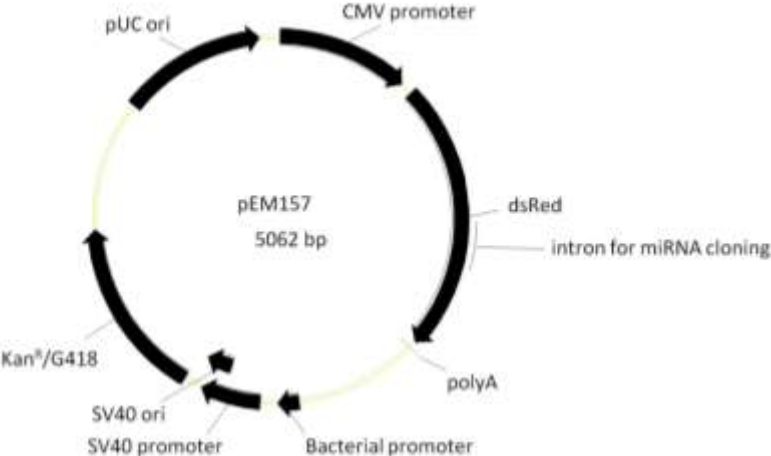
Table 2.1.4h: Double stranded miRNA mimics used for cell transfection
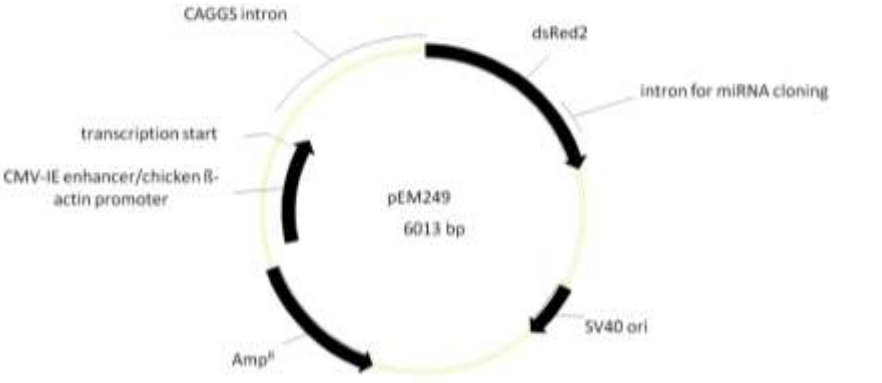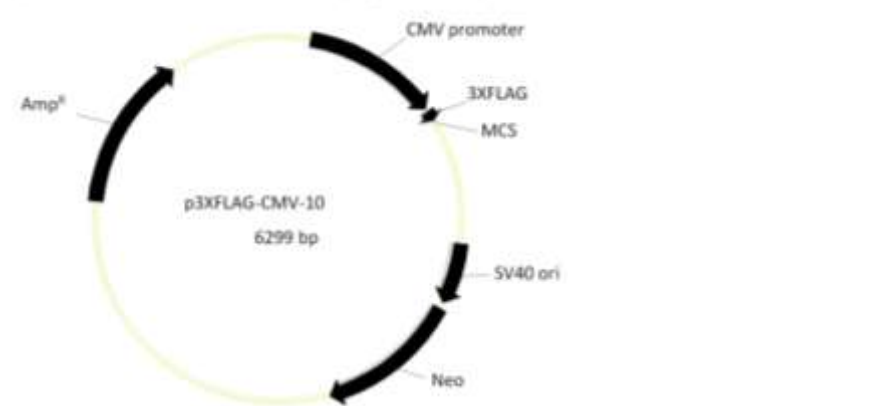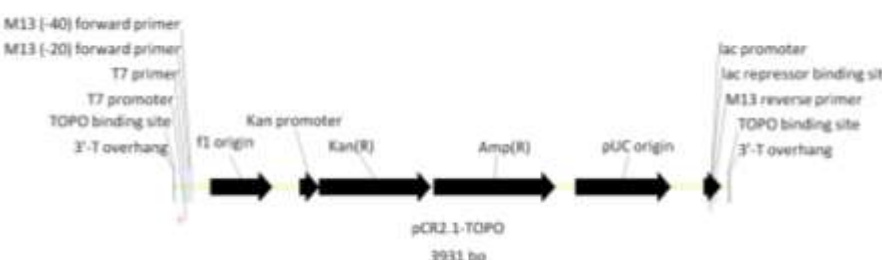
Name	Sequence
hsa-let-7a	UGAGGUAGUAGGUUGUAUAGUU
hsa-let-7e	UGAGGUAGGAGGUUGUAUAGUU
hsa-mir-125a	ACGGGUUAGGCUCUUGGGAGCU
hsa-mir-128b	UCACAGUGAACCGGUCUCUUU

Table 2.1.4i: siRNAs used for cell transfection

Name	Sequence
Dicer-1	ATCGATCATATGTCCAGTCTA
Dicer-4	AAGGCAGAATTTAAAGTTTGA

2.1.5 Veectors

pdsRED2-N1 backbone vector (Clontech):	Usage: pdsRED2-N1 has been mainly used as a marker for transfection efficensies *in vitro* and *in ovo*.
pEGFP-C1 backbone vector (Clontech):	Usage: Generation of : - miRNA-sensor (section 3.1.1.1) - target-gene sensor (section 3.1.1.3) - miRNA-inhibitor (sponges) (section 3.1.3)
pCMV-Intron-RED backbone vector:	Usage: Generation of miRNA overexession constructs (section 3.1.2.2) for *in vitro* transfection. Kindly provided by Tom Maniates (detailed description in Makeyev et al. 2007).

	Usage
pCAGGS-Intron-RED backbone vector: CAGGS intron transcription start CMV-IE enhancer/chicken ß-actin promoter pEM249 6013 bp Amp^R dsRed2 intron for miRNA cloning SV40 ori	Usage: Generation of miRNA overexpression constructs (section 3.1.2.2) for *in ovo* and *in utero* electroporation. Kindly provided by Tom Maniates (Makeyev et al. 2007).
p3xFLAG-CMV-10 backbone vector(Sigma-Aldrich): Amp^R p3XFLAG-CMV-10 6299 bp CMV promoter 3XFLAG MCS SV40 ori Neo	Usage: Generation of 3xFLAG tagged fusion proteins
pCR2.1-TOPO: M13 (-40) forward primer M13 (-20) forward primer T7 primer T7 promoter TOPO binding site 3'-T overhang f1 origin Kan promoter Kan(R) Amp(R) pUC origin lac promoter lac repressor binding site M13 reverse primer TOPO binding site 3'-T overhang pCR2.1-TOPO 3931 bp	Usage: Cloning of PCR products directly from a PCR reaction with A-overhangs for further restriction.

2.1.6 Constructs

- MBD-GFP (kindly provided by Kuniya Abe)
- pIRESneo-FLAG/HA Ago2 (Addgene)
- Myo6a

Plasmids that were generated for this thesis are listed in Section 2.2.5.

2.1.7 Bacterial strains

Strain	Genotype
Escherichia Coli XL-1 blue cells (Stratagene)	endA1 gyrA96(nal^R) thi-1 recA1 relA1 lac glnV44 F'[::Tn10 proAB$^+$ lacI^q Δ(lacZ)M15] hsdR17(r$_K^-$ m$_K^+$)

Escherichia Coli XL-10 gold cells (Stratagene)	endA1 glnV44 recA1 thi-1 gyrA96 relA1 lac Hte Δ(mcrA)183 Δ(mcrCB-hsdSMR-mrr)173 tet^R F'[proAB lacI^{q}ZΔM15 Tn10(Tet^R Amy Cm^R)]
Top10 cells (Invitrogen)	F- mcrA Δ(mrr-hsdRMS-mcrBC) φ80lacZΔM15 ΔlacX74 nupG recA1 araD139 Δ(ara-leu)7697 galE15 galK16 rpsL(Str^R) endA1 λ$^-$

2.1.8 Primary cells, cell lines, mouse strain and chicken eggs

- ES cells – murine embryonic stem cell line D3

- P19 EC cell– mouse embryonic carcinoma cell line (German Collection of Microorganisms and Cell Cultures, Braunschweig, Germany)

- HEK293 – Human Embryonic Kidney cells (German Collection of Microorganisms and Cell Cultures, Braunschweig, Germany)

- C57Bl/6J Mouse Line (FEM Berlin)

- E12 mouse progenitor cells generated from C57BL/6 Mouse

- Primary hippocampal neurons generated from C57BL/6 Mouse

- SPF certified eggs from "LOHMANN LSL CLASSIC Legehennen" (Lohmann Tierzucht, Cuxhaven, Germany)

2.1.9 Buffers, solutions and media:

Solutions used for immunostaining	Composition
PBS, 10×, pH = 7.4	2 g/L KCl, 2 g/L KH$_2$PO$_4$, 80 g/L NaCl, 14.4 g/L Na$_2$HPO4×2H$_2$O, with aqua bidest to 1 L
Paraformaldehyde (PFA, Sigma)	4% PFA in 1xPBS
Immunocytochemistry Blocking Solution	5% normal goat serum, 1% BSA, 0.1% fish gelatine, 1xPBS
Immunochistochemistry Blocking Solution	5% normal goat serum, 1% BSA, 1xPBST (1xPBS +0.1% Triton X100)
Washing Solution (PBST- I)	1xPBS, 0.1% Triton X100
Washing Solution (PBST-II)	1xPBS, 0.1% Tween20

Solutions used for Western blot	Composition
Protease inhibitors cocktail, 10×	0.2 mg/ml Pancreas extract, 0.02 mg/ml Chymotrypsin, 5 µg/ml Therolysin, 0.2 mg/ml Trypsin, 3.3 mg/ml Papain
Stacking gel buffer	0.5 M Tris, pH 6.8
Separation gel buffer	1.5 M Tris, pH 8.8
Stacking gel 4%	3 ml H$_2$O, 1.25 ml Stacking gel buffer, 540 µl 37.5:1% Acrylamid/Bis (Fluka), 50 µl 10% SDS 38 µl 10% APS, 13 µl TEMED
Separation gel 7.5%	5 ml H$_2$O, 2.7 ml Separation gel buffer, 2 ml 37.5:1% Acrylamid/Bis (Fluka), 100 µl 10% SDS, 50 µl 10% APS, 5 µl TEMED
Electrophoresis buffer for protein SDS-PAGE, 10×	0.25 M Tris (Base), 1.92 M Glycin, 1% SDS in 1 L distilled water

Western blotting buffer	192 mM Glycin, 25 mM Tris, 20% Methanol, in 1 L distilled water
PBT	1×PBS, 0.1% Tween 20

Solutions used for DNA electrophoresis	Composition
10x TBE buffer	108 g Tris base, 55 g boric acid, 40ml 0.5M EDTA(pH 8.0) with aqua bidest to 1 L
10X SB buffer	100 mM sodium hydroxide, pH adjusted to 8.5 with boric acid
Seakem LE Agarose	

Solutions used for bacterial culture	Composition
LB-media, pH=7.4	10 g NaCl, 10 g Peptone (Roth), 5 g yeast extract in 1 L distilled water
SOC-medium	0.5% yeast extract, 2% tryptone, 10 mM NaCl, 2.5 mM KCl, 10 mM MgCl2, 10 mM MgSO4, 20 mM glucose
Kanamycin	
Ampicilin	
Agar-Agar (Roth)	For Agar-Plates 15g Agar-Agar / 1 L LB-media was used.

2.1.10 Cell culture solution and Media

Cell culture solutions	Composition
Trypsin/EDTA solution, 0.25% (Gibco)	-
Penicilin/Streptamycin 100x solution (Gibco)	-
Glutamax 100x (Gibco)	-
Fetal Bovine Serum (PAN)	-
PBS, 10×, pH = 7.4	2 g/L KCl, 2 g/L KH_2PO_4, 80 g/L NaCl, 14.4 g/L Na$_2$HPO4×2H$_2$O, to 1 L with aqua bidest
0.1 % Gelatin solution (Merck)	0.1 g gelatin/100ml bidest →autoclaved
Poly-L-Ornithin (Sigma)	
Laminin (Millipore)	
Poly-L-Lysine ?	
Accutase (Sigma-Alldrich)	
FACS buffer	1xPBS, 5% Fetal bovine Serum
Cell type	**Composition**
P19 growth medium (P19GM)	α modified form of Eagle's minimal essential medium (αMEM, Sigma) supplemented with 10% heat inactivated fetal bovine serum (FBS, Gibco), 2 mM glutamine (Biochrom), 50 U/ml penicillin and 50 µg/ml streptomycin (Biochrom).
HEK293 growth medium	DMEM, containing 5% FBS, 2 mM glutamine, 50 U/ml penicillin and 50 µg/ml streptomycin
Primary neuron culture medium	Neurobasal Medium without L-Glutamine (Gibco) supplement with 1xB27 supplement

	(Gibco), 0.5 mM **L- glutamine,** 50 U/ml penicillin and 50 µg/ml streptomycin.
Neuronal Stem Cell Expansion Media **(NSCEx)**	Euromed-N (Euro-clone), 2mM L-Glutamine,1x N2-supplement (Gibco),1xPrimocin (Invivogen), 10nM Human recombinant insulin (Gibco), 20ng/ml FGF-2 (Millipore) and 20ng/ml EGF (Millipore)
Astrocytic neural stem cell differentiation media	NSEx media without FGF-2, + 5%FCS
Neuronal differentiation media for neural stem cells	NSEx media without EGF/FGF-2 supplemented with 10ng/ml FGF-2 and 1xB27 supplement (Gibco)

2.1.12 Antibodies

Antibody	Immununo-cytochemistry working solution	Western blotting working solution
Primary antibodies		
anti-β-III Tubulin, mouse monoclonal, clone SDL.3D10 (Sigma)	1/800	1/1000
anti-Lin28 MaxPab mouse polyclonal (Abnova)	1/2000	1/4000
anti-Lin28 rabbit polyclonal	1/1000	1/2500
anti-Oct-3/4 (C-10):sc-5279, mouse monoclonal (Santa Cruz Biotechnology)	1/200	-
anti-GFAP, mouse monoclonal, clone G-A-5 (Sigma)	1/1000	-
anti-SOX2 rabbit polyclonal, BIOZOL	1/1000	-
Anti-mLin41 Serum, rabbit, peptide, (Pineda Antikörper Service, Berlin)	1/5000	-
Anti-mLin41 Serum,guinea pig, peptide (Pineda Antikörper Service, Berlin)	1/200	-
anti-Flag, mouse monoclonal, clone M2 (Sigma)	1/2500	1/2000
Anti-RC-2, mouse monoclonal (Hybridoma Bank)	1/1000	1/1000
Secondary antibodies		
Alexa Fluor 488F(ab')2 anti-mouse IgG (Molecular probes)	1/1000	-
Alexa Fluor 568F(ab')2 anti-mouse IgG (Molecular probes)	1/1000	-
Alexa Fluor 488F(ab')2 anti-rabbit IgG (Molecular probes)	1/1000	-
Alexa Fluor 568 F(ab')2 anti-rabbit IgG (Molecular probes)	1/1000	-
HRP-labeled sheep anti-mouse IgG, Amersham Bioscience	-	1/5000
HRP-labeled sheep anti-rabbit IgG, Amersham Bioscience	-	1/5000

2.2 Methods

2.2.1 P19, HEK293 and neural stem cell (NSC) preparation and culture

All cell types were cultured at 37ºC in a humidified incubator with 5% CO_2. Preparation and electroporation of mouse E15-E18 primary cortical neurons is described in chapter 2.2.2.2.

P19 EC cells are developmentally pluripotent cells derived from a primary teratocarcinoma induced in the C3H/He mouse strain. These cells can differentiate into all cell types under the appropriate conditions. P19 EC cell cultures were started from a frozen stock by seeding cells into a 100-mm tissue culture dish with 10 ml of P19 growth medium (P19GM). To passage, cells were removed from the culture dish surface with a 0.25% trypsin/EDTA solution (Gibco). Trypsinization was stopped by adding P19GM. Cells were transferred into a 15-ml conical tube and pelleted in a centrifuge at 1000 rpm for 3 min. The cell pellet was resuspended in 5 ml of fresh medium and 0.5 ml was seeded dropwise into a 100-mm tissue culture dish with 10 ml of P19 growth medium.

HEK293 cells were grown as adherent monolayers in DMEM supplemented with 10% FBS, 2 mM glutamine, 50 U/ml penicillin and 50 µg/ml streptomycin. Under optimal conditions, HEK293 cells divide every 18-24 h and therefore were normally subcultured twice a week according to the same procedure as P19 EC cells.

Preparation and maintenance of neural Stem Cells

The uterus of a neck breaked C57BL/6 mother bearing E12 embryos was harvested with a scissor and transferred into an HBSS filled petri dish. The uterus was opened and the removed embryos were decaped. Under a microscope the brains were isolated with forceps the meningitis and hindbrain were removed. The isolated eight forebrains were collected in a 15ml Falcon tube containing HBBS and were washed 3 times. 3ml Accutase was added and the forebrains were incubated for 5min in a 37°C water bath. Afterwards Accutase was removed and the forebrains were washed 2 times with HBSS and transferred into a new 15mlFalcon tube containing 1ml of Neural Stem Cell Expansion media (NSCEx-Media). A firepolished glass pipette was used to disrupt the cells by repeated pipetting (around 30 times). The cell suspension was diluted by adding 6ml NSCEx-Media. The disruption of the cells and the number of cells was checked by using a Neubauer cell chamber. Cells were plated onto an untreated 10ml plastic plate with NSCEx-Media and incubated with a half volume of media exchanged every week for three Weeks. Small spheres were growing within these weeks and were collected by centrifugation at 700 rpm for 30s. The cells making the spheres were disrupted by re-dissolving the pellet with Accutase and repeated pipetting. The cells were plated again onto an uncovered 10ml dish in NSCEx-Media for one week. The

newly arisen neurospheres were transferred into an with 0.1% gelatin for one hour covered T25 flask with 5ml NSCEx-Media. Attachment and outgrowth of adherent cells occurred within 48 hours. These adherent cells were passaged 1:3 to 1:6 at 70% confluence every two – three days in a new with 0.1% gelatin covered T25 flask with NSCEx-Media for more than 30 passages. The NS cell line used in these experiments is Oct-4-, GFAP-, Sox2+, RC-2+, as confirmed by RT-PCR and immunocytochemistry (data not shown), consistent with the original description. For immunocytochemistry and microscopy applications, cells were plated onto covered 18mm glass cover slips in a 12 well plate. The glass cover slips were washed with sterile water, baked in an oven at 200°C for 2 hours. For astrocyte differentiation, the baked coverslips were covered with a 0.2% gelatine solution for at least one hour. For other applications the coverslips were incubated with 0.02% poly-ornithine solution overnight at RT, washed once with PBS and coated with a 7µg/mL laminin solution for at least two hours.

Cryopreservation and recovery of NS cells

From a 60-90% confluent T25 flask, cells were resuspend into 1 ml NSCEx-Media plus 10% DMSO. This suspension was split into two cryotubes and stored in Mr. Freeze at -80°C. After one day the cells were transferred to liquid nitrogen. NS cells are thawed by rapidly bringing the vial to 37°C followed by transfer to 5ml of pre-warmed NSCEx-Media. DMSO was removed by removing the supernatant after centrifugation. The cells were resuspended with 5ml NSCEx-Media and plated into a 0.1 gelatin covered T25 flask.

Differentiation of Neural Stem Cells

A) Astrocyte differentiation

The pellet of freshly passaged Neural Stem cells was dropwise resuspended in Astrocyte Differentiation Media (NS-Media, + 5%FBS (heat inactivated), +EGF, +Glutamax, +Insulin). $8x10^4$ cells were replated on a gelatin covered coverslip in a 12-well. The morphology of the Neural Stem cells changed rapidly within 24 to 48 hours to an astrocyte shape.

B) Neuronal differentiation

For neuronal differentiation NS cells are harvested using Accutase and $1-2 \times 10^5$ cells are re-plated into each12-well containing a poly-ornithine/laminin coated glass cover slip in Neural Differentiation Media. A half volume of medium is replaced every 2-3 days to maintain conditioning of medium.

2.2.2. Cell transfection with plasmid DNA and RNA

The exact amounts of DNA and RNA used for transfection experiments are shown in results. Transfection of Hek293 and P19 was performed by Lipofectamine reagent. Primary Neurons and NS-cells were electroporated by using the Amaxa Nucleofactor solution kit.

2.2.2.1 Transfection with Lipofectamine reagent

One day before transfection, 2×10^5 H293 or 2.5×10^4 P19cells were plated in monolayer per 12-well plate. Cells were transfected with 0.05 to 1 µg of the appropriate plasmid and/or 20pmol miRNA mimic using Lipofectamine reagent. Cells were processed for flow cytometry after 48 hours.

For RNA*i* experiments and ectopic miRNA expression, P19 cells were transfected with Lipofectamine RNA*i*-Max (Invitrogen GmbH, Karlsruhe, Germany), using the manufacturer's reverse transfection protocol. RNA*i* duplexes were obtained from Qiagen (Hilden, Germany) and used at 50 nM. The negative control siRNA (negative universal control, medium GC) was obtained from Invitrogen. Synthetic miRNA precursors (Section 2.1.4h) were obtained from Ambion (Ambion/Applied Biosystems, Darmstadt, Germany) and used at 50 nM.

2.2.2.2 Electroporatiopn of neural stem cells and primary cortical neurons

Transfection of Neural Stem Cells

Transfecion of Neural Stem Cells was performed with the Amaxa NSC-Nucleofactor Kit. The Nucleofactor solution was prepared by adding 0,5ml supplement to 2,25 ml Nucleofactor solution (this solution is stable for up to three month at 4°C). For each transfection ~ $1x10^6$ cells were resuspended in 100µl NSC-Nucleofactor solution together with 2-10µg Plasmid-DNA and transferred into an Amaxa electroporation cuvette. The cuvette was inserted into the Amaxa cuvette holder and electroporated with program A-33. After electroporation 500µl of ml NSCEx-Media was added immediately to the cuvette and the cells were plated onto a with 0.1 gelatine covered T25 flask containing 4,5ml of ml NSCEx-Media. After 16 hours non adherent cells and cell debris was removed by exchanging NSCEx-Media.

Preparation and transfection of Primary cortical neurons from E15 to E18 embryo
The brains of the embryos were selected as described above (see Preparation of neural stem Cells in Section 2.2.1). With forceps the cortices were isolated and treated with 3ml Trypsin in a 15ml Falcon tube for up to 10 minutes at 37°C. After adding 300 µl FCS and 2 times washing with Primary neuron culture media (NC-media) a firepolished glass pipette

was used to disrupt the cells by repeated pipetting (around 30 times). The supernatant containing the disrupted cells was collected in a new 15ml Falcon tube. The number of cells was determined by using a Neubauer cell chamber. For each Transfection, 1×10^6 cells were centrifugated at 300 rcf for 3 minutes. The Pellet was resuspended in Amaxa Primary Neuron Nuclefactor solution together with 1-2 µg Plasmid-DNA and transferred into an Amaxa electroporation cuvette. The Nucleofactor solution was prepared before by adding 0,5ml supplement to 2,25 ml Nucleofactor solution (this solution is stable for up to three month at 4°C). The cuvette was inserted into the Amaxa cuvette holder, and the cells were electroporated with program O-33. After the electroporation pulse, 500µl of ml NC-media was added immediately to the cuvette and plated onto a with poly-L-lysine covered 6 well plate. After 16 hours non adherent cells and cell debris was removed by exchanging NC-media.

2.2.3 *In Utero* and *in ovo* Electroporation

Preparation of micropipettes for DNA injection

Glass capillaries were pulled using a micropipette puller under following conditions: pressure 500/ heat 800/ pull 30/velocity 40/time 1. One mm of the micropipette tip was removed using a grinder. To make them ready to use for DNA injections the pipettes were sterilized under the UV lamp of a clean bench for 15 min.

DNA preparation

Plasmid preparation was done by using either the EndoFree Plasmid Kit (QIAGEN, Hilden, Germany) or NucleoBond Xtra EF (Macherey & Nagel, Düren, Germany) according to the manufacture's protocol. For microinjection, the DNA was diluted with PBS to a final concentration of one to four µg/µl. To make the DNA solution better visible 10ng Fast Green was added per 1µl DNA solution.

2.2.3.1 in utero Electroporation

A timed-pregnant mouse was anesthetized with an intraperioneal injection of 10% Nembutal solution (Nembutal diluted with saline to 10%). After narcotics of the mice the animal was fixed with tape on hands and feeds on a heating plate at 38°C with the abdomen upside.

The abdominal wall was rinsed with 70% ethanol. The abdominal skin was cut afterwards with scissors. With straight forceps the skin was cut vertical about two to three cm in length. The incision should be low enough on abdomen but higher than the fat pad. The incision through the abdominal muscle wall was done using a scalpel. Using ring forceps the uterus was gently pulled outside in order to find the uterine horn. After counting the embryos one to two embryos with an optimal head position were chosen for electroporation. The uterus was covered with pre-warmed saline every several minutes to prevent drying. With a DNA filled micropipette 1-3 µl DNA was injected into the ventricle using a mouth-controlled pipette

system. With forceps like electrodes parallel along its antero-posterior axis through the embryo and the positive paddle in direction of desired transfection the embryo was
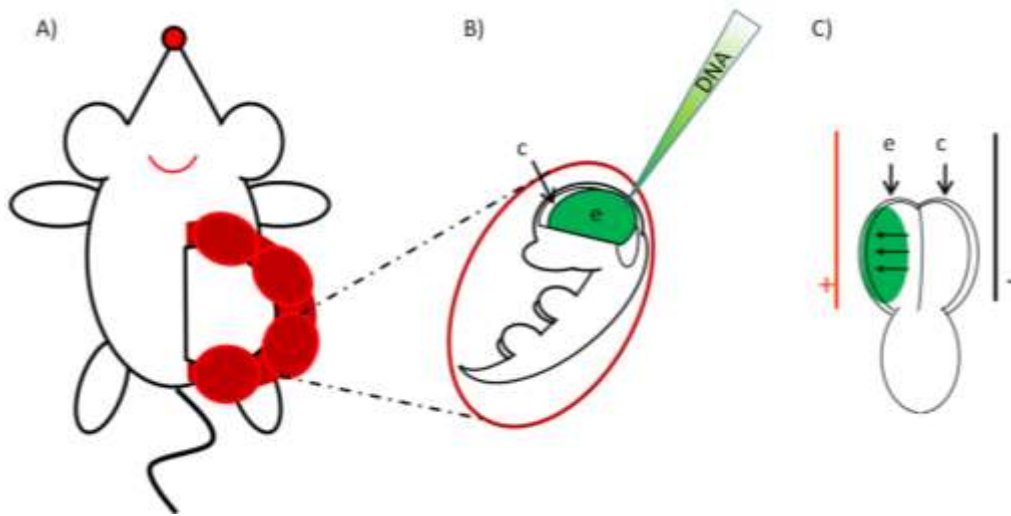

Figure 2.2.3.1: Schematic overview of the *in utero* electroporation technique. e: electroporated side of the brain c: control side. For a detailed explanation please refer to text.

And electroporated using 5 pulses with 30V for 50 ms for each pulse. The gap between the electrodes and the uterus was filled with PBS to ensure even electroporation. By using broad forceps and a needle holder the muscle layer was sutured in tight knot forms with silk suture. Afterwards the abdominal skin was sutured with synthetical suture.

For prenatal studies the electroporated embryos were removed out of the uterus of the neck-breaked mother. For postnatal studies the dsRED or GFP positive pups were identified by using a UV-lamp and tattooed for later identification.

2.2.3.2 *In ovo* electroporation

In ovo electroporation was originally established by Harukazu Nakamura and Jun-Ichi Funahashi. This technique allows misexpression using conventional plasmid expression vectors or knock-down studies using hairpin siRNA vectors in the developing neural tube, including very early stages. SPF certified eggs from "LOHMANN LSL CLASSIC Legehennen" were incubated in a breeding chamber at 38°C and 50 to 60 % relative humidity for 48 to 72 hours. A 2mm hole was pecked with a nail scissor at the flat end of the eggshell. About 3ml of the albumen was removed with a syringe. A tape was glued on the upper part of the laying egg and a 3 x 2cm oval lid was excised with a nail scissor to get access to the on the top of the yolk laying embryo. To be visible for the naked eye approximately 100µl of a 10% Indian ink/PBS solution was injected directly under the embryo. The injected DNA had a concentration between 1 and 4 µg/µl and was additionally stained with 0.05% Fast Green. Approximately 0,5 µl DNA was injected into the lumen of the neural tube. The needle electrodes were placed in parallel between the lower part of the neural tube. The distance

between both electrodes was 3 to 5mm. For electroporation at HH10-13 a 1mm electrode and at HH14-16 a 3mm electrode was used together with the electroporator CUY21. With five 15 V pulses for HH10-13 or five 25V pulses for HH14-16 , 50 milliseconds each in length, with an interval of 100 milliseconds between pulses the injected DNA was electroporated into one side of the neural tube. After removing the electrodes, the egg was sealed with Parafilm and incubated for two to three days at 38°C and 50 to 60 % relative humidity.
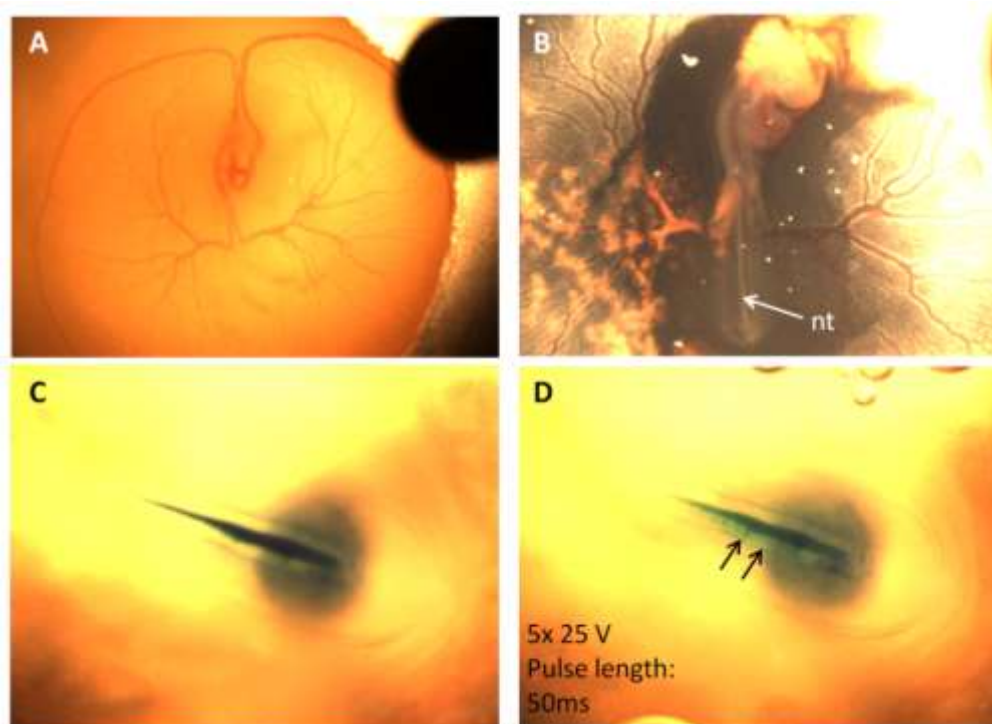

Figure 2.2.3.2: the *in ovo* electroporation of the neural tube A) A HH stage 16 chick with blood vessel surrounding the yolk sac **B)** A 10% non-phenolic ink solution was injected with a syringe under the embryo to visualize the neural tube (nt). **C)** The Figure shows the neural tube after injection of DNA containing ~1% fast green for visualization. **D)** After electroporation (five times 25V for 50ms) the DNA can be seen into the cathode side of the neural tube (black arrows).

Harvest of chicken embryos

The Parafilm was removed and the embryo was excised from the allantoic, and yolk sac sub-systems. The embryo was fixed ON in 4%PfA –PBS at 4°C, washed afterwards two times with PBS. For vibratome sections the head was discarded and the body was embedded in 50°C pre-warmed 4% Agarose-PBS. The embedded embryo was sectioned in 50µm slides using a vibratome.

2.2.4 Molecular biology methods

Standard molecular biology methods such as bacterial culturing, restriction digest, gel electrophoresis, etc. were performed according to "Current protocols in molecular biology" (Ausubel, 1994) and will not be described in detail.

2.2.4.1 Total RNA isolation and cDNA synthesis

Total RNA was isolated from mouse tissue and cell lines using TRIZOL reagent (Gibco) in accordance with the manufacturer's instructions. Briefly, cells were lysed by adding 1 ml of TRIZOL reagent per 35-mm diameter culture dish. Mouse brain samples were homogenized in 1 ml TRIZOL reagent per 100 mg of tissue. After adding 0.2 ml of chloroform the lysate was shaken by hand for 15 s, incubated at RT for 2-3 min and centrifuged at 12.000 g for 15 min at 4ºC to separate the phases. The upper, aqueous phase containing RNA was collected in a new tube. RNA was precipitated by addition of 0.5 ml of isopropyl alcohol per 1 ml of TRIZOL reagent by centrifugation at 12.000 g for 15 min at 4ºC. Pellets were washed with 70% ethanol and dissolved in RNAse-free water. RNA concentrations were measured using NanoDrop. The integrity of isolated RNA was checked by electrophoresis in a 1.5% agarose gel stained with ethidiumbromide (0.1 µg/ml).

Using Advantage RT PCR kit, 2 µg of total RNA were heated together with oligo(dT)18 primer at 70ºC for 2 min, and cooled rapidly on ice. Then the components listed below were added:

4 µl 5× reaction buffer

1 µl dNTP mix (10 mM each)

0.5 µl Recombinant RNAse inhibitor, 20 U

1 µl DNAse, 2 U (RNAse free)

The reaction was incubated at 37ºC for 30 min, then heated to 75ºC for 5 min, and placed on ice. After DNAse treatment, 1 µl of MMLV reverse transcriptase and 1 µl recombinant RNAse inhibitor were added to the reaction, and samples were incubated at 42ºC for 1 hour. To stop the cDNA synthesis, the reaction was heated at 94ºC for 5 min. The cDNA was diluted to a final volume of 100 µl by adding 80 µl of RNAse free water and stored at –70ºC.

2.2.4.2 Polymerase Chain Reaction (PCR)

DNA was amplified using a PCR block (MJ Research). PCR reactions (50 µl) were performed using either the CombiZyme DNA Polymerase mix (Invitek), GoTaq DNA polymerase (Promega) or the Phusion High-Fidelity DNA Polymerase (Finnzymes).

The following components were mixed:

CombiZyme reaction	Phusion Polymerase reactions	GoTaq polymerase reaction
1× OptiPerform Buffer III 2.5 mM MgCl2 250 µM dNTPs 1× OptiZyme Enhancer 0.5 µM forward primer 0.5 µM reverse primer 15-500 ng Template DNA 2 U CombiZyme DNA Polymerase H_2O to a final volume of 50 µl	1× Phusion HF Buffer 200 µM dNTPs 0.5 µM forward primer 0.5 µM reverse primer 15-500 ng Template DNA 1 U Phusion DNA Polymerase H_2O to a final volume of 50 µl	1× GoTaq master mix 1µM forward primer 1 µM reverse primer <250 ng Template DNA H_2O to a final volume of 50 µl

Programs for PCR reaction with CombiZyme Polymerase Mix, GoTaq green Master Mix or Phusion Polymerase:

Steps	CombiZyme	Phusion	GoTaq
Initial denaturation	95ºC for 2 min	98ºC for 2 min	95ºC for 5 min
Denaturation	94ºC for 30-60 s	98ºC for 10 s	95ºC for 15s
Annealing	60-70ºC for 1 min	58-65ºC for 15-30 s	3ºC below the calculated melting temperature of the primers
Extension	72ºC for 1 min	72ºC for 30-45 s/1kb	72ºC for 1 min/1kb
Cycles	25-35	25-30	25-30
Final extension	72ºC for 5 min	72ºC for 5 min	72ºC for 5 min
Storage	12ºC	12ºC	12ºC

2.2.4.3 General DNA cloning methods

Gel extraction:

DNA fragments were purified from agarose gels using the QIAquick Gel Extraction Kit (Qiagen) according to the manufacturer's instructions.

Plasmid linearization and dephosphorylation:

Vectors used for cloning were linearized with the appropriate restriction enzymes and 5'-phosphates were removed when necessary using Shrimp Alkaline Phosphatase (Promega). Both restriction enzymes and SAP were heat-inactivated for 15 min at 65ºC.

Ligation:

Insert restriction fragments were ligated into the linearized and dephosphorylated vectors using T4 DNA Ligase (BioLabs) in 20 µl reaction volume overnight at 16ºC. T4 DNA Ligase was inactivated by heating at 65ºC for 15 min and the vectors were transformed into chemically competent *E. coli* cells.

E. coli transformation:

XL-10 gold or Topo10 chemically competent *E. coli* cells were thawed on ice, 200-400 ng of plasmid DNA were added to 50 µl cells and incubated on ice for 30 min. The heat shock step was carried out at 42ºC for 30 s, 250 µl SOC-Medium was added and the cells were incubated at 37ºC for 1 h on a shaker. 100 µl from transformed bacterial cells were plated onto LB-plates containing ampicillin (100 µg/ml) or kanamycin (30 µg/ml) to select transformed bacteria. Plates were incubated at 37ºC overnight. Individual colonies were picked and grown in LB-medium with appropriate antibiotics for plasmid DNA preparation.
 Extraction of plasmid DNA:

Small-scale preparations of plasmid DNA were performed in 3 ml of LB-medium by Plasmid-Mini Kit (SeqLab). Medium culture (25 ml) or large culture (100-200 ml) preparations were carried out using Plasmid-Midi and Plasmid-Maxi kits (NucleoBond Macherey-Nagel) respectively, according to the manufacturer's protocols.

Restriction enzyme digestion:

To check the presence and the orientation of the insert of interest, plasmid DNA was digested with the appropriate restriction endonucleases at 37º C for 1-2 hours in 10-30 µl reaction volume. The product size and orientation was analyzed by agarose gel electrophoresis using 100-bp DNA Ladder, extended (Roth). For pC3xFLAG-Fusion proteins DNA Sequencing was performed by Sequenzierservice ABI BigDye-Terminator-Chemie, SMB Services in Molecular Biology (Berlin).

2.2.5 Plasmid constructs cloned for this work

For some molecular cloning, like the modification of the peGFP-C1 vector, insertion of artificial miRNA binding sites and miRNA sponge binding sites, pairs of synthetic oligonucleotides were used. Both single stranded oligonucleotides were designed in such a

way that annealing of both leads to a double-stranded oligonucleotide with certain restriction site overhangs. After linearization of the vector with corresponding restriction enzymes the double stranded oligonucleotide was inserted with T4-DNA ligase.

The annealing of both oligonucleotides was performed in an eppendorf tube containing both oligonucleotides (5µM each), 500 µl H_2O and 1x Taq PCR buffer. The reaction mix was incubated in a heating block for 2 min at 95°C and cooled down slowly at room temperature. For a 10µl ligation 2µl of the reaction mix was used.

2.2.5.1 Modification of the eGFP-C1 vector

In a first step, the annealed BglII-Stop--Not-HindIII oligonucleotide (shown in Table 2.1.5a) was ligated into the BglII/BamHI linearized peGFP-C1 vector in order to insert a stop codon and a NotI restriction site upstream of the multiple cloning site of the eGFP gene. To allow generation of tandem repeats of miRNA binding sites or miRNA sponge sites the peGFP vector was again modified. A double stranded oligonucleotide bearing a XhoI restriction site (shown in Table 2.1.4a) was inserted into the NotI/HindIII digested vector. This modified peGFP-C1 vector was renamed as pXho. A detailed scheme of these modifications is shown in Figure 3.1.1a.

2.2.5.2 Generation of miRNA sensor constructs and miRNA sponges

In order to generate miRNA sensor and miRNA sponges vector constructs with multiple binding sites the modified eGFP-C1 vector, pXho was used. The pXho vector contains downstream of the ribosomal stop codon the multiple clowning site: NotI-XhoI-HindIII-EcoRI-PstI-SalI whereas XhoI and SalI generate compatible overhangs. The insert of a pXho vector bearing an insert between the XhoI and SalI restriction site, can be duplicated due to vector linearization with NotI and XhoI and insert digestion with NotI and SalI with ongoing ligation. After each cloning step the number of inserts double and can be repeated as often as desired. The eGFP-miRNA sensor and eGFP-miRNA sponge constructs that were generated with this cloning strategy are listed in the following tables (A detailed scheme of this cloning strategy is also shown in Figure 3.1.1.2.

GFP-miRNA sensors:	Number of binding sites	Cloning stategy
GFP-let-7	1	Insertion of a let-7aBS (shown in Table 2.1.4b) into EcoRI/SalI digested pXho
GFP-2xlet-7	2	Excision of let-7 binding site with NotI/SalI out of GFP-let7→ Insertion into NotI/XhoI digested GFP-let-7
GFP-miR-124	1	Insertion of a miR-124BS (shown in Table 2.1.4b) into EcoRI/SalI digested pXho
GFP-2xmiR-124	2	Excision of miR-124 binding site with NotI/SalI out of GFP-miR124→ Insertion into NotI/XhoI digested GFP-miR-124
GFP-4xmiR-124	4	Excision of 2xmiR-124 binding site with NotI/SalI out of GFP-2xmiR-124→ Insertion into NotI/XhoI digested GFP-2xmiR-124
GFP-miR-125	1	Insertion of a miR-125BS (shown in Table 2.1.4b) into EcoRI/SalI digested pXho
GFP-2xmiR-125	2	Excision of miR-125 binding site with NotI/SalI out of GFP-miR125→ Insertion into NotI/XhoI digested GFP-miR-125
GFP-4xmiR-125	4	Excision of 2xmiR-125 binding site with NotI/SalI out of GFP-2xmiR-125→ Insertion into NotI/XhoI digested GFP-2xmiR-125
GFP-miR-128	1	Insertion of a miR-128BS (shown in Table 2.1.4b) into EcoRI/SalI digested pXho
GFP-2xmiR-128	2	Excision of miR-128 binding site with NotI/SalI out of GFP-miR128→ Insertion into NotI/XhoI digested GFP-miR-128
GFP-4xmiR-128	4	Excision of 2xmiR-128 binding site with NotI/SalI out of GFP-2xmiR-128→ Insertion into NotI/XhoI digested GFP-2xmiR-128

GFP-sponge miRNA vectors	Number of sponge binding sites	Cloning strategy
GFP-sp_let-7	64x let-7	1) Insertion of 2xLET7SP cassette (shown in Table 2.1.4c) into HindIII/SalI digested pXho→ pXho-2xlet-7sp 2) Cloning strategy was performed as previously described for GFP-miRNA sensors 5 times to generate GFP-sp_let-7 with 64 binding sites
GFP-sp_miR-125	32x miR-125	1) Insertion of 2xMIR-125SP cassette (shown in Table 2.1.4c) into HindIII/SalI digested pXho→ pXho-2xmiR-125sp 2) Cloning strategy was performed as previously described 4 times to generate GFP—sp_miR-125 bearing 32 binding sites
GFP-sp_miR-29	16x miR-29	1) Insertion of 2xMIR-29SP cassette (shown in Table 2.1.4c) into HindIII/SalI digested pXho→ pXho-2xmiR-29sp 2) Cloning strategy was performed as previously described 3 times to generate GFP-sp_miR-29 bearing 32 binding sites
GFP-sp_miR-125/ let-7	32x miR-125 + 32x let-7	1) Excision of 2xmiR-125sp cassette with NotI/SalI out of GFP-2xmiR-125sp→ Insertion into NotI/XhoI cutted GFP-2xlet-7sp 2) Cloning strategy was performed as previously described 4 times to generate GFP—sp_miR-125/let-7 vector bearing 32 binding sites for miR-125 and let-7

2.2.5.3 miRNA target gene constructs

3'UTRs of target genes, in order to generate GFP-target gene constructs, were directly amplified from mouse genomic DNA with GO-Taq Polymeras and Primersb shown in Table 2.1.4d. Beside the FoxP2 and Lin-28 PCR product, which were digested and ligated directly into the digested pXho vector, all other PCR-fragments were pre-cloned into the pCR2.1-TOPO vector. For each PCR product the correct insert size and its orientation within the TOPO vector was confirmed by restriction analysis. With appropriate restriction enzymes the

insert with small parts of the flanking TOPO vector was digested and ligated in the appropriate digested pXho vector. The Fox-P2 PCR fragment was directly digested with XhoI and KpnI while the PCR of Lin-28 was digested with EcoRI and BamHI. Both digested inserts were ligated into the appropriate linearized pXho vector.

For each GFP-target gene sensor construct the amplified part of the 3'UTR, including predicted miRNA binding sites of our interest, is schematically shown in Chapter 3.3.3.

2.2.5.4 Generation of premiRNA-RED constructs

In order to overexpress miRNAs based on expression plasmids we obtained two plasmids with different promoters (CMV and CAGGS) bearing an intron within the dsRED gene (vector maps are shown in Section 2.1.4). The CMV-intron-Red plasmid contained two unique restriction sites, Sac2 and NotI, within the intron. The intron of CAGGS-intron Red plasmid beared the two unique restriction sites PmeI and NotI. In order to clone stem loop precursors from let-7a, miR-128 and miR-29a into the intron-RED plasmids primers flanking 120 bp up and downstream of the loop precursors with added restriction sites were designed. PCR products were amplified from mouse genomic DNA and afterwards digested. After purification on a 1.5 % agarose gel, the fragments were ligated into the appropriate digested intron-RED plasmids. The lower Table shows all generated intron-RED constructs. The sequence of the primers are previously shown in Table 2.1.4e. A schematic of the expression strategy is shown in Figure 3.1.2.1.

Vector name	Inserted sequence (length)	Inserted with RE	Backbone vector
CMV-prelet-7a-RED	8790795-8790509 of NT_039580.7 (286 bp)	SacII and NotI	CMV-intron-Red
CAGGS-prelet-7a-RED	8790795-8790509 of NT_039580.7 (286 bp)	PmeI and NotI	CAGGS-intron Red
CMV-premiR128-RED	42755168-42755401 of NT_078297.6 (233bp)	SacII and NotI	CMV-intron-Red
CAGGS- premiR128-RED	42755168-42755401 of NT_078297.6 (233bp)	PmeI and NotI	CAGGS-intron Red
CAGGS- premiR29a-RED	260035- 259789 of NT_039341.7 (246bp)	PmeI and NotI	CAGGS-intron Red
CAGGS-premiR-124	Obtained by Eugene Makedev and Tom Maniatis (described in (Makeyev et al., 2007))		CAGGS-intron Red

2.2.5.5 Generation of pC3xFlag-fusion-protein constructs and site directed mutagenesis of pC3xFLAG-Lin-41

Two FLAG-tagged fusion-protein constructs were generated for this thesis: pC3xFLAG-Lin-41 and pC3xFLAG-Lin-28. The 630 nt long ORF of Lin-28 was directly amplified with the primers Lin28fwdNotI and Lin28revBamHI (shown in Table 2.1.4f) from mouse cDNA. The PCR fragment was cloned into pCR.2.1-TOPO, excised with NotI and BamHI and ligated into NotI/BamHI linearized pC3xFLAG vector.

In order to generate the 2568nt long Lin-41 ORF, several cloning steps were performed as illustrated in Figure 2.2.5.5. Several truncated Lin-41 sequences of the ORF (shown in Panel a of Figure 2.2.5.5) were used: Topo-Lin-41#9 bears the 5'-sequence, PCR Aga1+4 the 3'-sequence and TOPO-6-6 the intermediate sequence of the mLin-41 ORF. In a first step the
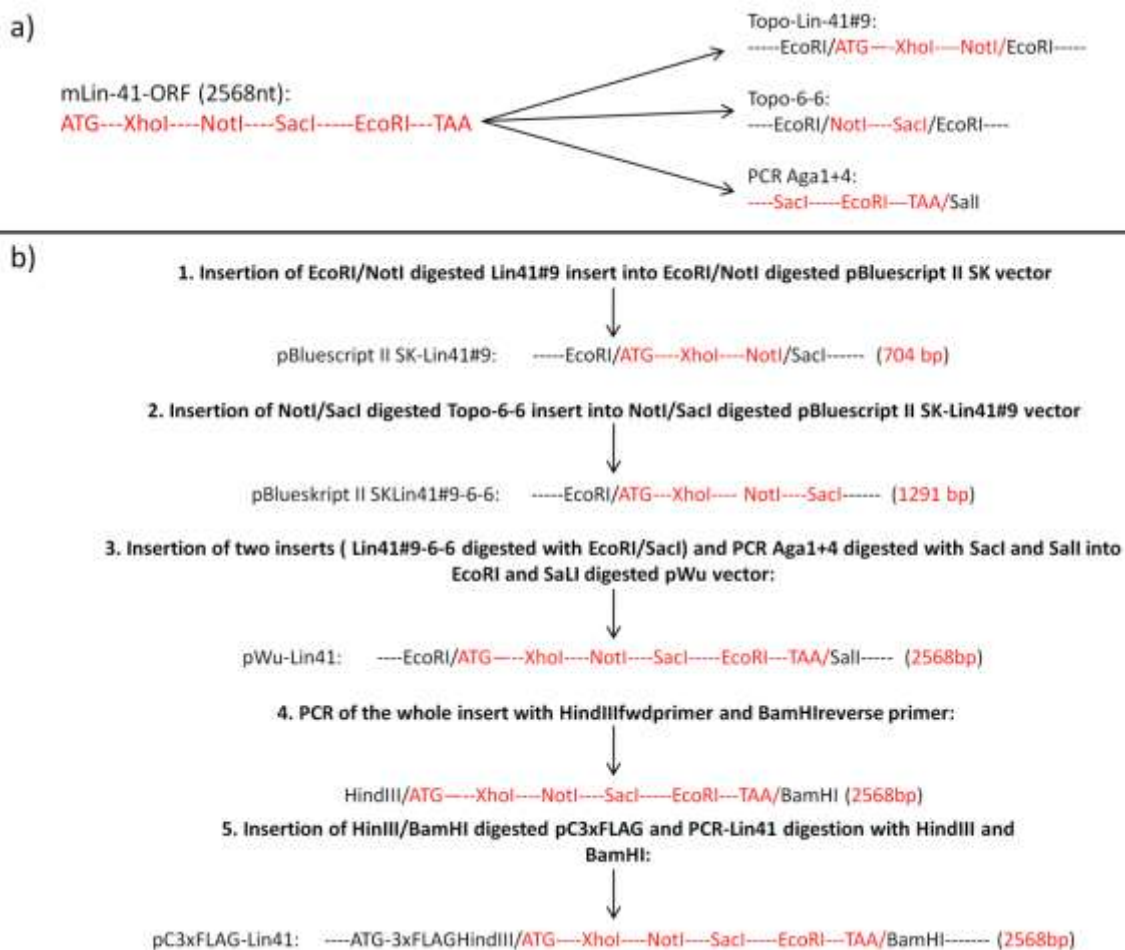

Figure 2.2.5.5: Generation of the pC3xFLAG-Lin41 construct a) Schematic illustration of the mLin-41 open reading frame (ORF) with unique restriction sites is shown on the left side. Truncated mLin-41 DNA sequences that were available to generate the whole ORF are displayed on the right. **b)** Cloning procedures which were performed in order to generate pC3xFLAG-Lin-41. Sequence and unique restriction sites of mLin-41 are highlighted in red letters. Unique restriction sites of plasmids are shown in black letters.

5'-sequence was excised with EcoRI/NotI and inserted into the appropriate cut pBluescript II SK plasmid (Step 1 in Figure 2.2.5.5). The SacI restriction site downstream of the NotI site from the new generated pBluescript II SK-Lin-41#9 allowed the insertion of the NotI/SacI cut intermediate sequence from TOPO-6-6 into pBluescript II SK-Lin-41#9. In a next step a triple Ligation was performed: the extended insert of pBluescript II SK-Lin-41#9-6-6 was excised with EcoRI and SacI and the SacI/SalI cut PCR AGA1+4 fragment was ligated into EcoRI/SalI linearized pWu vector (Step 3 of Figure 2.2.5.5). The pWu-Lin-41plasmid contained full length open reading frame. Next, a PCR was performed to flank the Lin-41 ORF with appropriate restriction sites (HindIII and BamHI). Because of the very high GC content within the 5'-sequence of Lin-41, 10% Betaine was added to the Phusion-PCR reaction mix to reduce secondary structure caused by its GC-rich region. The PCR fragment was digested with HindIII/BamHI and inserted in frame into the HindIII/BamHI linearized pC3xFLAG plasmid. The correctness of the ORF was verified by sequencing.

Mutagenesis of pC3xFLAG Lin-41:

To generate inactivating mutations in the RING domain of pC3xFLAG-Lin-41 the first two cysteine residues of the ring domain of pC3xFLAG- Lin-41 construct were exchanged to Leucin and Alanin. Therefore an internal BglII fragment was replaced with a PCR fragment generated using the forward mutagenesis primer Linmutfwd and the reverse primer Linmutrev (2.1.4g) and pc3xFLAG-Lin41 as a template to substitute Cys 12 for Leu and Cys 15 for Ala. The mutagenesis was verified by sequencing.

3. Results

3.1 Genetic tools to study miRNA functions

One major part of this thesis concerns the generation and validation of tools to detect and quantify miRNA activity in various cell types. Several of these strategies were then employed in the experimental validation of predicted miRNA target genes. Our group has chosen 4 mouse miRNA families for study: let-7/miR-98, miR-125/miR-351, miR-124 and miR-128. The mouse let-7/miR-98 family consists of 11 different let-7 gene loci and one locus for the related miR-98. The miRNA precursor encoded at each locus can be processed, leading to generation of eight different mature miRNAs (let-7a-g+let-7i) which share the same sequence in the 5'- region (nucleotides 1-8) (displayed in table 3.1.1.1). The miR-125/miR-351 family includes three different gene loci which are processed in two different mature miRNAs (miR-125a+b) and one miR-351 precursor. The mature unique miR-124 is encoded by three different and the mature unique miR-128 by two loci. The detailed mature sequence for all investigated miRNA families is shown in table 3.1.1.1. The let-7/miR-98 and miR-125/miR-351 family are expressed in many tissues, including the CNS, during early embryonic development. The miR-124 and miR-128 families are mainly restricted to neuronal development (Lagos-Qintana 2002; Smirnova 2005; Wulczyn 2007). To study miRNA activity and validate putative miRNA target sites in various cell types, GFP-sensor constructs were generated that are described in chapter 3.1.1. Misexpression tools to study miRNA function by miRNA over-expression are described in Chapter 3.1.2. Chapter 3.1.3 deals with plasmid-based tools to specifically inhibit endogenous miRNAs.

3.1.1 GFP sensor constructs: a tool to detect miRNA activity

Green fluorescent protein (GFP) has gained widespread use as a tool to visualize spatial and temporal patterns of gene expression *in vivo*. To use GFP as a so-called miRNA sensor, the CMV-eGFP-C1 vector from Clontech was chosen.
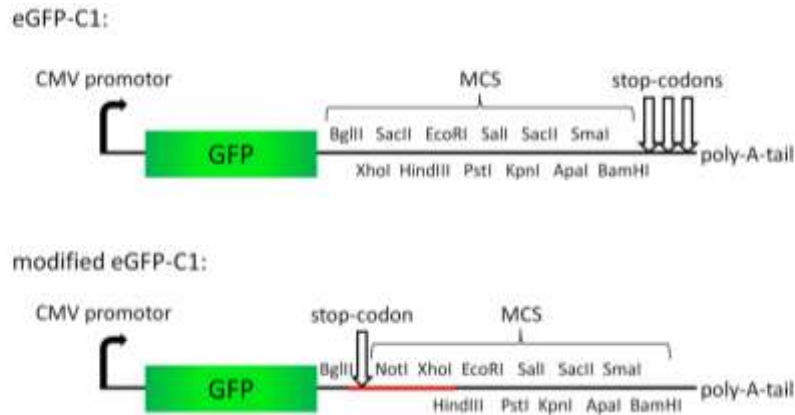

Figure 3.1.1a: Modification of the CMV-eGFP-C1 vector from Clontech To terminate translation proximal to the MCS in the 3' UTR of the eGFP gene an oligonucleotide containing a stop codon, NotI and XhoI restriction sites was inserted between the BglII and HindIII restriction sites in the vector. The inserted sequence is highlighted in red.

CMV-eGFP-C1 was originally generated to study N-term GFP-tagged fusion proteins in eukaryotic cells. A stop codon (taa) followed by NotI and XhoI restriction sites was inserted between the BglII and HindIII sites. This modification insured that ribosomes would not read through into the multiple cloning sites, allowing their use for the cloning of regulatory sequences (Figure3.1.1a) such as artificial miRNA binding sites or whole or partial 3'-UTRs of putative miRNA target genes. Inserted miRNA binding sites in the 3'-UTR of the GFP gene should mimic translational repression by miRNA. In this approach the GFP gene can be used as a quantitative reporter of gene expression (Smirnova et al., 2005).

3.1.1.1 GFP sensor constructs with artificial binding sites

To use the modified eGFP construct as a sensor for a distinct miRNA, synthetic oligos were inserted into the multiple cloning site to generate miRNA binding sites with the maximal possible sequence complementarity to the miRNA of interest. Binding sites for let-7a, miR-124, miR-125a and miR-128b were designed and inserted into the modified eGFP vector. The miRNA binding sites and corresponding miRNAs are displayed in Figure 3.1.1.1. An artificial binding site which is 100% complementary to a miRNA would form in the presence of that miRNA a double-stranded RNA duplex and undergo RNAi-induced silencing. Binding of other miRNA family members would also lead, because of their high complementarity, to a strong translation repression of the GFP gene. Therefore an eGFP sensor with an artificial miRNA binding site should show a much more sensitive response in contrast to a natural miRNA binding site.
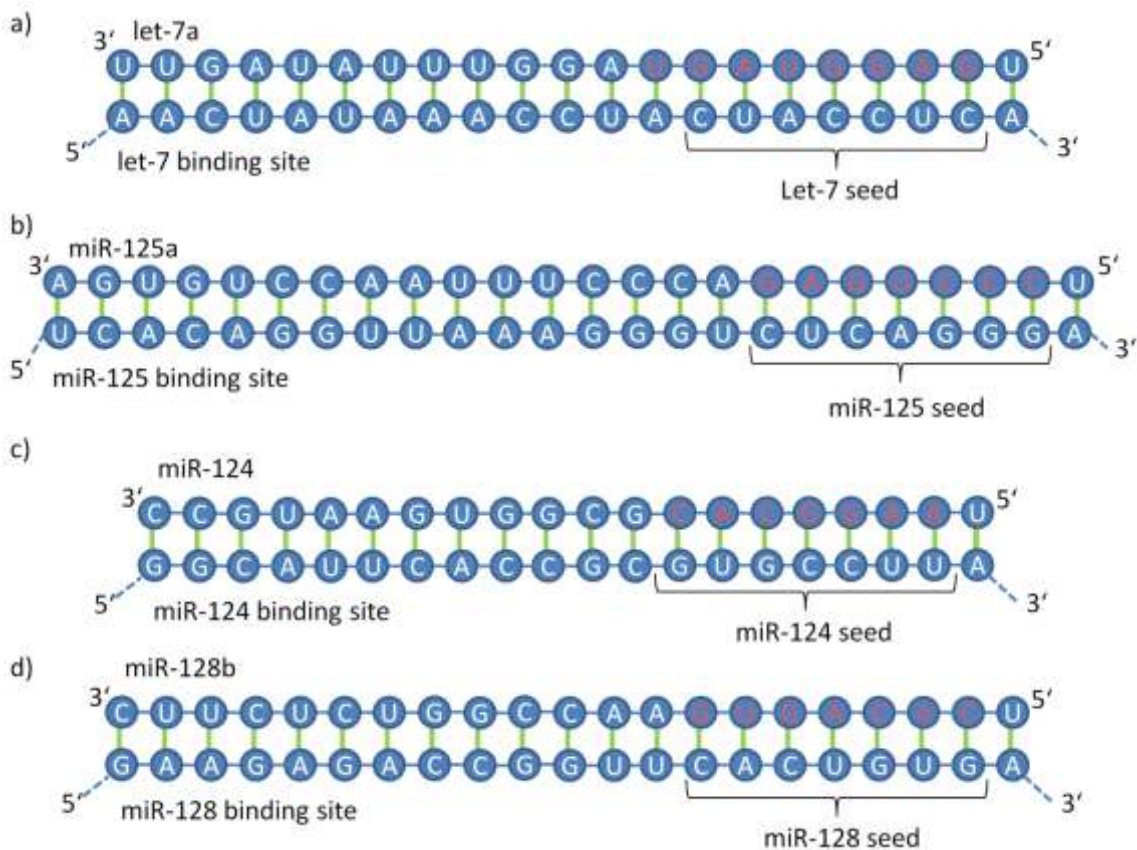

Figure 3.1.1.1: Sheme of miRNA-mRNA binding site duplexes for let-7, miR-125, miR-124 and miR-128 miRNA binding sites and members of each miRNA family which show 100% complementarity to the site are illustrated. The seed region for each miRNA is indicated in red letters.

To reduce the possiblity that the binding sites which were used to generate GFP sensor constructs might be recognized by other miRNAs each miRNA binding site was scanned for putative miRNA interaction partners. The miRNA search tool Microinspector V.1.5 (http://bioinfo.uni-plovdiv.bg/microinspector/) was used. The results are listed in Table 3.1.1.1

using a hybridization temperature of 37°C and < -20 kcal/mol as a cut off value for free energy.

Table 3.1.1.1: miRNA interactions for each binding site as calculated by Microinspector. Results are calculated using a hybridization temperature of 37°C and -20 kcal/mol as a cut off value for free energy. The miRNA seed regions are highlighted in red letters. **a)** For the let-7 binding site Microinspector identified all members of the let-7 miRNA family (let-7a-g+i) and miR-98. **b)** In addition to miR-125a and miR-125b, miR-351 is predicted to bind to the miR-125 binding site. All three share a common seed sequence. **c)** Microinspector identified the miR-124 binding site as a unique binding site for miR-124. **d)** For the miR-128 binding site an additional miRNA, miR-27 was predicted as an interaction partner.

a) let-7 binding site

miRNA	SEQUENCE OF MIRNA	FREE ENERGY (kcal/mol)
mmu-let-7a	UGAGGUAGUAGGUUGUAUAGUU	-39.2
mmu-let-7b	UGAGGUAGUAGGUUGUGUGGUU	-38.6
mmu-let-7c	UGAGGUAGUAGGUUGUAUGGUU	-38.6
mmu-let-7d	AGAGGUAGUAGGUUGCAUAGUU	-35.4
mmu-let-7e	UGAGGUAGGAGGUUGUAUAGUU	-34.9
mmu-let-7f	UGAGGUAGUAGAUUGUAUAGUU	-32.7
mmu-let-7g	UGAGGUAGUAGUUUGUACAGUU	-28.6
mmu-miR-98	UGAGGUAGUAAGUUGUAUUGUU	-27.9
mmu-let-7i	UGAGGUAGUAGUUUGUGCUGUU	-27.1

b) miR-125 binding site

NAME OF MIRNA	SEQUENCE OF MIRNA	FREE ENERGY (kcal/mol)
mmu-miR-125a	UCCCUGAGACCCUUUAACCUGUGA	-49.9
mmu-miR-125b	UCCCUGAGACCCUAACUUGUGA	-40.3
mmu-miR-351	UCCCUGAGGAGCCCUUUGAGCCUG	-36.4

c) miR-124 binding site

NAME OF MIRNA	SEQUENCE OF MIRNA	FREE ENERGY (kcal/mol)
mmu-miR-124	UAAGGCACGCGGUGAAUGCC	-43.5

d) miR-128 binding site

NAME OF MIRNA	SEQUENCE OF MIRNA	FREE ENERGY
mmu-miR-128	UCACAGUGAACCGGUCUCUUU	-41.7
mmu-miR-27b	UUCACAGUGGCUAAGUUCUGC	-20.1

The table reveals that the let-7 binding site seems to be a specific target for the whole let-7 miRNA family and miR-98. Because of its identical seed region (GAGGUAG) and overall sequence similarity, miR-98 is considered to be a let-7 family member (Hayes et al., 2006). A similar argument can be made for miR-351 and the miR-125 family. In contrast, miR-128 and miR-27b constitute an exception. The seed sequences of miR-128 (CACAGUG) and miR-27 (UCACAGU) overlap, but are not identical. Moreover, their expression pattern is very different. It has been shown that miR-27 is expressed in early osteoblast differentiation while miR-128 is mainly restricted to neurons (Smirnova et al., 2005; Wang and Xu, 2010).

3.1.1.2 Generating GFP constructs with multiple copies of miRNA binding sites

Studies have shown that the 3'-UTRs of many miRNA target genes often contain multiple binding sites (Lewis et al., 2003). Furthermore it has been shown with truncated 3'-UTRs of miRNA target genes that multiple miRNA binding sites exert a synergistic effect on miRNA mediated repression (Grimson et al., 2007). To maximize the sensitivity of the miRNA sensor

constructs, the following cloning strategy was used to generate tandem repeats of each miRNA binding site (see Figure 3.1.1.2).
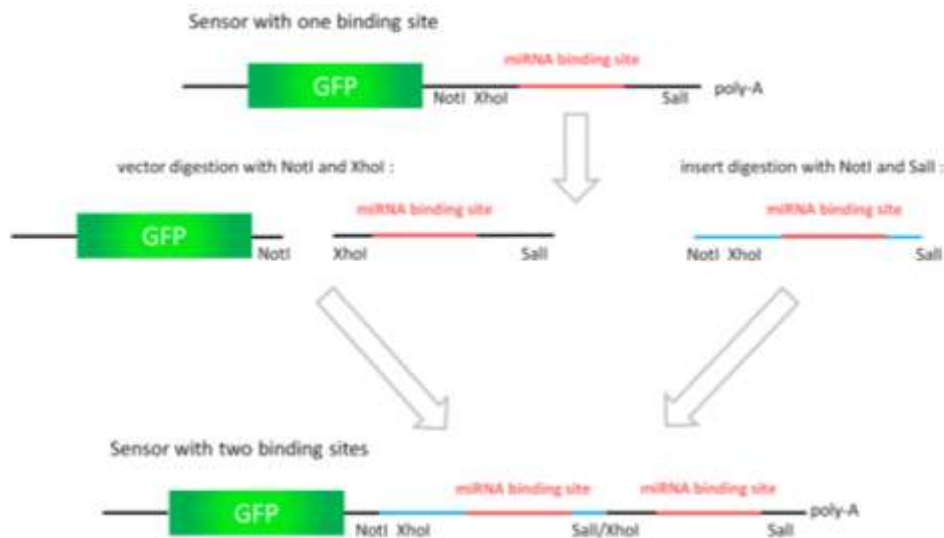

Figure 3.1.1.2: Cloning strategy for generating eGFP sensor constructs with multiple tandem copies of miRNA binding sites of interest. An eGFP vector bearing a binding site of interest was linearized with NotI and XhoI restriction enzymes. A fragment bearing the miRNA binding site was isolated after digestion with NotI and SalI. Ligation of the NotI/XhoI linearized vector and the NotI/SalI digested insert results in an eGFP-sensor with a duplication of the miRNA binding sites.

This cloning strategy can then be repeated as often as desired, each time doubling the number of binding sites.

3.1.1.3 GFP sensor constructs with 3'-UTR of target genes

In order to test bioinformatic predictions of miRNA target genes, sequences from the 3'-UTR of candidate genes were amplified by PCR and inserted into the 3'-UTR of the eGFP gene of the modified eGFP-C1 reporter plasmid as displayed in Figure 3.1.1.2. The amplified sequences were chosen to minimize the possibility of repression by other miRNAs, and were confined to those portions of the 3'-UTR containing clusters of putative binding sites.
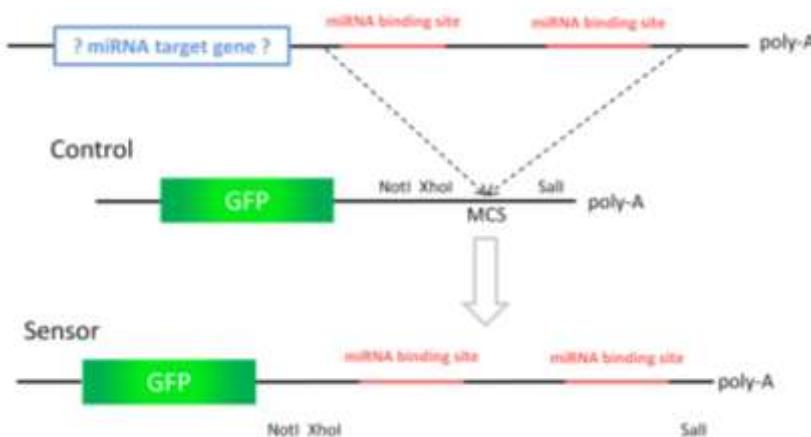

Figure 3.1.1.2: A cloning strategy to study regulation of distinct genes by miRNA Whole or partial sequences of 3'-UTRs bearing putative miRNA regulated sequences were inserted into the 3'UTR of the GFP gene of the modified eGFP-C1 vector. The GFP gene without any additional sequence in the 3'-UTR was used as a control.

3.1.2 Overexpression of miRNAs

In *C. elegans*, the temporal regulation of miRNA expression is a critical feature of the developmental pathways controlled by let-7 and lin-4 (homolog of the vertebrate miRNA miR-125). Overexpression-studies are one the major tools to study the effects of temporal misexpression on observable phenotypes in developmental assays.

3.1.2.1 Over-expression of miRNAs with synthetic precursor miRNA

"Pre-miR™ miRNA Precursor Molecules" from Ambion were used to overexpress miRNA in different cell lines. These artificial miRNAs mimics are small, chemically modified double-stranded RNA molecules designed and modified to ensure that the correct strand, representing the desired mature miRNA, is taken up into the RNA-induced silencing-like complex responsible for miRNA activity. The advantages of the ds-RNA molecules are that they are easier to transfect than vectors and can be used in dose response studies. In table 3.1.2.1 all Pre-miR™ miRNAs that were used are displayed.

Table 3.1.2.1: Synthetic miRNA precursors that were used for miRNA overexpression. The table shows the name of the mature sequence (based on nomenclature by Sanger) and their sequences.

miRNA	mature miRNA sequence
mmu-let-7a	UGAGGUAGUAGGUUGUAUAGUU
mmu-let-7c	UGAGGUAGUAGGUUGUAUGGUU
mmu-let-7e	UGAGGUAGGAGGUUGUAUAGUU
mmu-miR-125b	UCCCUGAGACCCUAACUUGUGA
mmu-miR-128a	UCACAGUGAACCGGUCUCUUU

We used these pre-miRNAs mainly to validate putative target genes. Therefore GFP-sensor constructs bearing artificial binding sites or 3'-UTR of putative target genes (described in detail in chapter 3.1.1) were co-transfected with synthetic precursor-miRNA specific for the target gene (Figure 3.1.2.1a). As a control the GFP-sensor was co-transfected with a pre-miRNA that is not predicted to bind to the target sequence (Figure 3.1.2.1).
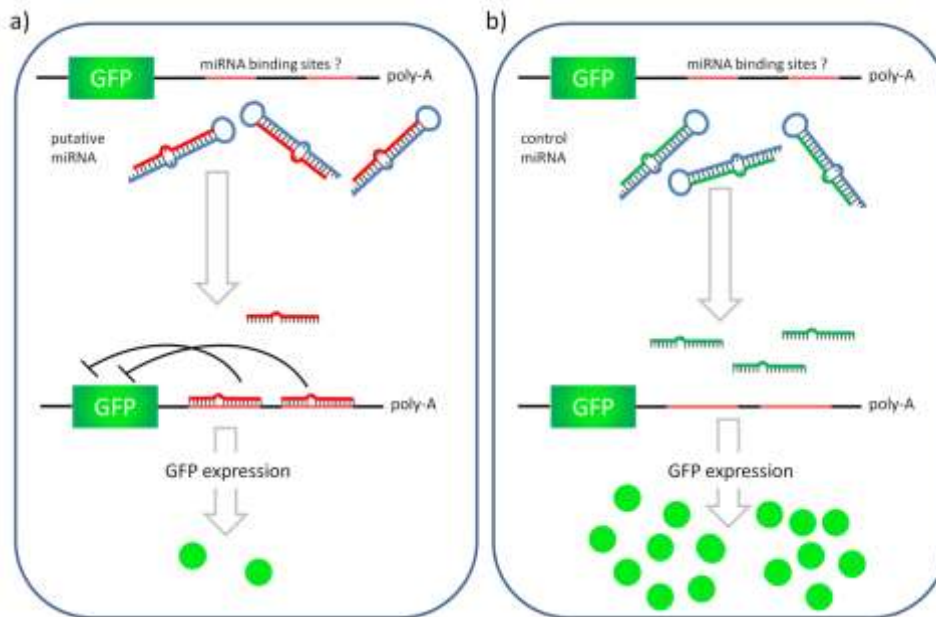
Figure 3.1.2.1: A genetic tool to validate miRNA regulated target genes a) A GFP plasmid bearing putative miRNA binding sites in the 3'-UTR of the modified eGFP gene was co-transfected with the corresponding synthetic precursor miRNA. Binding of processed miRNAs will result in translational repression of the GFP sensor and therefore a measurable decrease of GFP fluorescence compared to the control transfection shown in b. **b)** As a control, the same GFP sensor was co-transfected together with a non-corresponding pre-miRNA. The mature miRNA is not able repress the GFP gene yielding a background value for GFP expression.

3.1.2.2 Overexpression of miRNA with Intron-Red miRNA precursor constructs

A second strategy to overexpress miRNAs was based on a dsRed-expression plasmid. This strategy has the advantage of simultaneously marking transfected cells to allow tracing *in vivo*. For this purpose, we obtained a plasmid bearing an intron within the dsRED gene from Eugene Makeyev and Tom Maniatis (Makeyev et al., 2007). In this intronic sequence a stem loop precursor miRNA of interest can be inserted as displayed in Figure 3.1.2.2a.
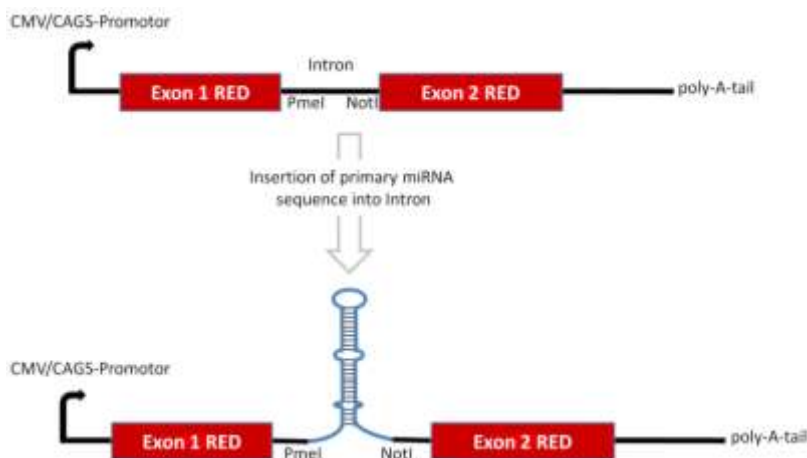

Figure 3.1.2.2a: Part of the "Intron-Red" vector showing the dsRED gene. An intron was placed between Exon1 and Exon2 of the dsRED gene bearing two unique restriction sites (PmeI and NotI). The Intron-RED vector was used to clone stem loop precursors of the miRNA of interest into the intron of the dsRED gene.

The intron-RED construct was available with two different promoters: CMV and ßActin-promoter with intronic enhancer elements (CAG). The constructs were designated as CMV-intron-RED or ßAct-intron-RED. Stronger over-expression was achieved with the ßActin-

promoter. These vectors were used for transfection in P19, E12 neural progenitor and HEK293 cells. Furthermore these construct were electroporated in the chick neural tube *in ovo* and in the mouse embryonic brain *in utero.*
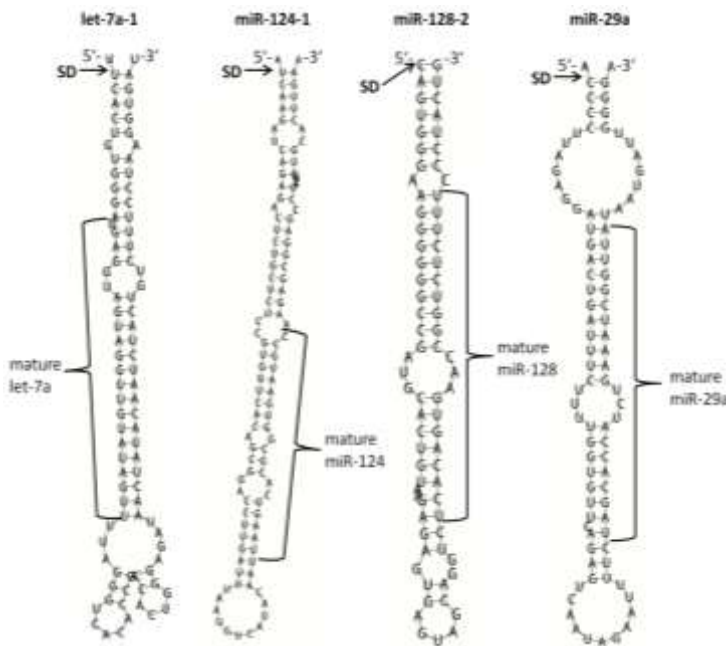

Figure 3.1.2.2b: Stem loop precursor structures from mouse that were inserted into the Intron-RED vector. Sequences of pre-let-7a-1, miR-124-1, miR-128-2 and miR-29a with ~50nt of upstream and downstream flanking sequence containing the so-called single strand-double-strand (SD) junction were inserted into the intron of the dsRED gene of the vector Intron-RED. Calculation of the pre-miRNA structure was performed with RNAfold webserver.

In addition to the Intron-RED cloning vector and the pre-miR-124-intron RED construct obtained from Makeyev (Makeyev et al., 2007), we generated intron-RED constructs with stem loop precursors from let-7, miR-128 and miR-29a (Figure 3.1.2.2b). A schematic of the expression strategy is shown in Figure 3.1.2.1.
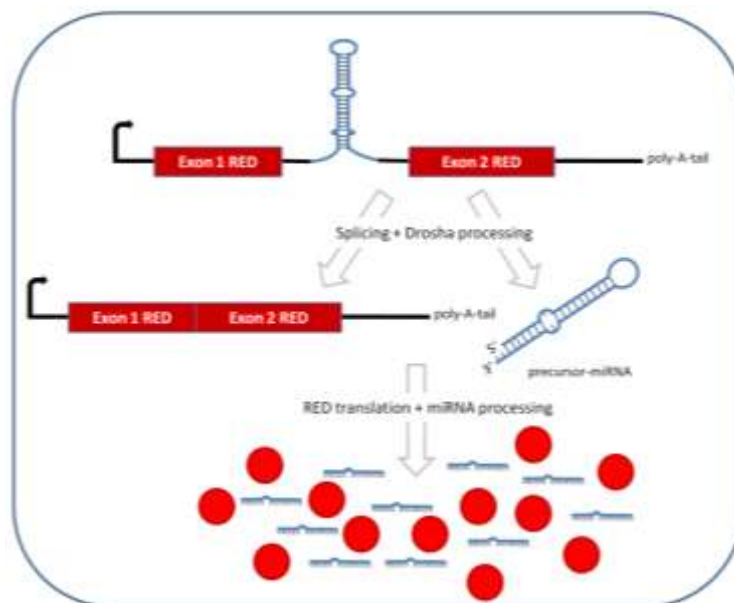
Figure 3.1.2.2c: Figure 3.1.2.1: A genetic tool for observing cells that over-express a distinct miRNA. A dsRED plasmid bearing the sequence of a stem loop miRNA precursor within an intron of the dsRED gene after transfection. After splicing and Drosha processing of the primary transcript, the dsRED-mRNA can be translated and the precursor-miRNA processed into its active form. Consequently the transfected RED fluorescent cell ectopically expresses the miRNA of interest.

3.1.3 Inhibition of miRNAs with GFP-sponge constructs

In order to inhibit endogenous miRNAs we generated GFP constructs with multiple tandem copies of imperfect miRNA binding sites in the 3'-UTR of the GFP gene to "mimic" a target gene. Between 16 and 64 imperfect miRNA binding sites with a high affinity to the miRNA were cloned using the method described in Chapter 3.1.1.2. The combination of high copy number and high affinity binding sites should sequester the endogenous miRNA, resulting in competitive inhibition of this miRNA and release of endogenous target mRNA repression (as shown in Figure 3.1.3.2a) (Ebert et al., 2007).
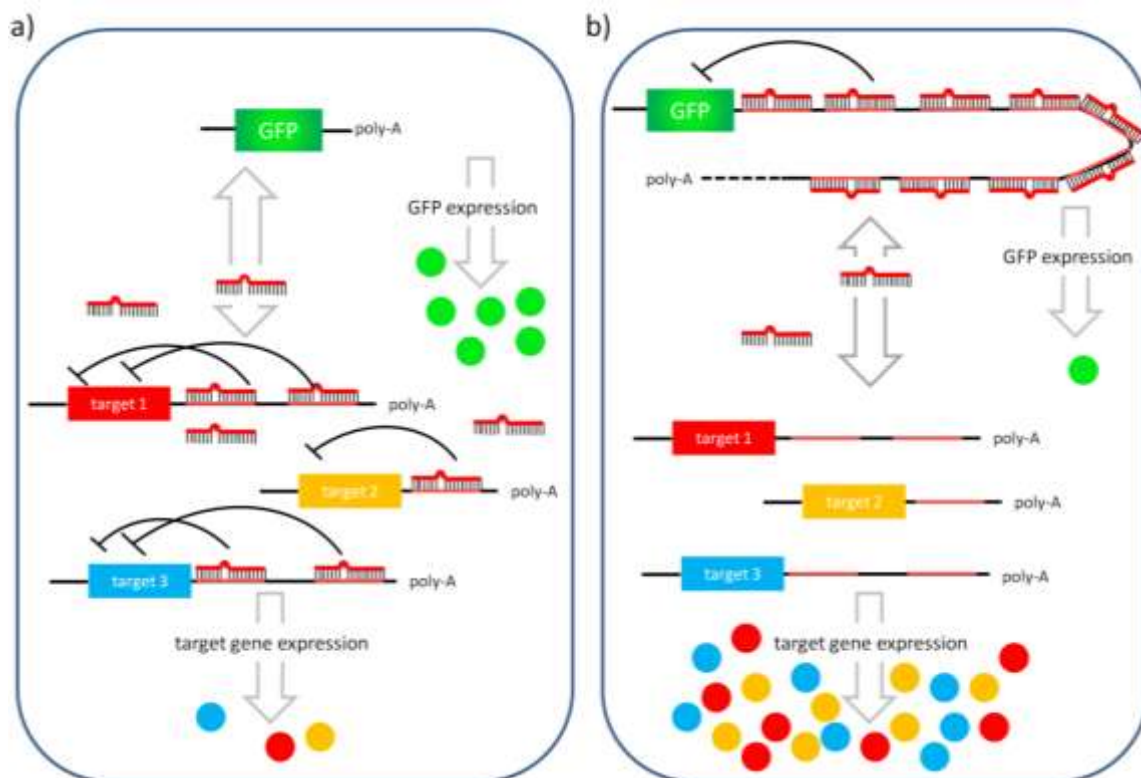

Figure 3.1.3.2a: "Knock-down" of an endogenous miRNA by competitive inhibition with a GFP-sponge construct a) Transfection of cells that show miRNA activity with the control plasmid expressing the eGFP gene has no effect on target gene expression: GFP is expressed and target genes are repressed by the endogenous miRNA. **b)** Transfection of the same cells with a GFP-miRNA sponge construct that codes for an eGFP gene bearing 16 to 64 imperfect binding sites for the endogenous miRNA competes with the target genes for the miRNA. Due to the high binding affinity and large number of sponge sites, the endogenous miRNA binds predominately to the sponge mRNA resulting in de-repression of the miRNA target genes.

In Figure 3.1.3.2b the miRNA binding sites that were used to generate the GFP-miRNA-"sponge" constructs with a corresponding binding representative for each miRNA family are shown. The mismatches were inserted to avoid rapid degradation the GFP-sponge mRNA by RNAi and to exclude binding of unwanted miRNAs. For example the mismatches in the miR-128 binding-site were positioned in the miRNA seed region to minimize unspecific binding of the related miRNA miR-27b. The miRNA specificity and binding energy was calculated with the web tool Microinspector.
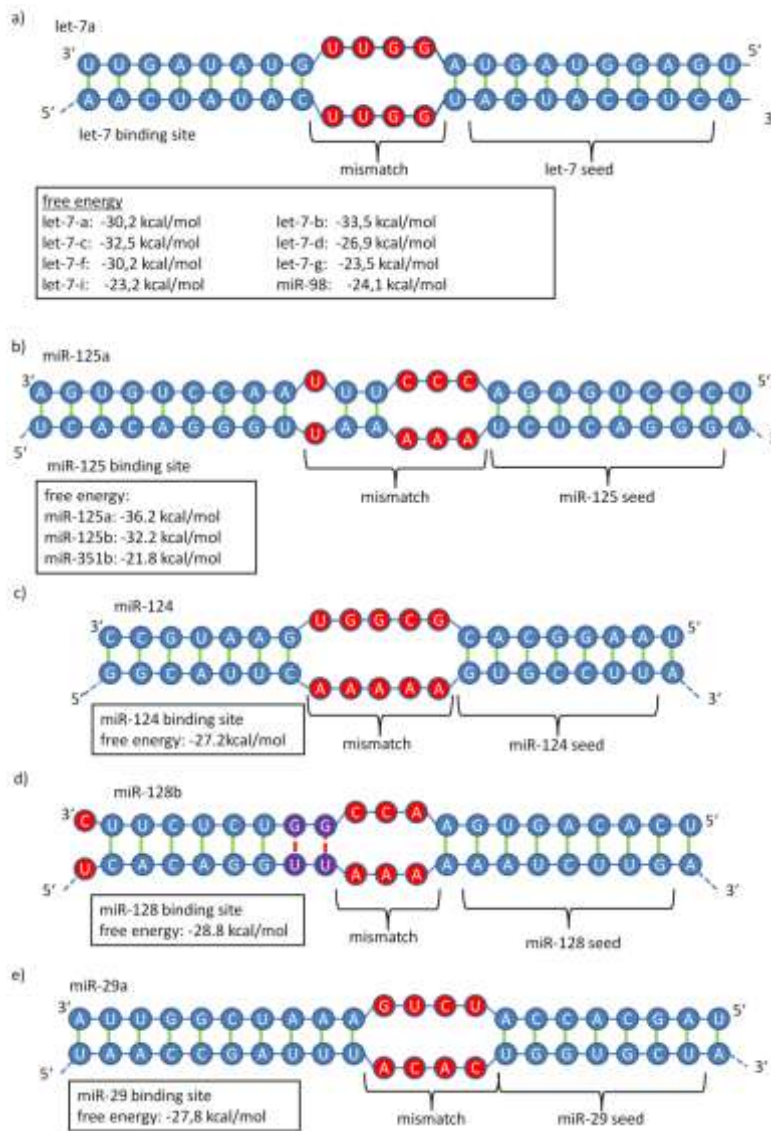
Figure 3.1.3.2b miRNA binding sites that were used to generate GFP-miRNA sponge constructs. All binding sites include in the middle of the sequence three to five mismatches (high-lighted in red) to their corresponding miRNAs. For all binding sites the maximum free energy for all miRNA interactions predicted by MicroInspector are shown.

a) Scheme of the let-7 binding site/let-7a duplex with four mismatches
b) Scheme of the miR-125 binding site/miR-125a duplex with four mismatches
c) Scheme of the miR-124 binding site/miR-124 duplex with four mismatches
d) Scheme of the miR-128 binding site/miR-128b duplex with five mismatches. In addition to the central mismatches, nucleotides at positions 1 (red) and 8-9 (violet) were designed to minimize rthe energy of binding for miR-27
e) Scheme of the miR-29a binding site/miR-29a duplex with 4 mismatches

Their ability to bind conjugate miRNAs was confirmed in a co-transfection assay with the conjugate pre-miRNA Red construct vs. non-conjugate pre-miRed construct in Hek293 cells. In all cases, the GFP expression of the GFP-sponges was significantly reduces by the conjugate pre-miR-RED vector (data not shown).

3.2 miRNA activity in different cell types

Preliminary experiments were performed to determine optimal conditions for the detection of miRNA activity using sensor plasmids. Criteria to be evaluated were choice of transfection reagent, cell density, time of incubation and amounts of sensor plasmid employed. The following is a description of the quantitative assay based on flow cytometry.

Cells co-transfected with GFP-sensor constructs and dsRED were incubated generally for 24 to 48h. The fluorescent intensity was measured by flow cytometry. Flow cytometry is a

technique for counting and examining cells by suspending them in a stream of fluid and passing them individually by an electronic detection apparatus. It allows simultaneous multiparametric analysis of the physical characteristics of up to thousands of cells per second. A laser light of a single wavelength is directed through the stream of fluid. A number of detectors are aimed at the point where the stream passes through the light beam: one in line with the light beam (Forward Scatter or FSC) and several perpendicular to it (Side Scatter (SSC) and one or more fluorescent detectors).
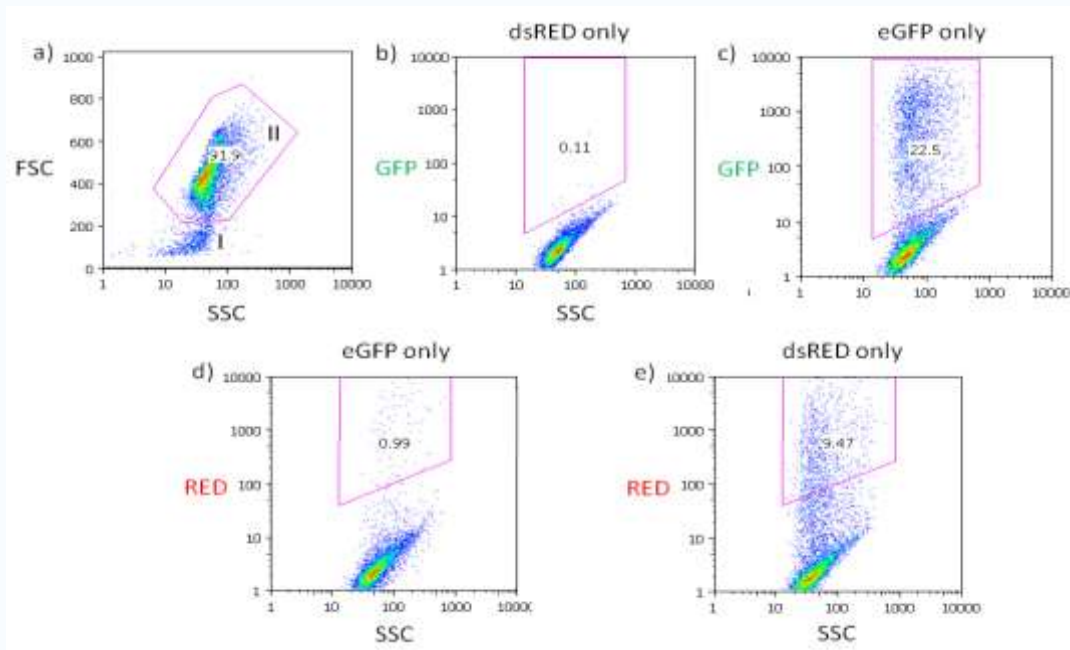

Figure 3.2.1a: Gating "living" fluorescent H293 cells with FLOWJO1.1 HEK293 cells were transfected with either 50ng eGFP or 200ng dsRED and harvested after 48h **a)** Comparison of the forward scatter (FSC) and the side scatter (SSC)b for each transfection reveals two distinguishable populations (I and II). Population I is composed of cell debris characterized by low FSC and broad SSC. Population II shows a much higher FSC and a narrower SSC and represents the living cell population. **b)** Gating GFP positive cells: living cells (gated as in **a**) which were transfected with dsRED were used for setting the gate of GFP positive cells. The gate was placed so that the number of false positive cells was not greater than 1% (in this example 0.11 % false positive cells. **c)** Gate for GFP positive cells: H293 cells were transfected with eGFP. **d**) Gating Red positive cells: eGFP transfected cells were used for setting the gate of Red positive cells. The parameter for setting the gate was the same as described in b (less than 1% false positive cells). e) Gated Red positive cells: The Red gate described in **d** was applied to cells transfected with dsRED.

Each suspended cell passing through the beam scatters the light, and fluorescent proteins or compounds in or attached to the cell may be excited into emitting light at a longer wavelength than the light source. This combination of scattered and fluorescent light is picked up by the detectors. By analyzing fluctuations in brightness at each detector for each fluorescent emission peak, it is possible to derive various types of information about the physical and chemical structure of each individual cell. FSC correlates with the cell volume while SSC depends on the inner complexity of the particle (i.e., shape of the nucleus, the amount and type of cytoplasmatic granules and the membrane roughness). These data were further analyzed using FLOWJO1.1 software. Cells with the desired cell volume (FSC) and

granularity (SSC) were chosen for analysis (see Figure 3.2.1a). A description of GFP and RED gating to quantify positive cells is shown Figure 3.2.1a.

One question that was encountered concerned the evaluation of GFP expression intensities. The average GFP intensity measured by the flow cytometry intrument is displayed by the geometric mean of the GFP. The use of the geometric mean of GFP for all cells was not useful because of the fluctuation of transfection efficiencies when comparing individual experiments. To control for transfection efficiency and to allow measurement of only the transfected cell population a second control plasmid, dsRED, was co-transfected with the GFP sensor.
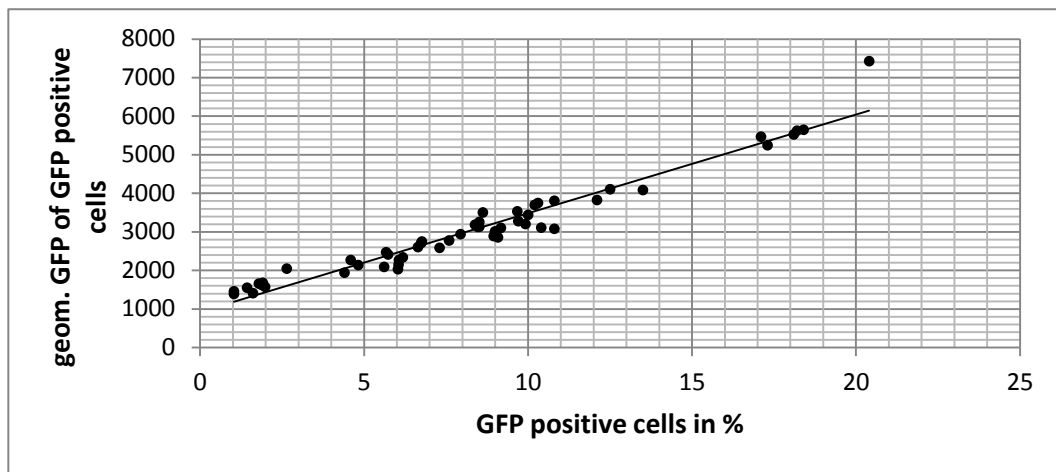

Figure 3.2.1b: Comparison of the percentage of GFP positive cells with their geometric mean of GFP based on 51 independent transfections in HEK293 cells. HEK293 cells were transfected with 50ng eGFP sensor constructs of various types and 200ng dsRED and measured by flow cytometry after 48h. The calculated correlation of both parameters is 0.9734.

The comparison of GFP positive cells and the geometric mean of GFP positive cells of 51 different transfections are displayed in Figure 3.2.1.1a. This result demonstrates a linear relationship between the two paramenters for these control transfections. Based on this result, the percentage of GFP positive cells was mainly used for data evaluation.

To compare miRNA-mediated sensor repression across different cell lines it is necessary to normalize the data records. Therefore beside the GFP-sensor/dsRED co-transfections, a GFP construct without any known regulatory elements was co-transfected together with dsRED. The GFP/dsRED transfection provides a basis for a non-regulated GFP sensor and was set to 1. All other values have been normalized to this negative control.

3.2.2 miRNA activity of endogenous let-7, miR-125, miR-124, miR-128 in primary cortical neurons

As a test of the artificial, perfectly complementary let-7 sensor, eGFP expression in transfected E15 primary neurons was compared to a sensor carrying regulatory sequences from a previously described natural let-7 target mRNA derived from the mouse Lin-41 gene (GFP-lin-41). As a control, a plasmid carrying inactivating point mutations in the let-7 binding sites (GFP-lin41LCS1+2) was used (Wulczyn et al., 2007). E15 primary neurons were electroporated with modified GFP-C1, GFP-lin-41, GFP-lin41LCS1+2 or GFP-2xlet-7 together with dsRED as a criterion for transfection efficiency. After 48h, cells were harvested and the GFP intensity was measured by flow cytometry. In Figure 3.2.2.1a the percentage of GFP positive cells normalized to the GFP-control are shown.
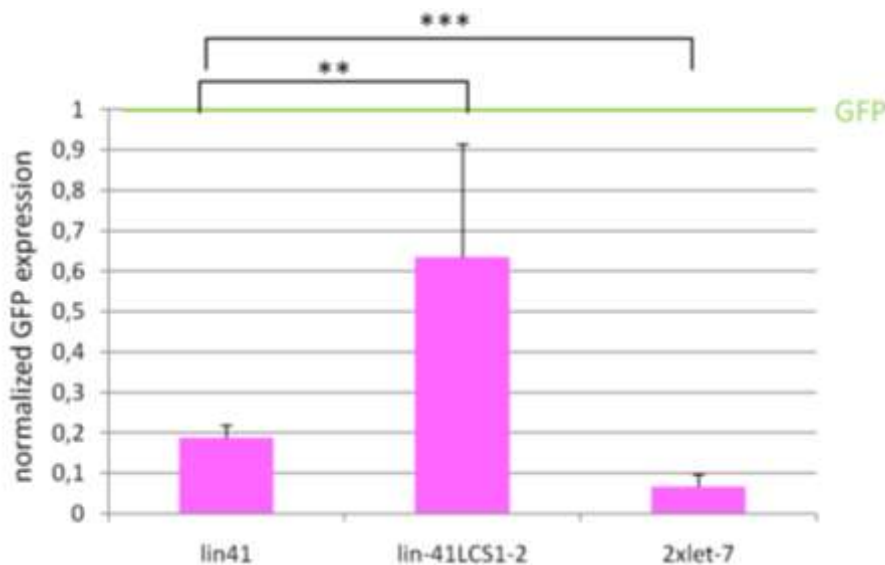

Figure 3.2.2a: Comparison of a "natural" GFP-let-7 sensor with an artificial GFP sensor.$1x10^6$ cortical neurons of mouse embryos were co-transfected with either 1µg eGFP-lin41 sensor, eGFP-lin-41LCS1+2 sensor or GFP-2xlet-7 binding sites together with dsRED and the fluorescence measured as described in chapter 3.2.1. An unpaired two tailed t-test (n≥5) was performed to reveal significant differences (** $p<0.01$, *** $p<0.001$).

The Lin-41 sensor with two validated let-7 sites is ~80% repressed in relation to the modified parent vector peGFP-C1. The same vector with point mutations in the let-7 conserved sites (LCS) displays a greater than threefold increase in GFP expression. The residual 40% repression in compared to the control vector may be due to the presence of additional regulatory sequences in the mutant mRNA. The strongest repression (~95%) is observed with the GFP-2xlet-7 sensor bearing two let-7 sites that are 100% complementary to let-7a. This result demonstrates the greater sensitivity of the GFP-2xlet-7 sensor compared to natural miRNA binding sites, even strongly regulated mRNAs like Lin-41 that were identified in genetic screens (Cullen, 2004). Recognition of the artificial GFP-2xlet-7 sensor by miRNAs other than let-7 is unlikely due to the minimal amount of sequence in the insert.

In a next step we tested let-7, miR-125, miR-124 and miR-128 activity in E18 primary cortical neurons with the GFP-miRNA sensor constructs described in Figure 3.1.1.1.
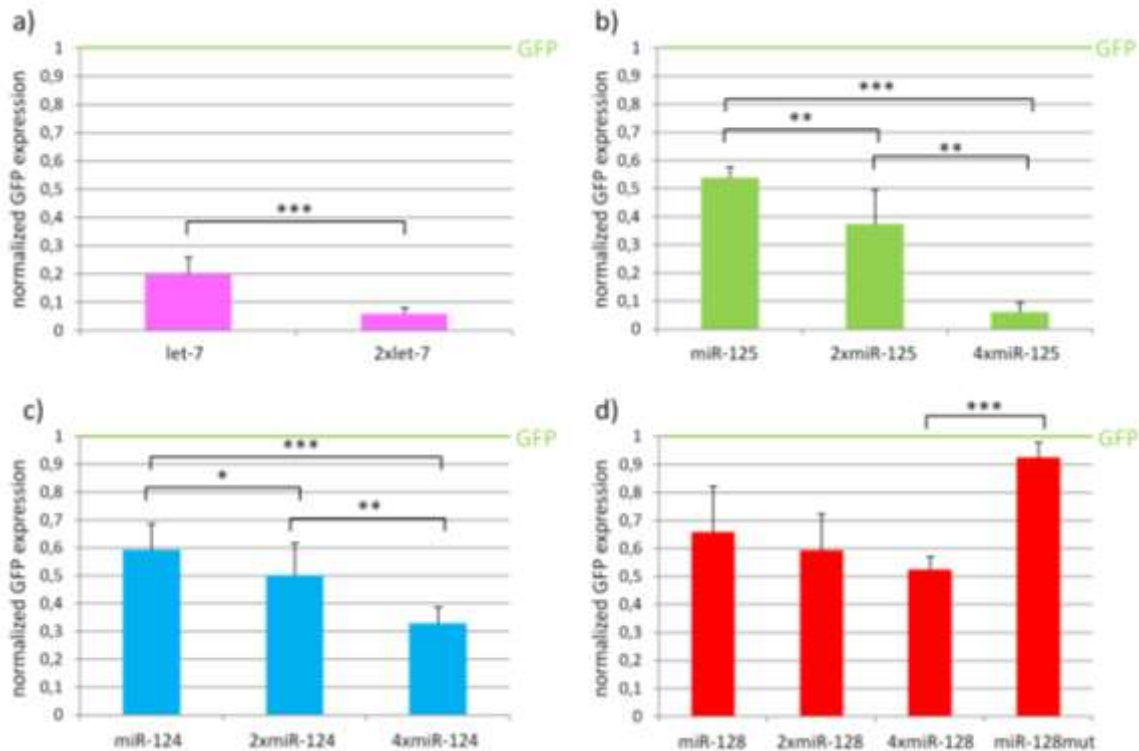

Figure 3.2.2b: Comparison of let-7-, miR-125-, miR-124- and miR-128-GFP sensor expression with different numbers of binding sites in E18 primary neurons 1×10^6 cortical neurons of E18 mouse embryos were transfected with 1µg GFP sensor construct together with 1µg dsRED. After 48h cells were harvested and the GFP/dsRED expression of cells was quantified by flow cytometry. The percentage of GFP positive cells were normalized to the GFP/dsRED control. An unpaired two tailed t-test (n≥3) was performed to reveal significant differences (* p< 0.05,** p<0.01,*** p<0.001) **a**) Comparison of let-7 GFP sensor expression with one and two complementary binding sites for let-7a **b**) miR-125 GFP sensor expression with one, two and four binding sites complementary to miR-125a **c**) Comparison of miR-124 GFP sensor expression with one, two and four binding sites complementary to miR-124 **d**) miR-128 GFP sensor expression with one, two and four binding sites complementary to miR-128. Additionally the GFP expression of a miR-128 GFP sensor with a truncated miR-128 binding site (miR-128 mut) was measured.

In this experimental series, the effect of one to four copies of the miRNA binding site was compared. In parallel miRNA sensor constructs with either one miRNA binding site or multiple binding sites were tested to reveal a synergistic effect on miRNA mediated repression. Forty-eight hours after electroporation the cells were harvested and the relative fluorescence activity for each sensor was measured by flow cytometry. eGFP expression was efficiently suppressed for all sensor constructs compared to the GFP control (Figure 3.2.2.).

The GFP expression of the GFP-let-7 sensor constructs is significantly reduced in E18 primary neurons. The GFP sensor construct with two binding sites shows a significantly lower expression (~95% repression) compared to the GFP sensor bearing one let-7 binding site (~80% repression). The GFP-miR-125 sensor constructs show a decreased GFP expression in E18 primary neurons. The GFP sensor construct with four miR-125 binding sites reveals a significantly lower expression (~93% repression compared with the GFP

sensor) compared to the single site (~43% repression). The GFP-miR-124 sensor constructs reveal a decrease of GFP expression as well. A GFP-sensor bearing one miR-124 binding site shows ~40% repression, with two binding sites 50% repression and with four binding sites ~ 68% repression in relation to the GFP/dsRED control. The GFP-miR-128 sensor constructs just show a moderate decrease of GFP expression in E18 primary neurons. In addition to GFP sensor constructs with one, two and four binding sites a GFP construct with a truncated miR-128 binding site was used as an additional control. The GFP sensor construct with fourmiR-128 binding sites was more efficiently repressed (~48%) than the other sensors and show a significant reduction of GFP expression compared to the GFP-sensor bearing a mutated miR-128 binding site which reached nearly the normal expression of the GFP/dsRED control. Apart from the miR-128 sensor, all the other sensors with multiple binding sites reveal a significant lower expression (n≥3, p<0.001) compared to the GFP sensors bearing just one miRNA binding site.

Beside of E18 primary cortical neurons, cortical neurons of an earlier stage (E15) were electroporated with the four miRNA constructs to test if they differ in miRNA activity. We choose eGFP sensor constructs bearing two binding sites for let-7 and four binding sites for miR-125, miR-124 and miR-128 because they showed the most sensitive response to miRNA activity (Figure 3.2.2c) and electroporated E15 primary cortical neurons as described above.
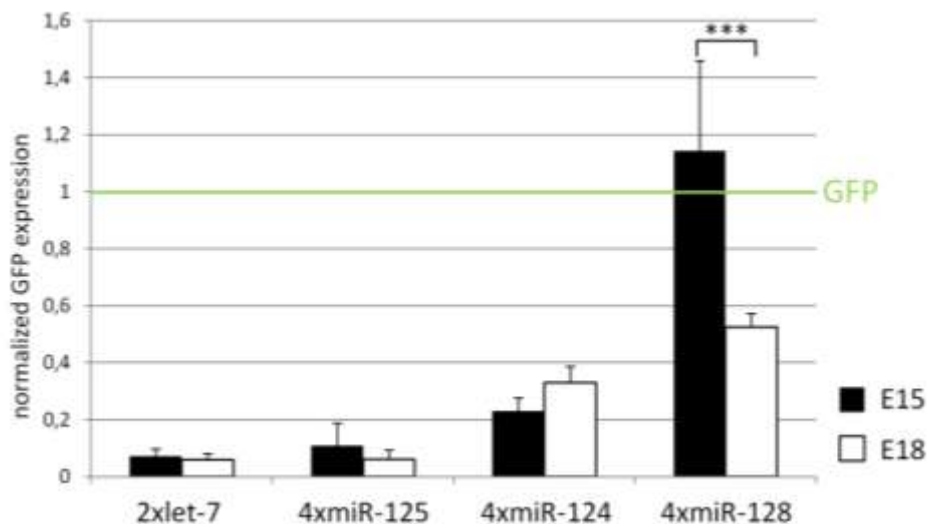
Figure 3.2.2c: miRNA activity of let-7, miR-125, miR-124 and miR-128 in E15 and E18 primary cortical neurons $1x10^6$ cortical neurons of E15 and E18 mouse embryos were electroporated with four different miRNA-sensors and the fluorescence of GFP measured as described in chapter 3.2.1. An unpaired two tailed t-test (n≥3) was performed to reveal significant differences (*** p<0.001). The black scale bars represent the normalized GFP intensity in E15; the white scale bars represent the normalized GFP intensity in E18 cortical neurons.

As shown in Figure 3.2.2c no significant in- or decrease of GFP expression was observed for the let-7, miR-125 and miR-124 sensor between E15 and E18 primary cortical neurons.

Interestingly E15 primary neurons do not show any miR-128 activity in comparison to E18 cortical neurons that show a significant (n≥3, p<0.001) ~55% repression of the miR-128 sensor. These data suggest that repression of target genes by miR-128 starts after E15 in cortical neurons.

3.2.3 miRNA activity of let-7, miR-125, miR-124, miR-128 in P19 cells (embryonic cell)

After the detection of let-7, miR-125, miR-124 in E15 and the start of miR-128 activity in E18 primary neurons, the activity of these miRNAs was examined in P19 EC cells. $5x10^4$ cells were transfected with 100ng GFP-miRNA sensor construct and 200ng dsRED as a criterion for transfection efficiency. After 48h, the fluorescent intensity of the cells were measured by flow cytometry and normalized to the parental GFP control (Figure 3.2.3).
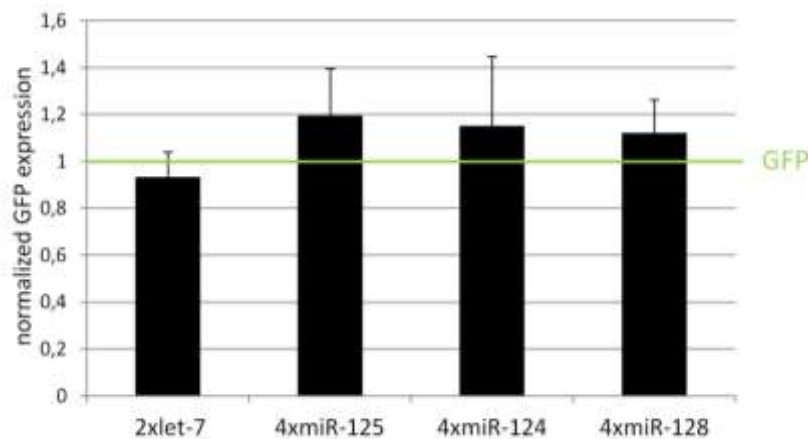
Figure 3.2.3: let-7-, miR-125-, miR-124-, and miR-128 GFP sensor expression in P19 cells $5x10^4$ were transfected with 100ng GFP sensor constructs and 200ng dsRED as a control for transfection efficiencies. After 48h, cells were harvested and the GFP expression was quantified by flow cytometry. The percentage of GFP positive cells was normalized to the modified parent vector eGFP-C1. The Figure represents the results of 5 independent transfections.

The experiments with P19 EC cultures reveal no miRNA activity of let-7, miR-125, miR-124 or miR-128. These miRNAs seem to be active at later stages during neural differentiation.

3.2.4 miRNA activity in E12 NSC

In order to study temporal expression of miRNAs in commited neural progenitor stem cells a cell line was generated using a protocol developed by Conti, Pollard and Smith (Pollard et al., 2006b). These cells were reported to share essential properties of bona fide radial progenitors and therefore can be considered to lie between P19 EC cells and primary neurons as a cell culture system. A detailed protocol for the generation, maintenance and characterization of these cells is provided in Material and Methods (2.1.2). To isolate a neural stem cell line from E12 neural tissue was dissected and cultured under conditions promoting

neurosphere formation. After formation of neurospheres these cell clusters were collected, triturated and allowed to attach to ornithine and laminin coated tissue culture flasks. Adherent cells were passaged every second or third day for over two month to remove differentiated and non-adherent neural progenitor cells. During the whole procedure the cells were cultivated in neural stem cell expansion media, which contains N-2 and the growth factors epidermal growth factor (EGF) and fibroblast growth factor2 (FGF-2). EGF and FGF-2 are necessary to promote proliferation of neural stem cells and to discourage differentiation.

3.2.4.1 Characterization of E12 NSC

Neural stem cells (NSCs), also called radial glia cells, have the ability to self-renew, generate a large number of progeny and differentiate into three of the principal cell types of the nervous system: neurons, astrocytes and oligodendrocytes. The NS cell line used in these experiments is Oct-4$^-$, GFAP$^-$, Sox2$^+$, RC-2$^+$, as confirmed by immunuhistochemistry (data not shown), consistent with the original description. In order to test their differentiation potential the E12 neural progenitor cell line was assayed under culture conditions previously described to promote their maturation to neurons or astrocytes (Pollard et al., 2006b). E12 neural stem cells at passage 39 (picture A in Figure 3.2.4.1) were collected and seeded on glass slides coated with 0.2% gelatine for astrocytes and ornithine plus laminin for neuronal differentiation. Medium containing 5% FCS without EGF and FGF promotes the differentiation primarily to astrocytes while adding 1xB27 without EGF promotes neuronal differentiation. After 6 days phase contrast pictures were taken from both cultures.
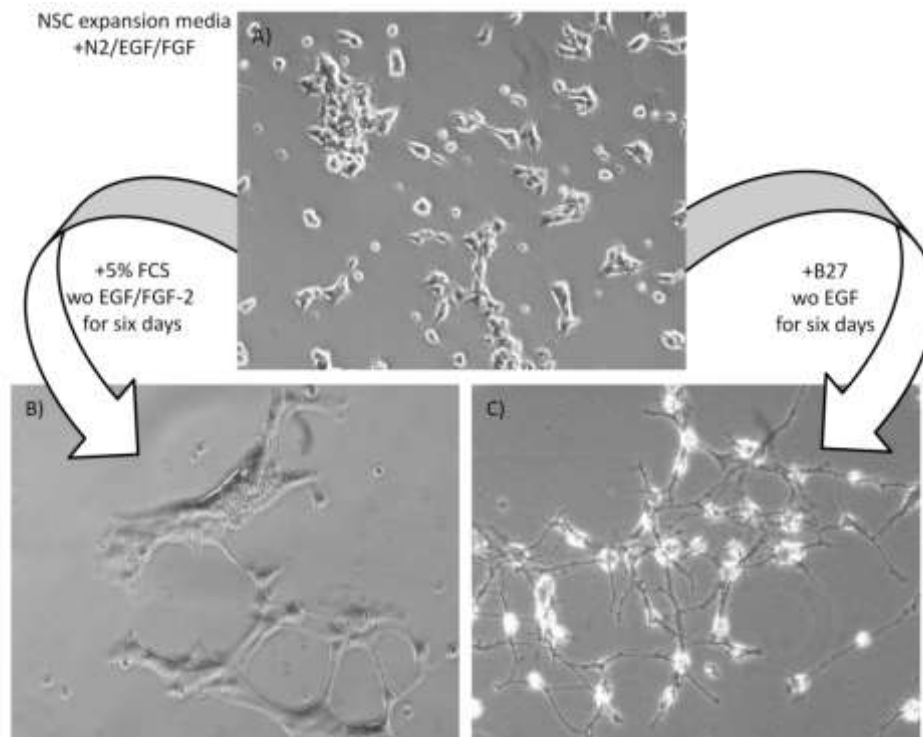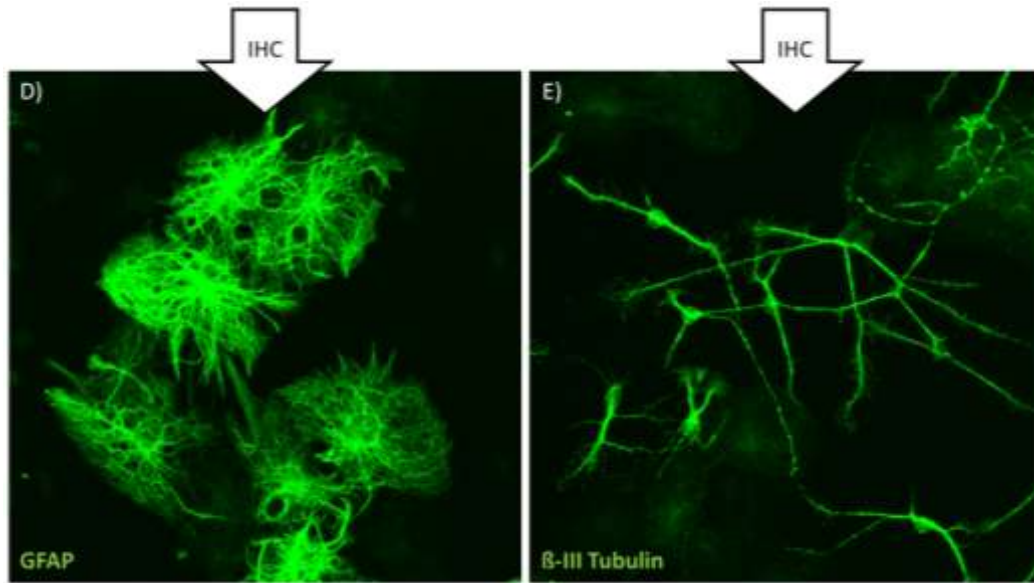
Figure 3.2.4.1: Testing the multipotency of the adherent E12 neural stem cells generated for this thesis A-C) Phase contrast images taken with 20x objective **D+E)** Fluorescent confocal z-stacks that have been merged with ImageJ **A)** Phase contrast image of E12 adherent glia at passage 39 **B)** In the presence of 5% FCS for six days these cells display increased size and a flattened morphology similar to cultured astrocytes **C)** Culture in the presence of B27 supplement without EGF for six days resulted in condensation of the cell body to the perinuclear area and significant polar cell extensions **D)** Fluorescent image of the cells cultured as in **B** using a monoclonal antibody against GFAP and anti-mouse-Alexa488 as a secondary antibody E) Fluorescent image of the cells cultured as in **C** using a monoclonal antibody detecting ⹀-III Tubulin and anti-mouse-Alexa488 as secondary antibody

The comparison clearly demonstrates the morphological differences between the astrocyte and the neuron culture (pictures B and C in Figure 3.2.4.1). Antibody staining was performed on these cells to demonstrate astrocytic and neuronal marker expression. For the astrocyte culture a GFAP (Glial fibrillary acidic protein) antibody and for the neuron culture a ß-III-tubulin antibody was used. In both cases the antibody-staining was positive which implies that the generated adherent neural progenitor cells were indeed multipotent at this stage.

3.2.4.2 miRNA activity of let-7, miR-125, miR-124, miR-128 in E12 NSC

As a next step, the miRNA activity of let-7, miR-124, miR-125 and miR-128 was examined with the previously described GFP sensor constructs. One difficulty encountered with the neural progenitor cells is that they are difficult to transfect by standard lipofection protocols. However, efficient transfection could be achieved using the Amaxa neural stem cell electroporation kit. For each transfection 1×10^6 cells were electroporated with 1µg GFP-miRNA sensor construct and 1µg dsRED. After 48h, the fluorescence of the cells was imaged with an inverse fluorescence microscope. Optimal exposure times for dsRED and GFP were determined for control transfections, and identical settings were used to acquire images of cells transfected with the sensor constructs (Rybak et al., 2008).
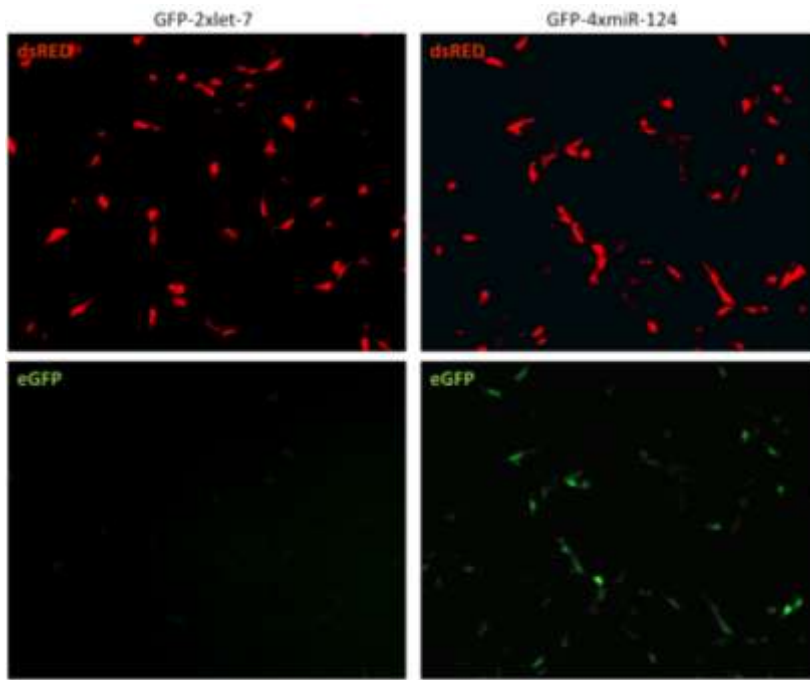
Figure 3.2.4.2a: DsRED and eGFP expression of E12 NSC with GFP-2xlet7/dsRED and GFP-4x124/dsRED 48h after transfection
eGFP/ dsRED expression of cells was visualized by reverse fluorescence microscopy (10x). For each picture an identical exposure time was choosen.

In Figure 3.2.4.2a images are shown for the let-7 GFP sensor (left side) and the miR-124 GFP sensor (right side). The pictures clearly demonstrate that eGFP expression of the cells transfected with the let-7 sensor is reduced in comparison to the GFP-4xmiR-124 transfection or eGFP controls (not shown). To obtain quantitative data transfected cells were assayed by flow cytometry after 48 hours. The GFP intensities for each sensor construct were normalized to control transfections with the parental GFP-C1 vector (green line)(Rybak et al., 2008).
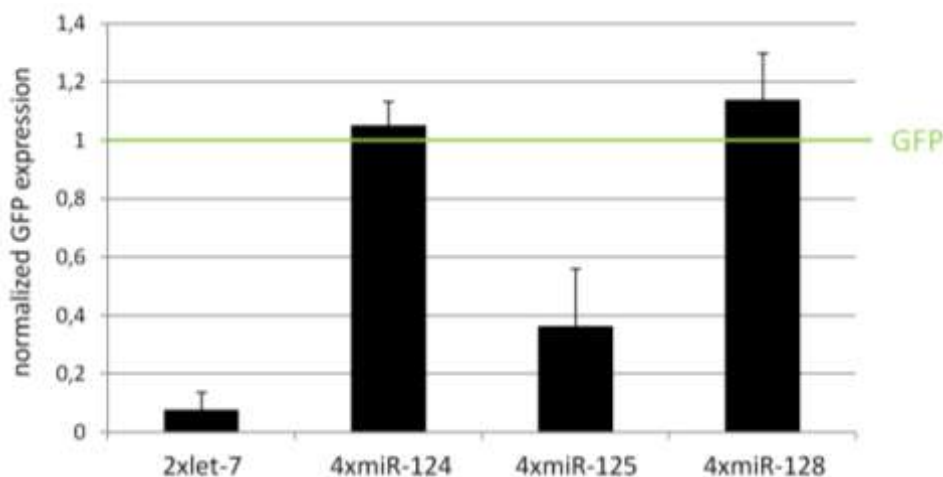
Figure 3.2.4.2b: let-7-, miR-125-, miR-124-, and miR-128 GFP sensor expression in E12 NSC
$1x10^6$ NSC were electroporated with 1µg GFP sensor constructs for let-7, miR-124, miR-125 and miR-128 and 1µg dsRED as a control for transfection efficiencies. After 48h, cells were harvested and the GFP expression was quantified by flow cytometry. The percentage of GFP positive cells was normalized to the modified parent vector eGFP-C1. The Figure represents the results of three independent experiments.

The results shown in Figure 3.2.4.2b reveals that the generated neural stem cells do not show any miR-124 or miR-128 activity: their GFP expression is similar to the GFP control

transfection. The results confirm significant activity of let-7 and miR-125 in the neural progenitors. Expression of the let-7 sensor was approximately 90% and the miR-125 sensor approximately 60% reduced in comparison to the control (green line). These results are consistent with the finding that miR-124 is first expressed after neuronal commitment in the embryonic central nervous system (Makeyev et al., 2007). Both miR-124 and miR-128 are restricted to neurons suggesting that there may be a temporal hierarchy between ubiquitous (let-7 and miR-125) and neuron-enriched miRNAs (miR-124 and miR-128) during stem-cell commitment in the central nervous system.

3.3 miRNA overexpression

Overexpression studies are one genetic tool to study miRNAs and their function during development. In the previous Chapter (3.1.2) two miRNA tools that were used in this thesis were described: synthetic Pre-miR™ miRNA Precursor Molecules and vector-based miRNA expression constructs. The synthetic precursors were mainly used to validate predicted miRNA target genes (see Chapter 3.3.3), while the vector-based pre-miRNA constructs were used to visualize cells that overexpress a distinct miRNA and to investigate possible phenotypes. Furthermore, the vector-based strategy was used for investigations of the miRNA biogenesis pathway. (Chapter 3.4).

3.3.1 Misexpression of miR-124 in E12 neural stem cells

As previously shown miR-124 is not active in neural stem cells but is activated in post-mitotic neurons but not astrocytes (Makeyev et al., 2007; Smirnova et al., 2005). The ability of miR-124 to regulate neurogenesis was therefore tested in neural stem cells undergoing astrocytic differentiation. 1×10^6 neural stem cells were electroporated with 4µg of either pre-miR-124-RED or Intron-RED vector. The cells were immediately seeded on 0.2% gelatin coated coverslips. After 12h the medium was exchanged to neural stem cell expansion containing 5% FCS without EGF and FGF to promote astrocytic differentiation (as described in Chapter 3.2.4.1). Three and six days after initiation of astrocytic differentiation the cells were fixed and stained with DAPI.

Figure 3.3.1a: miR-124 over-expression in neural stem cells three days after astrocyte differentiation On the left side differen-tiated neural stem cells are shown that have been transfected with the parental Intron-RED vector are shown. On the middle and right side two pre-miR-124-RED positive cells are shown. Noticeable on the right side are the DAPI stained nuclei which are standing abnormally close together (marked with white arrows).

Representative images are shown in Figure 3.3.1a and 3.3.1b. In comparison to the Intron-RED control the pre-miR-124-RED positive cells start to extend one primary outgrowth and a number of smaller outgrowths. Furthermore, the number of dsRED positive cells transfected with miR-124 was substantially decreased in comparison to the control (not shown observation).

Pictures were also taken from transfected neural stem cells which have been differentiated to astrocytes for additional three more days in order to check if these outgrowths of pre-miR-124-RED positive are preceded to extent or not (Figure 3.3.1b).

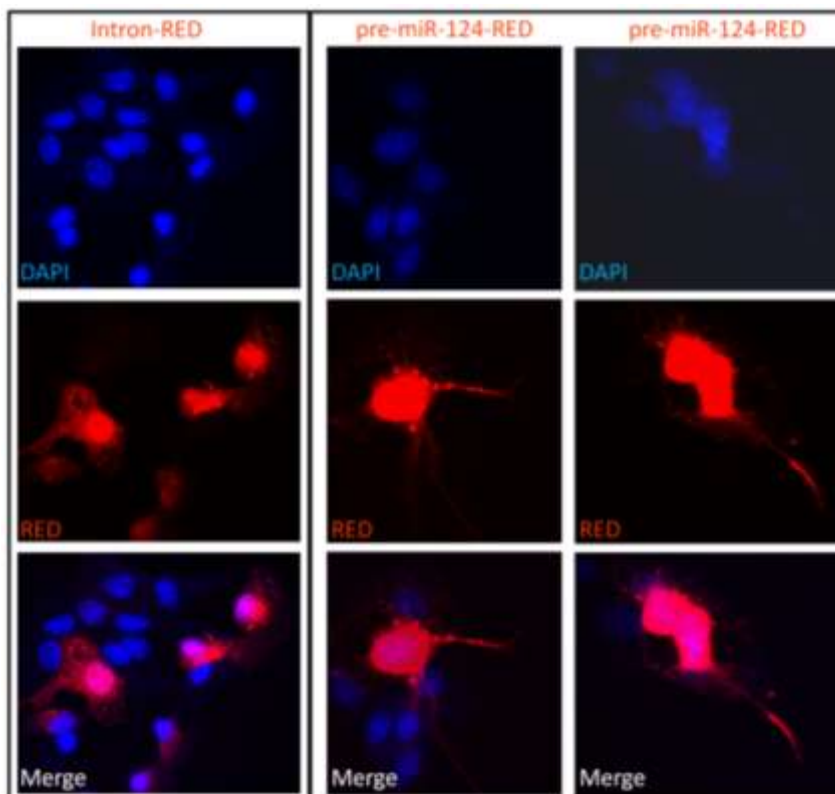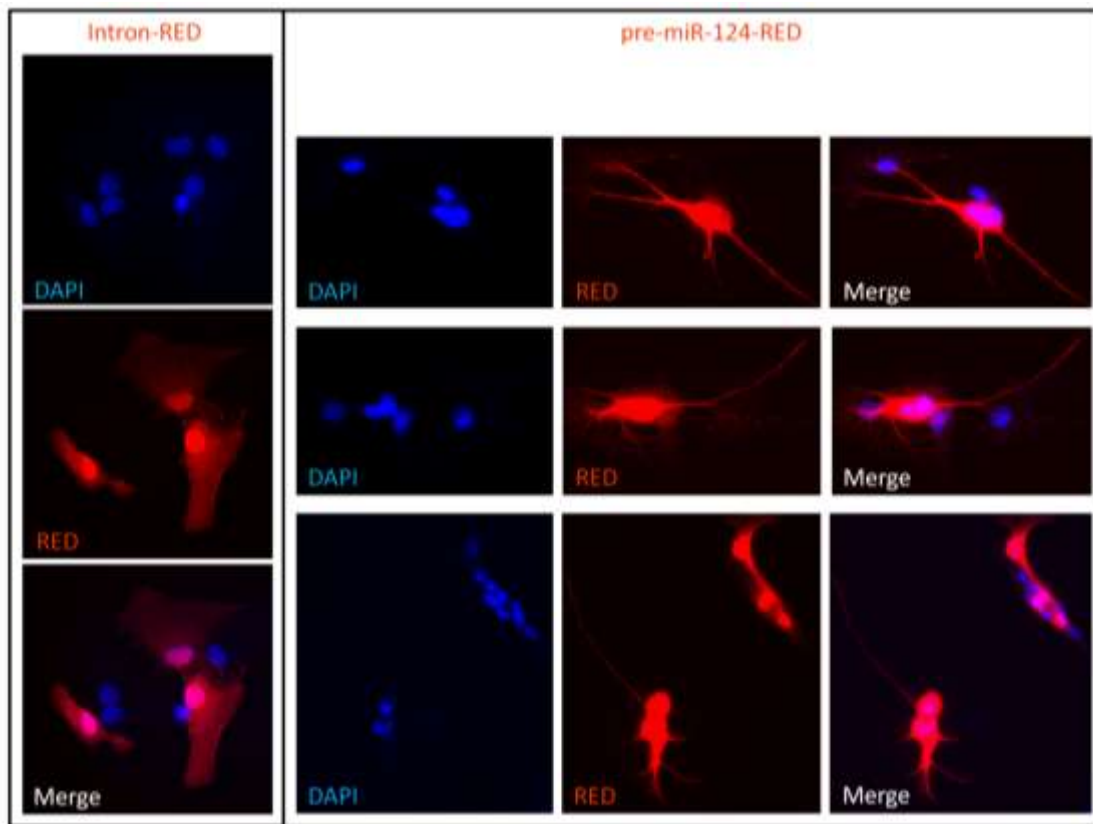**Figure 3.3.1b: miR-124 overexpression in neural stem cells six days after astrocyte differentiation** On the left side differentiated neural stem cells are shown that have been transfected with the parental Intron-RED vector are shown. The right panel shows pre-miR-124-RED positive cells.

The Intron-RED positive cells show the flat "fried egg" morphology typical for astrocytes growing on a cell culture dish (compare also Figure 3.2.4.1). Almost all pre-miR-124-RED positive cells reveal one very long cell outgrowths. These outgrowths are much longer in comparison to the pre-miR-124-RED positive that have been cultivated in astrocyte differentiation media for just three days (compare Figure 3.3.1a and 3.3.1b). Also smaller outgrowths, sometimes with numerous branches which are reminiscent of dendritic branches (exemplified in the middle picture of Figure 3.3.1b), occur. These results suggest that miR-124 is able to "override" the astrocytic differentiation program and induce a neuron-like

morphology. Moreover, the number of miR-124+ cells remained constant in 6 days of astrocytic differentiation (data not shown).

These preliminary results are supported by staining with neuron and astrocytic markers. For these experiments pre-miR-124-RED transfected neural stem cells were cultivated for five days in astrocyte differentiation medium. In a first approach an antibody staining with GFAP-antibody was performed to detect astrocytes. In Figure 3.3.1c fluorescent pictures of GFAP staining is shown, together with the signal from vector-derived dsRed. Comparison of GFAP and dsRed staining reveal a lack of GFAP expression in cells overexpressing miR-124. Occasional co-staining cells are marked with an arrow.
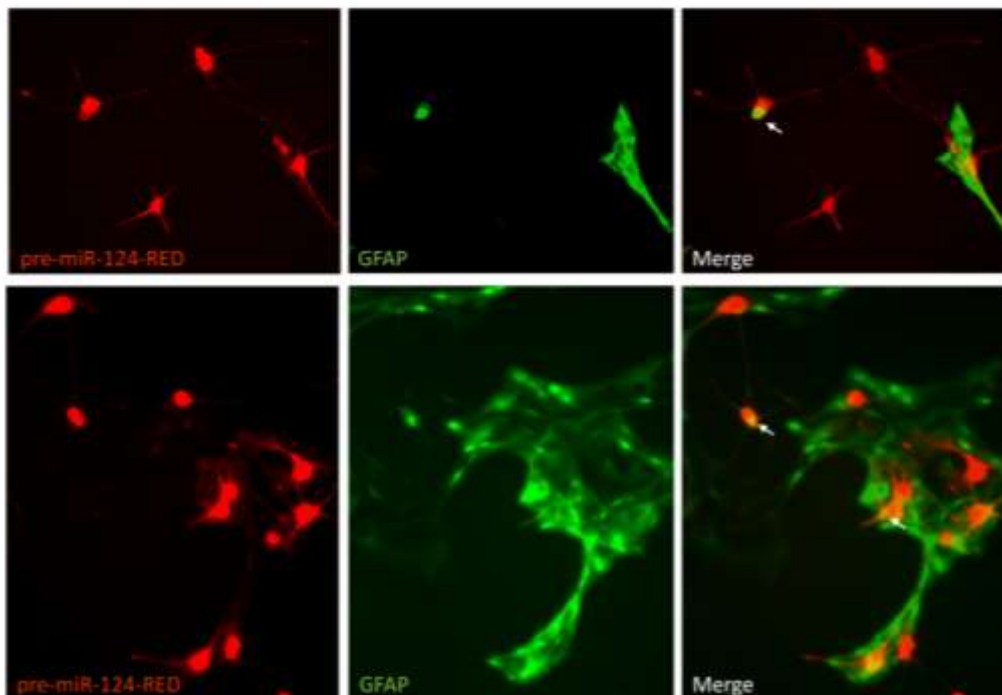
Figure 3.3.1c: miR-124 overexpression in neural stem cells five days after astrocyte differentiation show no or very weak expression of GFAP. Pre-miR-124-RED positive cells are shown on the left column. The middle column shows antibody-staining with monoclonal GFAP antibody which has been labeled with a secondary anti-mouse-Alexa488 antibody. The right column shows the merged pictures. GFAP staining which could be assigned to pre-miR-124-RED positive cells are marked with an arrow.

In order to check if these pre-miR-124 positive cells express neuron specific genes immunostaining with TuJ 1 antibody which detects ß-III Tubulin, was performed five days after transfection and cultivation in astrocyte media (Figure 3.3.1d).
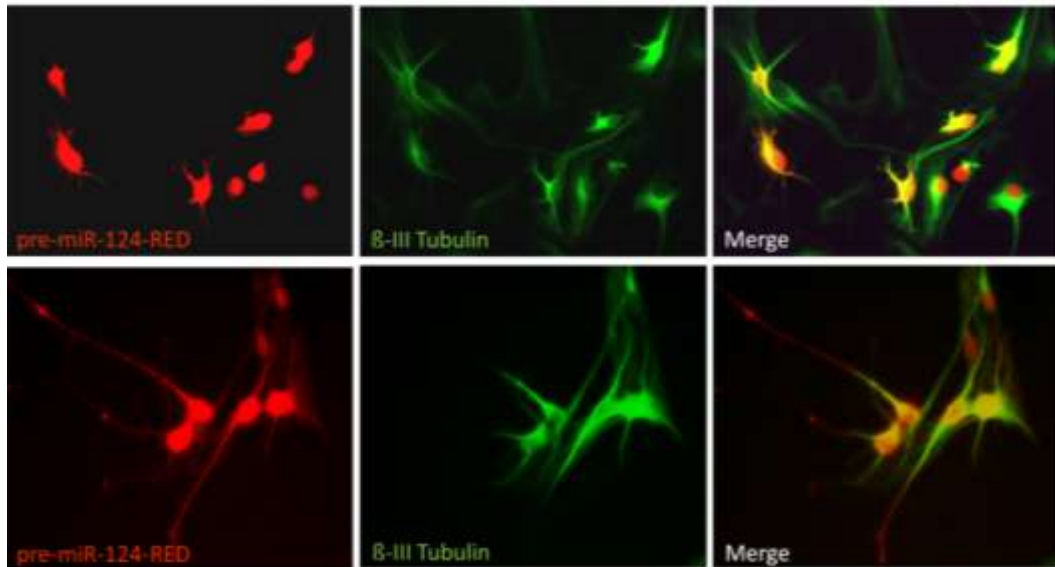
Figure 3.3.1d: Five days after astrocyte differentiation miR-124 positive neural stem cells reveal a strong expression of the neuronal marker anti ß-III Tubulin. Pre-miR-124-RED positive cells are shown on the left column. The middle column shows Alexa488-antibodystaining with monoclonal Tuj 1 antibody. The right column shows the merged pictures.

In all cases the pre-miR-124-RED positive cells show strong expression of ß-III tubulin, as is evident in the merged pictures on the right. The results in Figures 3.3.1a-d demonstrate that cells overexpressing miR-124 display the morphological characteristics of differentiating neurons.

Mir-124 seems to repress, at least in a first initial step, non-neural target genes causing induction of neurogenesis in cells. The question arise which miR-124 target genes are important to be down-regulated in order to induce neurogenesis.

A lot of effort was made to identify miRNA target genes. Since genes targeted by miRNA often undergo rapid degradation on mRNA level, several studies try to identify miRNA target genes by comparison of transcriptomes, based on RNA gene chips, between miRNA transfected cells and cells that were transfected with a control miRNA. However this method is not very precisely: decreased mRNA levels can be also the result of side- effects, such as miRNA mediated repression of transcription factors. For this thesis several GFP-based reporter gene constructs, bearing 3'UTRs of distinct miRNA target genes, were generated. The advantage of this strategy is that miRNA mediated repression of a target gene can be visual observed. The next section deals with the establishment of assay conditions to validate putative target genes and the validation of distinct predicted target genes.

3.3.2 Establishment of assay conditions to validate putative miRNA target genes using synthetic miRNAs

In order to validate target genes with eGFP sensor constructs, cells were chosen with low endogenous levels of the miRNA of interest. In a preliminary test, Hek293 cells were transfected with the GFP sensor constructs for let-7, miR-125, miR-124 and miR-128. After 48h we quantified the GFP expression by flow cytometry (Figure 3.3.2a).
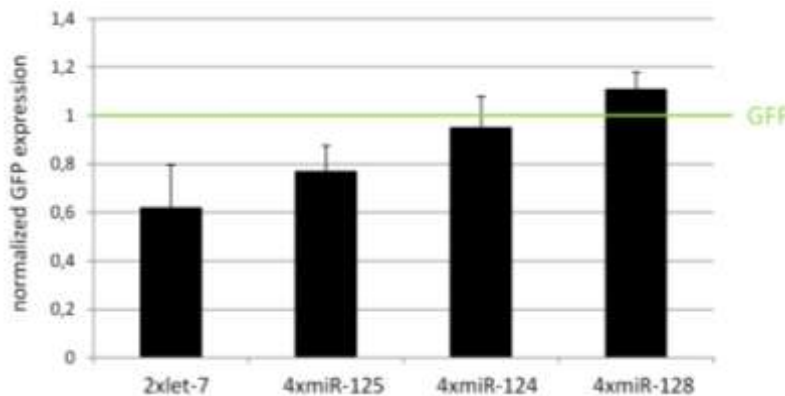
Figure 3.3.2a: let-7-, miR-125-, miR-124-, and miR-128 GFP sensor expression in Hek293 cells
4×10^5 were transfected with 100ng GFP sensor constructs and 200ng dsRED using lipofectamine as a transfection reagent. After 48h the GFP expression was quantified by flow cytometry. The percentage of GFP positive cells was normalized to the modified parent vector eGFP-C1. The Figure represents the results of 4 independent transfections.

As shown in Figure 3.3.2a, Hek293 cells reveal moderate let-7 and miR-125 activity: the sensor construct for let-7 reach ~60% GFP expression, and the miR-125 sensor ~75% GFP expression of the modified parental vector peGFP-C1. Sensors specific for miR-124 or miR-128 display control levels of GFP expression, indicating expression of these miRNAs is below the detection limit of this assay.

As a next step the synthetic miRNAs were tested to ensure that they are able to repress target genes in Hek293 cells. Both RNA molecules and miRNA-RNA duplexes are very sensitive to RNases and were therefore tested within a sensitive GFP-sensor assay to test their functionality (see Figure 3.3.2b).
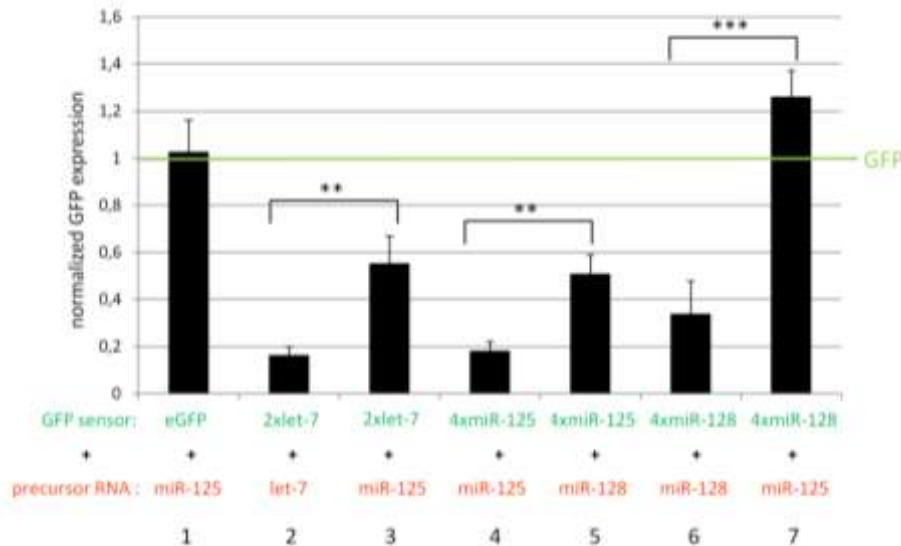
Figure 3.3.2b: let-7, miR-125, miR-124, and miR-128 GFP sensor expression in Hek293 cells co-transfected with different miRNA duplexes $4x10^5$ were transfected with 100ng GFP sensor constructs, 200ng dsRED and 20pmol precursor RNA using Lipofectamine2000 as a transfection reagent. After 48h the GFP expression was quantified by flow cytometry. The percentage of GFP positive cells was normalized to the modified parent vector eGFP-C1. Beside dsRED the following DNA and RNA was co-transfected : parental vector eGFP-C1 + premiR-125a (Column 1), eGFP-2xlet-7+prelet-7a (Column 2), eGFP-2xlet-7+premiR-125a (Column 3), eGFP-4xmiR-125+premiR-125a (Column4), eGFP-4xmiR-125+premiR-128b (Column 5), eGFP-4xmiR-128+premiR-128b (Column 6), eGFP-4xmiR-128+premiR-125a (Column 7). An unpaired two tailed t-test (n≥3) was performed to reveal significant differences (** p<0.01 ,*** p<0.001).

In Column 1 co-transfection of miR-125 and the eGFP-C1 vector did not reduce eGFP expression compared with transfection of the eGFP-C1 vector alone (green line). Furthermore, the eGFP expression of the eGFP sensor for let-7, miR-125 or miR-128 co-transfected with a non-corresponding miRNA (Column 3, 5 and 5) is similar to levels obtained without miRNA co-transfection (see Figure 3.3.2a), indicating that miRNA transfection did not interfere with low-level sensor regulation by endogenous miRNAs or with transfection efficiency. In all cases the cognate miRNA was able to significantly repress the GFP expression of its corresponding eGFP sensor. The let-7 sensor expression was reduced by 60% after co-transfection with let-7 (Column 2) compared with the co-transfection with miR-125 (Column 3). A similar result is revealed for the miR-125 sensor co-transfected with premiR-125 (Column 4) compared with co-transfection with premiR-128 (Column 5). The strongest repression of about 75% is shown for the eGFP-miR-128 sensor co-transfected with pre-miR-128 (Column 6) versus pre-miR-125 co-transfection. This assay was then employed in the validation of predicted miRNA target genes.

3.3.3 Validation of predicted miRNA target genes by co-transfection with doublestranded miRNA and GFP target gene constructs in Hek293 cells

As described in Chapter 1.4, in most instances target prediction algorithms like PicTar or TargetScan scan the 3'-UTR of mRNAs for conserved, perfect miRNA seed regions (nucleotide 1-7 or 2-8). The differences in miRNA-target gene predictions result from the different weighting of parameters such as seed conservation, binding energy, G:U base pairing outside or within the seed region and differences in the pools of investigated 3'-UTRs. An example is shown in table 3.3.3a where the number of conserved target genes for let-7, miR-125, miR-124 and miR-128, predicted either by PicTar or TargetScan, are displayed. In general TargetScan predicts ~ 1/3 more target genes for each miRNA than PicTar.

Table 3.3.3a: Number of conserved target genes for let-7, miR-125, miR-124 and miR-128 predicted by PicTar and TargetScan

miRNA	# of conserved target genes predicted by PicTar	# of conserved target genes predicted by TargetScan
let-7/mir-98	424	683
miR-125	342	472
miR-124	770	1047
miR-128	467	626

Table 3.3.3a illustrates the limits of current prediction databases, and the importance of experimental validation of target genes (Krek et al., 2005; Lewis et al., 2003). We therefore manually screened gene predictions for high likelihood targets with expression patterns or functions of interest for developmental neural biology, and generated the appropriate GFP-sensor constructs (see Table 3.3.3b). Target genes D4Ertd22e, Mll1, Rps6ka5 and FoxP2 were chosen as potential miR-128 targets. Interestingly FoxP2 is predicted by PicTar and TargetScan to be a let-7 target as well. As a miR-125 target gene the 3'-UTR of ZBTB71 was inserted into the 3'-UTR of the GFP gene. Partial 3'-UTRs of the putative let-7 target genes Arid3a, Arid3b, Nr6a1, Hic2 and Lin28 were inserted into 3'-UTR of the GFP gene.

Table 3.3.3b: Investigated putative miRNA target genes regulated by let-7, miR-125 and miR-128 Gene name, GenBank Accession #, the part of the amplified 3'-UTR that was inserted into the 3'-UTR of the GFP sensor, putative miRNA of interest with number of sites and their PicTar (Krek et al., 2005) or TargetScan (Lewis et al., 2003) rank is displayed for each investigated gene.

Gene name	Accession #	Amplified 3'-UTR (nt)	Definition	putative miRNA target/ maximum Number of sites	PicTar Rank/ TargetScan Rank
D4Ertd22e	NM_001025608	591-917	Mus musculus DNA segment, Chr 4, ERATO Doi 22, expressed , transcript variant 1	miR-128 / 4	3/2
Mll1	NM_001081049	13890-14362	Mus musculus myeloid/lymphoid or mixed-lineage leukemia 1	miR-128 / 3 miR-124 / 1	n.a./593 n.a./1036
Rps6ka5	NM_153587.2	3425-3722	Mus musculus ribosomal protein S6 kinase, polypeptide 5	miR-128 /2	15/18
FoxP2	NM_053242	2641-6124	Mus musculus forkhead box P2, transcript variant 1	miR-128/3 let-7/3	10/346 8/121
ZBTB7a	NM_010731	2458-2774	Mus musculus zinc finger and BTB domain containing 7a	miR-125/2	n.a./301
Arid3a	NM_007880.3	2492-4653	Mus musculus AT rich interactive domain 3A (BRIGHT-like)	miR-125/2 let-7/3	n.a./4 27/15
Arid3b	NM_019689	1706-3087	Mus musculus AT rich interactive domain 3B (BRIGHT-like)	miR-125/3 let-7/3	3/33 13/7
NR6a1	NM_010264.3	1842-3781	Mus musculus nuclear receptor subfamily 6, group A, member 1	miR-125/1 let-7/4	11/108 1/1

Noticeable is that apart from Hic2 and FoxP2, all putative let-7 target genes are also miR-125 target genes. A more detailed description of all investigated miRNA target genes, including the arrangement of miRNA binding sites within the amplified 3'-UTR, and probable miRNA-binding-site duplexes are shown in the following sections 3.3.3.1 to 3.3.3.6.

3.3.3.1 Validation of predicted three miR-128 target genes D4Ertd22e, Mll1 and Rps6ka5 in Hek293 cells

D4Ertd22e ranks number 3 for miR-128 targets predicted by PicTar and number 2 by TargetScan. The mRNA codes for two isoforms of a putative mitogen-activated protein kinase (MAPK) that are referred to as PM-20 and PM-21. It has been shown that PM-20 is a inhibitor of the oncogene Cdc25a, a molecule involved in the regulation of the p53-p21-Cdk checkpoint in carcinogenesis (Naeger et al., 1999; Saha et al., 1997). Furthermore PM-20 inhibits hepatocellular carcinoma growth (Kar et al., 2006). Therefore the targeting of D4Ertd22e by miR-128 might be one important regulatory step in the control of cell growth. The region of the 3'-UTR of D4Ertd22e containing four putative miR-128 binding sites used to generate a GFP sensor construct is shown in Figure 3.3.3.1a.

Figure 3.3.3.1a: A segment of the gene D4Ertd22e used to generate the GFP sensor construct.
a) A 327bp fragment was amplified from the 3'-UTR of D4Ertd22e gene. The four putative miR-128 binding sites are highlighted in bold red. **b)** Predicted miR-128a-mRNA duplexes for each binding site of D4Ertd22e. The seed region is highlighted in red. Standard base pairing is indicated by (|), G:U pairs by (:).

The **Mll1** protein is a histone methyltransferase. Methylated histones pack chromatin more tightly, inhibiting transcription. Mll1 is a global regulator of gene transcription and is involved in the epigenetic maintenance of transcriptional memory and the pathogenesis of human leukemia (See OMIM +159555). The sequence of the 3'-UTR of Mll1 with three potential miR-128 and one miR-124 binding sites used to generate a GFP sensor construct is shown in Figure 3.3.3.1b.

Figure 3.3.3.1b: A segment of the gene Mll1 used to generate the GFP sensor construct. a) A 472bp fragment was amplified from the 3'-UTR of the Mll1 gene. The sequence includes three putative miR-128 binding sites (red, bold letters) and one miR-124 binding site (blue, bold letters). The second miR-128 binding site, overlaps with the first binding site, is underlined. **b)** Predicted miRNA-mRNA duplexes for each binding site of Mll1. The seed region of miR-128 is highlighted in red letters, the miR-124 seed in blue. Base pairings are highlighted in bold letters.

The **Rps6ka5** gene, also known as MSK1 (Mitogen- and stress-activated protein kinase-1), has been shown to be directly activated by MAPK (mitogen activated protein kinase) and SAPK2 (stress activated protein kinase 2). MSK1 phosphorylates the NF-kB p65 subunit (also known as RelA) at Ser276. The modified RelA binds among other proteins to the SCF (stem cell factor, also known as Kit-1) intronic enhancer and enhances its transcription. SCF has been shown to promote early oocyte growth and development and is essential for the development of c-kit-expressing small- and medium-diameter primary sensory neurons. Figure 3.1.1.2.1.3 shows a small part of the Rps6ka5-3'-UTR including three putative miR-128 binding sites, in which two of them are overlapping. (see OMIM 603607)
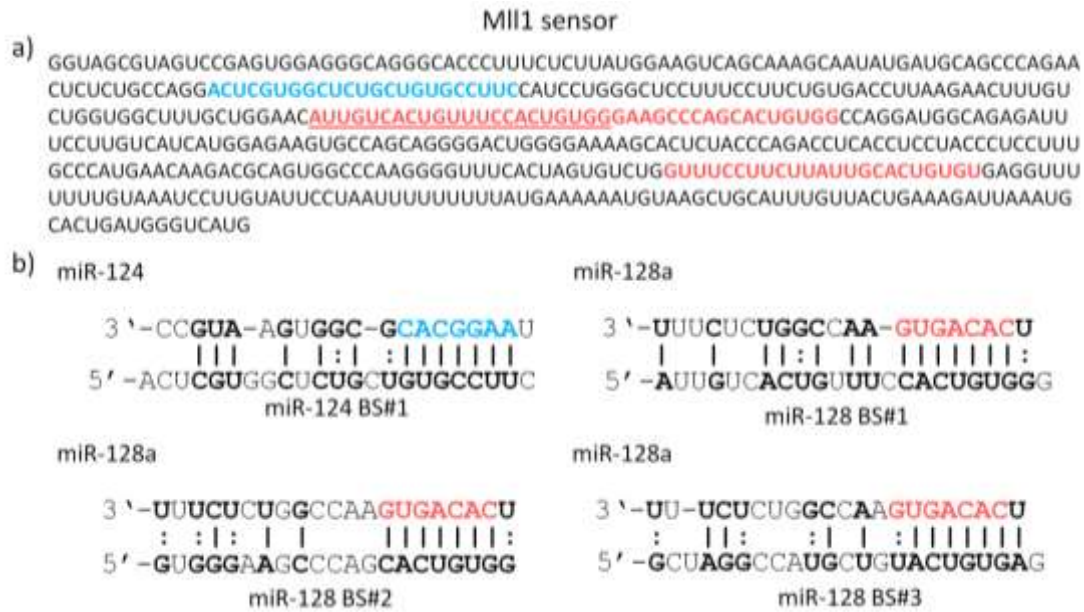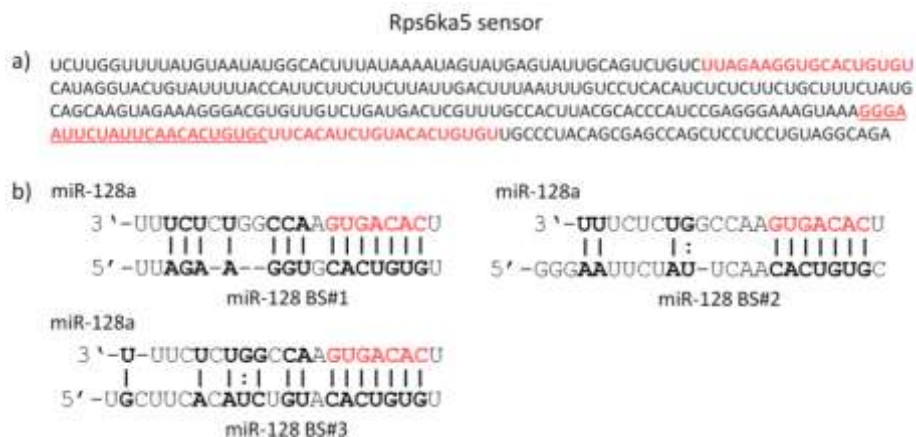

Figure 3.3.3.1c: A segment of the gene Rps6ka5 which was used to generate the GFP sensor construct. a) A 298bp fragment was amplified from the 3'-UTR of the Mll1 gene. The sequence includes three

putative miR-128 binding sites (red, bold letters). The second binding site which seed region overlaps with the third miR-128 binding site is underlined. **b)** Predicted miR-128a-mRNA duplexes for each binding site of Rps6ka5. The seed region of miR-128 is highlighted in red letters. Base pairings are highlighted in bold letters.

The three predicted miR-128 target gene GFP constructs (D4Ertd22e, Mll1 and Rps6ka5) were tested by co-transfection with miR-128 RNA (Figure 3.3.1.1a). miR-125 was chosen as a control because none of these putative miR-128 targets bears a predicted miR-125 binding site.
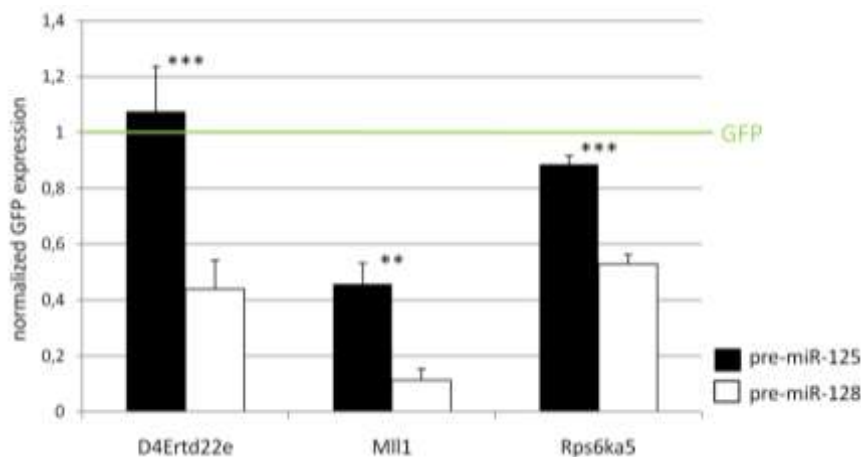
Figure 3.3.3.1d: Normalized GFP expression (48h after transfection) of Hek293 cells transfected with GFP-D4Ertd22e, GFP-Mll1 or Rps5ka6 together with either premiR-125(black scale bars) or premiR-128 (white scale bars) $4*10^5$ Hek293 cells were transfected with 100ng eGFP sensor, 200ng dsRED and 20pmol pre-miRNA RNA. After 48h the eGFP and dsRED expression was measured by flow cytometry. The percentages of positive cells were normalized to the parental vector eGFP-C1 (as previously described in Figure 3.3.1.1a). An unpaired two tailed t-test (n=4) was performed to reveal significant differences (** $p<0.01$, *** $p<0.001$).

The GFP-D4Ertd22e sensor showed a statistically significant repression by 60% in response to miR-128 in comparison to miR-125. A stronger ~75% repression by miR-128 is shown for GFP-Mll1. Noticeable is that the GFP-Mll1/premiR-125 control transfection shows a 55% reduction of the GFP expression in comparison to the parental GFP-C1 (green line). However the GFP expression was also reduced by transfection of the GFP-Mll1 without any miRNA mimic (data not shown). The weakest, but nevertheless statistically significant repression of ~40% by miR-128 is observed for the GFP-Rps6ka5 sensor. These results confirm D4Ertd22e, Mll1 and Rps6ka5 as miR-128 target genes in this assay.

3.3.3.2 The miR-128/let-7 target gene "forkhead box P2" (FoxP2)

This transcription factor is a member of the forkhead/winged-helix (FOX) family of transcription factors, and contains a FOX DNA-binding domain and a large polyglutamine tract. FoxP2 is sometimes referred to as the "speech gene" because humans with mutations in FoxP2 show a language disorder (see OMIM 605317). FoxP2 is thought to be required for proper development of speech and language regions of the fetal and adult brain. In finches it has been shown that young birds with FoxP2 mutations are unable to learn songs from adult male birds during the song learning phase. *In situ* hybridization with FoxP2 antisense probes

shows strong expression in the area X of the brain, also known as the "speech" area. The question arises as to whether the temporal or regional specificity of FoxP2 is regulated by let-7 or miR-128. We therefore generated a GFP sensor construct from the 3'-UTR of FoxP2 including three putative binding sites for let-7 and two binding sites for miR-128 (Figure 3.3.3.2a).
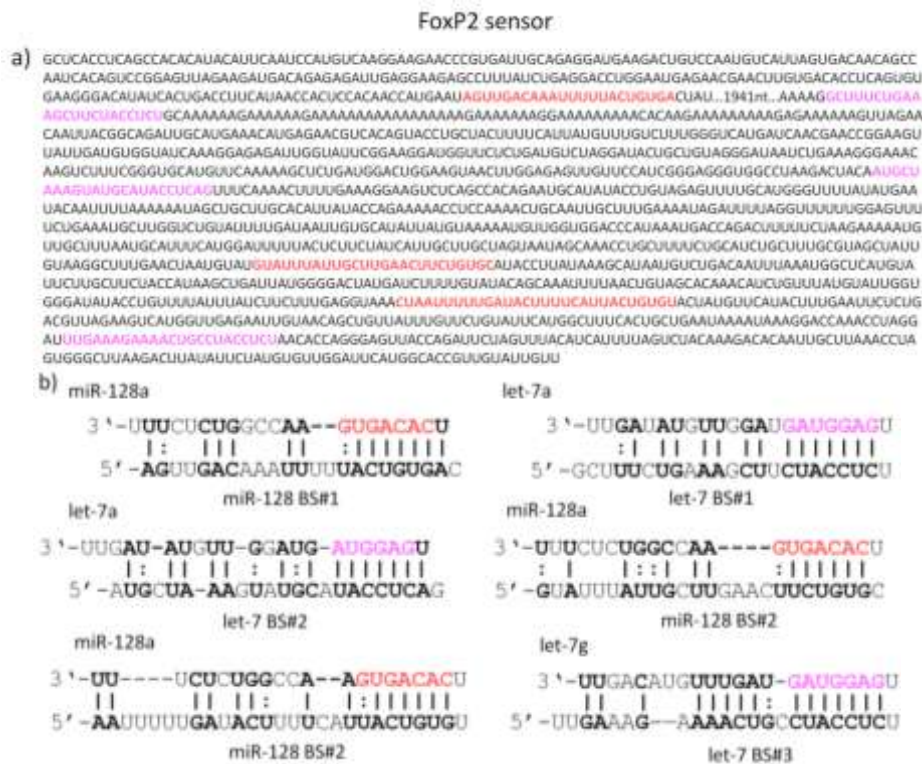
Figure 3.3.3.2a: The segment of the putative let-7/miR-128 target gene FoxP2 used to generate an eGFP sensor construct a) 3484 bp from the 3'-UTR of the FoxP2 gene were amplified and inserted into the modified eGFP vector. The sequence includes three putative let-7 binding sites highlighted in pink, bold letters and three miR-128 binding sites labelled in red letters. **b)** Predicted miR-128a-mRNA and let-7/mRNA duplexes for each binding site of FoxP2. The seed regions of miR-128 are highlighted in red letters, the let-7 seed is highlighted in pink. Base pairings between the miRNA and corresponding binding site are labelled in bold letters.

In order to check the potential repression the FoxP2 GFP sensor was co-transfected with let-7 or miR-128, or a combination of the two. As a control, the FoxP2 sensor was transfected with miR-125 or no miRNA precursor (Figure 3.3.3.2b).
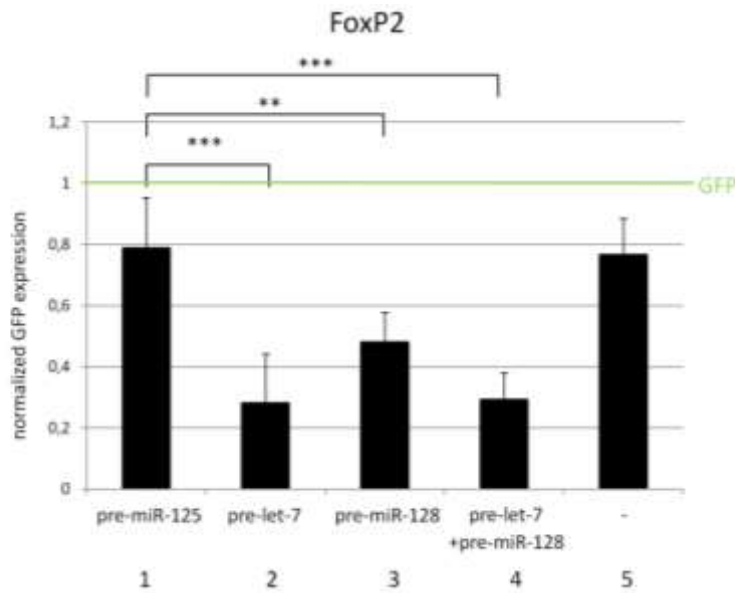
Figure 3.3.3.2b: Normalized GFP expression of Hek293 cells transfected with GFP-FoxP2 together with premiR-125, prelet-7 or premiR-128 $4*10^5$ Hek293 cells were transfected with 200ng dsRED, 100ng eGFP-FoxP2 sensor and either 20pmol premiR-125(Column 1), prelet-7a(Column 2), premiR-128(Column 3),prelet-7 + premiR-128(Column 4) or no miRNA precursor (Column 5). After 48h the eGFP and dsRED expression was measured by flow cytometry. The percentages of positive cells were normalized to the parental vector eGFP-C1 (green line). An unpaired two tailed t-test (n≥4) was performed to reveal significant differences (** $p<0.01$, *** $p<0.001$).

In Figure 3.3.3.2 GFP-FoxP2 transfection alone (Column 5) or co-transfection with the control precursor miR-125 (Column 1), reveals a moderate decrease of GFP expression of approximately 20% compared to the modified parental vector eGFP-C1 (green line). The decrease in GFP expression can be explained by the moderate let-7 activity in Hek-293 shown previously in Figure 3.3.1a+b. The GFP-FoxP2 sensor was repressed by let-7 by approximately 75% (Column 2) and repressed by ~27% by transfection with premiR-128 (Column 3). Cooperativity was not observed, as the GFP expression of GFP-FoxP2 co-transfected with prelet-7 was the same as the GFP-FoxP2 sensor transfected with let-7 and miR-128 precursor together (Column 4). However these data indicated that FoxP2 is a target of let-7 as well as miR-128.

3.3.3.3 The miR-125 target gene "zinc finger and BTB domain containing 7a" (ZBTB7a)

ZBTB7a, also known as FBI-1 is a nuclear factor that is preferentially associated with active chromatin. Furthermore, ZBTB7a interacts with the p65 subunit of NF-κB and enhances the transcription of the NF-κB response gene E-selectin. Like Rps6ka5, which is also involved in the NF-κB cascade, ZBTB7a is overexpressed in cancer. In Figure 3.3.3.3a, the part of the 3'-UTR of ZBTB7a with two putative miR-125 binding sites is shown.

ZBTB7a sensor

a) UGGUUGGUUUUAGGGGGUCUUAGACAGACCUUAAAUGCUCUGUCCACUAUGAGUGGACGUUAAAAUGGUCC
CCACCCUCCUUCCUCAGGGCACUUACUAAAGAGGGGGGUGUCCCCUCGGCCUCCCUCCCGGCCUGUGGCCUCC
GCAUCUCUGCACAUCCACCCUGGCCACCACUGACAUACAAAUCUAUUUAUUCCCAAGCCUGGAUGGCCAGAGC
GGGGAUUGGGGGGGGGCCGCUGGGGUCCCCGCCACCCUCCUUCACGGCACUUACACCUGACGGGGCCCUCGG
GGCCACUGCUCAGGGCGACCCCCCCCCC

b) miR-125a   miR-125a

3 '-AGU-GUUCAAUCCCAGAGUCCCU   3 '-AGUGUUC-AAUCCCAGAGUCCCU
     | | | | | | | | | | | | : : | | | | | | | | |
5' -UCCCCACCCUCCUUCCUCAGGGC   5' - CCCUCGGGGCCA-CUGCUCAGGGC

        miR-125 BS#1   miR-125 BS#2

Figure 3.3.3.3a: A segment of the putative miR-125 target gene ZBTB7a used to generate an eGFP sensor construct a) 317bp from the3'-UTR of the ZBTB7a gene were amplified and inserted into the modified eGFP vector. The sequence includes two putative miR-125 binding sites highlighted in green, bold letters. **b)** Predicted miR-125a-mRNA duplexes for each binding site of ZBTB7a. The seed regions of miR-125 are highlighted in green letters. Base pairings are highlighted in bold letters.

The 3'-UTR of ZBTB7a bears two putative miRNA binding sites for miR-125 predicted by TargetScan which are not predicted by PicTar. To check if ZBTB7a is a miR-125 target, we transfected Hek293 cells with the GFP-ZBTB7a sensor construct together with either miR-125 or miR-128 as a control in (Figure 3.3.1.1.3).
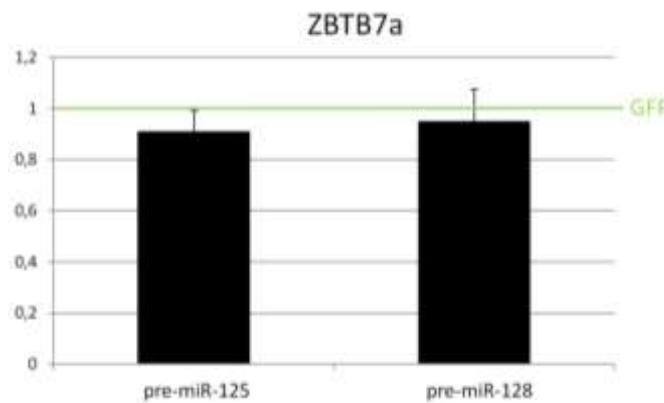
Figure 3.3.3.3b: Normalized GFP expression of GFP-ZBTB7a transfected with either premiR-125 or premiR-128 in Hek293 4*10^5 Hek293 cells were transfected with 200ng dsRED, 100ng eGFP-ZBTB7a sensor together with either 20pmol premiR-125 (left scale bar) or premiR-128 (right scale bar). After 48h the eGFP expression was measured by flow cytometry. The percentages of positive cells were normalized to the parental vector eGFP-C1 (green line).

As shown in Figure 3.3.3.3b, the GFP expression of GFP-ZBTB7a co-transfected with either premiR-125 or premiR-128 control miRNA is nearly the same. Although Hek293 cells show low level miR-125 activity as displayed in Figures 3.3.1a+b, the ZBTB7a sensor reaches the same GFP expression as its modified parental vector eGFP-C1 (green line). These results suggest that ZBTB7a is not a target gene of miR-125.

3.3.3.4 Validation of the putative let-7 and miR-125 target gene Nr6a1

It has been shown that **Nr6a1**, also known as germ cell nuclear factor (GCNF), represses the pluripotency gene Oct3/4 by recruiting the DNA methyltransferase 1 (Dnmt1) to the Oct3/4 promoter region and facilitating its methylation. Furthermore, Nr6a1 represses the pluripotency gene Nanog as well, suggesting an important role for Nr6a1 during ES cell differentiation. Using a lacZ reporter gene assay, Gu et al. found that Nr6a1 is predominantly expressed in spermatogenic cells and growing oocytes. Apart from the reproductive niches, LacZ staining was observed in other tissues, including hippocampus, cerebral cortex, cerebellum, and thalamus of brain. The sequence used to generate a GFP sensor construct for Nr6a1 includes four putative let-7 binding sites and one miR-125 binding site and is shown in Figure 3.3.3.4a.
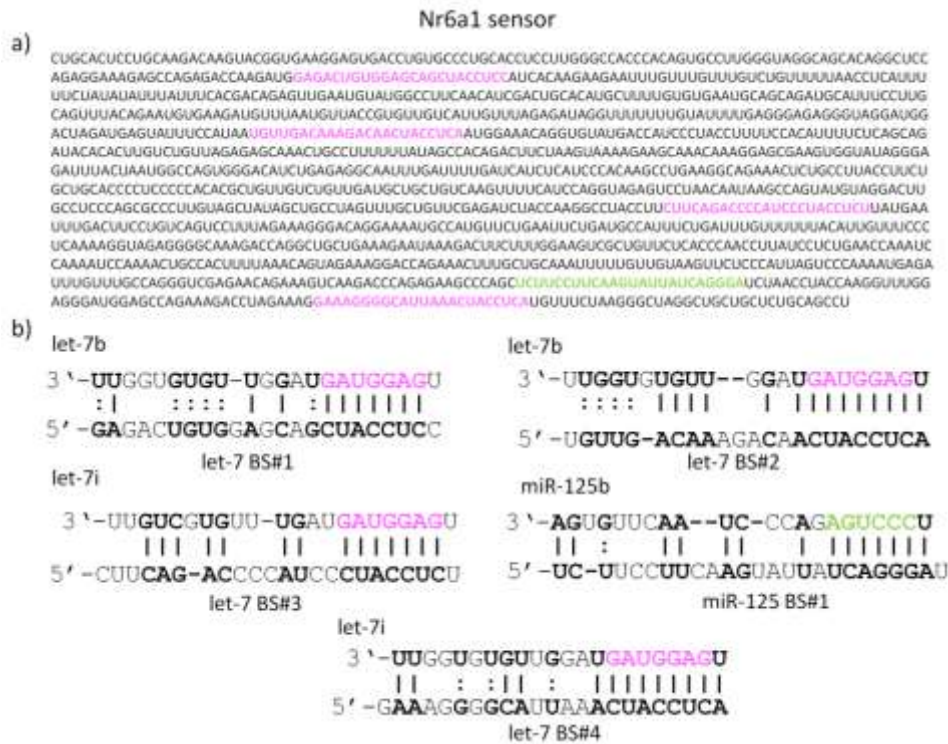
Figure 3.3.3.4a: Part of the 3'-UTR of the putative miR-125/let-7 target gene Nr6a1 used to generate an eGFP sensor construct a) 1305 bp from the 3'-UTR of the Nr6a1 gene were amplified and inserted into the modified eGFP vector. The sequence includes four putative binding sites for let-7 and one miR-125 binding site. The binding sites for let-7 are labelled in pink, bold letters while miR-125 binding sites are highlighted in green. **b)** Predicted miR-125a-mRNA duplex and let-7-mRNA duplexes for each binding site of Nr6a1. The seed region of miR-125 is highlighted in green, the let-7 seeds are shown in pink letters. Base pairings between the miRNA and corresponding binding site are labelled in bold letters.

The GFP-Nr6a1 sensor construct was co-transfected with pre-let-7, premiR-125 or premiR-128 RNA in Hek293 cells, and the GFP expression was quantified by flow cytometry 48 h later (Figure 3.3.3.4a).
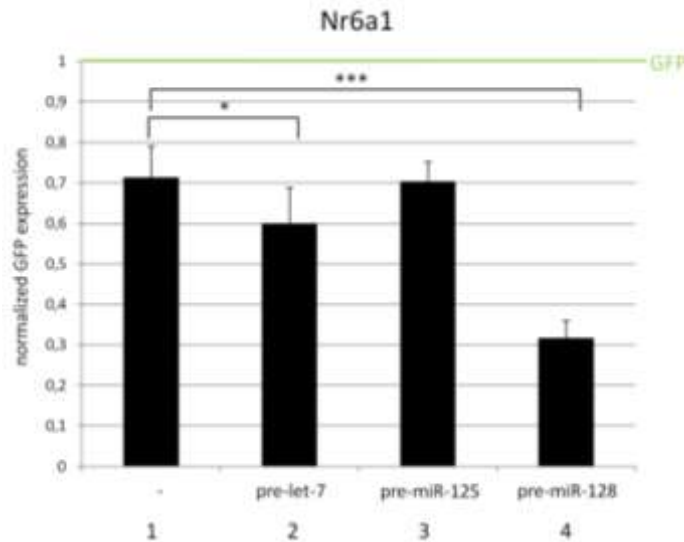
Figure 3.3.3.4b: Normalized GFP expression of GFP-Nr6a1 co- transfected with either prelet-7, premiR-125 or premiR-128 in Hek293 cells $4*10^5$ Hek293 cells were transfected with 200ng dsRED, 100ng eGFP-Nr6a1 sensor and either 20pmol premiR-125(Column 1), prelet-7a(Column 2), premiR-128(Column 3),prelet-7 + premiR-128(Column 4) or no miRNA precursor. After 48h the eGFP and dsRED expression was measured by flow cytometry. The percentages of positive cells were normalized to the parental vector eGFP-C1 (green line). An unpaired two tailed t-test (n≥3) was performed to reveal significant differences (* $p<0.05$, *** $p<0.001$).

Figure 3.3.3.4b reveals that GFP-Nr6a1 transfection alone (Column 1) shows a reduction of GFP expression of ~28% in comparison to the parental GFP-C1 vector (green line). The GFP expression of GFP-Nr6a1 co-transfected with no precursor miRNA (lane1) or premiR-125 (lane3) is identical, therefore the predicted miR-125 binding site does not seem to be biologically relevant. Although Nr6a1 is the highest ranked target of let-7 according to the PicTar and TargetScan. GFP-Nr6a1 expression was only reduced by ~18% by let-7, at the border of statistical significance (n=4, p=0.0467) detectable with this assay (lane2). Surprisingly, the GFP expression of GFP-Nr6a1 co-transfected with premiR-128 was strongly reduced (Column 4) in comparison to the control transfection (Column 1).

3.3.3.5 Validation of the putative let-7 and miR-125 target gene Arid3a

Arid3a encodes a member of the ARID (AT-rich interaction domain) family of DNA binding proteins that binds to AT-rich DNA sequences. It was found by homology to the Drosophila dead ringer gene, which is important for normal embryogenesis. Among other things, it has been shown that Arid3a protein is upregulated by forced expression of the transcription activator Trp5 (Transformation related protein, better known as p53)(Herrscher et al., 1995). p53 responds to diverse cellular stresses to regulate target genes that induce cell cycle arrest, apoptosis, senescence, DNA repair, or changes in metabolism. Mice deficient for p53

develop normally, but are susceptible to spontaneous tumors. This indirectly implicates Arid3a in the p53 cascade controlling cell growth. Figure 3.3.3.5a shows the part of the 3'-UTR of Arid3a with three miR-125 and two let-7 binding sites.


Figure 3.3.3.5a: A segment of the putative miR-125/let-7 target gene Arid3a which was used to generate an eGFP sensor construct a) 2164 bp from the 3'-UTR of the FoxP2 gene were amplified and inserted into the modified eGFP vector. The sequence includes two putative let-7 binding sites and three miR-125 binding sites. The binding sites for let-7 are labelled in pink, bold letters while miR-125 binding sites are highlighted in green. **b)** Predicted miR-125a-mRNA and let-7/mRNA duplexes for each binding site of Arid3a. The seed regions of miR-125 are highlighted in green, the let-7 seeds are shown in pink. Base pairings between the miRNA and corresponding binding site are labelled in bold letters.

The GFP-Arid3a sensor construct was co-transfected with either no pre-miRNA as a control, prelet-7, premiR-125 or premiR-128 RNA as a secondary control in Hek293 cells, and the GFP expression was quantified by flow cytometry 48 h later (Figure 3.3.3.5b).
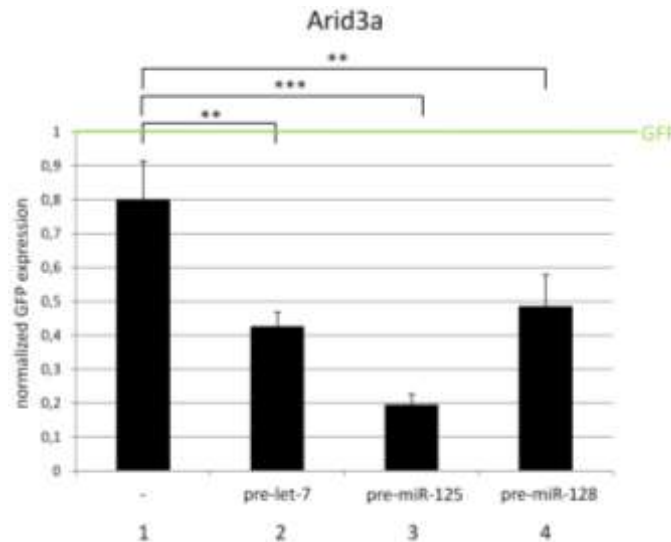
Figure 3.3.3.5b: Normalized GFP expression of GFP-Arid3a co- transfected with either prelet-7, premiR-125 or premiR-128 in Hek293 cells $4*10^5$ Hek293 cells were transfected with 200ng dsRED, 100ng eGFP-Arid3a sensor and either no precursor miRNA (Column 1), prelet-7a(Column 2), premiR-125(Column 3) or premiR-128(Column 4). After 48h the eGFP and dsRED expression was measured by flow cytometry. The percentages of positive cells were normalized to the parental vector eGFP-C1 (green line). An unpaired two tailed t-test (n≥3) was performed to reveal significant differences (** $p < 0.01$, *** $p < 0.001$).

In Figure 3.3.3.5b the GFP expression of the GFP-Arid-3a sensor transfected without any additional pre-miRNA(Column 1) was reduced by ~20% in Hek293 cells compared to the control transfection with parental GFP vector(green line). The GFP expression of GFP-Arid3a is significantly reduced by about 50% by co-transfection with prelet-7 compared with the GFP-Arid3a transfection alone. A stronger GFP repression compared with the GFP-Arid3a transfection alone is shown by co-transfection of the GFP-Arid3a sensor together with premiR-125 (lane3). The results are consistent with the potential regulation of Arid3a by let-7 and miR-125. Surprisingly, however, the GFP-Arid3a sensor shows a significant repression of GFP by co-transfection with premiR-128 (Column 4), even though miR-128 is not predicted to target Arid3a.

3.3.3.6 Validation of the putative let-7 and miR-125 target gene Arid3b

Kobayashi et al. showed that **Arid3b** plays an essential role in the development of the neural crest, a band cells derived from the ectoderm that are arranged along the outer surface of each side of the neural tube in the early stages of embryonic development. They also presented evidence that Arid3b is involved in the development of malignant neuroblastoma and might be useful as a tumor marker. 80% of stage IV tumors are Arid3b positive, whereas only 9% of stage I to III tumors are positive. siRNA experiments targeting Arid3b significantly suppressed the growth of several neuroblastoma cell lines while overexpression of Arid3b leads to an enhancement of tumor growth. Figure 3.3.3.6a shows the sequence which was

amplified to study miRNA mediated regulation of Arid3b is displayed. The sequence includes two putative let-7 binding sites and three miR-125 binding sites.
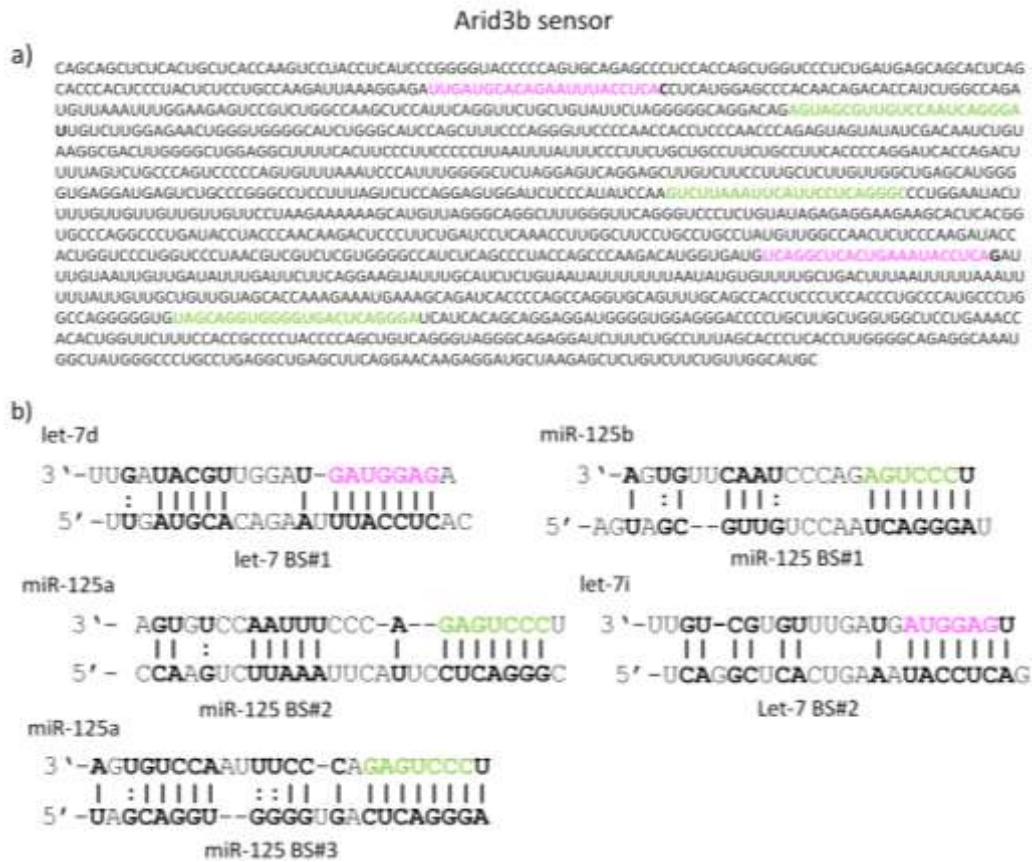

Figure 3.3.3.6a: Part of the 3'-UTR of the putative miR-125/let-7 target gene Arid3b used to generate an eGFP sensor construct a) 1382 bp from the 3'-UTR of the Arid3b gene were amplified and inserted into the modified eGFP vector. The sequence includes like Arid3a two putative binding sites for let-7 and three miR-125 binding sites. The binding sites for let-7 are labelled in pink, bold letters while miR-125 binding sites are highlighted in green. **b)** Predicted miR-125a-mRNA and let-7/mRNA duplexes for each binding site of Arid3b. The seed regions of miR-125 are highlighted in green, the let-7 seeds are shown in pink. Base pairings between the miRNA and corresponding binding site are labelled in bold letters.

In order to validate a possible regulation of Arid3b by let-7 and miR-125, a generated GFP-Arid3a sensor construct was co-transfected with either no pre-miRNA as a control, prelet-7, premiR-125 or premiR-128 RNA as a secondary control in Hek293 cells, and the GFP expression was quantified by flow cytometry 48 h later (Figure 3.3.3.6b).
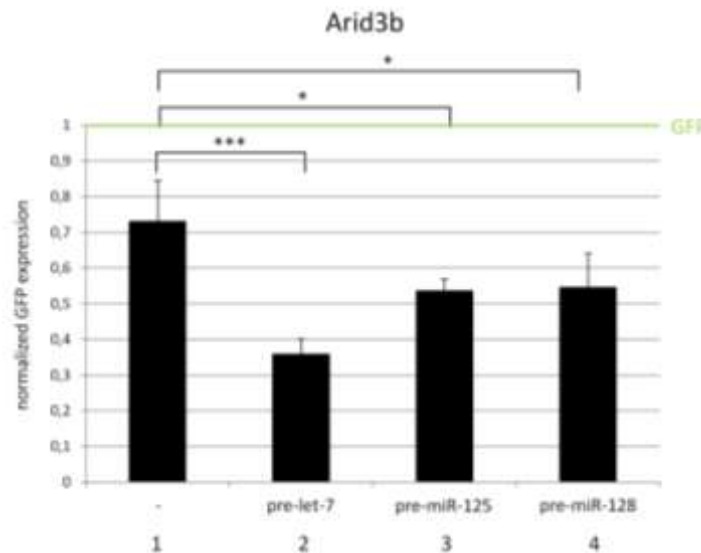
Figure 3.3.3.6b: Normalized GFP expression of GFP-Arid3b co- transfected with either prelet-7, premiR-125 or premiR-128 in Hek293 cells $4*10^5$ Hek293 cells were transfected with 200ng dsRED, 100ng eGFP-Arid3a sensor and either no precursor miRNA (Column 1), prelet-7a(Column 2), premiR-125(Column 3) or premiR-128(Column 4). After 48h the eGFP and dsRED expression was measured by flow cytometry. The percentages of positive cells were normalized to the parental vector eGFP-C1 (green line). An unpaired two tailed t-test (n≥3) was performed to reveal significant differences (*$p<0.05$, *** $p<0.001$).

The GFP expression was significantly reduced by 50% by co-transfection of GFP-Arid3b together with prelet-7 (Column 2) in comparison to the GFP-Arid3b transfection alone (Column 1) in Hek293 cells. This result suggest a potentially repression of Arid3b by let-7 during development. A much lower and less significant repression of approximately 25 % can be achieved by the co-transfection of GFP-Arid3b together with either premiR-125 (Column 3) or premiR-128 (Column 4) in comparison to the GFP-Arid3b transfection alone (Column 1). It is important to point out that both Arid3b and Arid3a and Nr6a1 appear to be regulated by miR-128, even those genes are not predicted to be miR-128 targets. Although it is not clear if this is the result of direct or indirect interactions, premiRNA transfection did not influence the expression of the eGFP control sensor as previously shown in Column 1 of Figure 3.3.2b or sensors containing synthetic miRNA binding sites (compare Column 6 and 7 of Figure 3.3.2b).

3.3.2 miRNA studies *in ovo*

The following chapter deals with studies of miRNA function during neurogenesis in the living chick embryo.

3.3.2.2 The *in ovo* electroporation technique

The following electroporations were performed, if not mentioned otherwise, 2.5 days after incubation at HH 14-16. At this time point the daughter cells of the neuroepithelial cells start to differentiate and migrate out of the ventricular zone into the mantle zone as previously shown in Figure 3.3.2.1.4. In a first approach, a CMV-eGFP vector was electroporated into the neural tube of a HH16 chick embryo. Two days later at HH26, the embryo was harvested and the electroporated area of the neural tube was cut in 50µm transverse sections. Figure 3.3.2.2b shows a typical distribution of GFP positive cells.
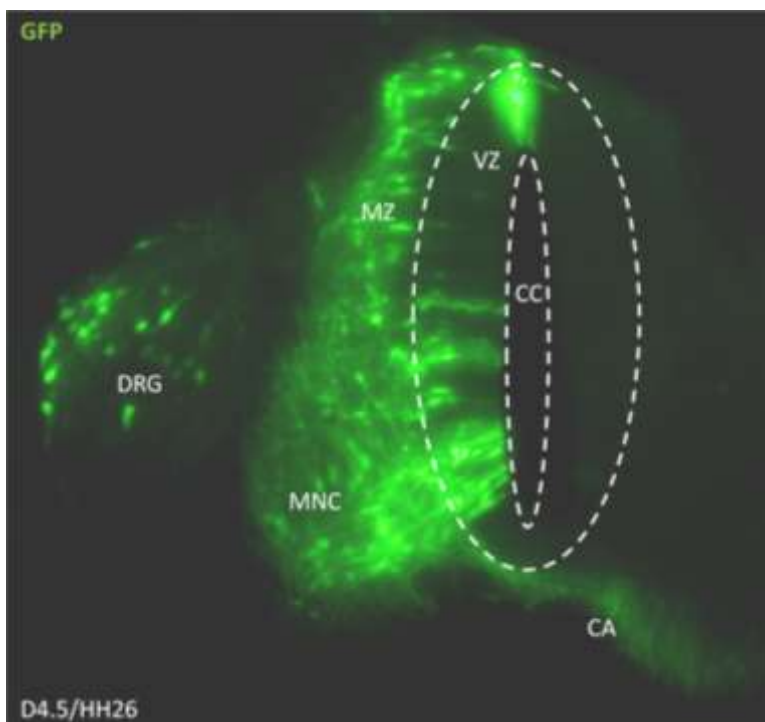
Figure 3.3.2.2b: Transversal section of a HH26 chick neural tube 48h after electroporation with CMV-eGFP CC: central canal, VZ: ventricular zone, ML: mantle zone, DRG: dorsal root ganglion, MNC: motor neural column, CA: commissural axons

In Figure 3.3.2.2b nearly all areas of the neural tube show the presence of GFP positive cells. Most of the GFP-transfected cells migrated from the ventricular zone (EL) into the mantle zone (ML). Migration to the motor neural column (MNC) and into the dorsal root ganglion (DRG) can also be observed. The transfected commissural neurons are indirectly visible by the outgrowth of commissural axons (CA) that migrate ventrally along the motor neural column of the untransfected side (check if that should be the path).

3.3.2.3 let-7 activity in the neural tube cells using GFP-2xlet-7 sensor constructs *in ovo*

Previously performed *in situ* hybridization experiments in our lab revealed that let-7 is highly expressed in the neural tube at early stages in the mouse embryo. These observations conform with *in situ* hybridizations against let-7a from the geisha webpage (Figure 3.3.2.3a)(Bell et al., 2004). Geisha (**G**allus **e**xpression **i**n **s**itu **a**nalysis) is an online database for gene expression detection by *in situ* hybridization in the chick embryo during the first six days of development.

Figure3.3.2.3a: let-7 expression in the neural tube of a chick embryo Horizontal section of a HH16 stage embryo**.** The DIG labelled let-7 antisense probe shows strong staining in the dorsal part of the neural tube.

A disadvantage of miRNA detection by *in situ* hybridization is that an antisense probe against the mature active form of a miRNA will also detect the primary transcripts and the precursor-miRNA. In order to detect let-7 activity in the neural tube *in ovo*, a DNA cocktail of 250ng GFP parental vector or 250ng GFP-2xlet-7 together with 500ng dsRED was injected in the neural tube of HH stage 14 chicken embryos and electroporated. Chickens were harvested after 36h. Pictures of embryos were taken with a stereo microscope using identical exposure times to reveal different fluorescent intensities (see Figure 3.3.2.3b).
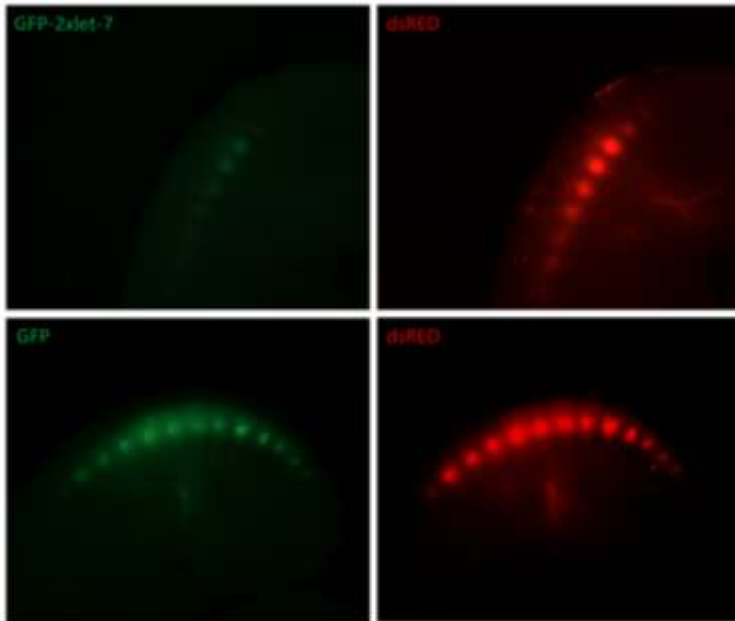
Figure 3.3.2.3b: let-7 activity in the neural tube of HH 26 embryo HH stage 14 chick embryos were electroporated with 250ng GFP together with 500ng dsRED or 250ng GFP-2xlet-7 sensor together with500ng dsRED. The pictures show the GFP/dsRED intensities after 36h. The upper row show the typical GFP/dsRED signal for a GFP-2xlet-7/dsRED co-electroporated chicken. The corresponding GFP/dsRED control electroporation is shown in the bottom row.

The picture shows a strong repression of the GFP-2xlet-7 sensor in comparison to the parental GFP construct which leads to the result that let-7 is indeed expressed and active in the neural tube.

Another advantage of the *in ovo* technique in combination with fluorescent GFP/dsRED constructs is shown in the following experiment. By using a fluorescent stereo microscope, the GFP/dsRED signal can be observed in the living chick embryo for several days. An example is shown in Figure 3.3.2.3c: the neural tube of a HH stage 13 embryo was electroporated with 250ng GFP-2xlet7 sensor together and 500ng dsRED construct. 24h, 48h and 72h after electroporation pictures were taken with identical exposure times for dsRED and GFP. 24h after electroporation, the GFP signal was equal to or stronger than the signal for dsRED (D and E). After 48h, the GFP intensity of the GFP-2xlet-7 was slightly reduced in comparison to the dsRED signal (I and J). A very strong reduction of GFP intensity in comparison to dsRED was observed 72h after electroporation (N and O).
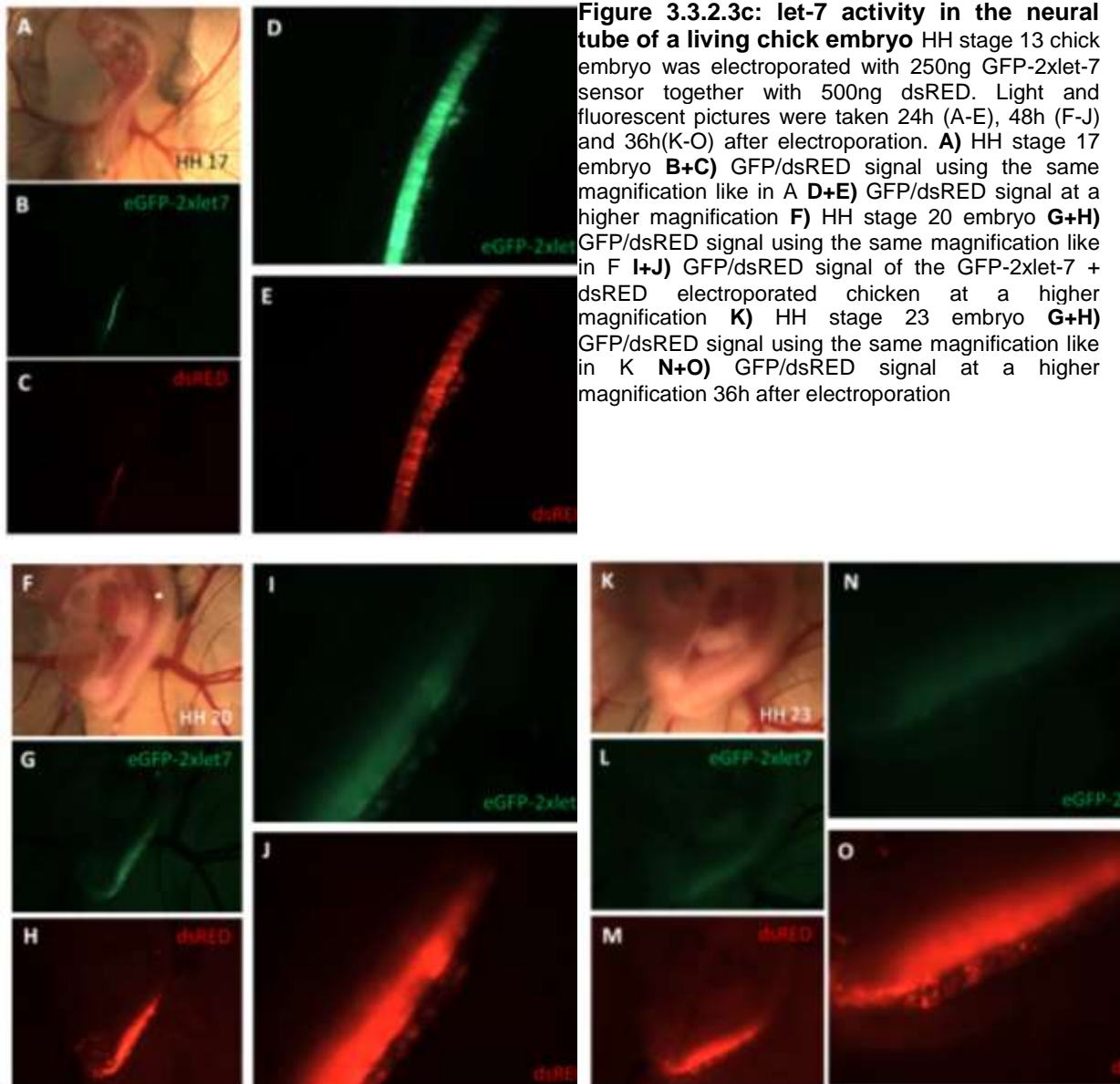
Figure 3.3.2.3c: let-7 activity in the neural tube of a living chick embryo HH stage 13 chick embryo was electroporated with 250ng GFP-2xlet-7 sensor together with 500ng dsRED. Light and fluorescent pictures were taken 24h (A-E), 48h (F-J) and 36h(K-O) after electroporation. **A)** HH stage 17 embryo **B+C)** GFP/dsRED signal using the same magnification like in A **D+E)** GFP/dsRED signal at a higher magnification **F)** HH stage 20 embryo **G+H)** GFP/dsRED signal using the same magnification like in F **I+J)** GFP/dsRED signal of the GFP-2xlet-7 + dsRED electroporated chicken at a higher magnification **K)** HH stage 23 embryo **G+H)** GFP/dsRED signal using the same magnification like in K **N+O)** GFP/dsRED signal at a higher magnification 36h after electroporation

3.3.2.4 miR-124 misexpression in the neural tube *in ovo*

miR-124 is one of the best-studied miRNAs in connection with neurogenesis. Maniatis and co-workers showed that miR-124 plays a key role in the differentiation of progenitor cells to mature neurons (Makeyev et al., 2007). Similar results were later obtained in a variety of additional experimental contexts. Therefore it was of major interest to test the effect of miR-124 overexpression in the neural tube *in vivo*. *In situ* data from the geisha webpage of the miR-124 family members miR-124a and miR-124b are shown in the following Figure 3.3.2.4a.

from GEISHA webpage
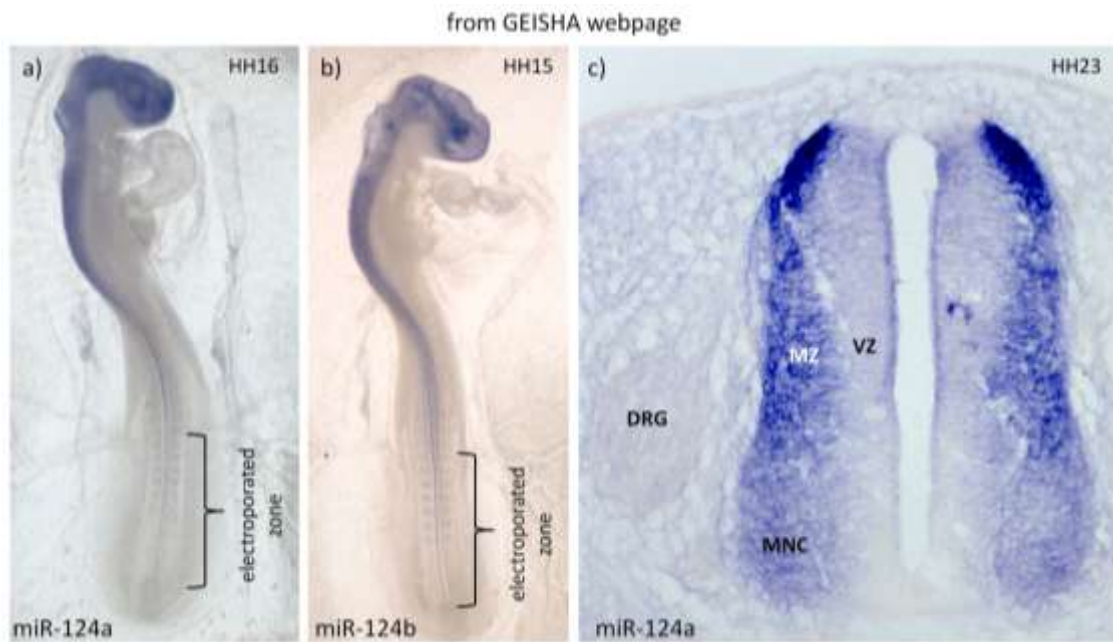
Figure 3.3.2.4a: miR-124a and miR-124b expression in the chick embryo a) whole mount *in situ* hybridization of an HH16 embryo with a DIG labeled miR-124a antisense probe b) whole mount *in situ* hybridization of an HH15 embryo with a DIG labeled miR-124b antisense probe c) *in situ* hybridization of a transversal section of a HH23 chick embryo with a DIG labeled miR-124a antisense probe. VZ: ventricular zone ML: mantle zone MNC: motor neural column DRG: dorsal root ganglion

The pictures show miR-124 expression in the developing brain and the neural tube. Interestingly the expression of miR-124 diminishes along the anterior to posterior axis of the neural tube, with the most posterior region apparently lacking miR-124. A transverse section of the neural tube at HH23 reveals miR-124 expression to be highly restricted to the mantle zone and the motor neural column of the neural tube. The dorsal root ganglion and the ventricular zone show no expression of miR-124.

In the following experiment miR-124 was overexpressed at HH16 in the posterior part of the neural tube where no miR-124 expression was observed during this time point (shown in brackets in Figure 3.3.2.4a). Electroporated cells were visualized via dsRed encoded on the pre-miR-124-RED vector (described in Chapter 3.1.2.2). 48h after electroporation at HH16 with either 2µg/µl Intron-RED or 2µg/µl pre-miR-124-RED the embryos were harvested and cut into 50µM transverse sections on a vibratome.
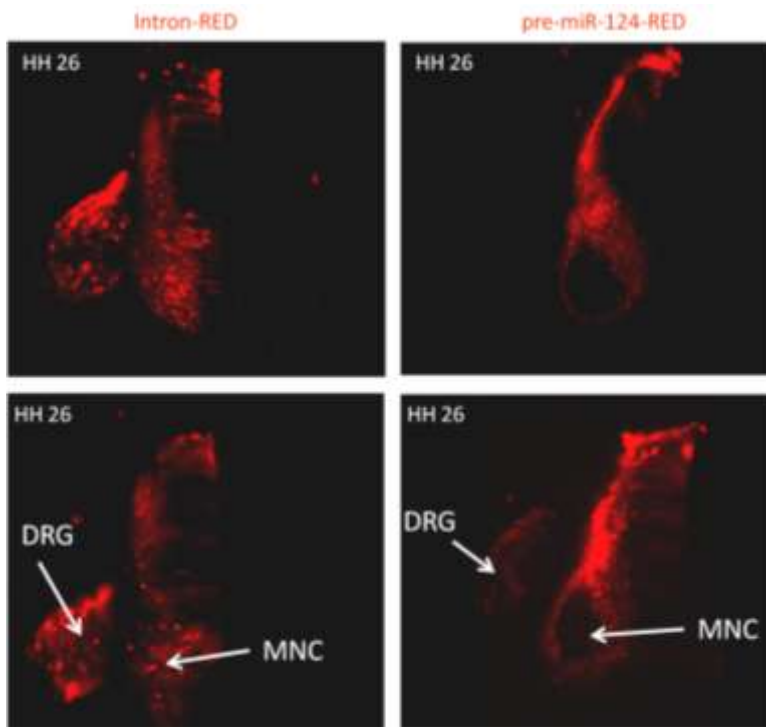
Figure 3.3.2.4b: miR-124 misexpression in the posterior part of the neural tube The posterior part of the neural tube of HH16 chick embryos were either transfected with 2µg/µl parental Intron-RED (or 2µg/µl pre-miR-124-RED vector). After 48 h the embryos were harvested and the posterior part of the embryo was cut in 50µm thick transverse sections. Two representative electro-porations of two different chick embryos that were electro-porated with the parental vector Intron-RED are shown on the left side. On the right side the neural tube of two different chick embryos transfected with pre-miR-124-RED are shown. (*n = 6)*

In Figure 3.3.2.4b, typical fluorescent images for both constructs are shown. It is particularly noticeable that cells expressing miR-124 fail to migrate to the dorsal root ganglion in comparison to the Intron-RED control. Furthermore the pre-miR-124-RED transfected neural tube shows a stronger RED signal surrounding the motor neural column, while the Intron-RED transfected neural tube shows a more homogenous RED signal.

Figure 3.3.2.4c: Merged z-stack of confocal images of the neural tube expressing Intron-RED (left) and pre-miR-124-RED (right) The posterior part of the neural tube was electroporated with either Intron-RED or pre-miR-124-RED as previously described in Figure 3.3.2.2.2b. The lower row shows the motor neural column at higher magnification.

A confocal microscope was used for a closer examination, and a z-stack of the neural tube was recorded. The z-stack was merged with ImageJ software. The results are displayed in Figure 3.3.2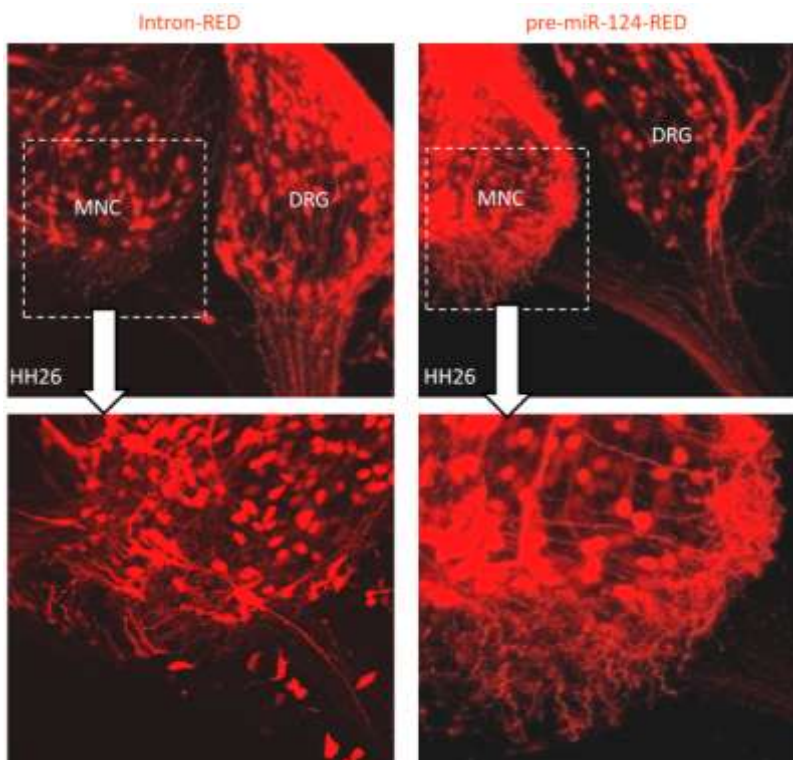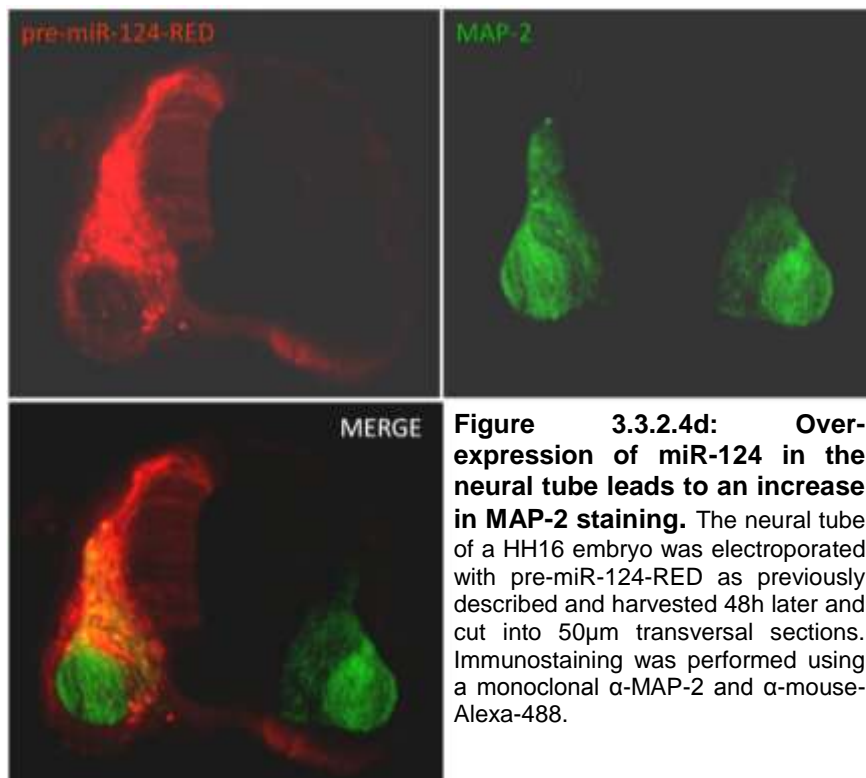.4c. As already shown in the previous Figure the dorsal root ganglion has fewer pre-miR-124-RED positive neurons compared to the Intron-RED control. The increased staining around the motor neural column after electroporation with pre-miR-124-RED is due to an increase in neuronal outgrowths.

To visualize dendritic outgrowth of transfected cells the sections were co-stained with MAP-2 antibody. MAP-2 is a neuron-specific microtubule associated protein that is enriched in dendrites.

Figure 3.3.2.4d: Over-expression of miR-124 in the neural tube leads to an increase in MAP-2 staining. The neural tube of a HH16 embryo was electroporated with pre-miR-124-RED as previously described and harvested 48h later and cut into 50μm transversal sections. Immunostaining was performed using a monoclonal α-MAP-2 and α-mouse-Alexa-488.

The neural tube shown in Figure 3.3.2.4d reveals strong MAP-2 staining within the motor neuron column and the ventral mantle zone in the vicinity of the commissural neurons on the non-electroporated right side. On the left side, miR-124 overexpression led to expanded MAP-2 staining into the dorsal mantle zone, indicative of either an increase in neuronal density or dendritic arbors in this region. Although preliminary, these results are in contrast to a published report describing much more limited effects of miR-124 overexpression after *in ovo* electroporation (Cao et al., 2007).

3.3.3 miRNA overexpression studies *in utero*

One technique that has been established in our institute during this work is the *in utero* electroporation technique. This technique allows the introduction of DNA or RNA into embryonic mouse brains at defined time points. The *in utero* electroporation was mainly done by injection of plasmid DNA into one of the lateral ventricles from which the surrounding cells generate the cortex.

For this thesis the two brain-specific miRNAs, miR-124 and miR-128 were overexpressed into the ventricular-layer of the lateral ventricle. To study a potential influence on migrating neurons, miR-124 and miR-128 were overexpressed at different stages between E12, when the first neurons migrate towards the pial surface, and E15, when the later neurons migrate to the superficial cortical layer.

3.3.3.3 miR-124 overexpression in the lateral ventricle of the mouse brain

As previously shown in Chapter 3.2.2, miR-124 is already active in E15 primary cortical neurons but not in radial progenitor cells. In addition, overexpression of miR-124 in the HH15 chicken neural tube led to clear phenotypic changes (described in section 3.3.2.4). In order to test if miR-124 also plays an important role in development of the cortex a gain of function approach using the pre-miR-124-RED vector was again chosen. As a control, the Intron-RED backbone vector or pre-miR-29-RED (data not shown) was electroporated. In a first experimental series, approximately 1μl DNA with a final concentration of 4μg/μl was injected into the lateral ventricle of E12 mice embryos and electroporated towards the lateral wall. The transfected brains were harvested six days later at E18. After fixation, 50μm coronal vibratome sections were mounted on glass slides and examined using a fluorescent microscope (Figure 3.3.3.a).
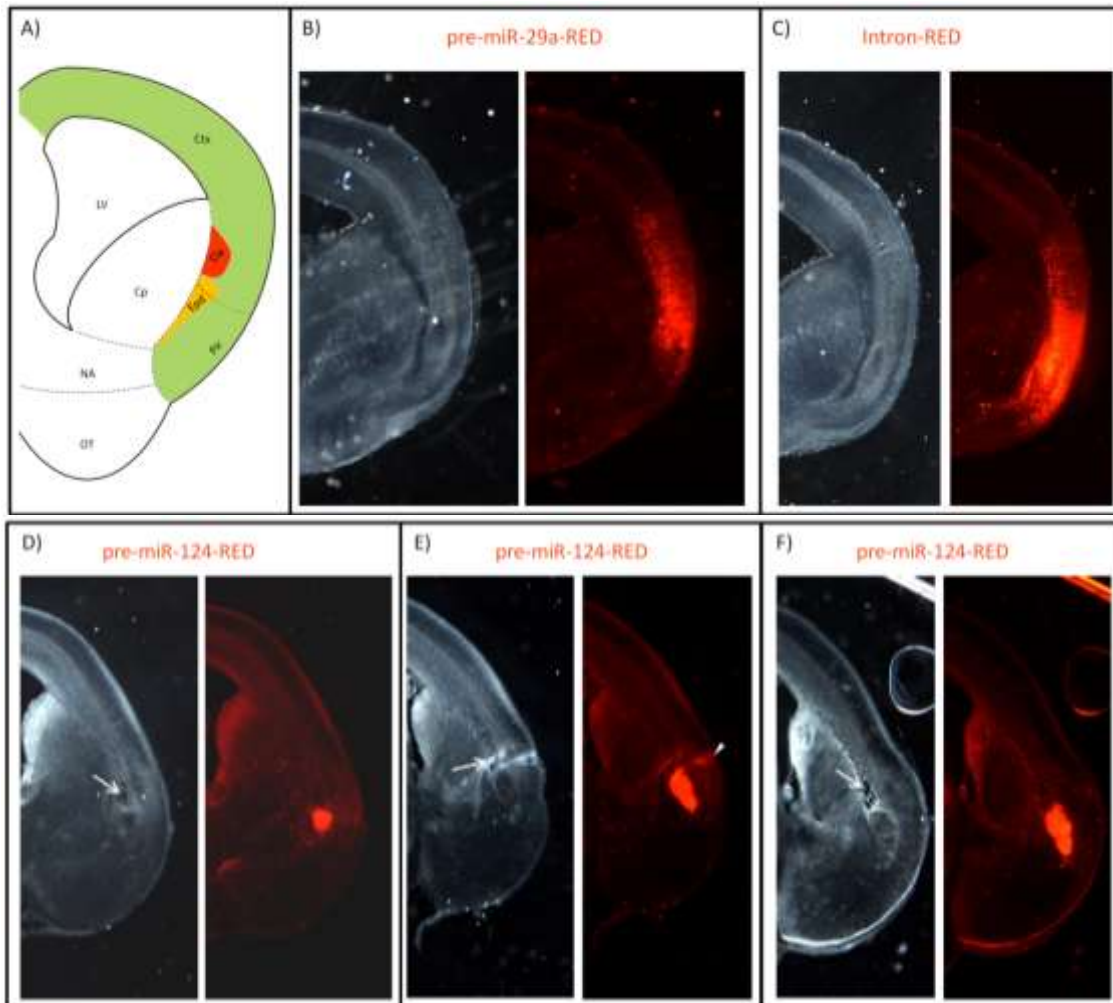
Figure 3.3.3.3a: miR-124 misexpression in the embryonic mouse brain A) Schematic coronal section of an E18 mouse forebrain at the level of the nucleus accumbens, the approximate region targeted in this series. Ctx: cortex(green), Pir: piriform cortex, LV: lateral ventricle, Cp: caudal putamen, Epd: endopiriform nucleus dorsal part, Cla: claustrum, NA: nucleus accumbens, OT: olfactory tubercle **B+C)** Two coronal sections of two different E18 brains that were electroporated at E12 with pre-miR-29a-RED or Intron-RED **D-F)** Three coronal sections of two different E18 brains that were electroporated at E12 with pre-miR-124-RED. In all three pictures abnormal morphology is apparent in the region containing electroporated cells. In picture E some cells have migrated into the cortical layer in a condensed ray (white arrowhead).

Figure 3.3.3.3a displays comparable pictures of five independent electroporations. In the upper row two control electroporations with the parental pre-miR-29a-RED or Intron-RED construct and in the bottom row three independent pre-miR-124-RED sections are shown. Cortical areas electroporated with Intron-RED show a widespread distribution of cells migrating into the cortical layers (pictures B and C). The pre-miR-124-RED positive cells in the pictures D-F displayed a highly abnormal migration and distribution. In majority of cases pre-miR-124-RED positive cells failed to migrate to the cortical layers. Just a few cells in picture E manage to reach the cortical plate (see white arrowhead). The majority of the pre-miR-124-RED positive cells are clustered within one subcortical area. Furthermore, the brain slides show a de-lamination effect near the miR-124-RED positive subcortical area (see white arrows). This misexpression phenotype is presented in more detail from merged confocal stacks spanning 30µm.
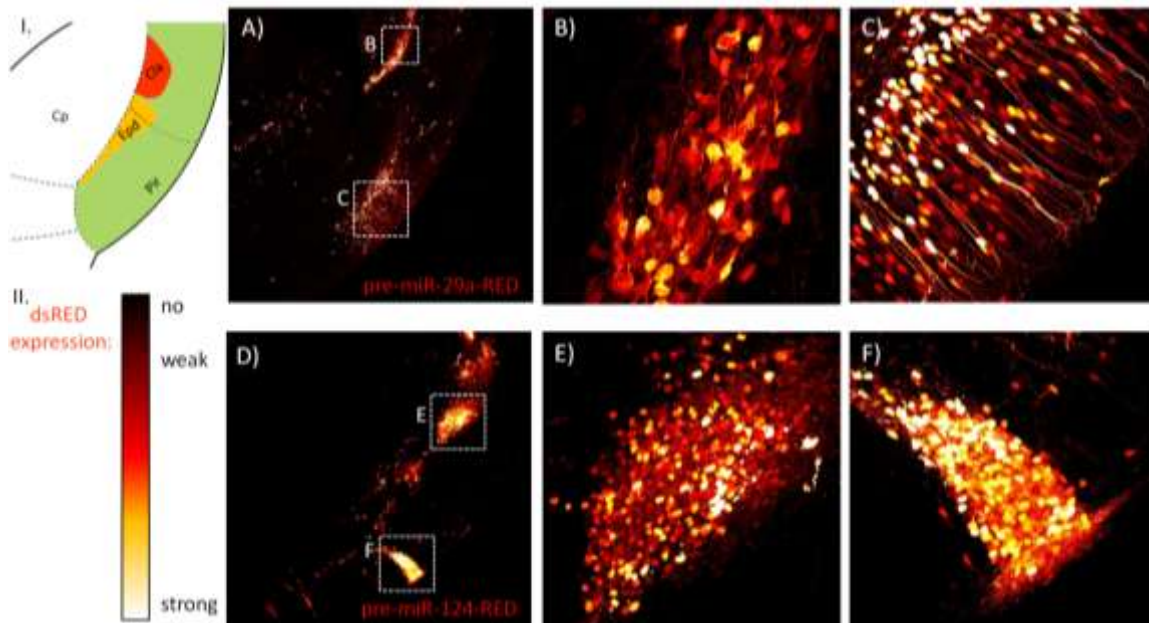
Figure 3.3.3.3b: miR-124 misexpression in the embryonic mouse brain I. Schematic coronal section of the dorsal cortex of an E18 mouse brain Pir: piriform cortex, Cp: caudal putamen, Epd: endopiriform nucleus dorsal part, Cla: claustrum shown in pictures A and D **II.** The firefly lut intensity bar. The Figure displays merged confocal stack pictures of E18 brains after electroporation with either pre-miR-29-RED **(A-C)** or pre-miR-124-RED **(D-F)** at E12 **A)** merged confocal stack of the brain area corresponding to the region shown in I. **B)** higher magnification of Intron-RED positive cells in the approximate area of the piriform nucleus **C)** higher magnification of Intron-RED positive cells in the piriform cortex region **D)** merged confocal stack of the electroporated cells, corresponding to the region shown in I. **E)** higher magnification of pre-miR-124-RED positive cells in the approximate area of the piriform nucleus **F)** higher magnification of pre-miR-124-RED positive cells in the approximate area of the piriform cortex.

In order to better visualize cells with strong fluorescent signal, the "firefly lut" (**l**ook **u**p **t**able) plug-in was used to convert fluorescent intensity along a black-red-white scale (see Figure 3.3.3.3b II.). In Panels B and E, cells in a subcortical location can be compared. In Panels C and F cortical cells are shown (Figure 3.3.3.3b). In the control electroporation, cells are primarily aligned in parallel. The outgrowths of these cells are arranged more or less in parallel to a combined centerline (picture B). As previously shown, a lot of pre-miR-29a-RED positive cells are distributed in the cortical piriform cortex. Most of their nuclei are arranged within one cortical layer whose outgrowths are arranged in parallel targeting the marginal layer (picture C).

pre-miR-124-RED electroporation at stage E12 reveals red positive cells in the same areas like the control but most of these cells are arranged in clusters (compare picture A and D). Far too much pre-miR-124-RED positive cells are observed in the piriform nucleus (picture A) in comparison to the control (picture D). Furthermore their outgrowths are spread in fuzzy different directions and the nuclei of the pre-miR-124-RED cells are arranged much closer together. Particular noticeable is the cell density of pre-miR-124-RED positive cells that have been migrated into the piriform cortical layer. These cells reach a much more narrow section of the in comparison to the control (picture D and F). The nuclei of pre-miR-124-RED positive cells are widespread in all layers of the piriform cortex and not located in a distinct layer like

shown for the control (compare picture C and F). Moreover the outgrowth of these cells point again in different directions with a fuzzy shape. The whole thing looks like a multiple pile-up.

In a following step, *in utero* electroporations were done at later stages to figure out if this observed phenotype caused by misexpression of miR-124 at E12 occurs in later stages too. Therefore pre-miR-124-RED or pre-miR-29a-RED as a control was injected into the lateral ventricle of E15 mice brains and electroporated. The brains were harvested at stage P1, cut in 50µm thick coronal sections and prepared for microscopic imaging as previously described. Interestingly, the differences between Intron-RED or pre-miR-124-RED electroporated brain slides were only slight to non-existent (data not shown).

3.3.3.4 miR-128 overexpression in the lateral ventricle at stage E15

In situ hybridization studies in our lab reveal that miR-128 is already expressed at embryonic mouse stage E12 in the neural tube and the developing brain. However, assays of miR-128 activity (Chapter 3.2.2) defined an induction time point between E15 and E18. Not very much is known about miR-128. Recent *in vitro* studies showed that miR-128 overexpression leads to a suppression of the genes Reelin and DCX (Doublecortin) in human neuroblastoma cells. Reelin plays an important role in neuronal migration and positioning of neurons in the developing brain. Moreover, Reelin stimulates dendrite and dendritic spine development. Doublecortin is expressed in neural precursor cells after exiting the cell cycle, and is therefore a marker for immature neurons. Another group showed that overexpression of miR-128 in glioma cells seems to suppress the transcription factor E2F3a. E2F3a is an important factor that regulates cell cycle progression. They observed that overexpression of miR-128 can inhibit cell proliferation in glioma cells. In summary, these data suggest a possible role for miR-128 in migration and maturation of neurons in the CNS. In order to check if overexpression of miR-128 in the developing cortex leads to a migration or proliferation phenotype, the pre-miR-128-RED and control constructs were electroporated into the lateral ventricle of E15 embryos, and the transfected brains were harvested 5 days later at P1. Coronal slices were do prepared as described in Chapter 3.3.3.3. In Figure 3.3.3.4a, coronal sections in the region of the sagittal fissure above the hippocampal formation are shown.
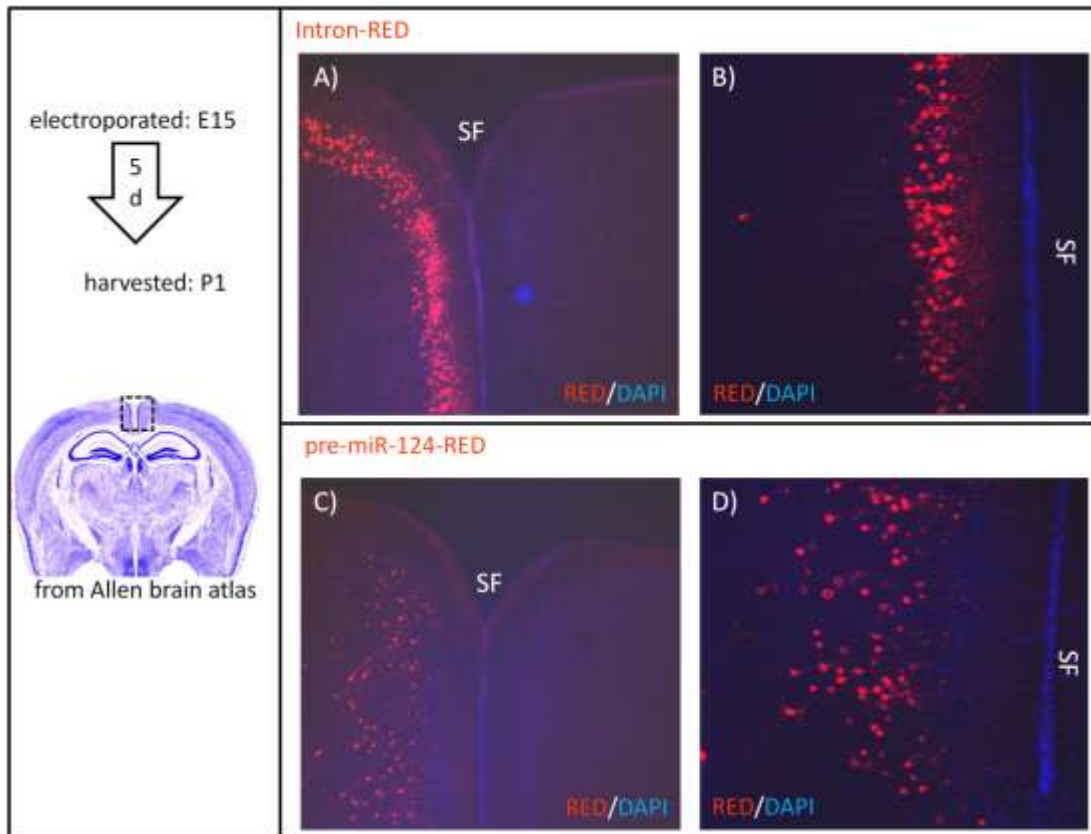
Figure 3.3.3.4a: miR-128 misexpression in the embryonic mouse brain E15 mice embryos were electroporated with either pre-miR-128-RED or Intron-RED and harvested six days later. The dotted square on the left marks the lateral commissural fissure of the cortex from where the pictures A-D originated. A-D) merged 30µm z-stack of fluorescent confocal pictures. The merged z-stack was afterwards merged with a DAPI-picture taken from that area. A) Intron-RED positive cells that are migrated to the cortical layers underlying the sagittal fissure (LCF) B) Enlarged picture of positive cells that migrated towards the sagittal fissure with the cortical layer Intron-RED C) pre-miR-128-RED positive cells that migrated close to the sagittal fissure D) Enlarged confocal z-series of pre-miR-128-RED positive cells near the sagittal fissure

Initial inspection of the results reveals that the pre-miR-128-RED positive cells are consistently arranged in deeper layers of the compared to the control. The Intron-RED positive cells of the control are densely packed in a small layer close to the molecular layer (Layer I). The pre-miR-128-RED positive cells are in contrast more widely distributed in deeper layers of the cortex. In order to roughly identify the cortical layers where the cellular bodies of the electroporated cells are arranged, confocal 30µm z-stacks of the RED fluorescent cells close to the pial surface were taken together with a picture of the DAPI staining (Figure 3.3.3.4b).
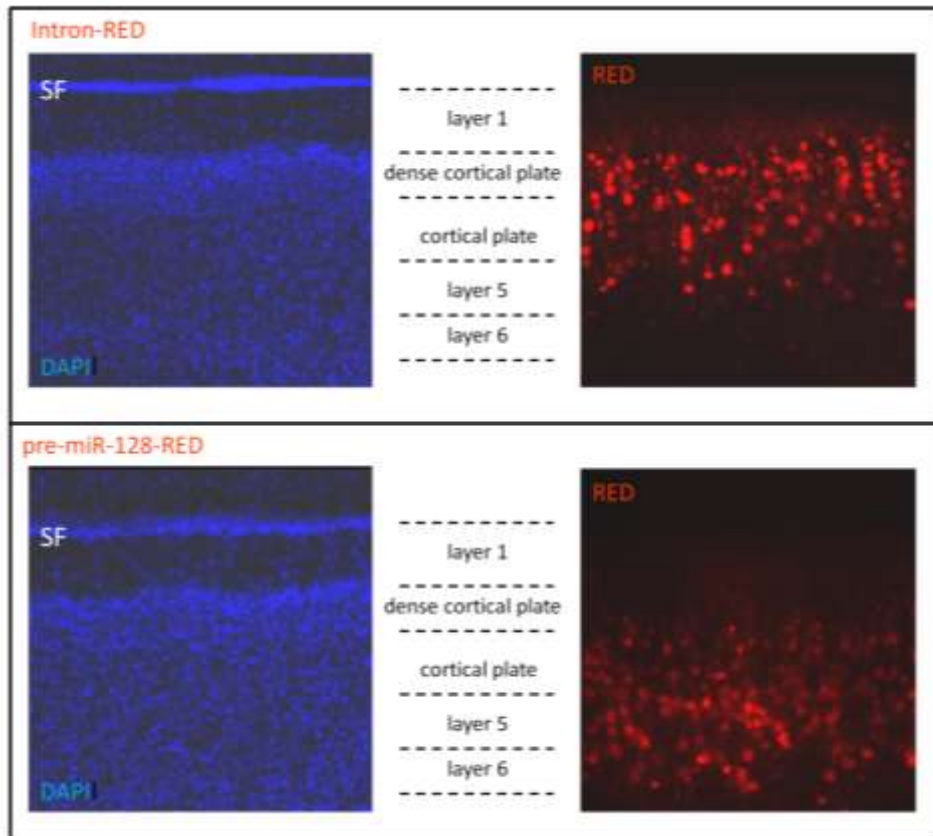
Figure 3.3.3.4b: Overexpression of miR-128 leads to a dispersion of electroporated cells in deeper cortical layers of the embryonic mouse brain E15 mice embryos were electroporated with either Intron-RED (upper panel) or pre-miR-128-RED(bottom panel) and harvested six days later. On the left the DAPI near the comissural fissure and on the right the corresponding red-fluorescent pictures are shown. The upper panel shows a brain slide that has been previously electroporated with the parental Intron-RED vector. In the middle the different cortical layers are displayed that have been derived from the different dispersion of DAPI stained nuclei for each layer.

By comparision of the DAPI staining with a coronal section of a P1 brain slide from the Allen mouse brain atlas it was possible to assign the nuclear distribution to distinct cortical layers: Layer 1 (molecular layer), the dense cortical plate, the cortical plate, Layer 5 and Layer 6. The brain which has been electroporated with the parental vector Intron-RED (upper row) shows the highest accumulation of electroporated cell bodies within the dense cortical plate and declining signal in lower layers until Layer 5. In contrast, cells that overexpress miR-128 (lower row) are most prominently found in Layer 5. miR-128^{+} cells are also observed in layer 6 and the cortical plate. These results are the first evidence that misexpression of miR-128 may interfere with cortical layering *in vivo*. It seems that premature miR-128 expression results in a "stop signal", preventing migration to the upper layers in late embryonic development.

3.4 Characterization of two miRNA regulated stemness genes: Lin-28 and Lin-41

3.4.1 Lin-28

Together with the embryonic stem cell specific genes Oct-4, Sox-2 and Nanog, Lin-28 cooperates to induce pluripotency when ectopically expressed in somatic cells (Thomson/Yu et al.). Induced pluripotent cells (iPS) seem to be nearly identical to natural pluripotent cells such as embryonic stem cells in many aspects, including expression of distinct stem cell genes, chromatin methylation, doubling time, embryoid body formation and ability to differentiate into various cell types. The regulation of Lin-28 by miR-125 in mammalian stem cells has been well characterized (Arasu et al., 1991; Moss et al., 1997; Moss and Tang, 2003), supporting an important role of miR-125 during stem cell differentiation.

3.4.1.1 Identification of Lin28 as a let-7 target gene

The 3'-UTR of Lin-28 bears two miR-125 binding sites, with additional evidence for at least one potential let-7 binding site. According to the current PicTar database of predicted miRNA binding sites, the mouse lin-28 3´UTR contains four conserved binding sites for members of the let-7 family in addition to the two experimentally validated sites for miR-125. Furthermore, the 3'-UTR of Lin-28 bears three additional predicted binding sites for miR-128. Two of them overlap with other putative miRNA binding sites as shown in Figure 3.4.1.1a.
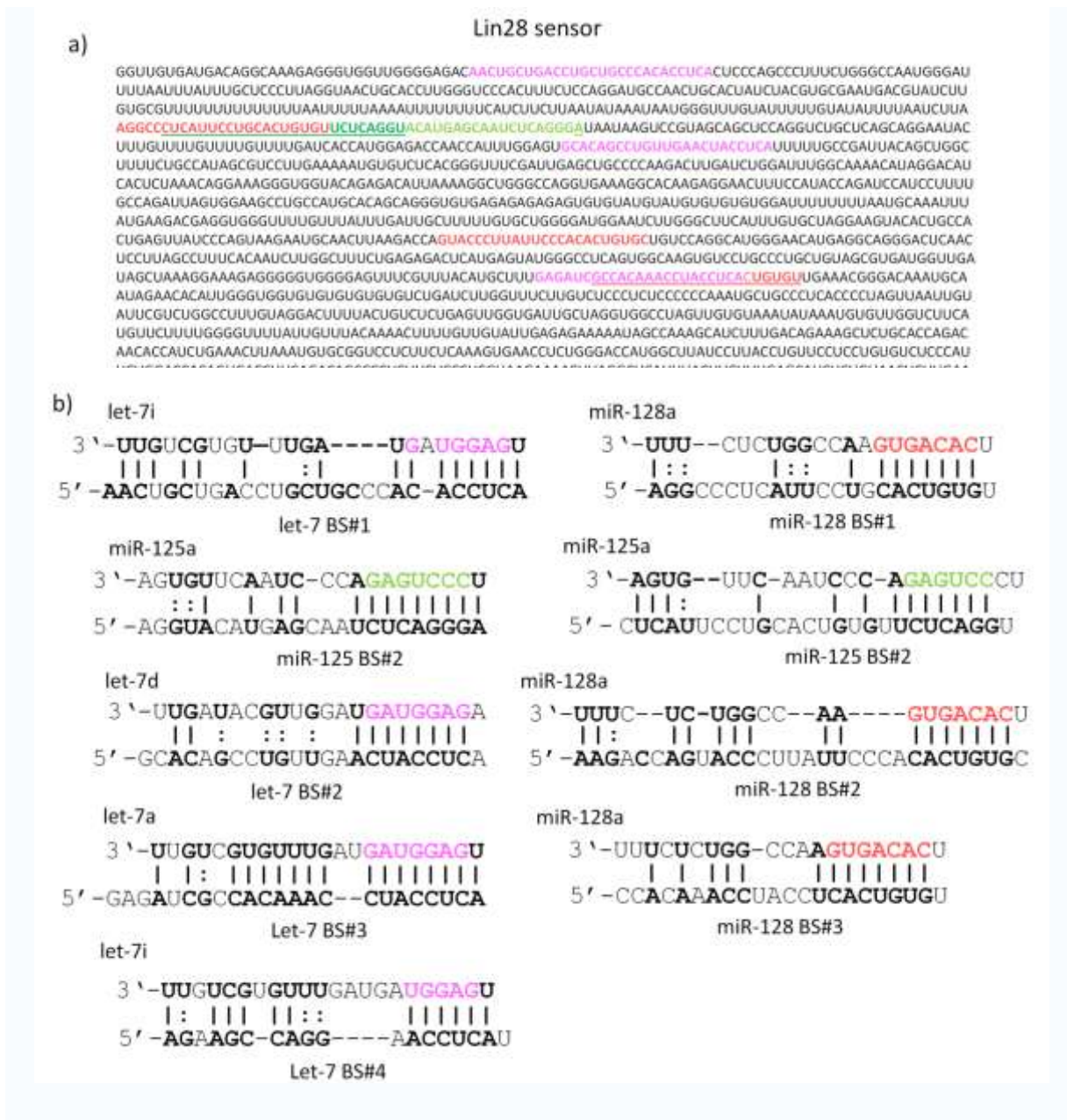
Figure 3.4.1.1a: Part of the 3'-UTR of the putative miRNA regulated gene Lin28 which was used to generate an eGFP sensor construct a) 1646 bp from the 3'-UTR of the Lin28 gene were amplified and inserted into the modified eGFP vector. The sequence includes binding sites for let-7, miR-125 and miR-128. The four binding sites for let-7 are labelled in bold pink letters. The two miR-125 binding sites are highlighted in green. The first miR-125 binding site (dark green underlined) extends deep into the first miR-128 binding site while the second miR-125 binding site overlaps with the first one. The 3'-UTR of Lin-28 contains three miR-128 binding sites as well. As mentioned above, the first binding site partially overlaps with the first binding site for miR-125 as well as the third one which extends with its sequence deep into the third let-7 binding site. **b)** Predicted miR-125a-mRNA duplex and let-7-mRNA duplexes for each binding site of Lin28. The seed region of miR-125 is highlighted in green, the let-7 seeds are shown in pink letters. Base pairings between the miRNA and corresponding binding site are labelled in boldface. Interestingly, the first let-7 binding site predicted by PicTar show s a short seed sequence.

In order to test whether Lin-28 is regulated by let-7 or miR-128, an eGFP sensor construct was generated bearing the 3'-UTR of Lin-28 (displayed in the upper part of Figure 3.4.1.1a). HEK293 cells were co-transfected with the GFP-Lin-28 sensor, together with synthetic

precursor miRNAs and pdsRed as a marker for transfection efficiency. After 48h, the fluorescence of the cells was measured by flow cytometry. Average eGFP fluorescence of dsRed-expressing cells is plotted for each miRNA and normalized to the parental GFP-vector in Figure 3.4.1.1b).
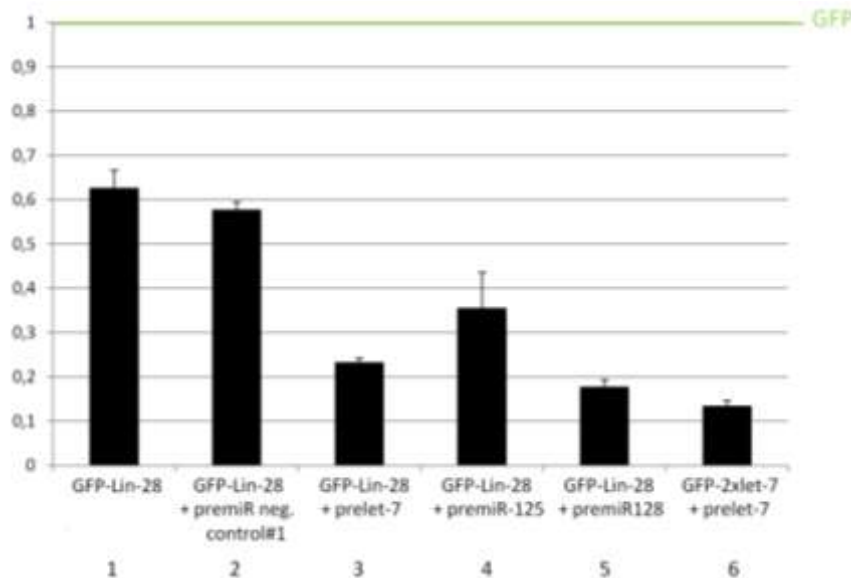
Figure 3.4.1.1b: Lin28 bears miRNA mediated regulatory binding sites for let-7, miR-125 and miR-128. For each transfection $4*10^5$ Hek293 cells were transfected with 100ng GFP sensor, 20pmol double stranded precursor miRNA and 200ng dsRED as a control for the transfection efficiency. After 48h the eGFP expression was measured by flow cytometry. The percentages of positive cells were normalized to the parental vector eGFP-C1 (green line). The normalized GFP expression of cells transfected with the GFP-Lin28 sensor (Column 1), GFP-Lin28 + a negative control precursor (Column 2), GFP-Lin28 + prelet-7 (Column 3), GFP-Lin-28 + pre-miR-125 (Column 4), GFP-Lin-28 + pre-miR-128 (Column 5) and GFP-let-7 sensor + pre-let-7 (Column 6) are shown. Data are mean ± sd. of four independent experiments.

In HEK293 cells the expression of the GFP-Lin-28 sensor itself (Column 1 and 2) was reduced in comparison to GFP- expression of the parental eGFP-vector (green line). However, expression of the Lin-28 sensor construct was found to be almost 3-fold downregulated by let-7 (Column 3) and ~2-fold downregulated by miR-125 (Column 4). The strongest repression could be observed as a result of co-electroporation with premiR-128 (Column 5) which nearly reaches the expression of the negative control where let-7 was co-transfected with a sensor containing two perfectly complementary let-7 binding sites.

3.4.1.2 Lin28 overexpression selectively represses miRNA activity in Hek293 cells

During this work we were able to demonstrate with biochemical assays that the pluripotency factor Lin-28 binds the pre-let-7 RNA and inhibits processing by the Dicer ribonuclease in ES and EC cells. Additional biochemical experiments revealed that Lin-28 binds pre-miR-128 in addition, but not pre-miR-124, suggesting sequence and secondary structure specific binding of Lin-28 to pre-miRNAs. To confirm this biochemical data, 3xFlag-Lin-28 or the empty 3xFLAG vector as a control was co-transfected with artificial GFP sensors for let-7, miR-124 and miR-128 together with intronic-dsRED constructs bearing the corresponding pre-miRNA sequences within the intronic sequence (Figure 4.4.1.1b).
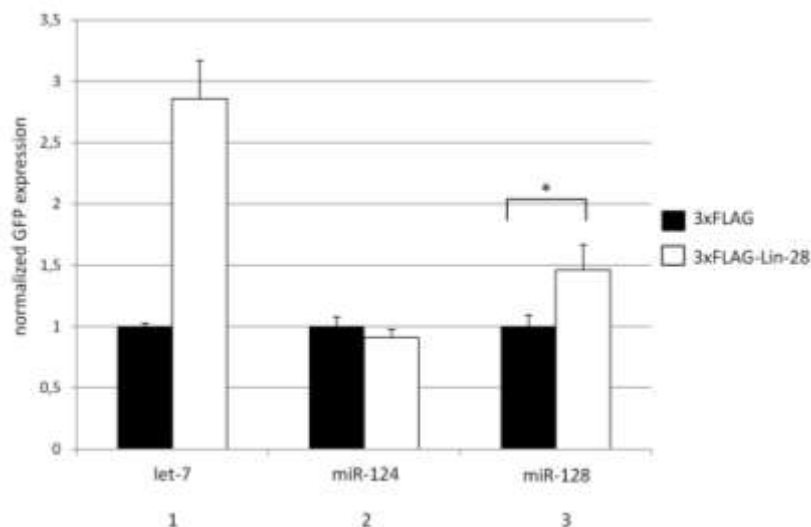
Figure 3.4.1.2: Lin28 selectively inhibits the activity of let-7 and miR-128 but not miR-124. For each transfection $4*10^5$ Hek293 cells were transfected with 100ng GFP sensor, 20pmol double stranded precursor miRNA and 200ng dsRED as a control for the transfection efficiency. After 48h the eGFP expression was measured by flow cytometry. The percentages of positive cells were normalized to the parental vector eGFP-C1 (green line). The normalized GFP expression of cells transfected with the GFP-Lin28 sensor(Column 1), GFP-Lin28 + a negative control precursor (Column 2), GFP-Lin28 + prelet-7 (Column 3), GFP-Lin-28 + pre-miR-125(Column 4), GFP-Lin-28 + pre-miR-128 (Column 5) and GFP-let-7 sensor + pre-let-7 (Column 6) are shown. Data are mean ± sd. of three independent transfections performed in duplicate.

In the case of let-7, Lin-28 was able to inhibit let-7 mediated silencing of the GFP-let-7 sensor up to 3-fold (Column 1). A weaker but significant 50% repression of pre-miR-128 activity could be observed for the GFP-miR-128 sensor in contrast to the 3xFLAG control (Column 3). However, the miR-124 sensor is not affected by Lin-28 (Column 2). These results confirm and support the biochemical data, that Lin-28 selectively binds the precursor miRNAs for miR-128 and let-7 and inhibits their processing by the Dicer ribonuclease (Heo et al., 2008; Rybak et al., 2008).

3.4.1.3 Lin28 overexpression in the chicken neural tube

Shortly after submission of our Lin-28 paper, another group headed by Richard Gregory published a paper where they showed in an *in vitro* assay that Lin-28, a developmentally regulated RNA binding protein, selectively blocks pri-let-7 processing in embryonic cells. They found that Lin28 is necessary and sufficient for blocking Microprocessor-mediated cleavage of the pri-let-7 miRNA in the nucleus. Their observations are in contrast to our results, because our model consists of a selective blockade of pre-let-7 in the cytoplasm. As one test of the two models, we analyzed the intracellular localization of Lin-28 *in vivo* after electroporation of HH16 chicken embryos. A pc3xFLAG construct bearing the ORF of Lin-28 was co-electroporated together with a construct coding for a GFP-MDB-NLS fusion protein into the neural tube of HH16 chicken. This construct encodes a nuclear targetted eGFP fusion protein with the methyl-CpG binding domain of MBD. Since neural progenitor cells in the neural tube undergo ongoing cell-divisions, this model allows observation of Lin-28 localization at all cell-cycle stages.

Figure 3.4.1.3 shows ectopic 3xFLAG-Lin-28/GFP-MBD-NLS expression in the chick embryonic neural tube at HH26. 3xFLAG-Lin28 was visualised with monoclonal anti-FLAG antibody and anti-mouse-Alexa-568. Pictures A shows a widespread distribution of 3xFLAG-Lin28 positive cells in the ventricular zone (EL), the mantle zone (ML) and a portion of the dorsal root ganglion (DRG). At a higher magnification (pictures D to I) ectopic expression of Lin-28 shows distinctly cytoplasmic staining. Noticeable is the perinuclear arrangement of ectopically expressed Lin-28 in small foci in cells close to the ventricular zone (pictures D and E). These observations support previous studies describing predominantly cytoplasmic localization of Lin-28 in cultured cells (Rybak et al., 2008) and extend the findings to the neuroepithelium *in vivo*. These results argue for a more central role for Lin-28 in cytoplasmic as opposed to nuclear miRNA processing.
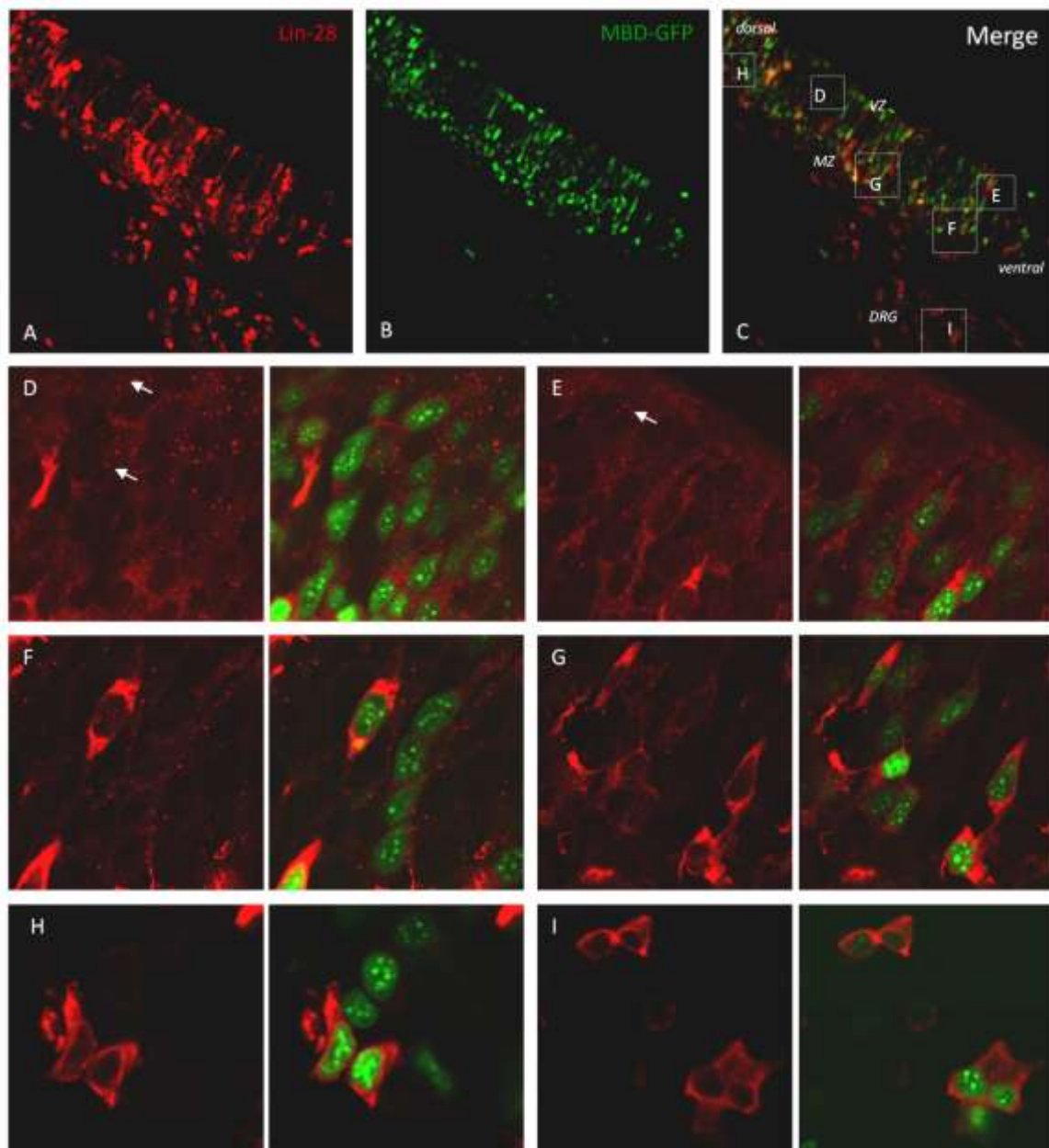
Figure 3.4.1.3: Overexpression of Lin-28 in the chicken neural tube shows distinct cytoplasmatic staining A-C: Rostral projections of confocal series **A**: Immunostaining of pC-3xFlag-lin28 positive cells **B**: MDB-GFP shows distinct nuclei staining **C**: Merged projections, confocal pictures on higher magnification were done for the areas D –I, DRG: dorsal root ganglion, VZ: ventricular zone, ML: mantle zone **D+E**: Confocal pictures from the ventricular layer. Lin-28 is localized as small dots in the cytoplasm (arrows) **F-H**: Confocal pictures from the mantle zone **I**: Confocal pictures of the dorsal root ganglion

As additional evidence for cytoplasmatic blockade *in vivo*, *in situ* hybridization was performed by A. Rybak to determine the localization of let-7 in EC cells. Probes complementary to let-7a or pre-let-7a both revealed predominantly granular staining in the perinuclear cytoplasm.

3.4.2 Lin-41

An additional part of this thesis involved the isolation of a full length clone of the predicted mammalian homolog of the original let-7 target gene of *C. elegans*, *lin-41*. Starting with a partial cDNA clone obtained from the Mammalian Gene Collection, 5' RACE was performed in an effort to isolate the 5'ORF. In the course of this work, a full length sequence was reported by Kanamoto et al. (Kanamoto et al., 2006), and was used to generate our own clone. Mouse and human Lin-41 was shown to encode a highly conserved, 855 aa long protein containing the full array of protein domains described for the *C. elegans* protein (Kanamoto et al., 2006): an N-terminal RING finger domain followed by a pair of B-Box-type Zinc fingers and the B-Box coiled coil domain, a filamin-type immunoglobulin domain and a C-terminal NHL domain (Figure 3.4.2a).

Figure 3.4.2a: Protein domains of mLin-41. **For a detailed explanation please refer to text.**

The combination of the Ring finger domain and the pair of B-Box-type Zinc fingers and the B-Box coiled coil domain have been found in a number of proteins, termed tripartite motif-containing Protein (Trim). The presence of the RING domain is often associated with E3 ligase activity, which mediates ubiquitination and therefore proteolysis of protein interaction partners. The NHL domain was first recognized as a repetitive structural motif in the Ncl-1, HT2A and Lin-41 proteins (Neumuller et al., 2008).The NHL domain is a six-bladed beta-propeller, each blade composed of a highly twisted four stranded antiparallel beta-sheet (Edwards et al., 2003).Using the partial sequence of the est clone, antibodies were produced and embryonic expression patterns of Lin-41 were investigated (Rybak et al., 2009).

3.4.2.1 Identification of Lin-41 as a miR-125 target gene

The reciprocal expression patterns of Lin-41, let-7 and miR-125 in ES and EC cells during neural differentiation strongly suggested that Lin-41 is regulated by these miRNAs in mammalian stem cells. A pair of let-7 binding sites corresponding to those found in the *C. elegans* mRNA were found to be conserved in the mouse. Analysis of the sequence revealed an additional binding site for miR-125. Site-directed mutagenesis of let-7 complementary sequences within the 3'-UTR of a GFP-Lin41 sensor led to an up-regulation of GFP in let-7 positive primary cortical neurons (Smirnova et al., 2005). As further support for conservation of let-7 regulation of Lin-41, and to test the activity of the miR-125 binding site, the GFP sensor construct bearing the 3'-UTR of mouse Lin-41 was co-transfected with double-stranded let-7 or miR-125 RNA mimics in HEK293 cells. After 48h, the eGFP intensity of the cells was measured by flow cytometry and the percentage of GFP-positive cells normalized to the modified parental control vector eGFP-C1 (Figure 3.4.2.1).
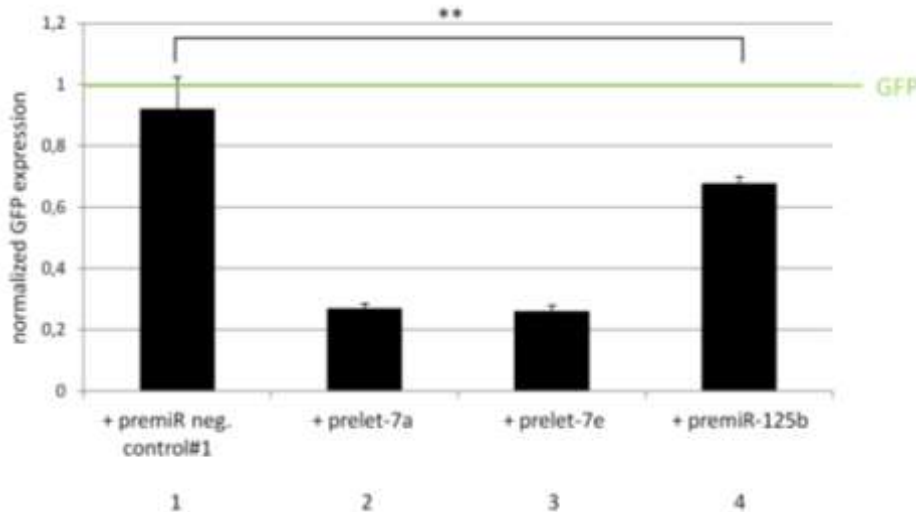
Figure 3.4.2.1: Lin-41 is a let-7 and miR-125 target gene $4*10^5$ Hek293 cells were transfected with 100ng GFP-Lin41 sensor together with 20pmol double-stranded miRNA and 200 ng dsRED as a control for the transfection efficiency. After 48h the eGFP expression was measured by flow cytometry and the percentages of counted positive cells were normalized to the parental vector eGFP-C1 (green line). The normalized GFP expression of the GFP-Lin-41 sensor co-transfected with pre-miR-negative control (Column 1), prelet-7a (Column 2), prelet-7e (Column 3) and premiR-125b (Column 4) are shown. An unpaired two tailed t-test (n≥3) was performed to reveal significant differences (** p<0.01).

As expected let-7a (Column 2) and let-7e (Column 3) reduced the GFP expression of the GFP-Lin41 sensor up to 70% in comparison to the GFP-Lin41 sensor co-transfected with the negative control (Column 1). A much weaker but significant (n=4 p=0.0072) ~30% reduction of GFP could be observed with miR-125 (Rybak et al 2009). Similar results were obtained by Kanamoto and Schulman (Kanamoto et al., 2006; Schulman et al., 2005).

3.4.2.2 Lin41 overexpression represses miRNA activity in Hek293 cells

Ago-2 is one of the core enzymes of the miRNA pathway, participating in which maturation of the precursor miRNA and in translational silencing. To test if Lin-41 reduces miRNA pathway activity by interacting with Ago2 we used the miRNA-dependent sensor assay in HEK293 cells. To determine if ubiquitination activity of Lin-41 is involved, wildtype and mutant Lin-41 were tested in parallel (Figure 3.4.1.3). The Figure displays the GFP intensity of pre-miRNA-RED positive cells 48h after transfection. The values were normalized to the corresponding GFP-sensor/pre-miRNA-RED transfections that were co-transfected with 800ng of the parental pc3xFLAG vector (dotted line).
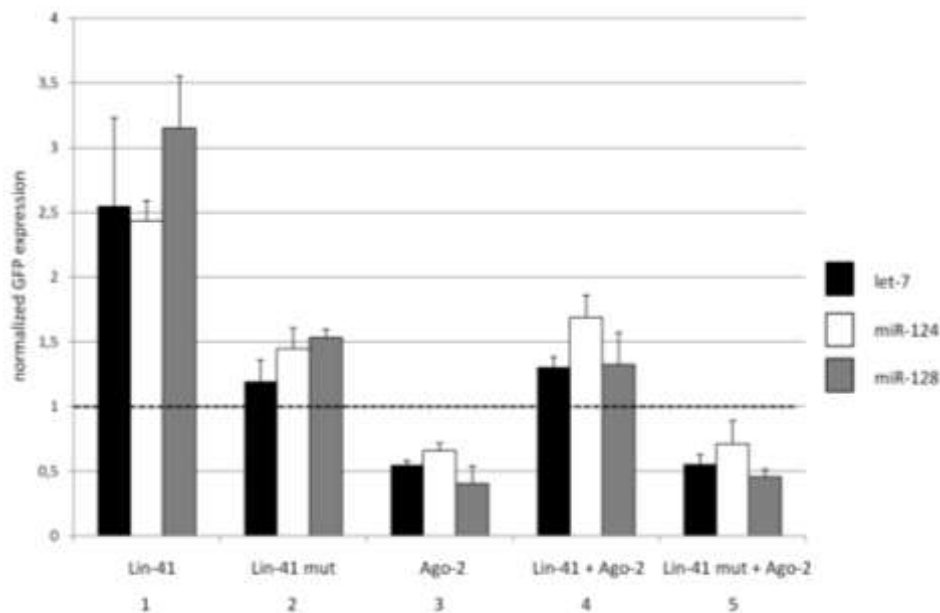
Figure 3.4.1.3: Lin-41 and Ago2 have inverse effects on miRNA-mediated reporter silencing in HEK293 cells $4*10^5$ Hek293 cells were transfected with either 200ng prelet-7-RED + 50ng GFP-2xlet-7 (black bars), 200ng premiR-124-RED + 50ng GFP-4xmiR-124 (grey bars) or premiR-128-RED + 50ng GFP-4xmiR-128 dsRED (white bars), together with 400ng of pcFLAG-Lin41 + 400ng pcFLAG (Column 1), 400ng pcFLAG-Lin41mut + 400ng pcFLAG (Column 2), 400ng pcFLAG-Ago-2 + 400ng pcFLAG (Column 3), 400ng pcFLAG-Lin-41 + 400ng pcFLAG-Ago-2 (Column 4) or pcFLAG-Lin41mut + 400ng pcFlag-Ago-2 (Column 5). After 48h, cells were harvested and analyzed by flow cytometry as described in the Methods. For each transfection eGFP expression is plotted relative to eGFP expression of the sensor in the presence of the cognate miRNA. The diagram displays the result of three independent transfections performed in duplicate.

As shown in Column three, each of the GFP-sensors tested was more strongly repressed by the corresponding miRNAs in the presence of Ago-2. The presence of Ago-2 reduces the GFP intensity by approximately 40% to 60% in comparison to control. This is consistent with published reports that Ago-2 is limiting for siRNA-mediated silencing (Diederichs). In contrast, the opposite effect was observed in the presence of Lin-41 (Column one). In the case of the let-7 and miR-124-GFP-sensor, Lin-41 is able to inhibit the repression mediated by the corresponding miRNA by about 2.5 fold. A 3-fold de-repression was observed for the GFP-miR-128 sensor. The Lin-41mut had little to no effect on miRNA-mediated silencing of the GFP-sensors (Column two) in comparison to the Lin-41 transfection (Column one),

indicating that an intact RING domain is required for miRNA pathway inhibition by Lin-41. As evidence for a direct interaction between Lin-41 and Ago-2, co-expression of both proteins led to intermediate values, indicating the two proteins cancel each other out (Column four). Once again, the RING mutant had no activity and Ago2 mediated, enhanced activity of the miRNA pathway was observed (Column 5).

3.4.2.3 Lin-41 studies in the chicken neural tube

Previous *in situ* experiments, performed by our group, have shown that Lin-41 is expressed in the ventricular zone of the neural tube of E12 mouse embryos. In order to check if Lin-41 is present at all in the neural tube of the chicken, vibratome sections of HH26 chicken have been immunostained with anti-Lin-41 antibody and Alexa488 as a secondary antibody (Figure 3.4.2.3a). The aa-sequence that was chosen to generate the mLin-41 antibody is specific for chicken Lin-41, as determined by BLAST.
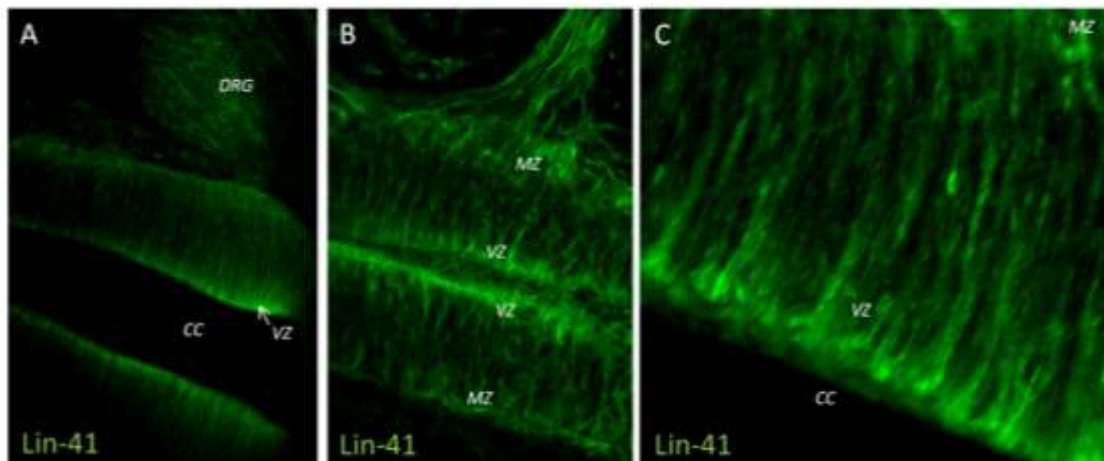
Figure 3.4.2.3b: Lin-41 expression in the chicken neural tube at HH26. Vibratome sections were stained with anti-mLin-41(green). DRG: dorsal root ganglion, CC: central canal, VZ: ventricular zone, ML: mantle zone A) Overview B) higher magnification of a more dorsally sliced section C) higher magnification of the ventricular zone. For a detailed explanation please refer to text.

Figure 3.4.2.3b reveals that Lin-41 is expressed in the neural tube and the dorsal root ganglion of the chicken (picture A). However Lin-41 is not ubiquitously present in the neural tube. In all pictures it is particularly noticeable that Lin-41 levels are highest in the apical part of the ventricular zone, and then once again in the basal mantle zone (pictures B and C).

Figure 3.4.2.3c GFP/dsRED expression in the chicken neural tube at HH26. Vibratome section of HH26 neural tube electroporated with CMV-eGFP-C1 [1µg/µl] and CMV-dsRED-N1 [1µg/µl] at HH16, stained with anti-FLAG (green). VL: ventricular zone, ML: mantle zone A) DAPI staining B) eGFP expression C) dsRED expression D) merged picture of B and C For a detailed explanation please refer to text.

To study the possible functional role of Lin-41 in spinal cord development, Lin-41 was overexpressed beginning at HH16 by *in ovo* electroporation. Figure 3.4.2.3c displays the result of a typical control experiment in which the marker proteins eGFP and dsRed were co-electroporated at HH16, with analysis 2.5 days later at HH26 As shown in picture B and C, eGFP and dsRED positive cells can usually be found in nearly every area of the neural tube 2.5 days after electroporation, as a result of ongoing proliferation and migration of the electroporated cells. Furthermore, every eGFP positive cell also expresses dsRED even if their fluorescent intensities are not always equal.

Figure 3.4.2.3d presents the results of obtained after electroporation of epitope-tagged Lin-41, allowing visualization by immunostaining with a monoclonal anti-FLAG antibody and anti-mouse-Alexa-488.

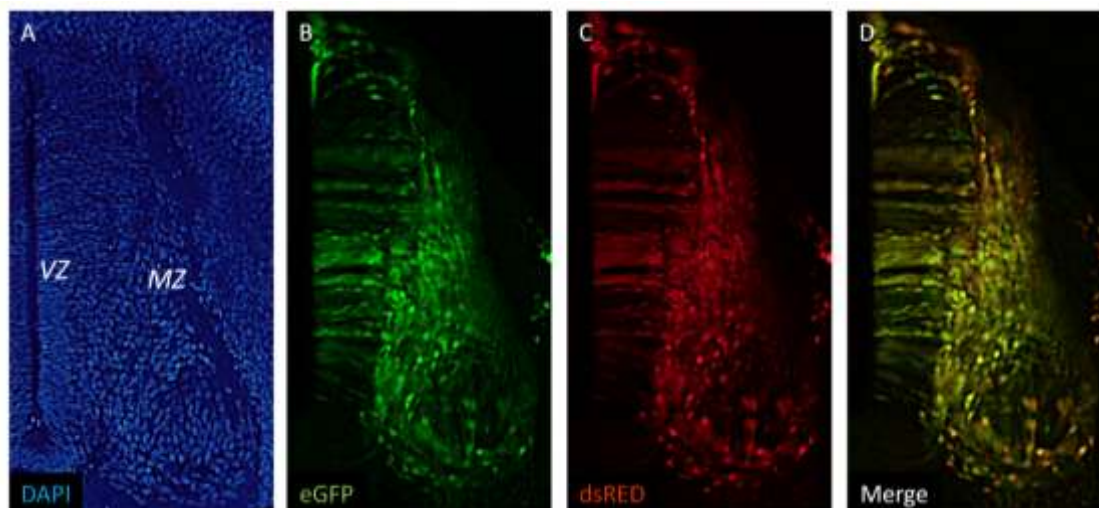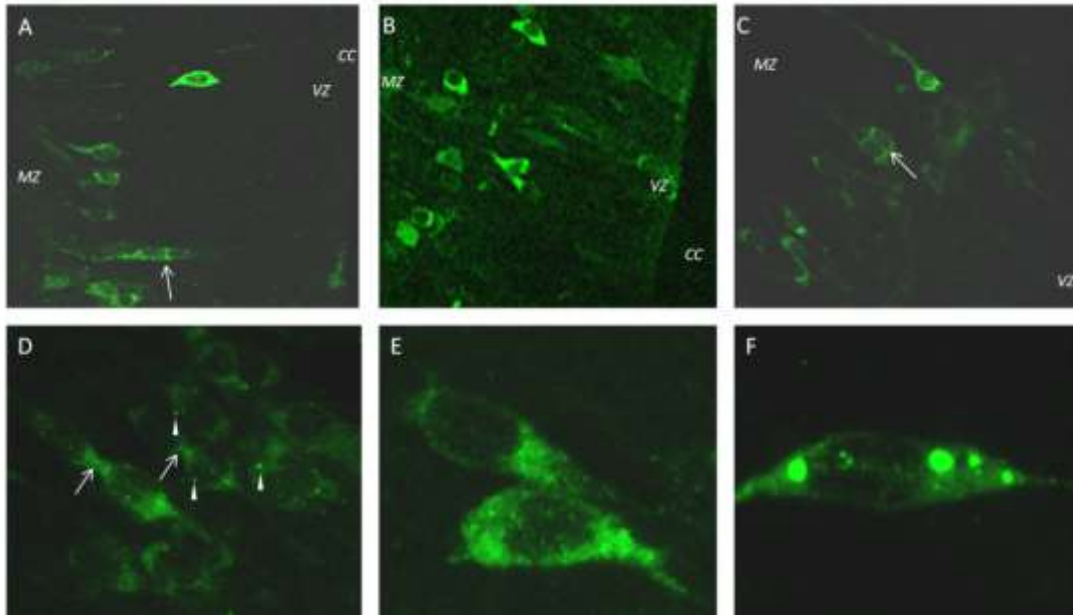**Figure 3.4.2.3d: Lin-41 overexpression in the chicken neural tube at HH26.** Vibratome sections of HH26 neural tube electroporated with pc3xFLAG-Lin-41[2µg/µl] at HH16 were stained with anti-FLAG (green). CC: central canal, VZ: ventricular zone, ML: mantle zone A-C) Overview spanning the area between the ventricular zone(VZ) and mantle zone (MZ) D-F) Higher magnification of pc3XFLAG-Lin-41 positive cells. For a detailed explanation please refer to text.

In clear contrast to the control, ectopic Lin-41 expression was observed in far fewer cells, which were typically arranged in a single layer located between the ventricular zone and the mantle zone (Figure 3.4.2.3). Furthermore, occasionally Lin-41 positive cells seemed to cohere (marked with arrows in the pictures A, C and D). At higher magnification (Figure 3.4.2.3.D), Lin-41 protein, like Lin-28, can be seen diffusely distributed in the cytoplasm and also accumulating in small foci reminiscent of P-bodies (marked with arrowheads). Picture E shows a more granular expression of Lin-41 while in picture F Lin-41 seems to be aggregated in larger clusters.

In co-electroporations of Lin-41 and dsRed, dsRed expression was seen to be restricted to the same cell populations as Lin-41 (Figure 3.4.2.3e). Therefore, the expression pattern must be the result of cellular events, such as cell cycle control, proliferation, differentiation or apoptosis, rather than differential regulation of Lin-41 protein at the post-transcriptional level in different cell populations.

Figure 3.4.2.3e: Lin-41 and dsRED misexpression in the chicken neural tube at HH26. Vibratome sections of HH26 neural tube that has been previously electroporated with pc3xFLAG-Lin-41[2µg/µl] and CMV-dsRED [250ng/µl] at HH16 were stained with anti-FLAG and Alexa-488 secondary antibody (green). The pictures were made of merged confocal z-stacks. EL: ventricular zone, MZ: mantle zone. Overview spanning the area between the ventricular zone and mantle zone is shown on the left. Higher magnification of the area is shown on the right.

3.4.2.4 Co-electroporation of Lin-41 and MyoVI in the chicken neural tube

One of the Lin-41 homologs in Drosophila, Brat, has been shown to be required for the execution and cell fate choice of assymetric divisions of neural progenitor cells (Betschinger et al., 2006).

During assymetric divisions Brat is transported by its interaction partner Miranda to the basal part of a dividing cell. Asymmetric Miranda distribution, in turn, is dependent on the Drosophila Myosin genes Zip and Jaguar. Of particular interest is the role of Jaguar, which is homologous to the vertebrate Myo6 proteins. Unlike typical myosins, Myo6 and Jaguar are unusual in that they move towards the minus (slow-growing) end of actin-filaments (Petritsch et al., 2003).
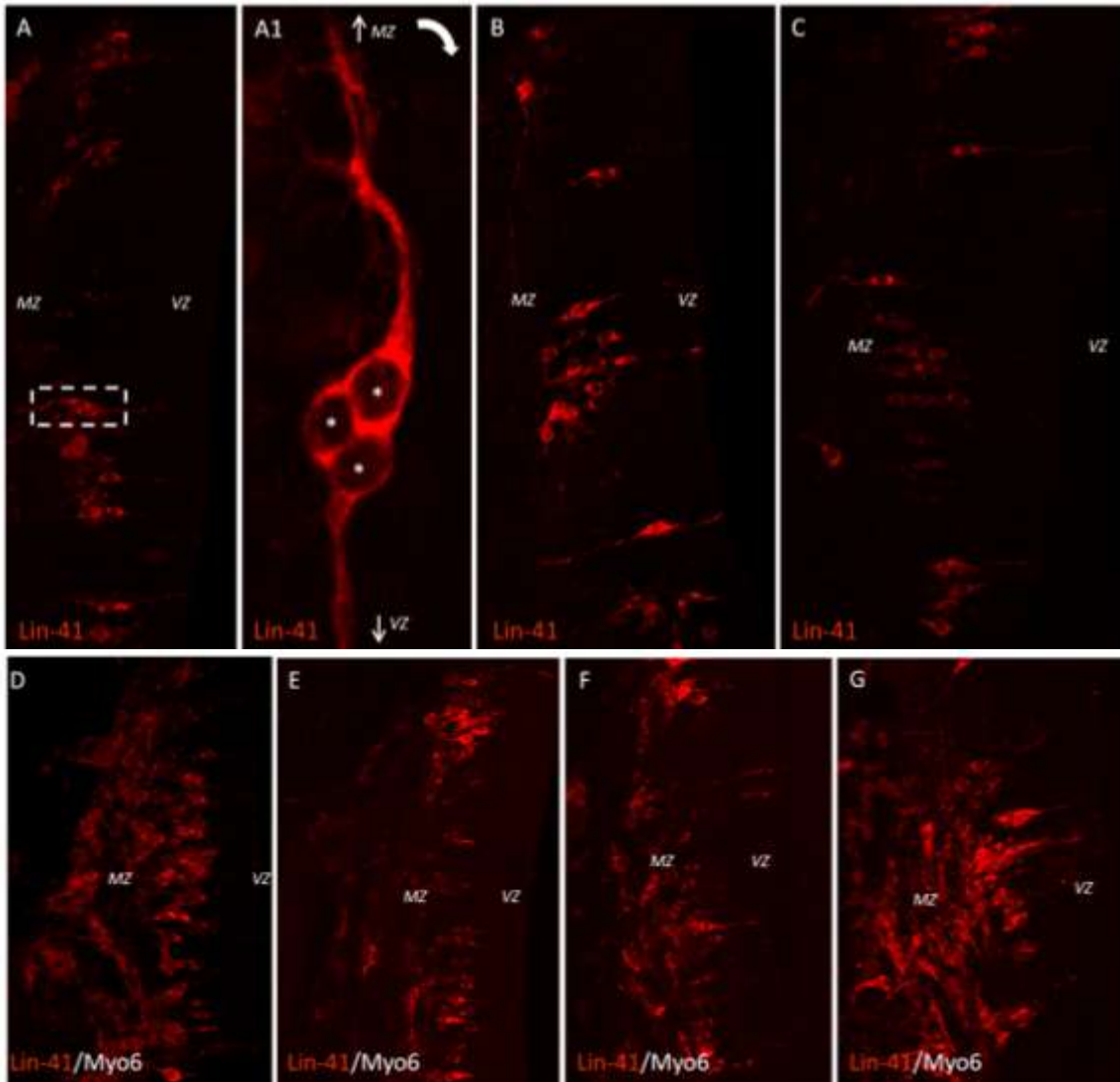
Figure 3.4.2.4: Co-expression of 3xFLAG-Lin41 and HA-Myosin VI leads to an increase of 3xFLAG-Lin-41 positive cells in the neural tube. Confocal pictures of HH26 neural tubes electroporated at HH16 with either pc3xFLAG-Lin-41[1µg/µl] (A-C) or pc3xFLAG-Lin-41[1µg/µl] + pHA-Myo6 [1µg/µl] (D-G). Lin-41 was visualized by staining with monoclonal anti-FLAG and Alexa568 conjugated secondary antibody (red). MZ: mantle zone, VZ: ventricular zone. A higher magnification of the dashed area in picture A shows a cluster of Lin-41 positive cells, as described above (marked with asterisks). For better illustration picture A1 has been rotated 90°.

Panels A-C present representative results for electroporation of Flag-tagged Lin-41, with results comparable to those of Figure 3.4.2.3d. Panels D-G present Lin-41 staining in the presence of ectopic Myo6. Co-expression of Myo6 led to increased numbers of Lin-41^{+} cells. In addition, Lin-41^{+} cells were readily detected throughout the ventricular progenitor zone, the mantle zone and the DRGs. These results are indicative of a functional interaction between Myo6 and Lin-41, whether direct or indirect. Given the known roles of both Myo6 and Lin-41 homologs in cell polarity in invertebrate model organisms, these results suggest that ectopic Lin-41 interferes with either cell division or fate choice in this assay.

3.4.3 Lin28 cooperates with Lin-41 in repression of let-7 activity

Functional analysis of Lin-28 showed that it acts as a selective inhibitor of let-7, and to a lesser extent miR-128, maturation. By virtue of its ability to promote Argonaute ubiquitination and turnover, Lin-41 acts as a global inhibitor of the miRNA pathway. Both proteins are co-expressed and co-regulated by let-7 and miR-125 in pluripotent cells. It was therefore of interest to determine if the two can act cooperatively in the inhibition of let-7. The sensor assay was chosen for these experiments using expression plasmids for let-7 and miR-124 together with their respective sensor constructs, as described in Section (3.1.2.2). Each miRNA and sensor pair was co-transfected with Lin-28, Lin-41 or mutant Lin-41 carrying inactivating point mutations in the RING domain (see Section 2.2.5.5).
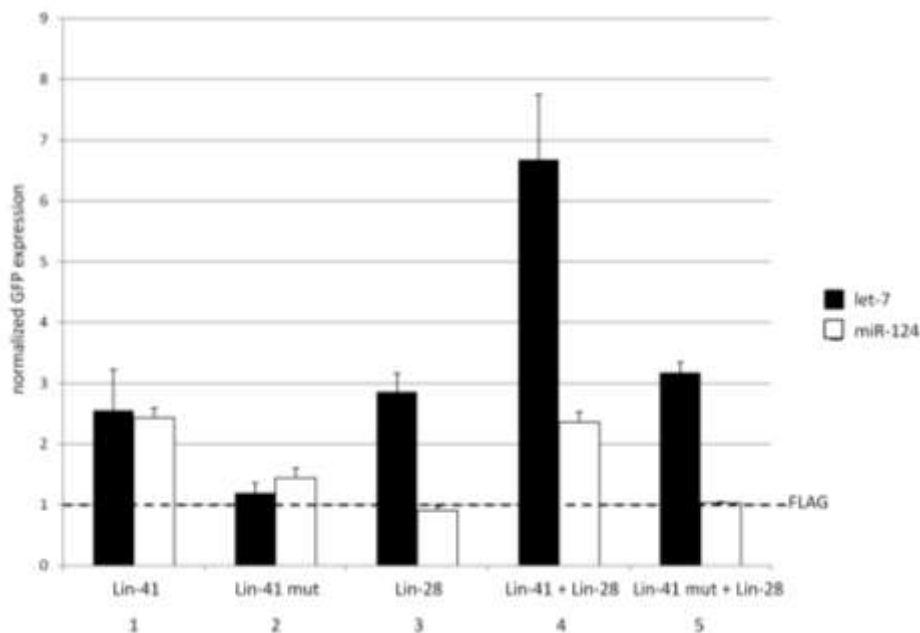
Figure 3.4.3: Lin-41 cooperates with Lin‑28 to suppress let‑7 mediated repression. $4*10^5$ HEK293 cells were transfected with either 200ng prelet-7-RED + 50ng GFP-2xlet-7 (black bars) or 200ng premiR-124-RED + 50ng GFP-4xmiR-124 (white bars) together with 400ng of pcFLAG-Lin41(Column 1), 400ng pcFLAG-Lin41mut (Column 2), 400ng pcFLAG-Lin-28 (Column 3), 400ng pcFLAG-Lin-41 + 400ng pcFLAG-Lin-28 (Column 4) or pcFLAG-Lin41mut + 400ng pcFlag-Lin-28 (Column 5). Additionally 400ng pcFLAG vector was used in transfections 1-3 to maintain consistent transfection conditions. After 48h, cells were harvested and analyzed by flow cytometry. RED fluorescent positive cells were gated with FlowJo2.1 . The geometric mean of GFP of the gated cells was normalized to the corresponding pre-miRNA-RED/GFP-miRNA sensor co-transfected with 800ng empty pcFLAG vector (black dashed line). The diagram displays the result of three independent transfections performed in parallel.

The increased GFP intensity in Column 1 compared with Column 2 reveals that overexpression of Lin-41, but not the RING domain mutant, reduced miRNA-mediated silencing efficiency for either let-7 or miR-124. Specific inhibition of let-7 by Lin‑28 is shown in Column 3. As previously shown, Lin-28 is not able to inhibit the activity of miR-124. In Column 4, Lin‑28 and Lin-41 cooperate to relieve repression of the let‑7 reporter but not the miR‑124 reporter, reflecting the specificity of Lin‑28 for let‑7. While either ectopic Lin-41 or Lin-28 itself results in a 2-3 fold higher GFP expression of the let-7 sensor, ectopic

overexpression of both proteins increase the GFP expression of the let-7 sensor by approximately 5.5-fold (Column 4) in comparison to the pcFLAG-control (dotted line). This cooperative suppression on let-7 silencing was not observed with the mutant form of Lin-41 (Column 5).

3.4.4 Inhibition of let-7 or miR-125 de-repress Lin-41 and Lin28 in E12 neural stem cells

To assess the relative contribution of miRNA-mediated control to regulation of Lin-41 and Lin-28 in neural stem cells, we employed plasmid-based miRNA inhibitors, so-called sponge vectors. Sponge-vectors bear up to 64 semi-complementary miRNA binding-sites inserted in the 3'-UTR of the eGFP gene. A detailed illustration of the binding sites and the mode of functioning is provided in Chapter 3.1.3.2. Efficient transfection of neural stem cells was achieved with the Amaxa electroporation kit. 72 hours after electroporation cells were harvested for protein or RNA extraction.

In Figure 3.4.4a the results of inhibiting let-7 or miR-125 on Lin-28 protein levels is examined by western blotting.

Figure 3.4.4a: Inhibition of let-7 or mir-125 de-repress Lin-28 in E12 neural stem cells NS cells were electroporated with water (Mock), sponge vectors specific for *mir-29* (sp_*mir-29*), *let-7* (sp_*let-7*), *mir-125* (sp_*mir-125*), or siRNA targeting the pre-miRNA processing core enzyme Dicer For comparison, Lane 1shows endogenous protein levels in EC cells. Lin-28 expression was analyzed by western blotting 72 h after electroporation (upper panel), and with β-actin as loading control (lower panel).

As positive control, Lin-28 expression in EC cells is displayed in Lane 1. whereas Lin-28 expression in neural stem cells is just above the detection limit (Mock transfection in Lane 2). However, the Western blot shows that Lin-28 is upregulated in response to the sponge antagonists for let-7 and miR-125 (Lanes 4 and 5), but not in response to the miR-29 antagonist (Lane 3). In four independent experiments, the sponge-mediated rescue of Lin-28 expression was similar to, or greater than, that seen after Dicer silencing (Lane 6). Although Dicer knockdown might be expected to fully de-repress miRNA targets, in practise Dicer knockdown is self-limiting because Dicer itself is required for siRNA-mediated silencing

In a nearly identical experiment the ability of sponge constructs to de-repress the let-7 and miR-125 target gene Lin-41 was tested (Figure 3.4.4b).
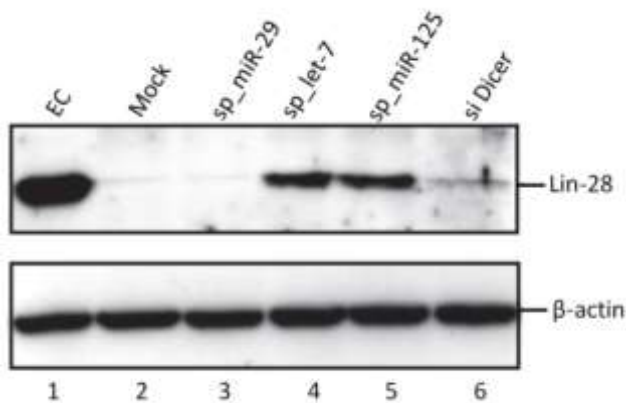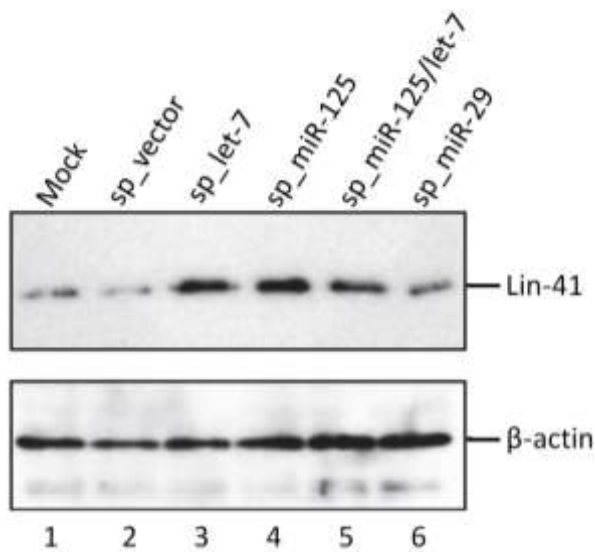

Figure 3.4.4b: Inhibition of let-7 or mir-125 de-repress Lin-41 in E12 neural stem cells NS cells were electroporated with water (Mock), empty sponge vector (sp_vector), or sponge vectors specific for let-7 (sp_let-7), miR-125 (sp_miR-125), miR-125 and let-7 (sp_miR-125/let-7) or miR-29 (sp_miR-29). In the upper panel, Lin-41 protein was detected by western blotting using a peptide antibody (indicated on the right). Lin-41 was present at low levels in mock, vector and miR-29 sponge electroporated cells. Sponge vectors for let-7 and miR-125 resulted in approximately a 2.5-fold increase in Lin-41 protein, compared with the miR-29 control sponge relative to β-actin shown in the lower panel (n = 4, P < 0.05, Student's t-test). Signals were quantified using LabImage 1D software.

Lin-41 is expressed at low levels in NS cells (Mock in Lane 1) and is not increased after electroporation of the sponge vector alone (Lane 2), or a sponge construct targeting *mir-29* (Lane 6). Electroporation of NS cells with sponge antagonists of let-7 (Lane 3), miR-125 (Lane 4) or let-7 and miR-125 (Lane 5) increased the level of Lin-41 protein Densitometric analysis of three independent experiments revealed an ~2.5 fold increase of Lin-41 protein in comparison to the sponge-miR-29 electroporation. These results demonstrate that mRNAs targeted by let-7 and miR-125, such as Lin-28 and Lin-41, are subject to ongoing post-transcriptional suppression in NS cells. The efficient de-repression of Lin-28 and Lin-41 by either inhibition of miR-125 or let-7 reveals that both miRNAs contribute to the inhibition of these pluripotency genes in neural stem cells.

3.4.5 Inhibition of let-7 or miR-125 inhibits pre-let-7a processing in E12 neural stem cells

Since both proteins cooperate to inhibit let-7 processing as previously demonstrated in Figure 3.4.3b, the sponge mediated inhibition of let-7 and miR-125 and therefore ongoing de-repression of Lin-28 and Lin-41 in neural stem cells should decrease pre-let-7 processing. In order to test this influence on let-7 processing in NSC an *in vitro* assay was performed. Radiolabelled pre-let-7a was incubated with cell extracts of NS cells after electroporation with different sponge constructs or an siRNA targeting Dicer (Figure 3.4.4c).
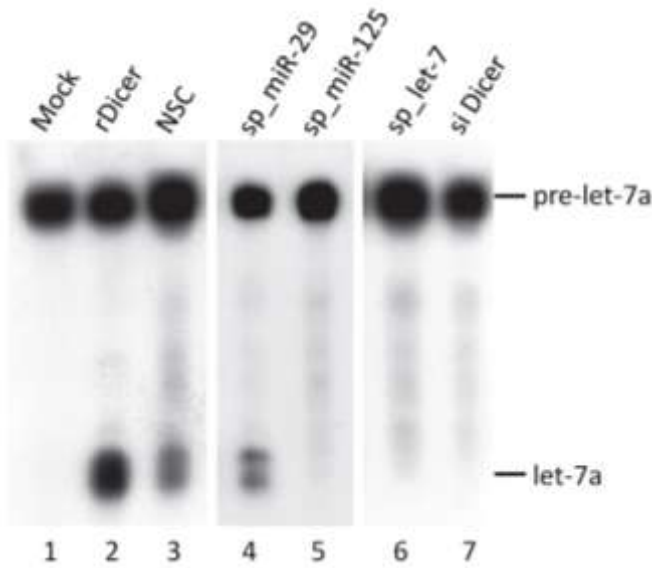
Figure 3.4.4c: Inhibition of let-7 or miR-125 inhibits pre-let-7a processing in neural stem cells. Cleavage reactions contained radiolabelled pre-let-7a and different electroporated NS cell extracts. Lane 1 is a mock reaction and Lane 2 is a control reaction using recombinant Dicer (rDicer). NS cells were non-electroporated (NSC) or electroporated with a control miR-29 sponge vector (sp_miR-29), miR-125 sponge vector (sp_miR-125), a let-7 sponge vector (sp_let-7) or a siRNA duplex against Dicer (si Dicer). Quantification of three independent experiments yielded an average 2.9-fold reduction for the let-7 sponge, compared with the miR-29 control (n = 3, P < 0.01, two-tailed Student's t-test).

The Mock reaction in Lane 1 shows the radiolabelled pre-let-7a RNA input. As a positive control, input pre-let-7a RNA was incubated with recombinant Dicer under limiting conditions to demonstrate release of mature, 22 nt let-7 (Lane 2). Activity of control NS cell extract is shown in Lane 3, and results in partial digestion of the precursor to mature let-7. Processing activity was retained after electroporation of a control sponge vector specific for miR-29 (Lane 4). The reduction in processing activity observed after inhibition of let-7 in Lane 6 was comparable to that attained by siRNA-mediated Dicer silencing (Lane 7). Similar results were obtained with the anti-miR-125 sponge construct (Lane 5).

In summary, suppressing let-7 activity with either the let-7- or miR-125-sponge construct led to a reduction in processing activity of let-7, presumably because of an increase in Lin-28 and Lin-41 protein levels.

4. Discussion

4.1 miRNA activity of let-7, miR-125, miR-124 and miR-128 during neural development

A basic prerequisite for understanding the function of miRNAs is to determine their spatial and temporal expression during development. Northern blot and *in situ* experiments performed previously in our lab revealed that let-7, miR-125, miR-124 and miR-128 are highly enriched in the CNS of embryonic stage E9.5 mouse embryos (Wulczyn et al., 2007). Similar results were also obtained by other groups (Krichevsky et al., 2006; Lukiw and Pogue, 2007; Sempere et al., 2004; Tang et al., 2007). Moreover these miRNAs are strongly induced during RA-induced neural differentiation of ES and EC cells (Smirnova et al., 2005). Northern blots of neuronal and astrocyte RNA identified several miRNAs with either neuron (miR-124, miR-128) or astrocyte (miR-23, miR-29) specific expression. The transfection of astrocytes or neurons with GFP-miRNA sensor constructs confirmed that miR-124 and miR-128 were preferentially active in neurons, establishing lineage specificity as an important property of brain miRNA populations. The temporal and lineage specific activity of many miRNAs is an important mechanism of post-transcriptional regulation during cellular differentiation and lineage determination (Bouhallier et al., 2010; Dugas et al., 2010; Leslie Pedrioli et al., 2010; Nakajima et al., 2006; Ramkissoon et al., 2006; Smirnova et al., 2005; Watanabe et al., 2005). Northern blots experiments with radiolabelled miRNA antisense probes revealed low levels of mature let-7 but high levels of precursor-let-7 in pluripotent cells, suggesting that regulation of let-7 occurs to a large extent at the post-transcriptional level. To allow the activity of additional miRNAs to be studied *in vitro* and *in vivo*, a series of eGFP-based reporter constructs, so-called miRNA sensors, were generated. These sensors bear artificial, perfectly complementary binding sites for one member of each miRNA-family (let-7a, miR-125a, miR-124 and miR-128b) within the 3'UTR of the GFP gene (Section 3.1.1.1). In transfected cells, the transcribed mRNA of the GFP sensor binds with a high affinity endogenous miRNAs. Depending on the level of complementarity between miRNA sequences and site sequences, this leads to efficient silencing of the mRNA either via the siRNA or miRNA pathway and therefore decreased GFP intensity.

As shown in Figure 3.2.2b) all four miRNAs were active in E18 primary cortical neurons, confirming our previous results obtained with less sensitive semi-complementary sensors (Smirnova et al., 2005). It has been previously shown that mRNA repression by multiple miRNAs results in more efficient inhibition than that expected from the sum of each individual binding site (Doench et al., 2003). In order to increase the sensitivity of this assay, GFP-sensors containing either two (for let-7) to four binding sites (for miR-125, miR-124 and miR-

128) were chosen for further analysis. In addition, the functionality of the GFP-sensors for let-7, miR-125 and miR-128 was tested in a co-transfection assay with synthetic miRNA mimics in Hek293 cells (Figure 3.3.2b). The GFP expression of all GFP-sensors was strongly reduced by the presence of the appropriate miRNA mimic, confirming the functionality of the GFP-sensors. Additionally, the functionality of the GFP-miR-124 was confirmed by overexpression of GFP sensor together with vector expressing miR-124 miRNA (data not shown).

A comparison of mir-128 expression between E15 and E18 cortical neurons revealed that miR-128 is not active in E15 neurons, but repression of the miR-128 sensor was observed at E18 (Figure 3.2.2c). It has been already shown that mir-128 expression increases during neuronal outgrowth in cell culture (Kim et al., 2007). The sensor assay was performed after two days in culture, when neuronal outgrowth is not yet induced. That could be one possible explanation why we did not observed mir-128 activity in E15 neurons.

The activity of let-7, miR-125, miR-124 and miR-128 was also examined in undifferentiated EC cells, revealing no activity of these miRNAs in the pluripotent state (showed in Section 3.2.3). To provide a new tool for the study of miRNA regulation in neural stem cells, a neural stem cell line from E12 mouse brain was generated, using a protocol first described in the Austin Smitl lab (Pollard et al., 2006a; Pollard et al., 2006b). Adherent cells, generated from neurospheres, are negative for the pluripotency factor OCT-4 and the astrocytic marker GFAP, but positive for the radial glia markers Sox2 and RC-2 and they showed ability to differentiate into neurons or astrocytes, as confirmed (see Section 3.2.4.1). Transfection of NS cells with the miR-sensor constructs showed a high activity of let-7 and miR-125, but absence of mature miR-124 or miR-128 (see Section 3.2.4.2) (Rybak et al., 2008).
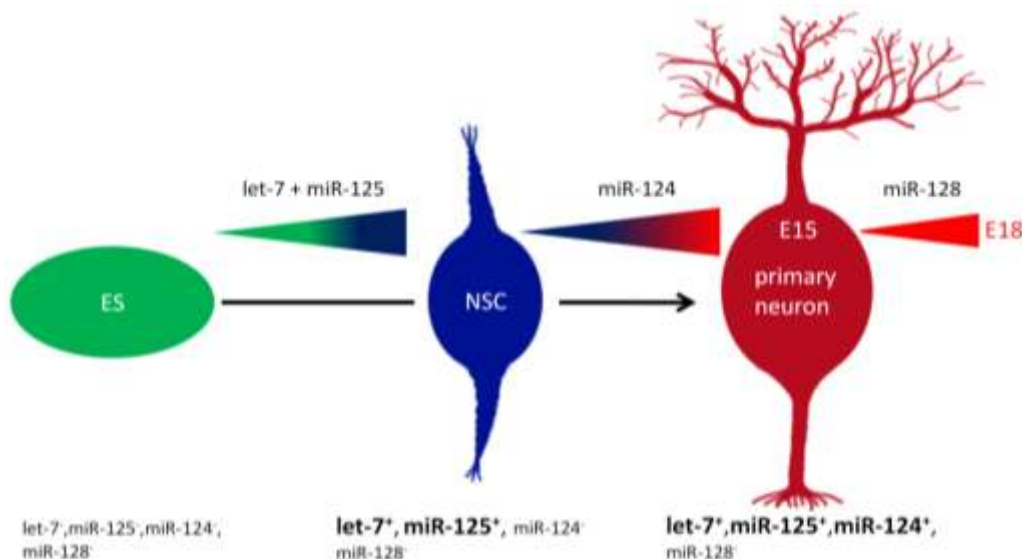

Figure 4.1: Schematic illustration of time-point and cell-specific let-7, miR-125, miR-124 and miR-128 activity during mouse neuronal development. For a detailed explanation please refer to text.

In summary, these data reveal that let-7 and miR-125 activity starts at a very early time point, suggesting a potential role for both miRNAs in the regulation of ES cell self-renewal. Recent publications from our and other groups have confirmed this suspicion (Bussing et al., 2008; Gunaratne, 2009; Liu et al., 2009; Melton et al., 2010; Nimmo and Slack, 2009; Yu et al., 2007a). Both the miR-124 activity in early newborn neurons and its neuronal lineage specificity suggests that miR-124 inhibits non-neural target genes and therefore promote neurogenesis (Makeyev et al., 2007; Smirnova et al., 2005). Activity of miR-128 starts at a later time point of embryonic neurogenesis after E15 (Section 3.2.2) and might be important for ongoing maturation of neurons and synaptic plasticity.

4.2 miRNA gain-of function studies

miR-124 gain-of-function *in vitro*

Recently overexpression of miRNAs has begun to be employed as another experimental approach to study miRNA function. Maniatis and co-workers previously showed that miR-124 overexpression in RA-induced differentiating EC cells led to an increased number of neurons (Makeyev et al., 2007). To reveal additional potential roles of miR-124, we overexpressed miR-124 in neural stem cells undergoing astrocyte differentiation. miR-124 is not expressed under these conditions, because of its neuronal specifity. The neuron-like outgrowths of miR-124 positive cells, undergoing astrocytic differentiation, shown in Section 3.3.1, suggest that miR-124 is able to promote neural lineage determination, even in the absence of RA or retinyl acetate (component of B27 supplement) and despite the presence of serum within the astrocytic differentiation media. Furthermore, these cells were negative for the astrocytic marker GFAP but positive for the neuronal marker ß-III Tubulin. This leads to the question, if miR-124 has the ability to re-program astrocytes towards neuronal cell fate. This question cannot be answered with these preliminary data. Interestingly, BMP-6 (bone morphogenetic protein 6) and BMPR1a (bone morphogenetic protein receptor 1a) are predicted by PicTar to be target genes of miR-124. Bone morphogenetic proteins (BMPs) are well-known astrocyte-inducing cytokines, which cause astrocytic differentiation and restrict neuronal differentiation. An increase of astrogliosis after injury of the CNS was reported by many groups (Guo et al., 2007; Kost-Mikucki and Oblinger, 1991; Tian et al., 2007; Vitellaro-Zuccarello et al., 2008). Astrogliosis is a common event upon injury of the CNS (Giulian et al., 1989; Nieto-Sampedro et al., 1985) and is believed to interfere with functional recovery. For this reason, genetic manipulations that can promote neurogenesis at the exposure of astrogliosis have

therapeutic potential suggesting a potential role of miR-124 for therapeutic purposes to manipulate gliosis (Berninger et al., 2007). MiR-124 is a potential novel candidate influencing the balance between astrogliosis and neurogenesis.

miR-124 gain-of-function *in ovo*

In situ hybridizations revealed that miR-124 is expressed in the developing brain and the anterior part, but not in the posterior part of the neural tube at HH16 stage (Figure 3.3.2.a). Moreover, *in situ* hybridization with a miR-124 antisense probe at HH23 stage shows that miR-124 expression is restricted to the mantle zone, where newborn post-mitotic neurons are arranged. Both, the dorsal root ganglion (DRG) and the ventricular layer lack miR-124 expression. In order to misexpress miR-124 in the neural tube, electroporation of the neural tube with the pre-miR-124-Red, or Intron-Red as a control, construct was performed at HH16 in the posterior part of the neural tube that lacks miR-124 expression. After 2.5 days, Intron-RED positive cells were nearly evenly distributed in the ventricular zone, the mantle layer zone and the dorsal root ganglion. In contrast, the pre-miR-124-Red positive cells preferentially migrate to the mantle zone but fail, with few exceptions, to migrate to the dorsal root ganglion (see Figure 3.3.2.4b). Additionally, the neural tube shows a stronger pre-miR-124-Red signal surrounding the motor neural column. Confocal pictures reveal that this pre-miR-124-RED signal is due to an increase in neuronal outgrowth. In order to investigate if miR-124 overexpression leads to an increase of postmitotic neurons, sections were immunostained, using a MAP-2 antibody. MAP-2 is a neuron-specific microtubule associated protein that is enriched in dendrites. Indeed, miR-124 overexpression led to an expanded MAP-2 staining into the dorsal mantle zone compared with the control side. The increased outgrowths around the motor-neural column, caused by miR-124 misexpression did not overlap with the MAP-2 staining, suggesting that these outgrowths have axonal origin. Therefore, additional immunostaining experiments should be performed with axonal or axional growth cone markers. Although preliminary, these results reveal that miR-124 misexpression, has an effect on neural tube development. These observation are in contrast to a published report describing much more limited effects of miR-124 overexpression after *in ovo* electroporation (Cao et al., 2007). Based on co-electroporation experiments with a non-fluorescent miR-124 expression construct and a GFP-plasmid, they found no evidence for enhanced neurogenesis. There primary finding was that ectopic miR-124 expression causes basal laminar defects near the dorsal root entry sites by repression of LAMC1 and ITGB1. Golding and Cohen showed that the basal lamina is partially intermitting at the dorsal root entry sites, allowing sensory afferents neurons to enter the spinal cord (Golding and Cohen, 1997). Interestingly, the *in situ* staining from Geisha web page reveals the strongest expression also in this area (Figure 3.3.2.4a). Although the basal lamina was not

investigated, our electroporation experiments showed, in contrast to their electroporations, a prominent staining of miR-124-Red near the dorsal root entry sites in comparison to the Intron-Red control (see Figure 3.3.2.4b). It is possible that such defect could contribute to a loss of migration to dorsal root ganglions. Because miR-124 is most highly expressed in sensory compared to motor neurons (Rajasethupathy et al., 2009), it would be interesting to determine if miR-124 overexpression affect specification as well.

miR-124 gain-of-function *in utero*

Different Cre-loxP-Dicer mutants have been generated in mice which lack Dicer expression at different stages in distinct areas of the developing brain (Davis et al., 2008; De Pietri Tonelli et al., 2008). These mutants showed decreased proliferation in the ventricular zone, widespread apoptosis and failure of cortical formation. These aberrations led to a reduced forebrain size and a reduced cortical thickness and reveal the importance of proper miRNA function during brain development. As the most strongly expressed miRNA in post-mitotic neurons (Lagos-Quintana et al., 2002; Lim et al., 2005), miR-124 is a certain candidate for mediating some of these effects.

In situ hybridization performed by Nicola Antonio Maiorano and Antonello Mallamaci on mouse embryonic brain slides at different stages revealed that miR-124 was not expressed at E 10.5 in the cortex but in post-mitotic neurons of the lateral and medial ganglionic eminence (Maiorano and Mallamaci, 2009). At E12.5, miR-124 was expressed in the developing cortex, showing a slight diffuse expression throughout the mitotically active ventricular zone and stronger expression in post-mitotic neurons of the cortical preplate. At E14.5, the most prominent staining was observed within the subplate, cortical plate and marginal zone. The subventricular zone showed a much weaker miR-124 expression, while the weakest expression was observed in the ventricular zone. This expression profile was retained for the remainder of embryonic development and diminished slightly around stage P4. Remarkably, the miR-124 expression pattern was more intense in the recently generated layers 2 to 4 at this stage. These results suggest that miR-124 expression in post-mitotic neurons starts soon after proliferation and increases during the migration to their designated cortical layers. Postnatally, after the neurons reached their designated layers, miR-124 expression decreases slightly.

In order to investigate if miR-124 plays a prominent role during cortical layering, a gain-of-function experiment was performed *in utero*. The CAGGS-pre-miR-124-RED construct was electroporated into the cortical ventricular zone of E12 stage mouse embryos, after the first wave of migrating neurons has reached the preplate of the cortex. As a control, the Intron-RED vector or pre-miR-29-RED construct (data not shown) was used.

Discussion

As displayed in Section 3.3.3.3, miR-124 misexpression shows remarkable effects on migrating neurons, six days after electroporation, at stage E18. In the majority of experiments, ectopic miR-124$^+$ cells were not observed in the cortical layers. In those cases where miR-124 overexpression was observed the cell bodies were tightly clustered and failed proper layering. In most instances, miR-124 positive cells failed to migrate to the cortical layers and were arranged in clusters within one subcortical area. Around this area the brain tissue seems to be disrupted (see Figure 3.3.3.3a), which is maybe related to the ability of miR-124 to downregulate laminin and integrin expression (Cao et al., 2007).

MiR-124 positive cells were also present in the piriform cortex (Figure 3.3.3.3b), where the cell bodies were more clustered and not located, in a distinct layer like shown for the control. This phenotype, caused by miR-124, diminished when pre-miR-124-RED was electroporated at later stages.

Overexpression of miR-124 was also performed by other groups (Maiorano and Mallamaci, 2009). They electroporated a pCMV-eGFP plasmid, bearing the primary transcript of miR-124, into the lateral ventricle of E12 stages mouse brains and performed immunostaining experiments with early and late neuronal markers 48 hours later at stage E14.5. Even if their and our experiments are not directly comparable, because of the usage of different backbone vectors and different time points, they observed that miR-124 overexpression stimulated direct neurogenesis and promoted transition of neural stem cells (radial glia cells) to short neural precursors (SNP) that mainly reside in the subventricular zone. However, they did not observe any dramatic migrational disorders.

It is to be expected that our expression vector, based on CAGGS promoter, would result in high miR-124 expression compared to the CMV construct used in their experiments. One danger of overexpression studies is the generation of artefacts, by overloading the processing machinery. However, the miR-124 specific phenotype was not observed in case of miR-29 electroporations (Figure 3.3.3.3b).

If the wrong layering of miR-124$^+$ cells is caused by neural pre-maturation alone is not clear. For example, neuropilin-1 (NP-1) is predicted by TargetScan to be a miR-124 target. It was shown that downregulation of the receptor NP-1 in newborn cortical neurons impedes their radial migration by disrupting their radial orientation. It would be interesting to know if a wild type rescue can be achieved by co-electroporation the NP-1 gene together with pre-miR-124-RED.

Alternatively, the inhibition of laminin and integrin, caused by miR-124, as described by Cao, might influence the migration. A third possible explanation is that miR-124 causes radial glia defects. Since newborn neuroblasts migrate along radial glia from the apical ventricular layer to the basal surface, a disruption of these tracks could also led to migrational disorders. Additional immunostaining experiments should be performed with radial glia cell and a

laminal marker, like integrin ß1 (a subunit of Laminin receptors), to test these last two hypothesises.

In summary, our miR-124 overexpression experiments led to three main observations. First, ectopic overexpression of miR-124 led to an increase of neuronal markers like MAP-2 and ß-III-Tubulin, suggesting that miR-124 stimulates neurogenesis. This observation is in consistent with other publications (Cheng et al., 2009; De Pietri Tonelli et al., 2008; Deo et al., 2006; Krichevsky et al., 2006; Makeyev et al., 2007). Second, ectopic miR-124 expression in neural stem cells undergoing astrocytic transition may override the astrocytic differentiation program and partial re-program them towards GFAP$^-$,MAP-2$^+$ "neurons". Finally, ectopic overexpression of miR-124 in the E12 stage mouse brain led to strong migrational and layering disorders, that main to be characterized in detail.

miR-128 Gain-of-function *in utero*

As previously shown, miR-128 activity was observed in E18 primary cortical neurons after two days in culture. Recent studies supported the evidence that miR-128 plays a role in neuronal maturation and synaptogenesis. First, microarray profiling of the mRNA response to ectopic miR-128 in EC cells led to an inhibition of developmental transcription factors while inducing neurogenesis and synaptogenesis genes (Gregory Wulczyn, unpublished observations). Second, synaptosomal RNA preparations of postnatal rat cortices revealed that miR-128 one of the most prevalent miRNA in synaptosomes (Vladimir Pekarik, Gregory Wulczyn and Wei Chen unpublished observations). A recent microarray analysis of regional miRNA expression patterns in the brain found that miR-128 is one of only seven miRNAs preferentially expressed in the hippocampus (Bak et al., 2008).

In order to investigate potential roles of miR-128 during neural development, a gain of function experiment was performed *in utero*. The CAGGS-pre-miR-128-RED vector was electroporated into the hippocampal region of mouse embryos at E15 stage. As a control, the CAGGS-Intron-RED vector was used. However, we were unable to consistently observe miR-128 overexpressing cells in the hippocampal formation. Electroporated cells were observed in the neighbouring cortex abutting the sagital fissure. Initial observations revealed that the cell bodies of Intron-RED$^+$ cells were densely packed close to the molecular layer. In contrast, the cell bodies of pre-miR-128-RED$^+$ cells were more widely distributed in deeper layers of the cortex (Figure 3.3.3.4a). To identify roughly the cortical layers confocal z-stacks were taken of the area together with a picture of DAPI staining. The nuclear distribution was assigned to distinct layers (Figure 3.3.3.4b). The cell bodies of Intron-RED$^+$ cells were most prominently found in the dense cortical plate with a diminished number in the more apical

Layer 5 (Layer 2 and 3). In contrast, the cell bodies of pre-miR-128-RED^{+} cells were mainly arranged in Layer 5. A lower number of cell bodies reached Layer 6 and the cortical plate.

During corticogenesis the cortex is build up in an inside out pattern. Different classes of projection neuron are born in overlapping temporal waves. Radial glia cells, which span from the apical ventricular zone to the basal pial surface are used as tracks for newborn neurons that are generated in the ventricular zone. In a first step at stage E11.5 the first born neurons migrate to the pial surface (Layer 1 /molecular layer). At stage E12.5 the next wave of newborn neuron migrates and forms the inner layer (Layer 6) of the cortex. At E13.5 a new wave of neurons migrates, passes Layer 6 and generates the upper Layer 5. The cortical plate is derived mainly from neurons that start to migrate at E14.5. The dense cortical plate (Layer 3 + 2) is generated by the latest born neurons starting around E15.5.

Since the electroporations were performed at around E15 one would expect that the targeted cells bodies would mainly be arranged in the dense cortical plate (Layer 2 and 3). The cell bodies of Intron-RED+ cells were indeed mainly present in this area. In contrast, the cell bodies of pre-miR-124-RED+ cells were mainly arranged in the "older" Layer 5 and failed to migrate into the dense cortical plate. These results are the first evidence that miR-128 may interfere with cortical layering *in vivo*. Ectopic overexpression of miR-128 in E15 stage neurons seems to have a pro-maturation effect, because these cells show migrational behaviour of neurons born at stage E13.5. However, additional immunostaining experiments have to be performed in order to identify their neuronal subtype.

Additional evidence that miR-128 plays a role in cortical layering is based on a recent publication from A. Ciafrè and co-workers. They showed that ectopic overexpression of miR-128 in neuroblastoma cells led to a repression of Reelin (Evangelisti et al., 2009). A Reelin autosomal recessive mutant mouse (called reeler mouse), was discovered nearly 50 years ago (Hamburgh, 1963), and revealed multiple defects such as inverted cortical lamination, abnormal positioning of neurons and aberrant orientation of cell bodies and fibers. In the cerebral cortex of the reeler mouse, neurons destined to form the subplate zone occupy ectopic positions in superficial cortical layers. A number of reports implicate the Reelin glycoprotein as an important regulator of corticogenesis by controlling neural migration and lamination (Chin et al., 2007; Nomura et al., 2008; Schaefer et al., 2008). Reelin-insufficiency caused inversion of cortical layers due to failure of neurons to migrate past earlier-generated neurons (Hammond et al., 2010; Tabata and Nakajima, 2002). In addition, Reelin overexpression studies showed that Reelin regulates structural and functional properties of synapses (Pujadas et al., 2010).

Summarized, these striking similarities between our miR-128 phenotype and Reelin deficiency phenotype, most notably the failure of neurons to migrate past earlier neurons, should be investigated further. A first approach could include a rescue experiment by co-

electroporation of Reelin expression construct and pre-miR-128-RED in the embryonic mouse brain *in utero*. These experiments are currently in progress. In order to check, which other genes are regulated by a certain miRNA, we established a GFP based sensor assay in Hek293 cells.

4.3 Validation of miRNA target genes

The prediction and validation of miRNA target genes are major research challenges to understand miRNA function. In animals, miRNA target sites are considered to be difficult to predict because they are just partial complementarity to their appropriate miRNAs. Several bioinformatic miRNA target prediction programs, based on a low number of experimental validated miRNA-target genes, have been developed (Bentwich, 2005; John et al., 2004; Krek et al., 2005; Lewis et al., 2003; Rusinov et al., 2005). However, it has been shown that these miRNA target prediction programs, like PicTar and MiRanda, are not able to recover all previous verified miRNA targets and give high number (around 24 to 39-%) of false positive target genes (Lewis et al., 2003). Therefore, several biological approaches have been established during the past years. One strategy is provided by the finding that miRNAs are often promote destabilization of targeted mRNAs by deadenylation (Eulalio et al., 2009; Fabian et al., 2009; Standart and Jackson, 2007; Wakiyama et al., 2007; Wu et al., 2006) or mRNA decay (Behm-Ansmant et al., 2006a; Behm-Ansmant et al., 2006b; Rehwinkel et al., 2005). mRNA profiling based on microarray analysis allows to screen for a large number of putative miRNA target genes after ectopic overexpression of a miRNA in a certain cell line (Lim et al., 2005). Although microarray analysis is a powerful tool to unshed the light on miRNA target genes, however this method alone is also limited, because miRNAs are not always silence their target genes by mRNA destabilization (Chendrimada et al., 2007; Kiriakidou et al., 2007; Wang et al., 2009).

Therefore, we have chosen a combination of both, informatics and biological strategies, to validate miRNA target genes of let-7, miR-125 and miR-128. To study miRNA mediated repression, we generated GFP constructs bearing 3'UTRs of putative miRNA target genes (shown in Section 3.3.3.1) and co-transfected them with complementary and control miRNA mimics in Hek293 cells. A preliminary test revealed that Hek293 cells have a moderate let-7 and miR-125 and no miR-128 activity (Figure 3.3.2a). The functionality of the miRNA mimics were confirmed by co-transfection with GFP-miRNA sensors in Hek293 cells (Figure 3.3.2b). As potential miR-128 target genes we generated eGFP target gene constructs for D4Ertd22e (PM20), MLL and Rps6ka5 and FoxP2. Previous microarray analysis revealed that the mRNA of these genes was reduced in EC cells which ectopically overexpressed miR-128 (F.

G. Wulczyn, unpublished observations) In addition, the genes were predicted by PicTar and TargetScan, to be target genes of miR-128 (Table 3.3.3b).

In all cases, the GFP expression of the GFP target gene constructs for D4Ertd22e, MLL, Rps6ka5 and FoxP2 was strongly reduced by co-transfection with the miR-128 mimic in comparison to the control (Figure 3.3.3.1d and Figure 3.3.3.2b), suggesting that all four genes are indeed miR-128 targets. Moreover, FoxP2 was predicted to be a let-7 target gene. In our assay we were able to confirm this prediction. However, a synergistically repression by ectopic overexpression of both, miR-128 and let-7, was not observed, suggesting that the repression of the GFP-FoxP2 by let-7 alone reached its maximum.

Additionally using similar assay for predicted miR-125 target gene (ZBTB7b) and three let-7/miR125 target genes (Nr6a1, Arid3a and Arid3b), we were able to demonstrate that, although ZBTB7a had been predicted by TargetScan as miR-125 target, this interaction cannot be validated by biological assays. The GFP-ZBTB7 sensor, bearing two predicted miR-125 sites with perfect seed matches (Figure 3.3.3.3a), was not repressed by miR-125 and reached the same GFP expression as the parental vector (Figure 3.3.3.3a). This result shows very plainly that the solitary presence of miRNA seed regions is not entirely sufficient to work as a regulatory sequence for a miRNA. Nr6a1 has four predicted let-7 and one miR-125 binding sites and is the highest ranking let-7 target prediction according to the PicTar and TargetScan database. However the results were ambiguous. Neither ectopic let-7 nor miR-125 significantly reduced the GFP expression of the GFP-Nr6a1 sensor. Noticeable is that the sensor alone was already about 30% reduced in comparison to the parental GFP vector. One possible explanation would be that endogenous let-7 and miR-125 of the Hek293 cells inhibit the GFP expression of GFP-Nr6a1. Also intriguing observation was the significant strong repression of GFP-Nr6a1 by ectopic miR-128.

A more slight GFP repression of GFP-Arid3a and GFP-Arid3b was also observed in response to ectopic miR-128. None of these genes are predicted to be targets of miR-128. At least, the GFP expression of GFP-Arid3a was strongly reduced by ectopic miR-125, suggesting that Arid3a is a miR-125 target gene. However, these results are not conclusive and are in contrast to previously performed RT-PCR experiments, where Arid3b and NR6a1 mRNAs were downregulated in response to mir-125 and let-7 in EC cells (A. Rybak, G. Wulczyn, unpublished data).

One problem in this assay could be the length of the 3'UTRs, which might bear too many additional regulatory sequences, which cause side effects. Another possibility could be the endogenous let-7 and miR-125 activity of the Hek293 cells, because all these construct were reduced, even without additional transfected miRNA mimics, in comparison to the parental GFP vector. Therefore, further experiments should be performed in other cells, using GFP-constructs bearing shorter 3'UTRs.

4.4 The let-7/miR-125 target genes Lin-41 and Lin-28 and their role during stem cell commitment

One additional aim of this study was to reveal potential functions of the mouse homologues of LIN-28 and LIN-41, a TRIM-NHL protein, in vertebrate development. Originally identified on the basis of their mutational phenotypes in stem-cell maturation, miR-125 and let-7 are strongly induced during neural differentiation of embryonic stem cells and embryocarcinoma cells (Smirnova et al., 2005; Wulczyn et al., 2007). As shown in Figure 3.4.2.1 and 3.4.1.1b we were able to confirm that let-7 and miR-125 target the two vertebrate pluripotency genes Lin-28 and Lin-41. The fact that both genes are let-7 and miR-125 targets has been also reported by other groups (Schulman et al., 2005),(reviewed in (Nimmo and Slack, 2009)).

In 2009, Schulman and co-workers showed that the TRIM-NHL protein TRIM32, is enriched in differentiating cells increase neural differentiation by ubiquitination of the pluripotent transcription factor c-Myc by its RING domain (Schwamborn et al., 2009). Furthermore, they showed that TRIM32 binds Ago-1, leading to an enhanced miRNA activity. Our group showed that Lin-41 ubiquitinates Ago-2 *in vitro* via its ring domain and therefore inhibits miRNA maturation. This result were supported by a miRNA-GFP sensor experiment in Hek293 cells, showing that Lin-41, but not the Lin-41 construct bearing a mutated RING domain, inhibits the activity of miR-124, miR-125 and let-7 (Figure 3.4.1.3) and therefore silence the miRNA activity in pluripotent cells (Rybak et al., 2009). These results suggest that both NHL-TRIM proteins play opposite roles during neural differentiation.

Lin-28 was identified as one of the pluripotency genes that cooperate together with Oct-4, Sox-2 and Nanog to induce pluripotency when ectopically expressed in somatic fibroblasts (Yu et al., 2007b). We showed that Lin-28 binds selectively certain precursor-miRNAs like let-7 and miR-128, and therefore inhibits their maturation by ribonuclease Dicer. These results were also confirmed by using a miRNA-GFP sensor assay (Figure 4.4.1.1b). Moreover, we showed that Lin-28 and Lin-41 can cooperate together in repression of let-7 activity and preventing therefore their own degradation during stem cell commitment (Figure 3.4.3). In addition, Heo et al. showed that Lin-28 binds pre-let-7 and promotes its degradation by 3`terminal oligouridylation (Heo et al., 2008; Heo et al., 2009). In contrast to Heo et al. and our report, Viswanathan et al. and Newmann et al. presented the evidence that Lin-28 binds pri-let-7 and therefore competes with the Microprocessor complex in the nucleus. However, ectopic expression in the neural tube of the chicken revealed that Lin-28 is not present in the Nucleus (Figure 3.4.1.3). Furthermore, *in situ* hybridization with probes complementary to let-7a or pre-let-7a both revealed predominantly granular staining in the perinuclear cytoplasm.

These evidences argue for a more central role for Lin-28 in cytoplasmic as opposed to nuclear miRNA processing.

Since neural stem cells are let-7[+] and miR-125[+] and nearly lack Lin-41 and Lin-28 expression, we tested the ability of so called miRNA-sponges (Cohen, 2009; Ebert et al., 2007), if competitive inhibition of either let-7 or miR-125 leads to a de-repression of both pluripotency genes Lin-28 and Lin-41.In both cases we could observe a de-repression of Lin-41 and Lin-28 in neural stem cells (Figure 3.3.4a and b), accompanied by a de-inhibition of let-7 maturation (Figure 3.4.4c).

Summarizing, in differentiated cells (Figure 4.4, left panel) the precursor-let-7 RNA is cleaved by the core-enzyme Dicer into the double- stranded let-7. The argonaute protein Ago2 is one of the core-enzymes which is involved in unwinding the double-stranded miRNA and associating the single stranded let-7 into the RNA-induced silencing complex (RISC). The mature, active let-7 inhibits on the posttranscriptional level, among other genes, the previously presented let-7/miR-125 target genes Lin-28 and Lin-41.
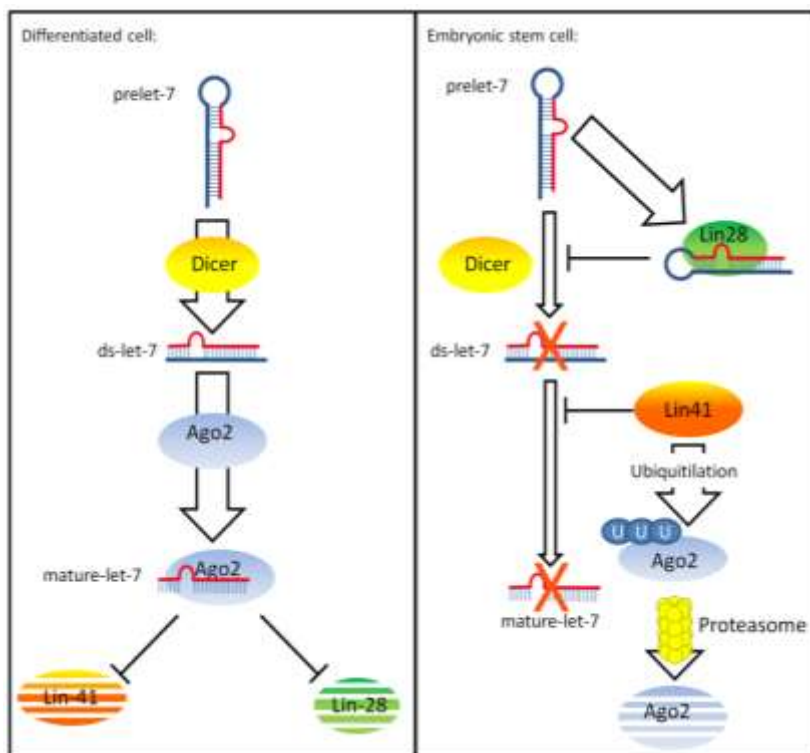
Figure 4.4: Illustration of the miRNA pathway in differentiated cells (left panel) and its inhibition by Lin-41 and Lin-28 in embryonic stem cells. Inhibited proteins are fasciated. For a detailed explanation please refer to text.

In embryonic stem cells Lin-41 and Lin-28 inhibit the processing of mature let-7 and thereby prevent their degradation by let-7 (Figure 4.4 right panel). Lin-28 regulates the miRNA pathway in a more specific way due to recognition and binding of specific double-stranded miRNA sequences and thus prevents the ribonuclease Dicer to cut the miRNA precursor into the double stranded miRNA. In contrast, Lin-41 represses miRNA maturation from the ds-miRNA to the mature form in a more general way by ubiquitylation of Ago-2, an important co-

factor which is necessary to process double stranded miRNAs into the single stranded mature forms.

4.5 Lin-41 in neural tube development

First question was where and when Lin-41 is expressed in the mouse during development. Lin-41 mRNA expression was detectable by RT-PCR in undifferentiated EC cells and was downregulated during retinoic acid-induced neural differentiation. Similar expression pattern was observed on protein level. Moreover we were able to demonstrate mLin-41 expression in the developing mouse embryo. Lin-41 was strongly expressed in early embryonic development E8.5-E10.5, and then gradually decreased (Rybak et al., 2009). Immunostaining experiments revealed strong mLin-41 expression in embryonic ectoderm (E7) and later on in the mid- and hindbrain, the spinal cord and in the dorsal root ganglion (E12). *In situ* hybridizations with probes against let-7 and Lin-41 on the neural tube of E12 mouse embryo showed reciprocal expression pattern, Lin-41 was highly expressed in the ventricular zone, whereas let-7 showed a strong prominent staining in the mantle zone, suggesting that both plays a prominent role during development of the CNS (A. Rybak, F.G. Wulczyn, unpublished observation).

Additional evidence that Lin-41 is important for vertebrate neurogenesis can be found in the publication from Schulmann and co-workers, where they demonstrated that Lin-41 gene-trap mutants demonstrated a striking neural tube closure defect during development (Maller Schulman et al., 2008). Several *Drosophila* studies support Lin-41 function as an important regulator of CNS development. Brat (Bain tumor), a Drosophila homolog of Lin41, is involved in the terminal differentiation of neural progenitors (Bello et al., 2006), absence of Brat leads to lethal hyperproliferation of these progenitors (Bowman et al., 2008).

Like Lin-41, Brat contains the NHL motif, although the TRIM domain is incomplete. Edwards et al. showed that the NHL domain is important to mediate protein-protein interactions with the PUF domain of Pumillo (Edwards et al., 2000). Pumillo itself binds, among other targets, the 3'-UTR of *hunchback*. Both proteins are necessary to repress the translation of the transcription factor hunchback (homolog of vertebrate PAX-1) in Drosophila. In addition it was shown that the NHL domain of Brat interacts with microtubule associated protein Miranda as well (Figure 4.2).
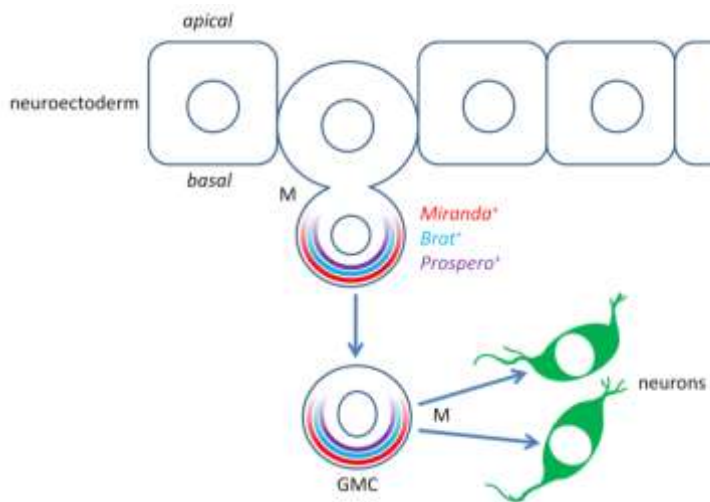
Figure 4.2: The Lin-41 homolog *Brat* is responsible for recruiting *Prospero* into the ganglion mother cell via the cargo protein Miranda during neuroblast division. For a detailed explanation please refer to text.

At early stages of Drosophila neurogenesis, neuroblast of the neuroectoderm divide asymmetrically into a new neuroblast and a mother ganglion cell (MGC). While the neuroblast retains multipotency the mother ganglion cell divides into two neuroblasts. As the asymmetric cell division starts, the cargo protein Miranda moves towards the basal membrane of the neuroblast and thereby recruits Brat (Lee et al., 2006). Brat in turn drags the transcription factor Prospero to the basal part of the dividing neuroblast. Prospero is found in early developing neurons and controls, among other things, dendrite development in growing neurons. Brat null mutants fail to recruit Prospero into the mother ganglion cell, leading to formation of two neuroblasts (Betschinger et al., 2006).

These findings raise the question, if mLin-41 plays a similar role during vertebrate neurogenesis as Brat. As a comparable model we chose the neural tube of the chicken embryos. Immunostaining of HH26 stage chicken embryo with mLin-41 antibody shows that mLin-41 is expressed, but not ubiquitously, in the neural tube (Figure 3.4.2.3b). High levels of Lin-41 were observed in the apical part of the ventricular zone and in the basal mantle zone. The presence of Lin-41 in the ventricular zone of the chicken neural tube is consistent previous study in mouse (Rybak A., Wulczyn G., unpublished observation). The high level of Lin-41 protein in the basal mantle zone, where post-mitotic neurons are arranged, is similar to Brat accumulation in differentiating ganglion mother cells. In a gain-of-function experiment, the pC3xFLAG-Lin-41 construct, bearing the full-length open reading frame of mouse Lin-41, was electroporated in the ventricular zone of the neural tube at HH16 stage, to check if disruption of the spatial Lin-41 expression pattern in the neural tube leads to developmental phenotype (Figure 3.4.2.3d). Two days after electroporation, at stage HH26, ectopic Lin-41 expression was observed just in a few cells, which were arranged in one layer, between the ventricular and the mantle zone and formed cohesive groups. In many cases, ectopic Lin-41 accumulated in small foci reminiscent of P-bodies. However, fact that just few lin-41 positive

cells were present in the one layer of the neural tube suggests that these cells have proliferation and/or differentiation defects. This suspicion is supported by a co-electroporation experiment with dsRED (Figure 3.4.2.3e). The dsRed expression was restricted to pC-3x-FLAG-Lin-41^{+} cells, suggesting that Lin-41 overexpression inhibits proliferation by cell cycle control or induced differentiation, or a combination of both.

Since Brat[-] mutants show uncontrolled proliferation, resulting in neuroblast-derived tumors, our results imply that ectopic Lin-41 expression leads to an opposite effect on proliferation. As shown for the Brat model in the neuroectoderm, Brat is important to recruit Prospero into the Ganglion mother cell, which in turn differentiates into two neuroblasts. A recent study showed that TRIM32, another TRIM/NHL protein which is ortholog to Brat, is asymmetric localized in one daughter cell during cell division of neural progenitor cells in the ventricular zone of the neocortex. Overexpression of TRIM32 leads to an increase of neural differentiation by ubiquitination of the pluripotent transcription factor c-Myc and binding of Ago-1, resulting in an increased miRNA activity (Schwamborn et al., 2009). Lin-41 has been shown to have a reverse effect, remaining pluripotency by ubiquitination of Ago-2 and therefore inhibits miRNA maturation, suggesting that both proteins have opposite roles in neural differentiation. The determinants of asymmetric Trim32 inheritance are not known. However, in the case of Brat interaction with Miranda is required. Asymmetric Miranda distribution, in turn, is dependent on the Drosophila Myosin genes Zip and Jaguar. Of particular interest is the role of Jaguar, which is homologous to the vertebrate Myo6 proteins. Unlike typical myosins, Myo6 and Jaguar are unusual, because they move towards the minus (slow-growing) end of actin-filaments (Petritsch et al., 2003). At present, little is known about vertebrate Myo6. Myo6 is involved in development of cochlear stereocilia (Karolyi et al., 2003). Several reports showed that humans, deficient in Myo6, show hearing loss (Hilgert et al., 2008; Sanggaard et al., 2008). More remarkable are the studies from Aschenbrenner, showing that Myo6 is required for the transportation of un-coated endocytic vesicles from the actin-rich periphery of epithelial cells (Aschenbrenner et al., 2003; Aschenbrenner et al., 2004).

With the exception of Lin-41, all mammalian TRIM-NHL proteins have been shown to interact with some forms of myosin (F. Gregory Wulczyn, 2010). To test if Myo6 is able to influence the Lin-41-effect in the neural tube, co-electroporation of HA-Myo6 and 3xFLAG-Lin-41 was performed (Figure 3.4.2.4). Co-expression of Myo6 led to increased numbers of Lin-41^{+} cells. Moreover, in contrast to the 3xFLAG-Lin-41 electroporation alone, ectopic Lin-41^{+} cells were widely distributed in the ventricular zone, the mantle layer zone, and the dorsal root ganglion. Although preliminary, these results are the first evidence that Lin-41 also direct or indirect interacts with Myosin during CNS development.

In conclusion, in this thesis it was shown that the pluripotency genes Lin-41 and Lin-28 are important regulators of the miRNA process machinery. Lin-28, together with Lin-41, inhibit let-7 maturation during stem-cell commitment. let-7 and miR-125 downregulate these pluripotency genes at the differentiation stage. Inhibition of either let-7 or miR-125 in differentiated neural stem cells leads to a restoration of Lin-41 and Lin-28 and therefore a partial rescue of the pluripotent state. These observations are of major interest for further studies, in particular for reprogramming differentiated cells into induced pluripotency cells (iPS).

In addition, gain-of function experiments with the neuron specific miRNAs miR-124 and miR-128 emphasized the importance of proper temporal and spatial miRNA activity during neural development. Overexpression of miR-128 or miR-124 *in utero* led to dramatic migrational disorders as well as miR-124 misexpression *in ovo*. These observations need to be characterized in more detail to understand these wide range interactions between miRNAs and their target genes during neural development.

5. Reference list

Arasu, P., Wightman, B., and Ruvkun, G. (1991). Temporal regulation of lin-14 by the antagonistic action of two other heterochronic genes, lin-4 and lin-28. Genes Dev *5*, 1825-1833.

Aschenbrenner, L., Lee, T., and Hasson, T. (2003). Myo6 facilitates the translocation of endocytic vesicles from cell peripheries. Mol Biol Cell *14*, 2728-2743.

Aschenbrenner, L., Naccache, S.N., and Hasson, T. (2004). Uncoated endocytic vesicles require the unconventional myosin, Myo6, for rapid transport through actin barriers. Mol Biol Cell *15*, 2253-2263.

Behm-Ansmant, I., Rehwinkel, J., Doerks, T., Stark, A., Bork, P., and Izaurralde, E. (2006a). mRNA degradation by miRNAs and GW182 requires both CCR4:NOT deadenylase and DCP1:DCP2 decapping complexes. Genes Dev *20*, 1885-1898.

Behm-Ansmant, I., Rehwinkel, J., and Izaurralde, E. (2006b). MicroRNAs silence gene expression by repressing protein expression and/or by promoting mRNA decay. Cold Spring Harb Symp Quant Biol *71*, 523-530.

Bell, G.W., Yatskievych, T.A., and Antin, P.B. (2004). GEISHA, a whole-mount in situ hybridization gene expression screen in chicken embryos. Dev Dyn *229*, 677-687.

Bello, B., Reichert, H., and Hirth, F. (2006). The brain tumor gene negatively regulates neural progenitor cell proliferation in the larval central brain of Drosophila. Development *133*, 2639-2648.

Bentwich, I. (2005). Prediction and validation of microRNAs and their targets. FEBS Lett *579*, 5904-5910.

Berninger, B., Costa, M.R., Koch, U., Schroeder, T., Sutor, B., Grothe, B., and Gotz, M. (2007). Functional properties of neurons derived from in vitro reprogrammed postnatal astroglia. J Neurosci *27*, 8654-8664.

Betschinger, J., Mechtler, K., and Knoblich, J.A. (2006). Asymmetric segregation of the tumor suppressor brat regulates self-renewal in Drosophila neural stem cells. Cell *124*, 1241-1253.

Beveridge, N.J., Tooney, P.A., Carroll, A.P., Tran, N., and Cairns, M.J. (2009). Down-regulation of miR-17 family expression in response to retinoic acid induced neuronal differentiation. Cell Signal *21*, 1837-1845.

Bhattacharyya, S.N., Habermacher, R., Martine, U., Closs, E.I., and Filipowicz, W. (2006). Stress-induced reversal of microRNA repression and mRNA P-body localization in human cells. Cold Spring Harb Symp Quant Biol *71*, 513-521.

Bohnsack, M.T., Czaplinski, K., and Gorlich, D. (2004). Exportin 5 is a RanGTP-dependent dsRNA-binding protein that mediates nuclear export of pre-miRNAs. RNA *10*, 185-191.

Bouhallier, F., Allioli, N., Lavial, F., Chalmel, F., Perrard, M.H., Durand, P., Samarut, J., Pain, B., and Rouault, J.P. (2010). Role of miR-34c microRNA in the late steps of spermatogenesis. RNA *16*, 720-731.

Bowman, S.K., Rolland, V., Betschinger, J., Kinsey, K.A., Emery, G., and Knoblich, J.A. (2008). The tumor suppressors Brat and Numb regulate transit-amplifying neuroblast lineages in Drosophila. Dev Cell *14*, 535-546.

Brengues, M., and Parker, R. (2007). Accumulation of polyadenylated mRNA, Pab1p, eIF4E, and eIF4G with P-bodies in Saccharomyces cerevisiae. Mol Biol Cell *18*, 2592-2602.

Brennecke, J., Stark, A., Russell, R.B., and Cohen, S.M. (2005). Principles of microRNA-target recognition. PLoS Biol *3*, e85.

Bussing, I., Slack, F.J., and Grosshans, H. (2008). let-7 microRNAs in development, stem cells and cancer. Trends Mol Med *14*, 400-409.

Cao, X., Pfaff, S.L., and Gage, F.H. (2007). A functional study of miR-124 in the developing neural tube. Genes Dev *21*, 531-536.

Cheever, A., and Ceman, S. (2009). Phosphorylation of FMRP inhibits association with Dicer. RNA *15*, 362-366.

Chendrimada, T.P., Finn, K.J., Ji, X., Baillat, D., Gregory, R.I., Liebhaber, S.A., Pasquinelli, A.E., and Shiekhattar, R. (2007). MicroRNA silencing through RISC recruitment of eIF6. Nature *447*, 823-828.

Chendrimada, T.P., Gregory, R.I., Kumaraswamy, E., Norman, J., Cooch, N., Nishikura, K., and Shiekhattar, R. (2005). TRBP recruits the Dicer complex to Ago2 for microRNA processing and gene silencing. Nature *436*, 740-744.

Cheng, L.C., Pastrana, E., Tavazoie, M., and Doetsch, F. (2009). miR-124 regulates adult neurogenesis in the subventricular zone stem cell niche. Nat Neurosci *12*, 399-408.

Chin, J., Massaro, C.M., Palop, J.J., Thwin, M.T., Yu, G.Q., Bien-Ly, N., Bender, A., and Mucke, L. (2007). Reelin depletion in the entorhinal cortex of human amyloid precursor protein transgenic mice and humans with Alzheimer's disease. J Neurosci *27*, 2727-2733.

Choudhary, S., Lee, H.C., Maiti, M., He, Q., Cheng, P., Liu, Q., and Liu, Y. (2007). A double-stranded-RNA response program important for RNA interference efficiency. Mol Cell Biol *27*, 3995-4005.

Cohen, S.M. (2009). Use of microRNA sponges to explore tissue-specific microRNA functions in vivo. Nat Methods *6*, 873-874.

Conaco, C., Otto, S., Han, J.J., and Mandel, G. (2006). Reciprocal actions of REST and a microRNA promote neuronal identity. Proc Natl Acad Sci U S A *103*, 2422-2427.

Cullen, B.R. (2004). Transcription and processing of human microRNA precursors. Mol Cell *16*, 861-865.

Daniels, S.M., Melendez-Pena, C.E., Scarborough, R.J., Daher, A., Christensen, H.S., El Far, M., Purcell, D.F., Laine, S., and Gatignol, A. (2009). Characterization of the TRBP domain required for dicer interaction and function in RNA interference. BMC Mol Biol *10*, 38.

Darnell, J.C., Jensen, K.B., Jin, P., Brown, V., Warren, S.T., and Darnell, R.B. (2001). Fragile X mental retardation protein targets G quartet mRNAs important for neuronal function. Cell *107*, 489-499.

Darnell, J.C., Warren, S.T., and Darnell, R.B. (2004). The fragile X mental retardation protein, FMRP, recognizes G-quartets. Ment Retard Dev Disabil Res Rev *10*, 49-52.

Davis, T.H., Cuellar, T.L., Koch, S.M., Barker, A.J., Harfe, B.D., McManus, M.T., and Ullian, E.M. (2008). Conditional loss of Dicer disrupts cellular and tissue morphogenesis in the cortex and hippocampus. J Neurosci *28*, 4322-4330.

De Pietri Tonelli, D., Pulvers, J.N., Haffner, C., Murchison, E.P., Hannon, G.J., and Huttner, W.B. (2008). miRNAs are essential for survival and differentiation of newborn neurons but not for expansion of neural progenitors during early neurogenesis in the mouse embryonic neocortex. Development *135*, 3911-3921.

Denli, A.M., Tops, B.B., Plasterk, R.H., Ketting, R.F., and Hannon, G.J. (2004). Processing of primary microRNAs by the Microprocessor complex. Nature *432*, 231-235.

Deo, M., Yu, J.Y., Chung, K.H., Tippens, M., and Turner, D.L. (2006). Detection of mammalian microRNA expression by in situ hybridization with RNA oligonucleotides. Dev Dyn *235*, 2538-2548.

Diederichs, S., and Haber, D.A. (2007). Dual role for argonautes in microRNA processing and posttranscriptional regulation of microRNA expression. Cell *131*, 1097-1108.

Doench, J.G., Petersen, C.P., and Sharp, P.A. (2003). siRNAs can function as miRNAs. Genes Dev *17*, 438-442.

Dugas, J.C., Cuellar, T.L., Scholze, A., Ason, B., Ibrahim, A., Emery, B., Zamanian, J.L., Foo, L.C., McManus, M.T., and Barres, B.A. (2010). Dicer1 and miR-219 Are required for normal oligodendrocyte differentiation and myelination. Neuron *65*, 597-611.

Ebert, M.S., Neilson, J.R., and Sharp, P.A. (2007). MicroRNA sponges: competitive inhibitors of small RNAs in mammalian cells. Nat Methods *4*, 721-726.

Edbauer, D., Neilson, J.R., Foster, K.A., Wang, C.F., Seeburg, D.P., Batterton, M.N., Tada, T., Dolan, B.M., Sharp, P.A., and Sheng, M. (2010). Regulation of synaptic structure and function by FMRP-associated microRNAs miR-125b and miR-132. Neuron *65*, 373-384.

Edwards, T.A., Trincao, J., Escalante, C.R., Wharton, R.P., and Aggarwal, A.K. (2000). Crystallization and characterization of Pumilo: a novel RNA binding protein. J Struct Biol *132*, 251-254.

Edwards, T.A., Wilkinson, B.D., Wharton, R.P., and Aggarwal, A.K. (2003). Model of the brain tumor-Pumilio translation repressor complex. Genes Dev *17*, 2508-2513.

Eulalio, A., Huntzinger, E., Nishihara, T., Rehwinkel, J., Fauser, M., and Izaurralde, E. (2009). Deadenylation is a widespread effect of miRNA regulation. RNA *15*, 21-32.

Evangelisti, C., Florian, M.C., Massimi, I., Dominici, C., Giannini, G., Galardi, S., Bue, M.C., Massalini, S., McDowell, H.P., Messi, E*., et al.* (2009). MiR-128 up-regulation inhibits Reelin

and DCX expression and reduces neuroblastoma cell motility and invasiveness. FASEB J *23*, 4276-4287.

F. Gregory Wulczyn, E.C., Eleonora Franzoni and Agnieszka Rybak (2010). miRNAs need a Trim Regulation of miRNA Activity by Trim-NHL Proteins. Madame Curie Bioscience Database.

Fabian, M.R., Mathonnet, G., Sundermeier, T., Mathys, H., Zipprich, J.T., Svitkin, Y.V., Rivas, F., Jinek, M., Wohlschlegel, J., Doudna, J.A.*, et al.* (2009). Mammalian miRNA RISC recruits CAF1 and PABP to affect PABP-dependent deadenylation. Mol Cell *35*, 868-880.

Gangaraju, V.K., and Lin, H. (2009). MicroRNAs: key regulators of stem cells. Nat Rev Mol Cell Biol *10*, 116-125.

Giraldez, A.J., Cinalli, R.M., Glasner, M.E., Enright, A.J., Thomson, J.M., Baskerville, S., Hammond, S.M., Bartel, D.P., and Schier, A.F. (2005). MicroRNAs regulate brain morphogenesis in zebrafish. Science *308*, 833-838.

Giulian, D., Chen, J., Ingeman, J.E., George, J.K., and Noponen, M. (1989). The role of mononuclear phagocytes in wound healing after traumatic injury to adult mammalian brain. J Neurosci *9*, 4416-4429.

Golding, J.P., and Cohen, J. (1997). Border controls at the mammalian spinal cord: late-surviving neural crest boundary cap cells at dorsal root entry sites may regulate sensory afferent ingrowth and entry zone morphogenesis. Mol Cell Neurosci *9*, 381-396.

Gregory, R.I., Chendrimada, T.P., Cooch, N., and Shiekhattar, R. (2005). Human RISC couples microRNA biogenesis and posttranscriptional gene silencing. Cell *123*, 631-640.

Gregory, R.I., Yan, K.P., Amuthan, G., Chendrimada, T., Doratotaj, B., Cooch, N., and Shiekhattar, R. (2004). The Microprocessor complex mediates the genesis of microRNAs. Nature *432*, 235-240.

Grimson, A., Farh, K.K., Johnston, W.K., Garrett-Engele, P., Lim, L.P., and Bartel, D.P. (2007). MicroRNA targeting specificity in mammals: determinants beyond seed pairing. Mol Cell *27*, 91-105.

Gunaratne, P.H. (2009). Embryonic stem cell microRNAs: defining factors in induced pluripotent (iPS) and cancer (CSC) stem cells? Curr Stem Cell Res Ther *4*, 168-177.

Guo, Y., Liu, Y., Xu, L., Wu, S., Yang, C., Wu, D., Wu, H., and Li, C. (2007). Astrocytic pathology in the immune-mediated motor neuron injury. Amyotroph Lateral Scler *8*, 230-234.

Hamburgh, M. (1963). Analysis of the Postnatal Developmental Effects of "Reeler," a Neurological Mutation in Mice. A Study in Developmental Genetics. Dev Biol *19*, 165-185.

Hammond, V.E., So, E., Cate, H.S., Britto, J.M., Gunnersen, J.M., and Tan, S.S. (2010). Cortical Layer Development and Orientation is Modulated by Relative Contributions of Reelin-Negative and -Positive Neurons in Mouse Chimeras. Cereb Cortex.

Han, J., Lee, Y., Yeom, K.H., Nam, J.W., Heo, I., Rhee, J.K., Sohn, S.Y., Cho, Y., Zhang, B.T., and Kim, V.N. (2006). Molecular basis for the recognition of primary microRNAs by the Drosha-DGCR8 complex. Cell *125*, 887-901.

Hausser, J., Landthaler, M., Jaskiewicz, L., Gaidatzis, D., and Zavolan, M. (2009). Relative contribution of sequence and structure features to the mRNA binding of Argonaute/EIF2C-miRNA complexes and the degradation of miRNA targets. Genome Res *19*, 2009-2020.

Hayes, G.D., Frand, A.R., and Ruvkun, G. (2006). The mir-84 and let-7 paralogous microRNA genes of Caenorhabditis elegans direct the cessation of molting via the conserved nuclear hormone receptors NHR-23 and NHR-25. Development *133*, 4631-4641.

Heo, I., Joo, C., Cho, J., Ha, M., Han, J., and Kim, V.N. (2008). Lin28 mediates the terminal uridylation of let-7 precursor MicroRNA. Mol Cell *32*, 276-284.

Heo, I., Joo, C., Kim, Y.K., Ha, M., Yoon, M.J., Cho, J., Yeom, K.H., Han, J., and Kim, V.N. (2009). TUT4 in concert with Lin28 suppresses microRNA biogenesis through pre-microRNA uridylation. Cell *138*, 696-708.

Herrscher, R.F., Kaplan, M.H., Lelsz, D.L., Das, C., Scheuermann, R., and Tucker, P.W. (1995). The immunoglobulin heavy-chain matrix-associating regions are bound by Bright: a B cell-specific trans-activator that describes a new DNA-binding protein family. Genes Dev *9*, 3067-3082.

Hilgert, N., Topsakal, V., van Dinther, J., Offeciers, E., Van de Heyning, P., and Van Camp, G. (2008). A splice-site mutation and overexpression of MYO6 cause a similar phenotype in two families with autosomal dominant hearing loss. Eur J Hum Genet *16*, 593-602.

Hillebrand, J., Barbee, S.A., and Ramaswami, M. (2007). P-body components, microRNA regulation, and synaptic plasticity. ScientificWorldJournal *7*, 178-190.

Horvitz, H.R., and Sulston, J.E. (1980). Isolation and genetic characterization of cell-lineage mutants of the nematode Caenorhabditis elegans. Genetics *96*, 435-454.

Ingelfinger, D., Arndt-Jovin, D.J., Luhrmann, R., and Achsel, T. (2002). The human LSm1-7 proteins colocalize with the mRNA-degrading enzymes Dcp1/2 and Xrnl in distinct cytoplasmic foci. RNA *8*, 1489-1501.

Iwasaki, S., Kawamata, T., and Tomari, Y. (2009). Drosophila argonaute1 and argonaute2 employ distinct mechanisms for translational repression. Mol Cell *34*, 58-67.

Jabri, E. (2005). P-bodies take a RISC. Nat Struct Mol Biol *12*, 564.

Jager, E., and Dorner, S. (2010). The decapping activator HPat a novel factor co-purifying with GW182 from Drosophila cells. RNA Biol *7*, 381-385.

Jang, L.T., Buu, L.M., and Lee, F.J. (2006). Determinants of Rbp1p localization in specific cytoplasmic mRNA-processing foci, P-bodies. J Biol Chem *281*, 29379-29390.

John, B., Enright, A.J., Aravin, A., Tuschl, T., Sander, C., and Marks, D.S. (2004). Human MicroRNA targets. PLoS Biol *2*, e363.

Kanamoto, T., Terada, K., Yoshikawa, H., and Furukawa, T. (2006). Cloning and regulation of the vertebrate homologue of lin-41 that functions as a heterochronic gene in Caenorhabditis elegans. Dev Dyn *235*, 1142-1149.

Kanellopoulou, C., Muljo, S.A., Kung, A.L., Ganesan, S., Drapkin, R., Jenuwein, T., Livingston, D.M., and Rajewsky, K. (2005). Dicer-deficient mouse embryonic stem cells are defective in differentiation and centromeric silencing. Genes Dev *19*, 489-501.

Kar, S., Wang, M., Yao, W., Michejda, C.J., and Carr, B.I. (2006). PM-20, a novel inhibitor of Cdc25A, induces extracellular signal-regulated kinase 1/2 phosphorylation and inhibits hepatocellular carcinoma growth in vitro and in vivo. Mol Cancer Ther *5*, 1511-1519.

Karolyi, I.J., Probst, F.J., Beyer, L., Odeh, H., Dootz, G., Cha, K.B., Martin, D.M., Avraham, K.B., Kohrman, D., Dolan, D.F.*, et al.* (2003). Myo15 function is distinct from Myo6, Myo7a and pirouette genes in development of cochlear stereocilia. Hum Mol Genet *12*, 2797-2805.

Kim, J., Inoue, K., Ishii, J., Vanti, W.B., Voronov, S.V., Murchison, E., Hannon, G., and Abeliovich, A. (2007). A MicroRNA feedback circuit in midbrain dopamine neurons. Science *317*, 1220-1224.

Kiriakidou, M., Tan, G.S., Lamprinaki, S., De Planell-Saguer, M., Nelson, P.T., and Mourelatos, Z. (2007). An mRNA m7G cap binding-like motif within human Ago2 represses translation. Cell *129*, 1141-1151.

Kost-Mikucki, S.A., and Oblinger, M.M. (1991). Changes in glial fibrillary acidic protein mRNA expression after corticospinal axotomy in the adult hamster. J Neurosci Res *28*, 182-191.

Krek, A., Grun, D., Poy, M.N., Wolf, R., Rosenberg, L., Epstein, E.J., MacMenamin, P., da Piedade, I., Gunsalus, K.C., Stoffel, M.*, et al.* (2005). Combinatorial microRNA target predictions. Nat Genet *37*, 495-500.

Krichevsky, A.M., King, K.S., Donahue, C.P., Khrapko, K., and Kosik, K.S. (2003). A microRNA array reveals extensive regulation of microRNAs during brain development. RNA *9*, 1274-1281.

Krichevsky, A.M., Sonntag, K.C., Isacson, O., and Kosik, K.S. (2006). Specific microRNAs modulate embryonic stem cell-derived neurogenesis. Stem Cells *24*, 857-864.

Lagos-Quintana, M., Rauhut, R., Yalcin, A., Meyer, J., Lendeckel, W., and Tuschl, T. (2002). Identification of tissue-specific microRNAs from mouse. Curr Biol *12*, 735-739.

Lee, C.Y., Wilkinson, B.D., Siegrist, S.E., Wharton, R.P., and Doe, C.Q. (2006). Brat is a Miranda cargo protein that promotes neuronal differentiation and inhibits neuroblast self-renewal. Dev Cell *10*, 441-449.

Lee, R.C., Feinbaum, R.L., and Ambros, V. (1993). The C. elegans heterochronic gene lin-4 encodes small RNAs with antisense complementarity to lin-14. Cell *75*, 843-854.

Lee, Y., Ahn, C., Han, J., Choi, H., Kim, J., Yim, J., Lee, J., Provost, P., Radmark, O., Kim, S.*, et al.* (2003). The nuclear RNase III Drosha initiates microRNA processing. Nature *425*, 415-419.

Lee, Y., Jeon, K., Lee, J.T., Kim, S., and Kim, V.N. (2002). MicroRNA maturation: stepwise processing and subcellular localization. EMBO J *21*, 4663-4670.

Leslie Pedrioli, D.M., Karpanen, T., Dabouras, V., Jurisic, G., van de Hoek, G., Shin, J.W., Marino, D., Kalin, R.E., Leidel, S., Cinelli, P.*, et al.* (2010). miR-31 functions as a negative

regulator of lymphatic vascular lineage-specific differentiation in vitro and vascular development in vivo. Mol Cell Biol.

Lewis, B.P., Burge, C.B., and Bartel, D.P. (2005). Conserved seed pairing, often flanked by adenosines, indicates that thousands of human genes are microRNA targets. Cell *120*, 15-20.

Lewis, B.P., Shih, I.H., Jones-Rhoades, M.W., Bartel, D.P., and Burge, C.B. (2003). Prediction of mammalian microRNA targets. Cell *115*, 787-798.

Li, S., Lian, S.L., Moser, J.J., Fritzler, M.L., Fritzler, M.J., Satoh, M., and Chan, E.K. (2008). Identification of GW182 and its novel isoform TNGW1 as translational repressors in Ago2-mediated silencing. J Cell Sci *121*, 4134-4144.

Lian, S.L., Li, S., Abadal, G.X., Pauley, B.A., Fritzler, M.J., and Chan, E.K. (2009). The C-terminal half of human Ago2 binds to multiple GW-rich regions of GW182 and requires GW182 to mediate silencing. RNA *15*, 804-813.

Lim, L.P., Lau, N.C., Garrett-Engele, P., Grimson, A., Schelter, J.M., Castle, J., Bartel, D.P., Linsley, P.S., and Johnson, J.M. (2005). Microarray analysis shows that some microRNAs downregulate large numbers of target mRNAs. Nature *433*, 769-773.

Lin, S.Y., Johnson, S.M., Abraham, M., Vella, M.C., Pasquinelli, A., Gamberi, C., Gottlieb, E., and Slack, F.J. (2003). The C elegans hunchback homolog, hbl-1, controls temporal patterning and is a probable microRNA target. Dev Cell *4*, 639-650.

Liu, J., Carmell, M.A., Rivas, F.V., Marsden, C.G., Thomson, J.M., Song, J.J., Hammond, S.M., Joshua-Tor, L., and Hannon, G.J. (2004). Argonaute2 is the catalytic engine of mammalian RNAi. Science *305*, 1437-1441.

Liu, J., Rivas, F.V., Wohlschlegel, J., Yates, J.R., 3rd, Parker, R., and Hannon, G.J. (2005a). A role for the P-body component GW182 in microRNA function. Nat Cell Biol *7*, 1261-1266.

Liu, J., Valencia-Sanchez, M.A., Hannon, G.J., and Parker, R. (2005b). MicroRNA-dependent localization of targeted mRNAs to mammalian P-bodies. Nat Cell Biol *7*, 719-723.

Liu, S.P., Fu, R.H., Yu, H.H., Li, K.W., Tsai, C.H., Shyu, W.C., and Lin, S.Z. (2009). MicroRNAs regulation modulated self-renewal and lineage differentiation of stem cells. Cell Transplant *18*, 1039-1045.

Liu, T., Papagiannakopoulos, T., Puskar, K., Qi, S., Santiago, F., Clay, W., Lao, K., Lee, Y., Nelson, S.F., Kornblum, H.I.*, et al.* (2007). Detection of a microRNA signal in an in vivo expression set of mRNAs. PLoS One *2*, e804.

Lukiw, W.J., and Pogue, A.I. (2007). Induction of specific micro RNA (miRNA) species by ROS-generating metal sulfates in primary human brain cells. J Inorg Biochem *101*, 1265-1269.

Ma, J.B., Yuan, Y.R., Meister, G., Pei, Y., Tuschl, T., and Patel, D.J. (2005). Structural basis for 5'-end-specific recognition of guide RNA by the A. fulgidus Piwi protein. Nature *434*, 666-670.

Maiorano, N.A., and Mallamaci, A. (2009). Promotion of embryonic cortico-cerebral neuronogenesis by miR-124. Neural Dev *4*, 40.

Makeyev, E.V., Zhang, J., Carrasco, M.A., and Maniatis, T. (2007). The MicroRNA miR-124 promotes neuronal differentiation by triggering brain-specific alternative pre-mRNA splicing. Mol Cell *27*, 435-448.

Maller Schulman, B.R., Liang, X., Stahlhut, C., DelConte, C., Stefani, G., and Slack, F.J. (2008). The let-7 microRNA target gene, Mlin41/Trim71 is required for mouse embryonic survival and neural tube closure. Cell Cycle *7*, 3935-3942.

Maniataki, E., and Mourelatos, Z. (2005). A human, ATP-independent, RISC assembly machine fueled by pre-miRNA. Genes Dev *19*, 2979-2990.

Mathonnet, G., Fabian, M.R., Svitkin, Y.V., Parsyan, A., Huck, L., Murata, T., Biffo, S., Merrick, W.C., Darzynkiewicz, E., Pillai, R.S*., et al.* (2007). MicroRNA inhibition of translation initiation in vitro by targeting the cap-binding complex eIF4F. Science *317*, 1764-1767.

Melton, C., Judson, R.L., and Blelloch, R. (2010). Opposing microRNA families regulate self-renewal in mouse embryonic stem cells. Nature *463*, 621-626.

Miska, E.A., Alvarez-Saavedra, E., Townsend, M., Yoshii, A., Sestan, N., Rakic, P., Constantine-Paton, M., and Horvitz, H.R. (2004). Microarray analysis of microRNA expression in the developing mammalian brain. Genome Biol *5*, R68.

Miyoshi, K., Tsukumo, H., Nagami, T., Siomi, H., and Siomi, M.C. (2005). Slicer function of Drosophila Argonautes and its involvement in RISC formation. Genes Dev *19*, 2837-2848.

Moss, E.G., Lee, R.C., and Ambros, V. (1997). The cold shock domain protein LIN-28 controls developmental timing in C. elegans and is regulated by the lin-4 RNA. Cell *88*, 637-646.

Moss, E.G., and Tang, L. (2003). Conservation of the heterochronic regulator Lin-28, its developmental expression and microRNA complementary sites. Dev Biol *258*, 432-442.

Naeger, L.K., Goodwin, E.C., Hwang, E.S., DeFilippis, R.A., Zhang, H., and DiMaio, D. (1999). Bovine papillomavirus E2 protein activates a complex growth-inhibitory program in p53-negative HT-3 cervical carcinoma cells that includes repression of cyclin A and cdc25A phosphatase genes and accumulation of hypophosphorylated retinoblastoma protein. Cell Growth Differ *10*, 413-422.

Nagele, R.G., Hunter, E., Bush, K., and Lee, H.Y. (1987). Studies on the mechanisms of neurulation in the chick: morphometric analysis of force distribution within the neuroepithelium during neural tube formation. J Exp Zool *244*, 425-436.

Nakajima, N., Takahashi, T., Kitamura, R., Isodono, K., Asada, S., Ueyama, T., Matsubara, H., and Oh, H. (2006). MicroRNA-1 facilitates skeletal myogenic differentiation without affecting osteoblastic and adipogenic differentiation. Biochem Biophys Res Commun *350*, 1006-1012.

Neumuller, R.A., Betschinger, J., Fischer, A., Bushati, N., Poernbacher, I., Mechtler, K., Cohen, S.M., and Knoblich, J.A. (2008). Mei-P26 regulates microRNAs and cell growth in the Drosophila ovarian stem cell lineage. Nature *454*, 241-245.

Nieto-Sampedro, M., Saneto, R.P., de Vellis, J., and Cotman, C.W. (1985). The control of glial populations in brain: changes in astrocyte mitogenic and morphogenic factors in response to injury. Brain Res *343*, 320-328.

Nimmo, R.A., and Slack, F.J. (2009). An elegant miRror: microRNAs in stem cells, developmental timing and cancer. Chromosoma *118*, 405-418.

Nomura, T., Takahashi, M., Hara, Y., and Osumi, N. (2008). Patterns of neurogenesis and amplitude of Reelin expression are essential for making a mammalian-type cortex. PLoS One *3*, e1454.

Nottrott, S., Simard, M.J., and Richter, J.D. (2006). Human let-7a miRNA blocks protein production on actively translating polyribosomes. Nat Struct Mol Biol *13*, 1108-1114.

Olsen, P.H., and Ambros, V. (1999). The lin-4 regulatory RNA controls developmental timing in Caenorhabditis elegans by blocking LIN-14 protein synthesis after the initiation of translation. Dev Biol *216*, 671-680.

Omarov, R.T., Ciomperlik, J.J., and Scholthof, H.B. (2007). RNAi-associated ssRNA-specific ribonucleases in Tombusvirus P19 mutant-infected plants and evidence for a discrete siRNA-containing effector complex. Proc Natl Acad Sci U S A *104*, 1714-1719.

Pasquinelli, A.E., Reinhart, B.J., Slack, F., Martindale, M.Q., Kuroda, M.I., Maller, B., Hayward, D.C., Ball, E.E., Degnan, B., Muller, P.*, et al.* (2000). Conservation of the sequence and temporal expression of let-7 heterochronic regulatory RNA. Nature *408*, 86-89.

Petritsch, C., Tavosanis, G., Turck, C.W., Jan, L.Y., and Jan, Y.N. (2003). The Drosophila myosin VI Jaguar is required for basal protein targeting and correct spindle orientation in mitotic neuroblasts. Dev Cell *4*, 273-281.

Pham, J.W., Pellino, J.L., Lee, Y.S., Carthew, R.W., and Sontheimer, E.J. (2004). A Dicer-2-dependent 80s complex cleaves targeted mRNAs during RNAi in Drosophila. Cell *117*, 83-94.

Pillai, R.S., Artus, C.G., and Filipowicz, W. (2004). Tethering of human Ago proteins to mRNA mimics the miRNA-mediated repression of protein synthesis. RNA *10*, 1518-1525.

Plante, I., Davidovic, L., Ouellet, D.L., Gobeil, L.A., Tremblay, S., Khandjian, E.W., and Provost, P. (2006). Dicer-derived microRNAs are utilized by the fragile X mental retardation protein for assembly on target RNAs. J Biomed Biotechnol *2006*, 64347.

Pollard, S., Conti, L., and Smith, A. (2006a). Exploitation of adherent neural stem cells in basic and applied neurobiology. Regen Med *1*, 111-118.

Pollard, S.M., Conti, L., Sun, Y., Goffredo, D., and Smith, A. (2006b). Adherent neural stem (NS) cells from fetal and adult forebrain. Cereb Cortex *16 Suppl 1*, i112-120.

Pujadas, L., Gruart, A., Bosch, C., Delgado, L., Teixeira, C.M., Rossi, D., de Lecea, L., Martinez, A., Delgado-Garcia, J.M., and Soriano, E. (2010). Reelin regulates postnatal neurogenesis and enhances spine hypertrophy and long-term potentiation. J Neurosci *30*, 4636-4649.

Rajasethupathy, P., Fiumara, F., Sheridan, R., Betel, D., Puthanveettil, S.V., Russo, J.J., Sander, C., Tuschl, T., and Kandel, E. (2009). Characterization of small RNAs in aplysia reveals a role for miR-124 in constraining synaptic plasticity through CREB. Neuron *63*, 803-817.

Ramkissoon, S.H., Mainwaring, L.A., Ogasawara, Y., Keyvanfar, K., McCoy, J.P., Jr., Sloand, E.M., Kajigaya, S., and Young, N.S. (2006). Hematopoietic-specific microRNA expression in human cells. Leuk Res *30*, 643-647.

Rehwinkel, J., Behm-Ansmant, I., Gatfield, D., and Izaurralde, E. (2005). A crucial role for GW182 and the DCP1:DCP2 decapping complex in miRNA-mediated gene silencing. RNA *11*, 1640-1647.

Reinhart, B.J., Slack, F.J., Basson, M., Pasquinelli, A.E., Bettinger, J.C., Rougvie, A.E., Horvitz, H.R., and Ruvkun, G. (2000). The 21-nucleotide let-7 RNA regulates developmental timing in Caenorhabditis elegans. Nature *403*, 901-906.

Richards, S.A., Lounsbury, K.M., and Macara, I.G. (1995). The C terminus of the nuclear RAN/TC4 GTPase stabilizes the GDP-bound state and mediates interactions with RCC1, RAN-GAP, and HTF9A/RANBP1. J Biol Chem *270*, 14405-14411.

Ronemus, M., Vaughn, M.W., and Martienssen, R.A. (2006). MicroRNA-targeted and small interfering RNA-mediated mRNA degradation is regulated by argonaute, dicer, and RNA-dependent RNA polymerase in Arabidopsis. Plant Cell *18*, 1559-1574.

Rusinov, V., Baev, V., Minkov, I.N., and Tabler, M. (2005). MicroInspector: a web tool for detection of miRNA binding sites in an RNA sequence. Nucleic Acids Res *33*, W696-700.

Rybak, A., Fuchs, H., Hadian, K., Smirnova, L., Wulczyn, E.A., Michel, G., Nitsch, R., Krappmann, D., and Wulczyn, F.G. (2009). The let-7 target gene mouse lin-41 is a stem cell specific E3 ubiquitin ligase for the miRNA pathway protein Ago2. Nat Cell Biol *11*, 1411-1420.

Rybak, A., Fuchs, H., Smirnova, L., Brandt, C., Pohl, E.E., Nitsch, R., and Wulczyn, F.G. (2008). A feedback loop comprising lin-28 and let-7 controls pre-let-7 maturation during neural stem-cell commitment. Nat Cell Biol *10*, 987-993.

Saha, P., Eichbaum, Q., Silberman, E.D., Mayer, B.J., and Dutta, A. (1997). p21CIP1 and Cdc25A: competition between an inhibitor and an activator of cyclin-dependent kinases. Mol Cell Biol *17*, 4338-4345.

Sanggaard, K.M., Kjaer, K.W., Eiberg, H., Nurnberg, G., Nurnberg, P., Hoffman, K., Jensen, H., Sorum, C., Rendtorff, N.D., and Tranebjaerg, L. (2008). A novel nonsense mutation in MYO6 is associated with progressive nonsyndromic hearing loss in a Danish DFNA22 family. Am J Med Genet A *146A*, 1017-1025.

Schaefer, A., Poluch, S., and Juliano, S. (2008). Reelin is essential for neuronal migration but not for radial glial elongation in neonatal ferret cortex. Dev Neurobiol *68*, 590-604.

Schulman, B.R., Esquela-Kerscher, A., and Slack, F.J. (2005). Reciprocal expression of lin-41 and the microRNAs let-7 and mir-125 during mouse embryogenesis. Dev Dyn *234*, 1046-1054.

Schwamborn, J.C., Berezikov, E., and Knoblich, J.A. (2009). The TRIM-NHL protein TRIM32 activates microRNAs and prevents self-renewal in mouse neural progenitors. Cell *136*, 913-925.

Seggerson, K., Tang, L., and Moss, E.G. (2002). Two genetic circuits repress the Caenorhabditis elegans heterochronic gene lin-28 after translation initiation. Dev Biol *243*, 215-225.

Sempere, L.F., Freemantle, S., Pitha-Rowe, I., Moss, E., Dmitrovsky, E., and Ambros, V. (2004). Expression profiling of mammalian microRNAs uncovers a subset of brain-expressed microRNAs with possible roles in murine and human neuronal differentiation. Genome Biol *5*, R13.

Sheth, U., and Parker, R. (2003). Decapping and decay of messenger RNA occur in cytoplasmic processing bodies. Science *300*, 805-808.

Smirnova, L., Grafe, A., Seiler, A., Schumacher, S., Nitsch, R., and Wulczyn, F.G. (2005). Regulation of miRNA expression during neural cell specification. Eur J Neurosci *21*, 1469-1477.

Song, J.J., Liu, J., Tolia, N.H., Schneiderman, J., Smith, S.K., Martienssen, R.A., Hannon, G.J., and Joshua-Tor, L. (2003). The crystal structure of the Argonaute2 PAZ domain reveals an RNA binding motif in RNAi effector complexes. Nat Struct Biol *10*, 1026-1032.

Standart, N., and Jackson, R.J. (2007). MicroRNAs repress translation of m7Gppp-capped target mRNAs in vitro by inhibiting initiation and promoting deadenylation. Genes Dev *21*, 1975-1982.

Tabata, H., and Nakajima, K. (2002). Neurons tend to stop migration and differentiate along the cortical internal plexiform zones in the Reelin signal-deficient mice. J Neurosci Res *69*, 723-730.

Tang, X., Gal, J., Zhuang, X., Wang, W., Zhu, H., and Tang, G. (2007). A simple array platform for microRNA analysis and its application in mouse tissues. RNA *13*, 1803-1822.

Tian, D.S., Dong, Q., Pan, D.J., He, Y., Yu, Z.Y., Xie, M.J., and Wang, W. (2007). Attenuation of astrogliosis by suppressing of microglial proliferation with the cell cycle inhibitor olomoucine in rat spinal cord injury model. Brain Res *1154*, 206-214.

Tucker, M., Valencia-Sanchez, M.A., Staples, R.R., Chen, J., Denis, C.L., and Parker, R. (2001). The transcription factor associated Ccr4 and Caf1 proteins are components of the major cytoplasmic mRNA deadenylase in Saccharomyces cerevisiae. Cell *104*, 377-386.

Vitellaro-Zuccarello, L., Mazzetti, S., Madaschi, L., Bosisio, P., Fontana, E., Gorio, A., and De Biasi, S. (2008). Chronic erythropoietin-mediated effects on the expression of astrocyte markers in a rat model of contusive spinal cord injury. Neuroscience *151*, 452-466.

Wakiyama, M., Takimoto, K., Ohara, O., and Yokoyama, S. (2007). Let-7 microRNA-mediated mRNA deadenylation and translational repression in a mammalian cell-free system. Genes Dev *21*, 1857-1862.

Wang, S., Liu, N., Chen, A.J., Zhao, X.F., and Wang, J.X. (2009). TRBP homolog interacts with eukaryotic initiation factor 6 (eIF6) in Fenneropenaeus chinensis. J Immunol *182*, 5250-5258.

Wang, T., and Xu, Z. (2010). miR-27 promotes osteoblast differentiation by modulating Wnt signaling. Biochem Biophys Res Commun *402*, 186-189.

Watanabe, T., Takeda, A., Mise, K., Okuno, T., Suzuki, T., Minami, N., and Imai, H. (2005). Stage-specific expression of microRNAs during Xenopus development. FEBS Lett *579*, 318-324.

Wightman, B., Ha, I., and Ruvkun, G. (1993). Posttranscriptional regulation of the heterochronic gene lin-14 by lin-4 mediates temporal pattern formation in C. elegans. Cell *75*, 855-862.

Wu, L., Fan, J., and Belasco, J.G. (2006). MicroRNAs direct rapid deadenylation of mRNA. Proc Natl Acad Sci U S A *103*, 4034-4039.

Wulczyn, F.G., Smirnova, L., Rybak, A., Brandt, C., Kwidzinski, E., Ninnemann, O., Strehle, M., Seiler, A., Schumacher, S., and Nitsch, R. (2007). Post-transcriptional regulation of the let-7 microRNA during neural cell specification. FASEB J *21*, 415-426.

Yan, N., Lu, Y., Sun, H., Tao, D., Zhang, S., Liu, W., and Ma, Y. (2007). A microarray for microRNA profiling in mouse testis tissues. Reproduction *134*, 73-79.

Yu, F., Yao, H., Zhu, P., Zhang, X., Pan, Q., Gong, C., Huang, Y., Hu, X., Su, F., Lieberman, J.*, et al.* (2007a). let-7 regulates self renewal and tumorigenicity of breast cancer cells. Cell *131*, 1109-1123.

Yu, J., Vodyanik, M.A., Smuga-Otto, K., Antosiewicz-Bourget, J., Frane, J.L., Tian, S., Nie, J., Jonsdottir, G.A., Ruotti, V., Stewart, R.*, et al.* (2007b). Induced pluripotent stem cell lines derived from human somatic cells. Science *318*, 1917-1920.

Yu, Z., Raabe, T., and Hecht, N.B. (2005). MicroRNA Mirn122a reduces expression of the posttranscriptionally regulated germ cell transition protein 2 (Tnp2) messenger RNA (mRNA) by mRNA cleavage. Biol Reprod *73*, 427-433.

Zekri, L., Huntzinger, E., Heimstadt, S., and Izaurralde, E. (2009). The silencing domain of GW182 interacts with PABPC1 to promote translational repression and degradation of microRNA targets and is required for target release. Mol Cell Biol *29*, 6220-6231.

Zhao, C., Sun, G., Li, S., and Shi, Y. (2009). A feedback regulatory loop involving microRNA-9 and nuclear receptor TLX in neural stem cell fate determination. Nat Struct Mol Biol *16*, 365-371.

Zhou, H., Yang, L., Li, H., Li, L., and Chen, J. (2009). Residues that affect human Argonaute2 concentration in cytoplasmic processing bodies. Biochem Biophys Res Commun *378*, 620-624.

6. Appendix

6.1 Statement

Hiermit erkläre ich, daß ich die vorliegende Dissertation selbständig verfaßt und mich keiner anderen als der angegebenen Hilfsmittel bedient habe.

Berlin, den _____

_____

Unterschrift des Doktoranden

6.2 Publications

Rybak, A., Fuchs, H., Smirnova, L., Brandt, C., Pohl, E.E., Nitsch, R., and Wulczyn, F.G. (2008). *A feedback loop comprising lin-28 and let-7 controls pre-let-7 maturation during neural stem-cell commitment*. Nat Cell Biol *10*, 987-993.

Smirnova L, Rybak A, Fuchs H, Pekarik V, Wulczyn FG (2008) *miRNAs in Neurobiology*. In Encyclopedia of Neuroscience Binder, M.D.; Hirokawa, N.; Windhorst, U.; Hirsch, M.C. (Eds.).Springer Verlag ISBN: 978-3-540-29678-2

Rybak, A., Fuchs, H., Hadian, K., Smirnova, L., Wulczyn, E.A., Michel, G., Nitsch, R., Krappmann, D., and Wulczyn, F.G. (2009). *The let-7 target gene mouse lin-41 is a stem cell specific e3 ubiquitin ligase for the mirna pathway protein ago2*. Nat Cell Biol *11*, 1411-1420

6.3 Danksagung

Diese Arbeit entstand am Institut für Anatomie in der Abteilung Zell- und Neurobiologie. Ich möchte mich an dieser Stelle recht herzlich bei all jenen bedanken, die mir während dieser Zeit mit Rat und Tat zur Seite standen um dies Arbeit anzufertigen.